Valorisation of CO2 capture agents for soil decontamination

Clara Tosi

N°d'ordre NNT : 2022LYSE1010

THESE de DOCTORAT DE L'UNIVERSITE DE LYON
Opérée au sein de
L'Université Claude Bernard Lyon 1

Ecole Doctorale N° 206
Chimie, Procédés, Environnement

Spécialité de doctorat : Chimie
Discipline : Chimie Organique

Soutenue publiquement le 28/01/2022, par :

Clara Tosi

Valorisation of CO_2 capture agents for soil decontamination

Devant le jury composé de :

Amgoune, Abderrahmane	Professeur, Université Lyon 1	Examinateur
El Khamlichi, Aicha	Ingénieure, ADEME	Examinatrice
Lebigue-Julcour, Carine	Directrice de recherche CNRS	Rapporteur
Legrand, Yves-Marie	Ingénieur de Recherche CNRS	Rapporteur
Leclaire, Julien	Professeur, Université Lyon 1	Directeur de thèse
Barnes-Davin, Laury	Directrice R&D, VICAT	Co-Directrice de thèse

Université Claude Bernard – LYON 1

Président de l'Université	M. Frédéric FLEURY
Président du Conseil Académique	M. Hamda BEN HADID
Vice-Président du Conseil d'Administration	M. Didier REVEL
Vice-Président du Conseil des Etudes et de la Vie Universitaire	Mme Céline BROCHIER
Vice-Président de la Commission de Recherche	M. Petru MIRONESCU
Directeur Général des Services	M. Pierre ROLLAND

COMPOSANTES SANTE

Département de Formation et Centre de Recherche en Biologie Humaine	Directrice : Mme Anne-Marie SCHOTT
Faculté d'Odontologie	Doyenne : Mme Dominique SEUX
Faculté de Médecine et Maïeutique Lyon Sud - Charles Mérieux BURILLON	Doyenne : Mme Carole
Faculté de Médecine Lyon-Est	Doyen : M. Gilles RODE
Institut des Sciences et Techniques de la Réadaptation (ISTR)	Directeur : M. Xavier PERROT
Institut des Sciences Pharmaceutiques Biologiques (ISBP)	Directrice : Mme Christine et VINCIGUERRA

COMPOSANTES & DEPARTEMENTS DE SCIENCES & TECHNOLOGIE

Département Génie Electrique et des Procédés (GEP)	Directrice : Mme Rosaria FERRIGNO
Département Informatique	Directeur : M. Behzad SHARIAT
Département Mécanique	Directeur M. Marc BUFFAT
Ecole Supérieure de Chimie, Physique, Electronique (CPE Lyon)	Directeur : Gérard PIGNAULT
Institut de Science Financière et d'Assurances (ISFA)	Directeur : M. Nicolas LEBOISNE
Institut National du Professorat et de l'Education	Directeur : M. Pierre CHAREYRON
Institut Universitaire de Technologie de Lyon 1	Directeur : M. Christophe VITON
Observatoire de Lyon	Directrice : Mme Isabelle DANIEL
Polytechnique Lyon	Directeur : Emmanuel PERRIN
UFR Biosciences	Administratrice provisoire : Mme Kathrin GIESELER
UFR des Sciences et Techniques des Activités Physiques et Sportives (STAPS)	Directeur : M. Yannick VANPOULLE
UFR Faculté des Sciences	Directeur : M. Bruno ANDRIOLETTI

Acknowledgments

There are many people I need to thank for this accomplishment, which is not only mine but partially theirs too.

I would like to thank the CSAp group Florent, Laurent, Julien for welcoming me and teaching me the fine and frustrating art of scientific research. Julien, I thank you sincerely for giving me the opportunity of this thesis, when it seemed I could go no further in chemistry. To the fellows PhDs Fanny, Benji, Alex, Francesca, Maxime, Marc and Tituoan, thank you for making life in the lab so fun, and scientific and personal discussions so interesting.

Francesca, Bronsina mia, we have accomplished so much. Having you at my side during this rollercoaster of emotions, known as the PhD, was the greatest gift. Thank you for the support and for the many, many laughs.

To *La Mif*, the weirdest group of Italians (and one French) anybody could find in Lyon. Kevin, Matilde, Carolina, Paolo & Paolo, Francesco, the PhD would not have been the same without you and our ateliers, I am so very glad to have met you all.

To my friends and family, thank you for being my support system throughout the years, the sorrows and the joys, regardless of how many borders were separating us.

To Simona, lifelong chemistry partner, from the roofs of La Sapienza to Marseille, Amsterdam, Graz and Lyon, the world is ours, sweetie. To Francisco, long-lost brother, thank you for everything, from walking barefoot in Marseille to surprising me at the wedding.

To Kostia, my husband, my слоник, my love. Thank you for supporting my brightest moments just as lovingly as my darkest, you are and always will be my greatest source of marvel.

To my Father, and my Mother. Thank you for listening to my chemistry related speeches at every dinner, thank you for not understanding that a mass spectra is not a bunch of ghosts and thank you for giving me the tools to always be creative and artistic in life.

The mermaid in this thesis goes to you, miei piccoli amici piumati.

Table of contents

Résumé en Français

Du fait de l'industrialisation et des besoins énergétiques en croissance, la concentration des gaz à effet de serre est en constante augmentation. Dans les années 2000-2010, 49 Gt de CO_2 ont été émis, dont 78% par des activités industrielles[1]. En 2021, la concentration de CO_2 dans l'atmosphère a atteint 420 ppm[2]. La solution à cette problématique repose certainement sur l'utilisation des énergies renouvelables, mais des technologies capables de réduire les émissions anthropogéniques peuvent aider à minimiser l'effet néfaste des gaz à effet de serre pendant la période de transition.

Pour répondre à cette problématique, nous proposons de développer des technologies CCUS (Carbon Capture Utilization and Storage), impliquant le captage du CO_2 par des solutions d'amines et la carbonatation minérale. C'est dans ce contexte qui se situe ce travail de thèse, où l'objectif principal est de définir et optimiser un système moléculaire, à base d'acide aminés, capable de capter le CO_2, de transférer le CO_2 au sol pour le carbonater et d'en extraire simultanément les métaux polluants qu'il contient, par lixiviation. Ce travail est donc divisé en deux volets :

1. Le captage du CO_2 par des acides aminées en milieu aqueux
2. L'utilisation de ces solutions comme extractants pour la décontamination et la carbonatation des sols, en investiguant au préalable leur efficacité pour la carbonatation des métaux, tels que les alcalino-terreux.

Trois acides aminés, la glycine, *L*-lysine et *L*-cystéine, ont été étudiés pour leurs propriétés de captage du CO_2 par une approche de type Chimie Combinatoire Dynamique, en se focalisant sur les adduits carbamates et carbonates formés et ainsi que sur les propriétés structurales qui déterminent leur stabilité.

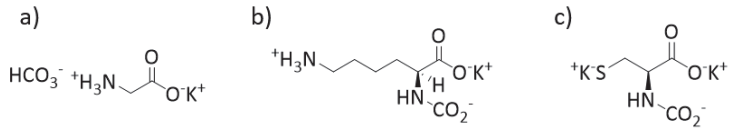

Figure 1 Adduits potentiel entre acides aminées et CO_2. a) Sel de bicarbonate de glycine ; b) alpha monocarbamate de *L*-lysine ; c) monocarbamate de *L*-cystéine.

Dans le troisième chapitre ces bibliothèques combinatoires dynamiques, acide aminés-CO_2, sont étudiées en présence d'un sel de métal soluble, pouvant interagir comme « template »,

ou patron, ($MgCl_2$, $CaCl_2$). L'intérêt est d'observer si le métal possède une affinité envers un ou plusieurs ligands CO_2-sourcé, qui peut modifier leur distribution au sein du mélange en formant un ou plusieurs complexes stables. Les αAA ont été ensuite testés pour le développement d'un procédé de « Integrated Absorption Mineralization (IAM) », i.e. pour le captage du CO_2 intégré à la carbonatation minérale d'oxides métalliques. Ces tests ont été effectués par voie mécanochimique liquide/solide et solide/solide.

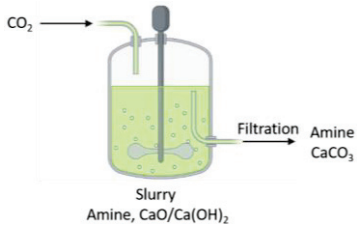

Figure 2 Example de réaction IAM. Le CO_2 est introduit dans une suspension d'amine et d'oxyde/hydroxyde de métal. Suite à filtration le carbonate métallique, préalablement formé, est séparé de la solution d'amine, qui peut être potentiellement réutilisée pour d'autres cycles de captage/carbonatation minérale.

La dernière partie de ce travail est l'utilisation des solutions d'acides aminés, en présence et en absence de CO_2, pour la remédiation des sols. L'étude s'est focalisée sur un sol contaminé en Eléments-Traces Métalliques (ETM), provenant des déchets industriels. Cette partie regroupe l'extraction des métaux, le stockage du CO_2 sous forme de carbonate métallique et la régénération de l'agent extractant.

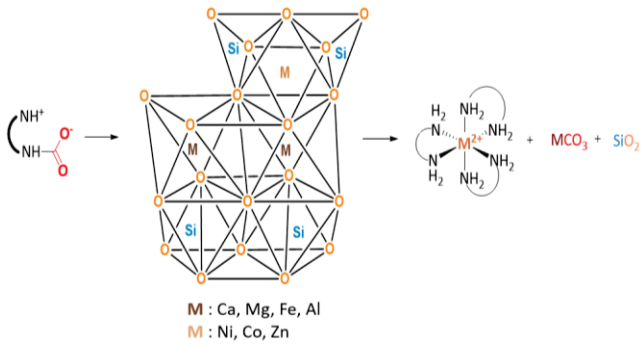

Figure 1 Principe de dépollution des sols par des solution d'amines chargées en CO_2. Extraction de métaux par complexation d'amine et formation simultanée de carbonates métalliques.

Ce travail de thèse s'inscrit dans le cadre d'une collaboration de recherche et développement industrielle en collaboration avec l'ADEME et l'entreprise Vicat, et vise comme objectif l'utilisation des émissions CO_2 comme ressource pour la carbonatation des déchet industriels, qui pourront ensuite être réutilisés dans la production du ciment.

Nomenclature and abbreviations

α: CO_2 loading

δ: chemical shift (NMR)

$\Delta_r G^\circ$ = standard free reaction energy

$\Delta_r H^\circ$ = standard reaction enthalpy

$\Delta_r S^\circ$ = standard reaction entropy

λ: wavelength

σ: standard deviation

μ: micro

ν: frequency of vibration (FT-IR)

αAA: α amino acid

AAS: Amino Acid Salts

AF: Amplification Factor

ADA: N-2-(acetamido)iminodiacetic acid

Ala: Alanine

AMP: Amino methyl propanol

APCs: amino polycarboxylates

Arg: Arginine

Asp: Aspartic Acid

atm: atmosphere

°C: Celsius

$\overline{C}_P$= specific heat capacity of the solvent (kJ/kg*K)

CAPEX: Capital Expenditures

CC: Cyclic Capacity

CCS: Carbon Capture and Storage

CCU: Carbon Capture and Utilization

CCUS: Carbon Capture Storage and Utilization

cEF: complete E factor

CHNS: Carbon, Hydrogen, Nitrogen, Sulfur elementary analysis

CKD: Cement Kiln Dust

Cys: Cysteine

D: Deuterium

DCC: Dynamic Combinatorial Chemistry

DCL: Dynamic Combinatorial Library

DEEA: Diethylethanolamine

DETA: Diethylenetriamine

DPTA: Diethylenetriamine pentaacetic acid

ds: dried soil

€: euros

EDA: Ethylenediamine

EDDS: Ethylenediamine-disuccinic acid

EDTA: Ethylenediaminetetraacetic acid

EOR: Enhanced Oil Recovery

ETM : Eléments-Traces Métalliques

FT-IR: Fourier-transform Infrared spectroscopy

g: gram

GHG: Greenhouse Gas

Gly: Glycine

Gton: Gigaton

IAM: Integrated Amine Mineralization

ICP-OES: Inductively Coupled Plasma-Optical Emission Spectroscopy

i.e.: in example

h: hour

HM: heavy metal

K: Kelvin

kJ: kilojoule

Lys: Lysine

M: mol/L

m: meter

$\bar{m}_{solv}$ = average mass flow rate (kg/s)

MC: Mineral Carbonation

MEA: Monoethanolamine

min: minutes

MHz: MegaHertz

mL: milliliters

mm: millimeters

mol: moles

NMR: Nuclear Magnetic Resonance

NOx: Nitrogen Oxides

NTA: Nitrile triacetic acid

OPEX: Operational Expenses

P: pressure

p: partial pressure

PCC: Post Combustion Capture / Power Compensated Calorimetry

PDA: Propanediamine

pH: potential of hydrogen

ppm: part per million

PTFE: Polytetrafluoroethylene

PZ: Piperazine

qNMR: quantitative NMR

Q_{Reb}: reboiler duty (kJ/s)

Q_{Reg}: regeneration duty (kJ/kg)

rpm: round per minute

$: dollar

s: second

$SCCO_2$: Super Critical CO_2

SOx: Sulphur Oxides

t: time / ton

T: Temperature

TGA-MS: Thermogravimetric Analysis coupled with Mass Spectrometer

TMPCl: Tetramethyl phosphonium chloride

TMS: Tetramethylsilane

W: watt

w/w: weight/weight concentration

WC: Tungsten Carbide

wt%: weight percentage

x: molar fraction

XRD: X-Ray Diffraction

y: year

General Introduction

The constantly uprising CO_2 concentration in the atmosphere is urging the development of Carbon Capture Utilization and Storage technologies.

The purpose of this thesis is to develop an integrated carbon capture and mineral carbonation process coupled to the decontamination of a soil, provided by the cement industry. The main objective is to identify a molecular system based on amino acids, which is capable to capture CO_2, store it permanently as carbonate products into a polluted soil, and simultaneously extract the metal contaminants via leaching techniques.

The first chapter reports the state of the art on carbon capture technologies, focusing on CO_2 capture by amine scrubbing, conventional mineral carbonation as well as Integrated Absorption Mineralization (IAM), and a general overview of soil remediation techniques.

In the second chapter, the CO_2 capture properties of three amino acids (αAA), such as glycine, *L*-lysine and *L*-cysteine, were investigated via a Dynamic Combinatorial Chemistry approach. The study quantified the populations of carbamates and carbonated adducts formed in solution, as well as the structural properties influencing their stability.

The third chapter presents the study of these Dynamic Combinatorial Libraries (DCLs), in the presence of a soluble metal salt ($MgCl_2$, $CaCl_2$), which can act as a "template". The interest of this study resides in determining if the affinity of each metal cation towards one or more library member, modifies their distribution, by forming one or more soluble complexes.

The αAA were then tested in an Integrated Absorption Mineralization (IAM) set-up, in which CO_2 capture was coupled with the mineral carbonation of metal oxides. These experiments were conducted by a mechanochemical approach both in solid/solid and solid/liquid conditions.

The fourth and final chapter of this work explores the utilization of amino acids, both under CO_2-loaded and unloaded forms, as washing solutions for soil remediation. The study focuses on a soil polluted by heavy metals, derived from industrial wastes. In this section, metal extraction CO_2 capture as metal carbonates and amine regeneration are merged and combined in a single, two-pots CCUS process.

Chapter 1
Introduction

Chapter 1

1 A general introduction on CO_2

During the last decades, the greenhouse effect has dramatically escalated, owed partly to CO_2 emissions. Due to the uprising industrialization, with ever-growing need for energy, the greenhouse gas (GHG) emission is constantly increasing. Only in the years 2000-2010 were released 49Gt of CO_2, 78% of which were produced by the industrial processes and fossil fuel combustion[1]. Since 2010 the tendency of carbon dioxide emission has been constantly uprising[2], until reaching a CO_2 concentration level of 420 ppm in the atmosphere as of 2021 (Fig.1a).

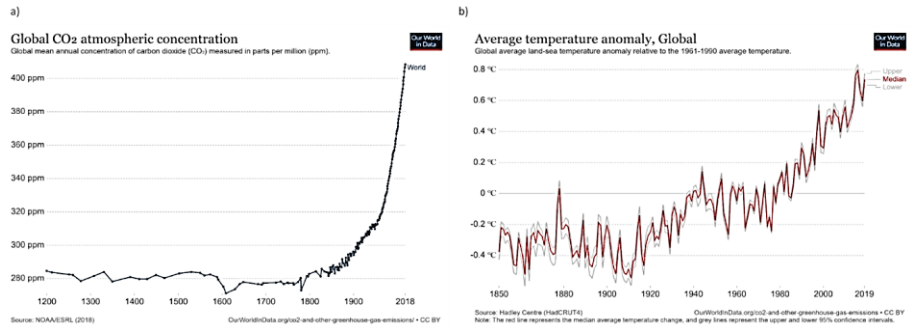

Fig. 1 a) Atmospheric carbon dioxide concentration from 1200 to 2018, measured in parts per million (ppm). Atmospheric concentrations - Our World in Data[3]; b) Global average (red) land-sea temperature anomaly from 1850 to 2019, expressed in degrees Celsius (°C). Average temperature anomaly, Global (ourworldindata.org)[4].

In order to slow down the exponential growth of CO_2 atmospheric concentration, the energy sources for modern way of living should be immediately revolutionized, which currently does not seem realistic.

The most impacting consequence of this continuous CO_2 emissions growth is global warming and, subsequently, climate change. Global warming modifies the average global temperature, influences rainfall patterns, amplifies coastal erosion, lengthens the growing season in some regions and melts ice caps and glaciers, presenting the most dreadful prospective for the future of humanity.

In Fig.1b is represented the variation of the average temperature (red line), in comparison to the period from 1961 and 1990, represented by the 0 °C baseline. The impressive increase in CO_2 concentration in the atmosphere since the beginning of the industrialized era (Fig.1a) and

the rise of average temperature from 1980 until now (Fig.1b) are extremely off-putting and point to the worldwide necessity for radical actions.

If the long-term solution undoubtedly relies on the use of renewable energies, new developing technologies based on reducing anthropogenic emissions will help to stay on course during the transition time[5].

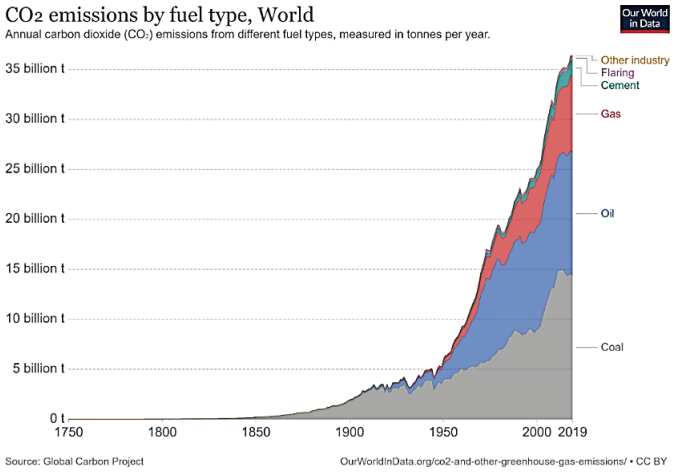

Fig. 2 Carbon dioxide emissions, expressed in billion tons, divided by fuel type, in a period span from 1750 to 2019[6]. CO_2 emissions by fuel - Our World in Data

Carbon dioxide emissions from energy and material production can arise from various sources and fuel type: coal, oil, gas, cement production and gas flaring, as shown in Fig.2.

As production of coal and oil fuels represent the two most important sources of CO_2, the research for reducing GHG emissions focuses on finding valuable environmentally friendly alternatives to those energy sources, as well as reducing CO_2 emissions in the atmosphere.

Several processes targeting those goals fall into the classification of Carbon Capture and Storage (CCS), Carbon Capture and Utilization (CCU), and Carbon Capture Utilization and Storage (CCUS).

1.1 Carbon Capture and Storage (CCS)

Carbon Capture and Storage technologies focus on the carbon dioxide cycle, which includes its separation from flue gases, its compression at 20 bars and lastly its transportation to its final storing location.

Flue gases are composed of around 15% of carbon dioxide mixed with inert N_2, as well as sulfur and nitrogen oxides (SOx and NOx). In order to perform an effective carbon capture step, the reactive oxides of sulfur and nitrogen have to previously be separated from the mixture, for instance via an alkaline scrubber[7] (eq.1-3).

$$CaCO_3 + SO_2 \longrightarrow CaSO_3 + CO_2 \quad (1)$$

$$Ca(OH)_2 + SO_2 \longrightarrow CaSO_3 + H_2O \quad (2)$$

$$4NH_3 + O_2 + 2NO_2 \longrightarrow 3N_2 + 6H_2O \quad (3)$$

Within the different methods for CO_2 capture currently investigated, is possible to find *calcium looping*[8], *pre-combustion* and *post combustion*[9].

Calcium looping uses calcium oxide to extract CO_2 to form $CaCO_3$. The carbonated product is then calcinated at 950 °C, producing a highly concentrated CO_2 gas flow and regenerating CaO, which can be reused for further capture cycles (eq.4)[10-12].

$$CaO \xrightarrow{\text{flue gas}} CaCO_3 \xrightarrow[CO_2]{950°C} CaO \quad (4)$$

The *pre-combustion capture* involves the separation of carbon dioxide from fossil fuel, or biomass fuel, before the combustion step. A first step of partial oxidation of fossil fuel leads to the formation of syngas (eq.5), which is rich with carbon monoxide and hydrogen.

$$C_xH_y + (x/2)\,O_2 \longrightarrow xCO + (y/2)\,H_2 \quad (5)$$

$$CO + H_2O \longrightarrow CO_2 + H_2 \quad (6)$$

Syngas then reacts with water vapor to form CO_2 (eq.6) , which is then separated from the gas mixture[13]. *Pre-combustion* capture is cheaper than *post-combustion capture* by 21–24% [14], nevertheless its implementation in industrial plants is still in progress due to the complexity of the set-up[15].

Finally, *post combustion capture* separates CO_2 from flue gases with the use of chemical solvents[16], usually aqueous alkanolamines, which are then regenerated by stripping carbon dioxide via high temperature desorption, a process which will be furtherly discussed in section 1.3 (page 26).

After the capture step, carbon dioxide is carried to its final storing site. Due to the large volumes of CO_2 involved, the gas is transported from the capture plant to the storing site via pipeline[17]. For logistical and economical reason, CO_2 is compressed at 20 bars and converted from gaseous to supercritical state.

The final storing site should be able to contain large quantities of CO_2, to deal with the 35 Gton of carbon dioxide emitted each year[18], and should ensure a long-term sequestration[16]. At present day there are two possible storage solutions: *ex situ* mineral carbonation and *in situ* geological storage. While the former will be furtherly discussed in section 2 of this chapter, the latter is depicted in Fig.3.

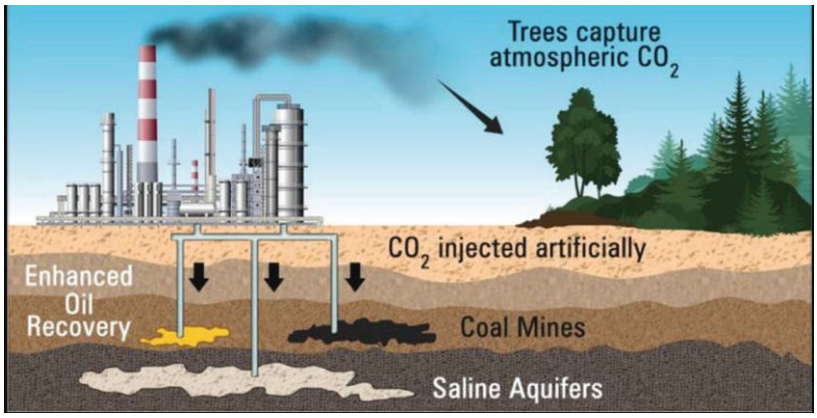

Fig. 3 Geological storage options for CO_2: unmineable coal seams, saline water-saturated reservoirs and oil reservoirs (Enhanced Oil Recovery).

Geological storage is considered the most mature option for the isolation of CO_2 from the atmosphere. It consists in injecting gas, liquid or supercritical CO_2 into oil reservoirs, saline aquifers or coal bed formation which are usually located at 800-1000m underground. Several pilot-scale and industrial-scale projects have already been developed and the Sleipner project, which stores approximately 1 million tons of CO_2 annually, has been in operation since 1996[17]. Studies showed that a well-regulated storage presents few risks of leakage (less than 0.0008%/year) and enables a long-term storage for CO_2, over 10000 years[19-20]. In addition, the presence of Mg^{2+}, Ca^{2+} oxides and silicates in a geological reservoir allow the transformation of carbon dioxide in magnesium and calcium carbonates via mineral carbonation reaction (eq.7-10)[21].

$$CaO + CO_2 \longrightarrow CaCO_3 \quad (7)$$

$$MgO + CO_2 \longrightarrow MgCO_3 \quad (8)$$

$$CaSiO_3 + CO_2 + 2H_2O \longrightarrow CaCO_3 + H_4SiO_4 \quad (9)$$

$$Mg_3Si_2O_5(OH)_4 + 3CO_2 + 2H_2O \longrightarrow 3MgCO_3 + 2H_4SiO_4 \quad (10)$$

$$H_4SiO_4 \longrightarrow SiO_2 + 2H_2O \quad (11)$$

The extent of the CO_2-water-mineral interaction depends on the pressure, temperature and metal abundance of the storing site. These factors can inhibit the gas-solid or liquid-solid mass transfer, slowing the mineral carbonation rate[22]. In addition, the formation of passivating silica layers (eq.11) within the minerals, furtherly hinders the reaction. Mineral carbonation is the only downhill pathway involving CO_2 as a reactant, since the enthalpies of formation of carbonates are between -179[23] and -118[24] kJ/mol of CO_2 (calcium carbonate and magnesium carbonate, respectively). In current times, geological storage is one of the only technologies capable to meet the Gt scale of storage [16].

1.2 Operational and Capital Expenses (OPEX and CAPEX)

Although many different capture plant configurations and technologies have already been developed, the post-combustion carbon capture step still presents prohibitive costs[8]. These costs are usually divided into operational expenses, OPEX, and capital expenses, CAPEX.

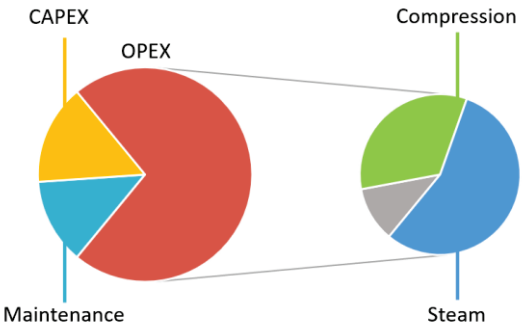

Fig. 4 Operational expenses (OPEX) and Capital expenses (CAPEX) of a post-combustion carbon capture plant. Reproduced from Marocco *et al.*, 2019[25].

In general, OPEX indicate the energy costs required for the separation of CO_2 from flue gases. If the capture plant itself needs an important amount of energy to run, it will force a higher production of coal, higher CO_2 emissions and so on. Taking a Post-Combustion amine-

scrubbing capture plant as an example, the regeneration step of the absorber represents around 50% of the operational costs while 30% is used for the compression of carbon dioxide[26, 27].

On the other hand, CAPEX correspond to the costs of the capture infrastructure. They include the cost of the capturing solvent, the material of the set-up which should resist to high temperature and corrosion form acid gas and basic amine, as well as the plant size[28]. The latter is related to the chemistry of the process. Henry's Law states that the dissolution of a gas (CO_2) into a liquid (amine sorbent) is directly proportional to its partial pression over the liquid. Since CO_2 capture is performed at atmospheric pressure, the contact surface between liquid and gas must be wide to ensure high capture performances, which consequently means large plants.

In 2018 the price of CO_2 capture by monoethanolamine (**MEA**) in a post-combustion capture facility was 50$/ton of CO_2[27], while the carbon tax in France was around 45$/ton of CO_2.

This economic gap lowers the interest of industries to construct CO_2 capture plants, which could instead be promoted by introducing an additional economic incentive in the CCS process. In this context can be introduced Carbon Capture and Utilization (CCU) and Carbon Capture Utilization and Storage (CCUS).

1.3 Carbon Capture Utilization (CCU)

CCU refers to the use of captured-CO_2 as a feedstock for industrial and chemical processes to yield valuable carbon-containing products[8].

As shown in Fig.5b CCU technologies can vary from chemical synthesis to food and beverage industry. For the latter CO_2 can be used as a carbonating agent for beverages, packaging gas for food preservation and, in its supercritical state, for the extraction of caffeine and cannabis from seeds and beans[29-30].

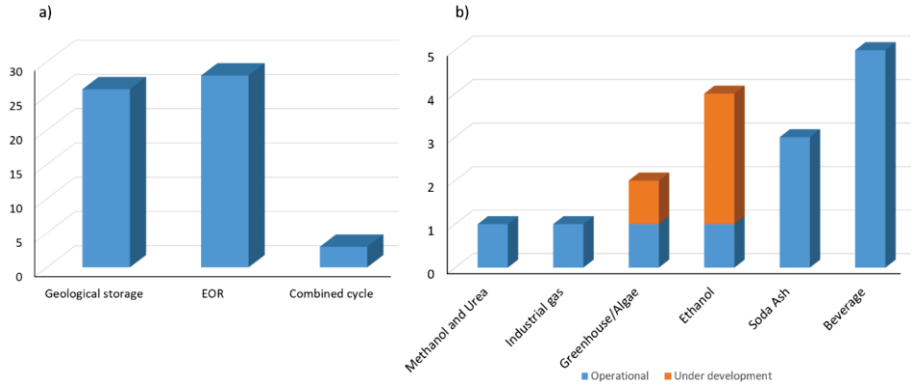

Fig. 5 a) Number of active CCU plants and their repartition between Geological storage (26), Enhanced Oil Recovery (28) and other combined cycles (5) in 2020; b) number of operational (blue) and under development (orange) CCU plants for different CO_2-products in 2020. Reproduced from: https://co2re.co/FacilityData.

Furthermore, algae such as *Dunaliella salina* or seaweed[31] can be used for CCU processes. The algae can fix CO_2 from three sources: atmosphere, flue-gases and soluble carbonates. Carbon dioxide is transformed into glucose via photosynthesis, increasing the algae growth. The biomass can later on be harvested, dried and used for the production of biofuels[32]. In 2008 the cost of dried biomass was estimated at 2.55 €/kg, which was considered too high to justify biofuel production[32].

CO_2 can also be used as a synthon for the chemical synthesis of polymers, cyanate[33], carbamates or hydrocarbons[34]. As an example, in eq.12 is reported the synthesis of a five-membered cyclic carbonate, which can be used as solvents or for further reactions with ammonia to yield polyurethane[33, 35].

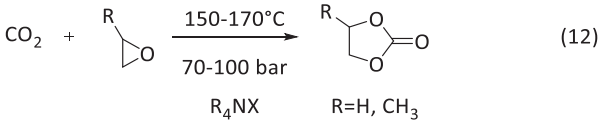

(12)

Carbon dioxide can be used for the catalyzed synthesis of methanol starting from syngas (CO, H_2, CO_2), a reaction studied and performed for many years already[36]. Another example is the industrial synthesis of urea[37] (eq.13, 14):

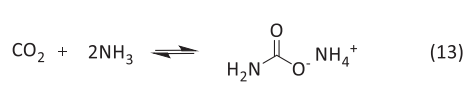

(13)

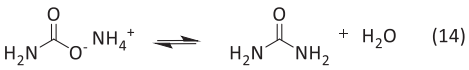

(14)

It is one of the industrial examples of the largest conversion of CO_2 into valued products, with a production of $1.5*10^8$ t/year and a consumption of carbon dioxide of $1.12*10^8$ t/year[37]. CO_2 is also used in its supercritical form ($SCCO_2$) for the synthesis of salicylic acid, in presence of a base catalyzer (eq.15)[38]:

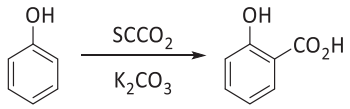

(15)

Finally, in Table 1 are reported the consumption of CO_2 to produce Urea, salicylic acid and cyclic carbonates and the market shares of those products.

Table 1 Production of Urea, Methanol and Carbonates with respective CO_2 use expressed in ton/year (t/y). Data provided by Marocco *et al*.[25]

Compound	Production (t/y)	CO_2 consumption (t/y)	Market share
Urea	$1.5*10^8$	$1.12*10^8$	75%
Salicylic Acid	$7.0*10^4$	$3.0*10^4$	40%
Carbonates	$8.0*10^4$	$4.0*10^4$	50%

1.4 Carbon Capture Utilization and Storage (CCUS)

A most deployed example of Carbon Capture Utilization and Storage (CCUS) technology is Enhanced Oil Recovery (EOR) (Fig.8), with 28 operational facilities in 2021 (Fig.5a).

After being captured and compressed, supercritical CO_2 is injected in oil reservoirs to enhance oil extraction, resulting in a production increase of 30% to 60% higher than regular oil extraction technologies[39]. In this way carbon dioxide is permanently stored in the geological reservoir[18]. While EOR represents an additional economic incentive for CCS, it also promotes the use of oil-based energy and the increase of anthropogenic emissions.

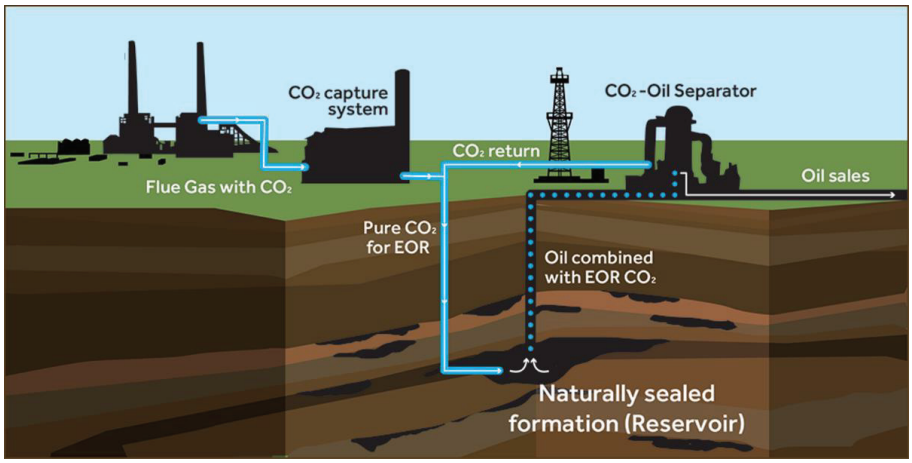

Fig. 6 Enhanced Oil Recovery (EOR) technology, from capture to geological storage. The captured and compressed CO_2 is transported via pipeline to an oil reservoir. The injection of CO_2 in the reservoir enhances oil extraction.

Another example of CCUS technology is Enhanced Gas Recovery (EGR) in which CO_2 in injected in depleted gas reservoir for the recovery of methane (CH_4). Depleted gas reservoirs present few risks of gas leakage and a wide storing volume of 140 Gt worldwide[40].

1.5 Integrated CCUS

Integrated CCUS indicates a process in which the CO_2 loaded solution is used to yield new carbamated/carbonated products in a step prior to desorption.

In 2020 our group developed an integrated CCUS pathway coupling CO_2 capture by amine scrubbing and metal separation[41]. A CO_2-loaded solution of Diethylenetriamine was used for the separation of lanthanum, cobalt and nickel contained in lithium batteries. Carbon dioxide is stored as $La_2(CO_3)_3$ and the metals are separated with high purity (> 97%), providing a potential new way to integrate CO_2 capture and storage with metal recovery[41].

An important example of integrated CCUS is *mineral carbonation*, where ores, tailings, fly ashes, or brines can be transformed into mineral carbonates[25]. The latter can then be integrated in construction fillers, cement additive and other industrial applications.[42] The integrated CO_2 absorption and carbonation of metals and minerals represents one of the three subjects of this work and will be furtherly discussed in section 2 of the introduction.

1.6 Post combustion amine scrubbing

Post combustion amine scrubbing is one of the most deployed technology for CO_2 capture. The basic process of amine scrubbing, patented by Bottoms in 1930[43], aimed at removing H_2S and CO_2 from natural and fuel gases using Piperazine (**PZ**)[44]. As shown in Fig.7, in the first steps the fuel passes through the boiler and the alkaline sulfur removal step (eq.1,2,3, page 23). The resulting gas mixture is then cooled at 40 °C and introduced in the absorber tank. There, the sorbent is loaded with CO_2 (CO_2-rich sorbent) and transferred to the stripper where the solution is heated at 100-120 °C. After the thermal-desorption step, the pure CO_2 gas flow is compressed and the regenerated amine (CO_2-lean sorbent) is reintroduced in the absorber tank[7].

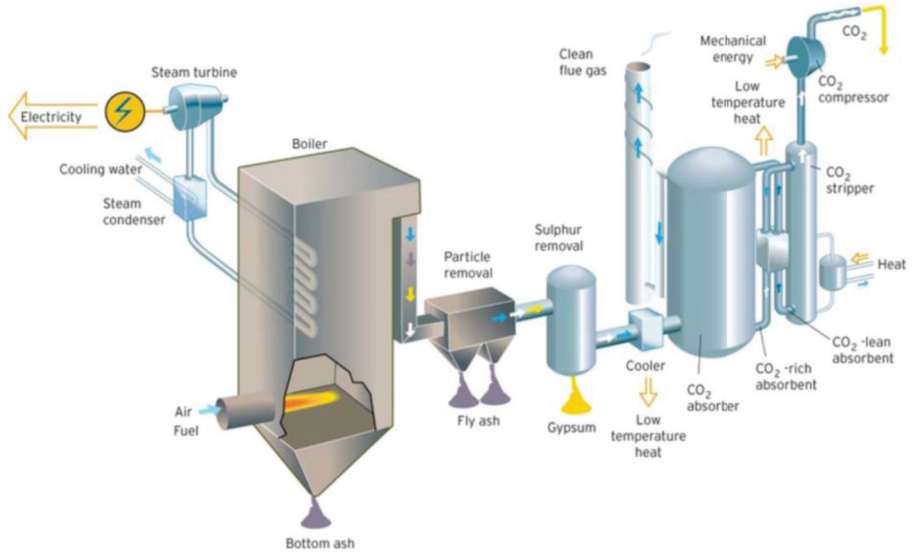

Fig. 7 Post-combustion capture system. The fuel is introduced in the boiler and transferred to an alkaline washing step for SOx and NOx removal. The gas mixture is cooled at 40 °C and introduced in the CO_2 absorber where is captured by the amine solution. The CO_2-rich sorbent is transferred in the stripper, the elevated temperature (100-120 °C) enables the desorption of CO_2 with the regeneration of the lean sorbent. Carbon dioxide is finally pressurized at 20 bars and ready to be transferred for further utilization or to its final storing site[45].

1.6.1 Absorption

In the absorption step, an aqueous solution of amine circulates in the absorber tank to capture CO_2 at ambient pressure and 40 °C. Due to the electrophilic character of the carbon, CO_2 can undergo an attack by a nucleophile or by a Lewis Base:

$$AH + CO_2 + B \rightleftharpoons ACO_2^- + BH^+ \quad (16)$$

$$2R_2NH + CO_2 \rightleftharpoons R_2NCO_2^- + R_2NH_2^+ \quad (17)$$

$$CO_2 + OH^- \rightleftharpoons HCO_3^- \quad (18)$$

Eq.16 presents the general nucleophilic attack on carbon dioxide, with abstraction of the proton by a Bronsted base (B). Eq.17 presents a carbamation reaction, where the amine plays the role of both nucleophile and base. The presence of water leads to a carbonation reaction (eq.18), in which the role of the nucleophile is played by the hydroxide, initially present as such or deprotonated by another base[46].

As every covalent associative process, carbamation and carbonation equilibria display a strongly negative reaction enthalpy. Studies in literature report that the reaction enthalpy for CO_2 capture from flue gases varies from -60/-80 kJ/mol for carbamation, to -45/-50 kJ/mol for carbonation[41, 47-50]. The heat dissipated by the exothermic reaction is then partially recycled in the heat exchanger of the PCC set up. For both pathways the gas capture into a liquid displays a negative entropy (-70/-90 J/K*mol)[51] due to the loss of free molecules in gaseous state[52].

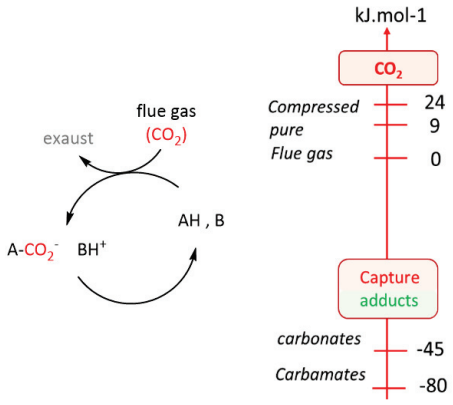

Fig. 8 On the left a carbon capture cycle in presence of a nucleophile (AH) and a base, on the right the enthalpy associated with CO_2 capture reactions. Courtesy of Prof. J. Leclaire.

To date, two mechanisms are proposed for carbamation[46]: termolecular and zwitterionic. The termolecular mechanism presents the formation of carbamic acid[53-54] as a transient species (eq.19), which is directly deprotonated by a base (eq.20)[55-56]:

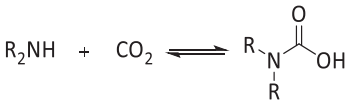

(19)

(20)

For the zwitterionic mechanism, the nucleophilic attack of the amine on carbon dioxide yields an ammonium-carbamate zwitterion (eq.21), which is then deprotonated (eq.22)[57-58].

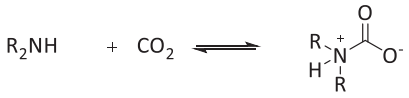

(21)

(22)

1.6.2 Desorption

As mentioned in the previous section, the capture of gaseous CO_2 presents a negative entropy, hindering the desorption step, while the negative enthalpy of formation of both ammonium carbamates and carbonates favors the capture step. In the operating conditions, the enthalpic gain is higher than the entropic loss. Therefore, Gibb's free energy is negative, resulting in an exothermic spontaneous reaction (eq.23).

$$\Delta G_R^0 = \Delta H_R^0 - T\Delta S_R^0 \quad (23)$$

In order to regenerate the solvent and separate carbon dioxide, the CO_2-rich solution obtained in the absorption step is transferred to the stripper tank, where carbon dioxide is thermally desorbed at 100-120 °C. The energetic cost of this process is defined as the reboiler duty (Q_{reb}) and depends on the heat of desorption, the sensible heat and the heat of vaporization (eq.24)[26].

$$Q_{Reb} = \left(n_{CO_2}\Delta H_{CO_2}\right) + \left(\bar{m}_{\,solv}\bar{C}_{\,P}(T_{in} - T_{out})\right) + \left(n_{vap,H_2O}H_{vap,H_2O}\right) \quad (24)$$

$\mathbf{Q_{Reb}} = \text{reboiler duty (kJ/s)}$

$\mathbf{n_{CO_2}} = \text{stripping molar flow rate (kg/s)}$

$\Delta\mathbf{H_{CO_2}} = \text{heat of } CO_2 \text{ desorption (kJ/kg)}$

$\bar{\mathbf{m}}_{\mathbf{solv}}$= average mass flow rate (kg/s)

$\bar{\mathbf{C}}_{\mathbf{P}}$ = specific heat capacity of the solvent (kJ/kg ∗ K)

$\mathbf{T_{in}} - \mathbf{T_{out}}$ = temperature difference in and out of the stripper (K)

$\mathbf{n_{vap,H_2O}}$ = molar flow rate of vaporised water

$\mathbf{H_{vap,H_2O}}$ = latent heat of water vaporization

The first component indicates the heat of desorption ($n_{CO_2}\Delta H_{CO_2}$) required to release CO_2 from the amine solvent. It depends on the capture reaction enthalpy and the quantity of captured CO_2, also defined as loading (eq.28-31, page 35). The second component $\left(\bar{m}_{solv}\bar{C}_P(T_{in} - T_{out})\right)$ refers to the energy required to heat the solvent circulating in the stripper tank, where ΔT is the temperature difference of the solvent entering and leaving the desorption tank. The third component $\left(n_{vap,H_2O}H_{vap,H_2O}\right)$ indicates the heat of water vaporization required to regenerate the solvent. Finally, the regeneration duty (Q_{reg}, kJ/kg) is calculated dividing the reboiler duty by the molar flow rate (eq.25)[26].

$$Q_{reg} = \frac{Q_{reb}}{n_{CO_2}} \qquad (25)$$

Considering the enthalpy of formation of ammonium carbamates and carbonates previously discussed, amine sorbents which preferably form the latter should require less energy for the CO_2 stripping/amine regeneration step.

After the desorption, the stripped amine solvent is reintroduced in the absorber tank and pure CO_2 can be compressed at 20 bar for further use or sequestering[52]. In a post combustion capture plant, most of the energy cost of the process comes from the low-temperature (100-120 °C) stripping step for the desorption of CO_2.

Concerning the industrial limitations of PCC, its main disadvantages are: dimension of the equipment, consumption of water (millions of liter per hour[27]), toxic byproducts deriving from amine degeneration and the disposal of expired solvents[16]. On the other hand, PCC units do not require the construction of new facilities, but they can directly be implemented onto already existing coal-fired power plants.

In order to maximize the advantages of PCC, the scientific community has focused on the determination of the ideal solvent for CO_2 absorption.

The latter should be[59]:

- non-toxic and environmentally friendly. Since amine emissions may occur through the cleaned exhaust gas it is important that the chemicals have low or no environmental effects[60]
- resistant to thermal degradation, to limit the solvent losses
- non-corrosive, to preserve the stainless-steel units and limit metal pollution in the solvent
- have low viscosity, to enhance gas-liquid mass transfer and consequently CO_2 capture
- present fast reaction kinetics with CO_2, to reach maximum loading in short time spans
- high absorption capacity, to assure an efficient capture process
- low desorption energy requirement, to reduce the overall energy costs (OPEX)
- preferably inexpensive, to limit the CAPEX

1.6.3 First generation solvents

Amine-based scrubbing solvents are divided into first generation (aqueous solution of one amine, most frequently an alkanolamine)[61-62], and second generation solvents (aqueous solution of mixed amines)[44]. Monoethanolamine (**MEA**) is probably the most extensively studied first generation absorbent used for post combustion CO_2 capture[63] which has been implemented into commercial facilities. It is subject to oxidative and thermal degradation[7] into 2-oxazolidone (eq.26) and dihydroxyethylurea[64] (eq.27), occurring during the stripping step, but it is inexpensive (42$/kg) and presents high initial absorption rates[65] (7.66* 10^{-7} mole/s-Pa-m^2, for 7M **MEA**)[66].

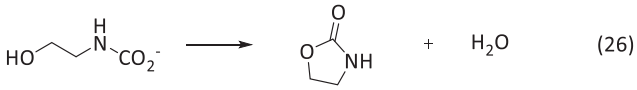

MEA-carbamate 2-Oxazolidone (26)

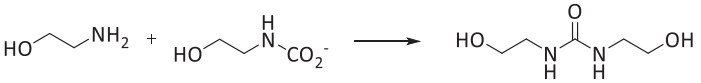

MEA **MEA**-carbamate N,N'-di(2-hydroxyethyl)urea (27)

The capture performance of a solvent is measured via several parameters, such as loading ($\alpha(CO_2)$). The literature presents several loading definitions[47, 49, 67] resulting in a lack of unity

in the reported data, which complicates the task of solvent benchmarking and impedes a clear comparison between published results.

Hereafter are listed four different expressions of α(CO_2):

$$\alpha_{alk}(CO_2) = \frac{moles_{CO_2}}{moles_{alkalinity}} \quad (28)$$

$$\alpha^{g}_{R_2NH}(CO_2) = \frac{g_{CO_2}}{kg_{solution}} \quad (29)$$

$$\alpha^{n}_{R_2NH}(CO_2) = \frac{moles_{CO_2}}{moles_{R_2NH}} \quad (30)$$

$$\alpha_{N}(CO_2) = \frac{moles_{CO_2}}{moles_{R_2NH} * \#N} \quad (31)$$

The CO_2 loading aims at quantifying the carbon dioxide content in an absorbent solution, and it can be expressed per moles of alkalinity (eq.28)[66], mass of total solution (eq.29)[49], moles of amine (eq.30) or normalized per moles of nitrogen (eq.31).

Another factor used to compare the efficiency of solvent is the called Cyclic Capacity (CC). The calculation of the cyclic capacity is shown in eq.32:

$$\Delta\alpha = \alpha_{rich} - \alpha_{lean} \quad (32)$$

Where α(rich) is the loading value after absorption and α(lean) the loading value after desorption. This parameter helps to determine the capture yield and the productivity of a solvent. Unfortunately, the literature presents heterogeneity cyclic capacity, for many values are determined in different operating conditions (T of absorption/desorption, concentration, partial CO_2).

For the CO_2 capture mechanism by **MEA** solutions, two moles of **MEA** are needed to fix one mole of CO_2 through carbamation (eq.33), and one mole of **MEA** per mole of carbon dioxide for the carbonation reaction (eq.34). The bicarbonate ion shown in eq.18 can also be obtained by hydrolysis of the carbamate (eq.35).

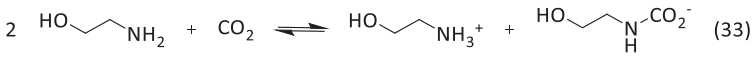

(33)

(34)

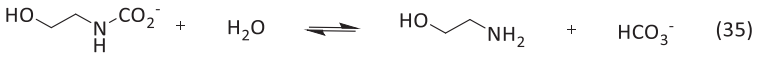

(35)

The carbamation/carbonation distribution of a CO_2-loaded solution of **MEA** was investigated by NMR analysis, only to confirm that the carbamate is indeed the most abundant specie. However, the exact share between the ammonium carbamate and carbonate is not yet reported in the literature[68-69].

As mentioned at the beginning of this section, **MEA** displays some drawbacks, such as thermal and oxidative degradation during the stripping step, and corrosion of the stainless steel tanks (16.44 miles per year at 80 °C with loading 0.2) at high concentration (5M)[70]. However, the biggest disadvantage is the high energy requirement for desorption, which is estimated to be around 3.8 MJ/kg of CO_2 captured[61].

Another first generation solvent is Piperazine (**PZ**)[71]. In a study conducted in 2019, Kim *et al.*[65] investigated the rate of CO_2 absorption of a 3.5M solution of **PZ** at 40 °C, proving a fast rate of 9.12 (mol of $CO_2/m^2*s*kPa$)[65], while Freeman *et al.*[66] determined that the absorption rate of a 8M solution of Piperazine is two times faster than a 7M solution of **MEA** ($1.98*10^{-6}$ and $7.66*10^{-7}$ mole/s-Pa-m^2, respectively)[66]. The presence of two amine groups allows an intramolecular extraction of the hydrogen atom, giving rise to a zwitterionic monocarbamate **PZ-1** (eq.36), as well as dicarbamate **PZ-2** (eq.37), although the latter is usually followed by hydrolysis of the ammonium carbamate in carbonate (eq.35).

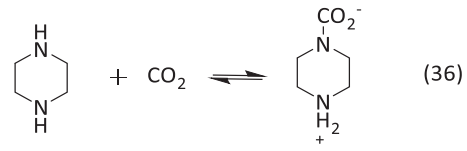

(36)

PZ **PZ-1**

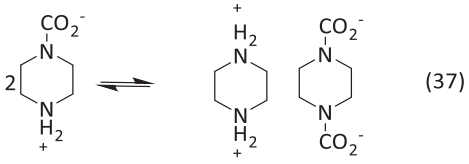

(37)

PZ-1 **PZ^{2+}** **PZ-2**

Studies have shown that 8M **PZ** is two orders of magnitude more resistant to oxidative and thermal degradation compared to 7M **MEA**[67]. Piperazine is also more resistant to temperature, since it can be used up to 150 °C without significant thermal degradation[62], while **MEA** presents thermal degradation from 110-125 °C[72]. Finally, the energy required for the regeneration of an 8M solution of Piperazine was estimated at 2.9 MJ/kgCO_2[73]. Despite several advantages, **PZ** is more expensive than **MEA** (83 €/kg compared to 42 €/kg) and may presents precipitation and solubility issues at high concentrations (8M)[73].

1.6.4 Second generation solvents

Second generation solvents consist in a mixture of two amines, each with one or more performant capture qualities (absorption rate, absorption capacity, low volatility). Second generation solvents were introduced trying to enhance the qualities of single-amine sorbents while reducing their drawbacks. Two examples can be given of such systems: blended solution of **MEA** with diethylethanolamine (**DEEA**), and Piperazine (**PZ**) with Amino methyl propanol (**AMP**) (Fig.9).

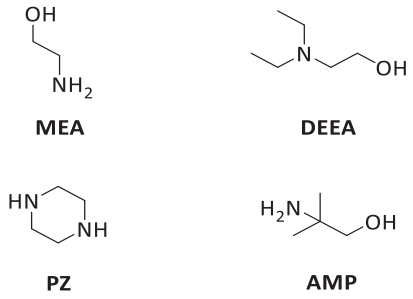

Fig. 9 Structures of amines combined in second generation solvents.

Tertiary amines and hindered amines such as **DEEA** and **AMP** capture CO_2 by forming ammonium-bicarbonate salts, thus presenting a slow initial absorption rate. On the other hand, this allows an overall high capture capacity for a total of one mole of CO_2 per mole of nitrogen. Furthermore, since the enthalpy of formation of ammonium carbonates is lower compared to that of ammonium carbamates, CO_2 desorption can attend higher extent using sterically hindered amines compared to primary and secondary amines[63, 74].

As previously mentioned, **MEA** presents a carbamation loading of 0.5 mole CO_2/mole of amine, while **DEEA** shows a loading of 1 mole CO_2/mole amine. A study performed by Luo *et al.* in 2016 [75] showed that a blended solution of **MEA**/**DEEA,** with molar ratio of 2.5:2.5 and a

total amine concentration of 5M, presented a 32% increase in absorption capacity compared to single-blended 5M **MEA**[75].

A study conducted in 2011 by Bruder *et al.*[76], stated that Piperazine enables faster mass transfer compared to other alkanolamines, and could be used as a promoter for CO_2 capture by **AMP**. In 2016, Rabesteiner *et al*.[77] led a pilot plant study on a mixed solution of 3M **AMP** and 2M **PZ**. Their results showed that the overall CO_2 loading of the second-generation solvent was higher compared to benchmark 5M **MEA** (3 mols of CO_2/kg of solvent compared to 2.7 mols of CO_2/kg of solvent) and that the system showed a regeneration energy of 3.15 MJ/kgCO_2, resulting in an energy saving of 17% compared to the standard solvent 5M **MEA**[77].

1.6.5 Polyamines and α-amino acids as substitutes for MEA

As shown for **PZ**, polyamines can form zwitterionic ammonium carbamates and polycarbamates[78]; in the case of a general α,ω-diamine the reaction can be described as eq.38:

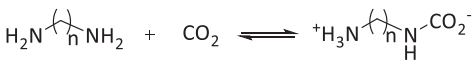

(38)

This indicates that, at same concentration, a solution of polyamine may theoretically capture more CO_2 through carbamation, compared to a solution of **MEA**. A key pending question is of course the energy cost of this capture. Primary and secondary polyamines can yield ammonium bicarbonates salts by hydrolysis of carbamates (eq.39), although the reaction is deterred by the high stability of the zwitterionic intramolecular ammonium carbamate.

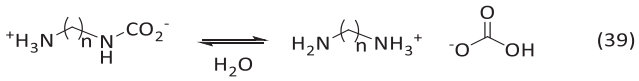

(39)

In 2017, Muchan *et al.*[79] studied the correlation between the absorption capacity of 2M Ethylenediamine (**EDA)**, Diethylenetriamine (**DETA)**, triethylenetetramine (**TETA)** and tetraethylenepentamine (**TEPA),** and the number of amines moieties on the absorbent backbone.

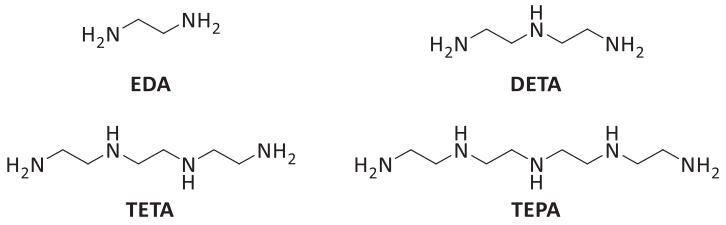

Fig. 10 Polyamines investigated by Muchan *et al.* [79].

In Table 2 are reported the results obtained by Muchan *et al.*, where it can be observed that the overall loading and the initial absorption rate increase with an increasing number of amine groups [79]. The increasing secondary amine groups present additional reaction sites for the formation of ammonium carbamates and polycarbamates, thus increasing the absorption rate of the amine[80-81].

Table 2 CO_2 loading at 25 °C, initial absorption/desorption rate, heat duty for solvent regeneration, and enthalpy of absorption for 2M **MEA**, **EDA**, **DETA**, **TETA**, and **TEPA**. Data reported by Muchan *et al.*[79]

R_2NH 2M	**α(CO_2) (mol CO_2/mol amine)**	**In. absorption rate (10^{-2} mol/min)**	**In. desorption rate (10^{-2} mol/min)**	**Q_{reg} (kJ/mol)**	**-ΔH (kJ/mol)**
MEA	0.55	0.67	1.23	175.72	55.94
EDA	0.95	0.57	1.42	127.55	48.58
DETA	1.33	0.59	2.35	67.01	56.49
TETA	1.66	0.67	2.63	63.14	56.64
TEPA	2.12	0.74	4.14	41.13	70.18

It can be observed that with an increasing number of amine sites the desorption rate increases and the heat of regeneration decreases. The authors suggest the hypothesis that the CO_2-loaded species yielded by **TEPA**, **TETA** and **DETA** are more labile than those yielded by **EDA** and **MEA**, thus require less energy for the desorption of CO_2. Their hypothesis is partially supported by a study conducted by Ermatchkov *et al.*[82] on a CO_2-loaded solution of **PZ** 1.5M. The investigation determined that the enthalpy of formation of **PZ**-monocarbamate (eq.36, page 36) and **PZ**-dicarbamate (eq.37, page 36) was -30.07 kJ/mol and -10.99kJ/mol respectively, therefore showing a lower stability of the dicarbamate. On the other hand, while the **PZ** yields dicationic-dianionic dicarbamate species, **TEPA** could yield more stable zwitterionic polycarbamates. It can be observed that the enthalpy of formation decreases with an increasing number of amine groups, which suggests that the ammonium-carbamates yielded by **TEPA** are more stable than the ammonium-carbamates yielded by **MEA**. The discrepancies in the data reported by Muchan *et al.* could be clarified with an NMR study of

the ammonium carbamate/carbonate species yielded by each amine in the operating conditions.

The repartition between ammonium carbamate and carbonate of a CO_2-loaded amine can also be influenced by the length of the chain between two primary amine groups. Zhang *et al.* [83] observed that, at same operational conditions, Propanediamine (**PDA**) formed 3.6 times more carbonate compared to Ethylenediamine (**EDA**), concluding that polyamines with longer carbon chains have a higher tendency to form ammonium carbonates, while polyamines with short carbon chains tend to form zwitterionic ammonium carbamates[83].

In the shortest polyamines the anion/cation couple of the intramolecular zwitterionic carbamate can fold into a seven membered ring (Fig.11). Although five and six membered rings are reported to be more stable for entropic and enthalpic reasons (tension with respect to the ideal tetrahedral configuration and number of frozen degrees of freedom respectively)[84] , this is the most stable and any further chain extensions would attenuate the extra stabilization observed with respect to the intermolecular pairing.

A study published in 2017 by Pike *et al.*[85] discussed the Gibb's free energy loss, principally of entropic origin, caused by the formation of an intermolecular hydrogen bond. Experimentally it was measured to be around 6 kJ/mol[85]. This is basically what is gained when comparing the stability of a zwitterionic intramolecular, versus intermolecular, ammonium carbamate salt bridge.

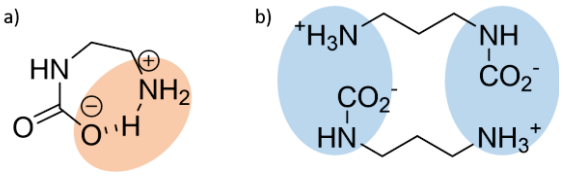

Fig. 11 a) Favored seven membered ring intramolecular salt bridge of an **EDA** monocarbamate zwitterion, b) disfavored intermolecular salt bridge of a **PDA** monocarbamate.

In longer polyamines, zwitterionic carbamates are not as stable as the ring size increases and its stability decreases. Carbamation becomes less favorable, and the proportion of carbonation increases.

Previously introduced ethylenediamine (**EDA**)[80] and diethylentriamine (**DETA**) are studied at laboratory scale as polyamines candidates for commercial CO_2 capture. These were considered as substitutes for **MEA** due to several advantages, such as higher CO_2 loading and

higher absorption rate. However, they also present some drawbacks, such as high energy for regeneration (-85 kJ/mol for **EDA** 12M, 40 °C)[86] and degradation through oxidation of the amine (to cyclic urea for instance[72,87]).

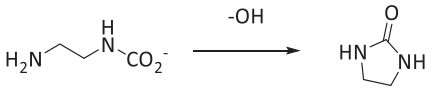

EDA-carbamate Cyclic urea (40)

It is also essential to consider the life cycle analysis, i.e. the footprint associated with the synthesis, use and final disposal of the absorber solvent.

For this reason, many studies have focused on amino acid salts (AAS) as alternative promising candidates for CO_2 absorption. The absorbent solutions have to be produced by deprotonation of neutral amino acids with either an organic or an inorganic base. Compared to industrial amine solvents they can be synthetized from biological sources[88] (i.e. extraction from protein hydrolysates, enzymatic processes, fermentation by microorganisms)[89].

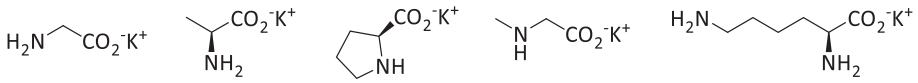

GlyK ***L*-AlaK** ***L*-ProK** **SarK** ***L*-LysK**

Fig. 12 Structures of amino acids investigated for CO_2 capture.

AAS such as proline, sarcosine and glycine (Fig.12) have only been studied at laboratory scale, but show high absorber efficiency. Glycine, for instance, showed a loading capacity similar to **MEA**[90], due to the presence of a single primary amine group on its bone structure.

In 1997, Hook[63] reported that amino acid potassium salt solutions such as **GlyK** and **AlaK** have lower volatility compared to alkanolamines, due to the ionic nature of the solutions[91,92]. Unfortunately, the comparison is difficult to make, since the literature presents incomplete and sometimes incoherent studies on volatility of αAA. In Table 3 are summarized the values reported by the literature for neutral (i.e. zwitterionic) amino acids, compared to **MEA**.

Table 3 Vapor pressure of **MEA**, *L*-lysine (***L*-Lys**), *L*-cysteine (***L*-Cys**) and *L*-aspartic acid (***L*-Asp**) at 25 °C. Values reported by the literature.

Amine	Vapor Pressure (mm Hg)
MEA	0.404
***L*-Lys**	$5.28*10^{-9}$ [93]
***L*-Cys**	$6.73*10^{-7}$ [94]
***L*-Asp**	$2.6*10^{-7}$ [94]

Hook also claims that AAs present fewer oxidative degradation issues[63, 95-96] during the removal of acid gases from oxygen-rich gas streams like flue gases in comparison to alkanolamines. On the other hand, thermal degradation of amino acids solution, such as sodium *L*-Sarcosinate, *L*-Alaninate and Glycinate, was proved to be more rapid than **MEA**[90]. In Table 4 are reported the results obtained by Huang *et al.*[90] which show a higher amine loss for amino acids compared to **MEA**.

Table 4 Thermal degradation of amino acid salts compared to **MEA**, at 2.5M and 135 °C[90].

Amine	C (M)	T °C	Amine loss after 50h
MEA	2.5	135	3%
Na-Sarcosinate	2.5	135	8%
Na-Alanine	2.5	135	38%
Na-Glycine	2.5	135	58%

An investigation conducted by Weiss *et al.*[97] in 2018, observed four possible degradation products of glycine between 185 °C and 280 °C, shown hereafter in Fig.13.

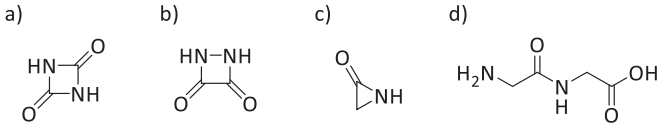

Fig. 13 Thermal degradation products of glycine for temperatures between 185 °C and 200 °C observed by Weiss *et al.*[97]. a) 1,3-Diazetine-2,4,dione; b) Isomer of Fig.12a, 1,2-Diazetine-3,4-dione; c) 2-Aziridinone; d) intermediate dimer, **Gly**-**Gly**.

In 2017, Zhao *et al.*[91] indicated that a solution of Potassium Lysinate presents higher loadings than **MEA** (1 mole of CO_2 per mole of lysine), explained by the presence of a second primary amine group on the amino acid[82]. In addition, the heat of absorption of a 3.3 M solution of ***L*-LysK** was estimated at -55/-70 kJ/mol of CO_2 which is lower than -80/-85 kJ/mol of CO_2 for conventional 5 M **MEA** at 0.1–0.5 loading range (mol CO_2/mol of amine)[91, 95].

The carbon capture chemistry of polyamines and amino acids such as **EDA**, **DETA**, *L*-lysine, glycine and *L*-cysteine will be furtherly discussed in Chapter 2. In Chapter 3 and 4 the CO_2

amine sorbents will be investigated as potential metal chelating and metal mineralization agents for an integrated CCUS process.

2 Mineral carbonation

As introduced in section 1.4, mineral carbonation can be listed as an example of CCUS, as it encompasses capture from flue gas and sequestration of CO_2 under the form of carbonates, which can be subsequently commercialized as filling material or cement component. In this perspective, the utilization provides an incentive for capture and sequestering. Mineral carbonation is defined as the reaction between minerals containing alkaline earth metals and carbon dioxide, to yield solid metal carbonates (eq.41, 42):

$$MO + CO_2 \longrightarrow MCO_3 + heat \quad (41)$$

$$MSiO_3 + CO_2 \longrightarrow MCO_3 + SiO_2 + heat \quad (42)$$

Formation of carbonates provides a solution of long-term stable storage[98], through a thermodynamically downhill pathway[99]. While the enthalpy of formation of ammonium carbamates and carbonates, yielded by CO_2 amine-capture, is around -80kJ/mol of CO_2 and -45kJ/mol of CO_2, respectively, it reaches -118kJ/mol for magnesium carbonate and -179 kJ/mol, for calcium carbonate. This underlines the stability of these CO_2 sequestering products (Fig.14).

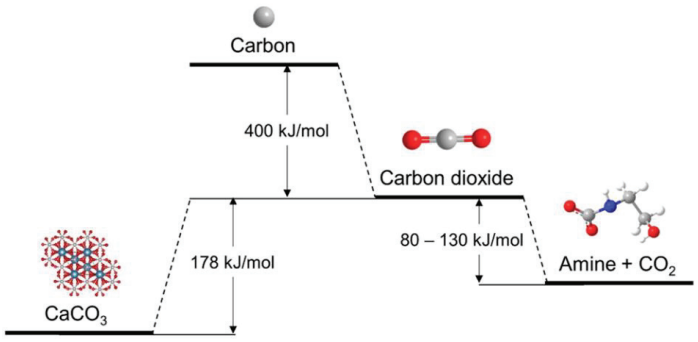

Fig. 14 Reaction enthalpies from carbon dioxide to the formation of CO_2-loaded amines and $CaCO_3$. Reproduced from Hong *et al.*, 2020[23].

The important availability of raw materials, such as magnesium and calcium bearing minerals, constitutes one of the great advantages of mineral carbonation. Natural silicates such as serpentine ($(Mg, Fe, Ni)_3Si_2O_5(OH)_4$) (100,000Gt) [100], olivine ($(Mg,Fe)_2[SiO_4]$) and wollastonite

($CaSiO_3$) (90 Mt)[101] (Fig.15) are used both for *in situ* and *ex situ* mineralization since they have low material costs, high reactivity, and can be readily available near CO_2 emission sources[102].

Fig. 15 a) Serpentine ($(Mg, Fe, Ni)_3Si_2O_5(OH)_4$), b) olivine ($(Mg,Fe)_2[SiO_4]$), c) wollastonite ($CaSiO_3$).

On the other hand, metal oxides (CaO and MgO) are available in alkaline industrial by-products such as fly ash and cement kiln dust (CDK), which production is around 750 million tons and 220 million tons per year, respectively[103]. Studies have reported that 200−300 Mt of CO_2 can be stored annually in alkaline industrial residues[99], while up to 10,000–1000,000Gt of carbon[42] could be stored by mineral carbonation (Table 5).

Table 5 Sequestration capacity by reservoir type[24].

Reservoir type	Range of storage capacity (Gt of CO_2)
Mineral carbonation[42]	10,000 – 1,000,000
Saline aquifers	1000 – 10,000
Oil and gas fields	675 - 900

Mineral carbonation can be conducted *in situ*, *ex situ* or integrated to carbon capture. These different strategies and pathways will be detailed and discussed hereafter.

2.1 *In situ* mineral carbonation

After capture and compression, CO_2 is stored in its supercritical or fluid state in reactive geologic formations at > 800 m depth. In the presence of CO_2, the starting mineral substrate slowly dissolves (mineralysis) into soluble metal ions, which are then carbonated. This mineralization step is generally the rate determining step, since the solubilization of metal cations can be impeded by the formation of passivating silica layers (eq.9-10, 43-44). The reactions occurring during the global carbonation process from Mg, Ca, Fe-rich silicate are listed below.

$$Mg_2SiO_4 + 2CO_2 \longrightarrow 2MgCO_3 + SiO_2 \quad (43)$$

$$Mg_3Si_2O_5(OH)_4 + 3CO_2 \longrightarrow 3MgCO_3 + 2SiO_2 + 2H_2O \quad (10)$$

$$Fe_2SiO_4 + 2CO_2 \longrightarrow 2FeCO_3 + SiO_2 \quad (44)$$

$$CaSiO_3 + CO_2 \longrightarrow CaCO_3 + SiO_2 \quad (9)$$

At a depth > 800 m the *in situ* carbonation reaction occurs at around 40 °C - 80 °C and from 74 to 200 bars of CO_2[104].

Two examples of in situ operating sites are the Columbia River flood basalts in Washington State and the Hellisheiði geothermal power plant in southwest Iceland. The former is a pilot demonstration project which stored 1,000 t of pure liquid CO_2 in 2013. The latter currently captures and stores 33% of CO_2 emitted by the Hellisheiði power plant, corresponding to ~12,000 t annually[105].

2.2 Conventional *ex situ* mineral carbonation

Ex situ pathways designate a reaction between either pre-extracted minerals or leached solution of oxides and silicates with carbon dioxide above-ground. Both necessitate rock mining and ore grinding as pre-requisites[24].

Mineral carbonation can also be divided in direct and indirect carbonation. The former implies a direct reaction between minerals and CO_2 (can be performed *in situ*/*ex situ*), while the latter requires the upstream extraction of Ca and Mg from raw material followed by the reaction of the leached metals with CO_2 (*ex situ*).[106]

Leaching of the minerals can be performed by chemical means with acids and/or organic ligands, which are reported to improve the mineralysis rate[107]. After dissolution of calcium and magnesium cations, the acidic aqueous solutions are treated with a base, triggering an important pH swing, then with CO_2 to form mineral carbonated salts. The pH swing is necessary to prevent the dissolution of carbonates[98]. A study conducted by Kim *et al.*[106] showed that 10.5 was the optimal end-of carbonation pH to obtain high CO_2 storage via $CaCO_3$ coherently with the pKa of CO_3^{2-}/HCO_3^- of 10.32.

The choice of the acid is important, not only regarding its environmental impact, but also for the mineral dissolution efficiency and the overall metal carbonation. The use of strong concentrated acids, such as hydrochloric or nitric, can be problematic since their recovery can

make the overall process energy-intensive[42]. It is also necessary to consider that the use of strong acid dramatically lowers the pH of the resulting solution, thus a fraction of the base needed in the process will be sacrificed to swing back the overall pH of the solution and will not serve as carbon capture agent, while substantial amount of salt will be co-produced by the neutralization.

The use of acetic or citric acid, on the other hand, would provide conjugated bases which will act as chelating agents toward Mg^{2+} and Ca^{2+}, increasing the availability of these cations in solution for further carbonate formation[108]. Several organic chelating agents, such as gluconic acid, **EDTA** (Ethylenediaminetetraacetic acid), oxalic acid, and glutamic acid[109], were studied for their ability to enhance the dissolution rates and yields of Ca- and Mg-bearing minerals. The conjugated base, i.e. the active form of these ligands is presented in Fig.16.

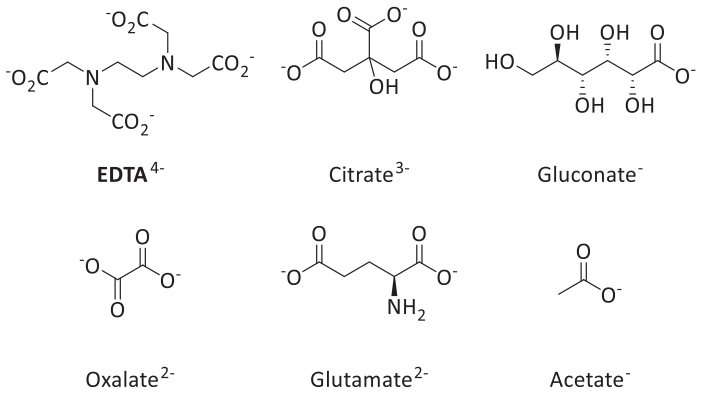

Fig. 16 Ligands deriving from organic carboxylic acids used for metal dissolution.

It must be mentioned that the choice of the organic chelating agents has to be tailor-made with respect to the mineral composition, in order to avoid the formation of insoluble or highly stable metal-chelant complexes which would overall hinder the carbonation reaction. An example can be given by the oxalate-Magnesium couple for the mineral carbonation of olivine (Mg_2SiO_4) discussed by Bonfils *et al.*[110]. The study showed that a solution of olivine and 0.1M disodium oxalate, at 120 °C and 20 bars of CO_2 did not yield $MgCO_3$, but rather a Mg-oxalate complex[110].

Other strategies have been reported where the dissolution and carbonation of minerals was performed in absence of acid and chelating agents, but in presence of $NaHCO_3$ and NH_3.

Studies have reported the 85% conversion of Mg_2SiO_4 (olivine) to $MgCO_3$ (magnesite) at 185 °C, with a CO_2 pressure of 139 atm, for 3h with $NaHCO_3$, while $CaSiO_3$ (wollastonite) was converted completely to calcium carbonate at 100 °C, pressure of CO_2 (pCO_2) of 40 atm in distilled water for one hour[99, 109, 111].

$$Mg_2SiO_4 \xrightarrow[NaHCO_3,\ 185°C,\ 3h,\ P(CO_2)=139\ atm]{CO_2} 2MgCO_3 + SiO_2 \qquad (45)$$

For the carbonation reaction reported in eq.45 it was observed that increasing concentrations of $NaHCO_3$ promoted higher carbonation rates of olivine (9.5% carbonation for 0.32M $NaHCO_3$, 70% carbonation for 0.64M HCO_3). Although the precise role of $NaHCO_3$ was not defined by the authors[111], it is hypothesized that $NaHCO_3$ plays the role of pH buffer, releasing readily-accessible carbonate ions and promoting further carbonation of olive by carbon dioxide.

A strategy designed by a Finnish group, known as "the ÅA (Åbo Akademi) route" consists in the treatment of serpentine with ammonium salts and CO_2[112].

$$Mg_3Si_2O_5(OH)_4(s) + 3(NH_4)_2SO_4(s) \xrightarrow[400°C]{} 3MgSO_4(s) + 2SiO_2(s) + 2H_2O(g) + 2NH_3(g) \qquad (46)$$

$$MgSO_4(s) + 2H_2O(l) + 2NH_3(g) \xrightarrow[T_{amb},\ P_{amb}]{} Mg(OH)_2(s) + (NH_4)_2SO_4(aq) \qquad (47)$$

$$Mg(OH)_2(s) + CO_2(g) \xrightarrow[500°C,\ 20\ bar]{} MgCO_3(s) + H_2O(g) \qquad (48)$$

First, a water-soluble Mg sulphate is produced (eq.46), then converted into Mg hydroxide and ammonium chloride by ammonia solution (eq.47). $Mg(OH)_2$ is finally carbonated in a pressurized reactor (eq.48) achieving > 50% of conversion. In this specific example it was observed than for a same CO_2 partial pressure, carbon dioxide could be used either as a pure gas or as a simulated flue gas with no effect on the carbonation rate[112-113].

This last example shows the possibility to directly use flue gases, rather than purified and compressed CO_2, for mineral carbonation. This integrated approach would imply that CO_2-rich solutions could be directly used as CO_2 feedstock without the need of separating, stripping and compressing CO_2. In the specific case of CO_2 separation by amine scrubbing technology,

the CO_2 rich solution formed in the absorber tank could be used for mineral carbonation via an Integrated Absorption Mineralization (IAM) approach.

2.3 Integrated Absorption Mineralization (IAM)

The integrated absorption mineralization pathway focuses on the optimization of both the rate-determining mineralization step and the Carbon Capture Utilization and Storage chain. In the IAM process the use of CO_2-rich solutions as CO_2 feedstock would allow to skip the energy-costly stripping and compressing steps. At the same time, the CO_2-loaded absorbents could act as chelating agents for Calcium and Magnesium, thereby accelerating mineralysis.

In section 1.6.4 of this chapter (page 37) was mentioned that, tertiary or sterically hindered amines produce mostly ammonium carbonates upon CO_2 capture (eq.48). Therefore, when tertiary or sterically hindered amines are led to react with CO_2 and metal oxides (MgO, CaO), the following reaction may proceed:

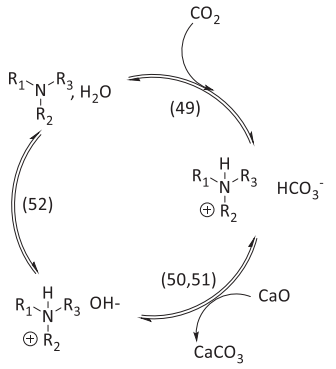

$$R_3N + H_2O + CO_2 \longrightarrow R_3NH^+ + HCO_3^- \quad (49)$$

$$CaO + H_2O \longrightarrow Ca(OH)_2 \quad (50)$$

$$HCO_3^- + Ca(OH)_2 \longrightarrow CaCO_3 + H_2O + OH^- \quad (51)$$

$$R_3NH^+ + OH^- \longrightarrow R_3N + H_2O \quad (52)$$

Fig. 17 Pathway of carbon capture by an aqueous amine solution with formation of ammonium carbonates (eq.49), and transcarbonation of metal oxide CaO into $CaCO_3$ (eq.50,51), with concomitant regeneration of the amine (eq.52).

First the amine captures CO_2 by forming ammonium-bicarbonate salts (eq.49), then CaO is introduced in the reaction and hydrolyzed into $Ca(OH)_2$ (eq.50). The bicarbonates are transferred from the ammonium salt to $Ca(OH)_2$, yielding $CaCO_3$ (eq.51). In this step HCO_3^- are consumed, releasing OH^- in solution which can regenerate the amine sorbent (eq.52).

In the case of a primary or secondary amine solvent (i.e. **MEA**, **GlyK**) which preferably capture CO_2 as ammonium carbamates, the mechanism is similar:

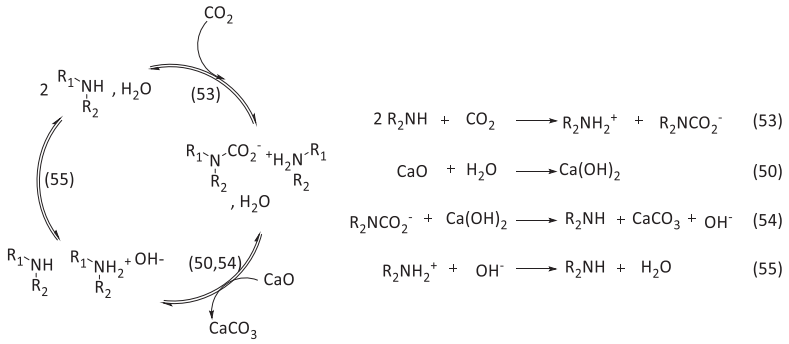

Fig. 18 Mechanism of carbon capture by an aqueous amine solution with formation of ammonium carbamates (eq.53), hydrolysis of CaO into and its carbonation to $CaCO_3$ (eq.50,54), accompanied by regeneration of the amine (eq.55).

First CO_2 is captured as an ammonium carbamate by two equivalents of amine (eq.53), then the solution is mixed with CaO which is hydrolyzed into $Ca(OH)_2$ (eq.50). The carbamate is then hydrolyzed into bicarbonate and transferred to the alkaline earth hydroxide, yielding $CaCO_3$. This reaction simultaneously regenerates one amine equivalent and releases OH^- in solution (eq.54). Finally, the second amine equivalent is regenerated (eq.55), thus completing the IAM cycle. In case of polyamines such as **EDA** and **DETA** the mechanism is the same, except that only one equivalent of amine would be required to yield the ammonium-carbamate (section 1.6.5, page 38).

For both Fig.18 and Fig.19, the first step is the formation of ammonium carbamates and carbonates in solution, whose chemistry mostly depends on the nature of the amine sorbent. Since CO_2 is an acid gas, the overall pH of the solution decreases by several units in this step (49, 55), potentially going below the pKa of CO_3^{2-}/HCO_3^- (10.32 at 25 °C).

The increase in pH which accompanies the mineral carbonation step entails the precipitation of metal carbonates without the need of an additional base treatment[108] (section 2.2, page 45). Furthermore, the regeneration of the capture solvents occurs through an internal pH swing, at 50–75 °C, which is significantly below the thermal regeneration of solvents at 100–120 °C[108]. This enables a 38% reduction of the energy duty, compared with the traditional steam-based regeneration process[102]. Finally, compared to the operating conditions observed for conventional *ex situ* mineral carbonation (400 °C, 139 atm of CO_2), the IAM pathway allows us to work in mild conditions.

Another advantage of the one-step pathway is that mineral-bearing solvents undergo continuous looping between the CO_2-rich and lean states, which are respectively neutral and basic from a pH perspective thereby facilitating the accelerated conversion of calcium and magnesium oxides to carbonate.[99]

In the literature, several examples of IAM operate on **MEA**-containing slurries of calcium or magnesium oxides[102, 109, 114-116]. Park's group in Korea obtained a conversion of calcium oxide of 67% using 5M **MEA**, 20wt% of CaO (aq) at 30 °C, stirring for 24h at 220 rpm [116]. Other studies showed complete conversion of CaO into calcium carbonate and 70% conversion of MgO to hydrated magnesium carbonate at 50 °C with 5M **MEA** and 15 wt% solid for a reaction time of 3h[109].

Table 6 IAM reactions with **MEA** 5M, with CaO and MgO obtained by Kang *et al.*[116] and Liu *et al.*[109].

R_2NH	C (M)	MOx	C (wt%)	T (°C)	rpm	t (h)	MCO_3
MEA	5	CaO	20	30	220	24	67%
		CaO	15	50	/	3	100%
		MgO	15	50	/	3	70%

As previously mentioned in section 1.6, **MEA** is a vastly used, yet not optimal, carbon sorbent. An environmentally benign alternative to its use in the IAM processes can be provided by amino acids.

Sodium Glycinate (**GlyNa**) is currently being investigated as a solvent for IAM processes. Experiments ran by Gadikota's group in 2021 showed about 94% conversion of calcium oxide to calcium carbonate at 75 °C in 1.0 M **GlyNa** and a reaction time of 3h, while works with $CaSiO_3$ and MgO showed a conversion of 31% and 87% in the same reaction conditions[115].

Table 7 Results reported by Liu *et al.*[115] on the conversion of metal oxides to metal carbonate via IAM reaction with 1M **GlyNa** at 75 °C, 300 rpm for a reaction time of 3h.

R_2NH	C (M)	MOx	C (wt%)	T (°C)	rpm	t (h)	MCO_3
GlyNa	1	CaO	15	75	300	3	94%
		$CaSiO_3$					31%
		MgO					87%

Liu and Gadikota state that **GlyNa** undergoes multiple CO_2 capture/regeneration cycles in the aqueous phase, increasing availability of aqueous carbon species for carbonate precipitation, thus achieving high mineral carbonation rates[115]. This shows that Na-glycinate is an alternative to aqueous industrial amines for simultaneous CO_2 capture/ mineral carbonation coupled to chemical regeneration of the solvent.

In Fig. 19 are reported the thermodynamic features of the IAM process. The first circle (red) presents the CO_2 capture loop starting from flue gases, while the second circle (blue) shows the metal dissolution loop starting from metal oxides and silicates.

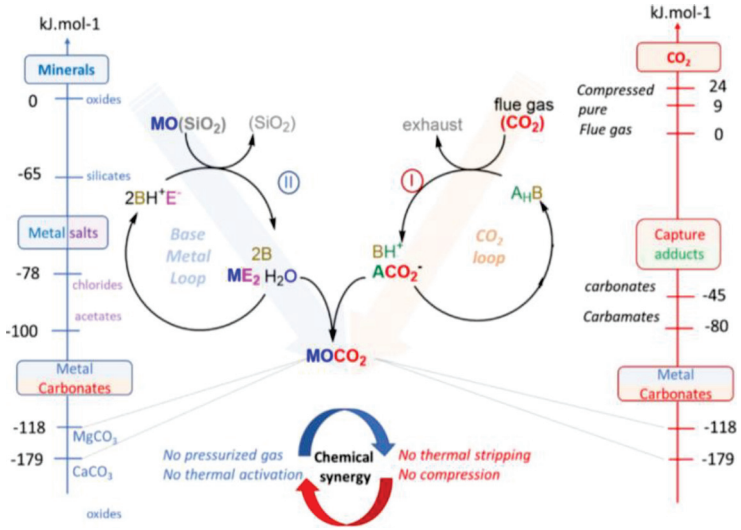

Fig. 19 Thermodynamic features and simplified view of integrated CO_2 absorption and mineralization. Dark blue M: major metals (Mg, Ca); E- = metal extractant; AH B = CO_2 absorbent (incl. base); $MOCO_2$: metal carbonate; $MO(SiO_2)$: base metal oxide or silicate. On the left: base-metal loop, dissolution of major metals from minerals by extractants E and their regeneration upon carbonation. On the right: CO_2 capture loop and absorbent regeneration upon carbonation. Left and right Gibb's enthalpy of formation of CO_2-loaded products expressed in kJ/mol. Courtesy of Prof. J. Leclaire.

Taking a step back, it can be claimed that the IAM process has significant advantages both compared to classical amine scrubbing and classical mineral carbonation. As per the latter, it reduces the reaction time from days to hours, operating conditions from 500 °C, 139 atm to 40 °C, 1 atm. For the former, it reduces energy duty associated to absorbent regeneration and CO_2 compression. The IAM involves a reduced energy cost, since CO_2 carbonation reaction takes place at a mild temperature of 40 °C, and the heat released from the exothermicity of the mineral carbonation reaction could be reused.[102]

This approach of simultaneous capture, conversion, and storage of CO_2 to carbonates exemplifies the importance and potential impact of integrated pathways.

Mineral carbonation also brings benefits from a circular economy perspective, since it can be applied to both natural resources and industrial waste (fly ash, CDK), valorizing the latter[102, 106].

A study ran by Zhao's group in Beijing in 2018 confirmed the technical feasibility of an IAM process operating from fly ash, reporting a calcium carbonation extent of 53% using a 2M solution of Piperazine at 40 °C[102].

In terms of market perspectives, a process converting two wastes stream into a valued product may be implemented in the cement and concrete production chains. In the same paper, Ji states that carbonation of fly ash improves the properties that are requested for a use as an ingredient in cement and concrete[102]. There are indeed several markets for carbonate-based products, such as cement voids filler, cement additive, $MgCO_3$ boards for construction and stabilizers.[42] This underlines the potential important economic incentive to develop efficient, environmentally sensible IAM processes.

3 Depollution of soils

As mentioned in the previous paragraph, cement and concrete industries represent an interesting target for the use of recycled waste materials. Carbonates and siliceous phases, for instance, can be used to produce binding agents, mineral aggregates, and concrete, necessary for commercial construction products (i.e. bricks, pavers, etc).

Within the class of industrial wastes, one can find polluted soils, which can, similarly to fly ash, be turned into valuable and environmentally friendly products. The interest in the use of polluted soils as renewable sources resides in their components, which are silicates, oxides, clays and various metal salts. These are potential substrates for mineral carbonation.

Soils are usually composed of three phases: solid, liquid and gas. The solid material usually presents a width < 2mm and can be constituted of organic or inorganic components. The organic components mainly derive from dead vegetation, and they are usually found in the humus fraction of the soil (organic and topsoil layer, Fig.20). The topsoil also contains clay and iron oxides which can be leached by natural weathering, descending in the subsoil. The latter contains other inorganic constituents such as silicates, carbonates, iron oxides and alkaline earth soluble salts. Finally, the parent material and bedrock are constituted by limestone, sandstone, granite and unweathered rocks. The repartition between those components varies from soil to soil and it is usually determined by XRD analysis.

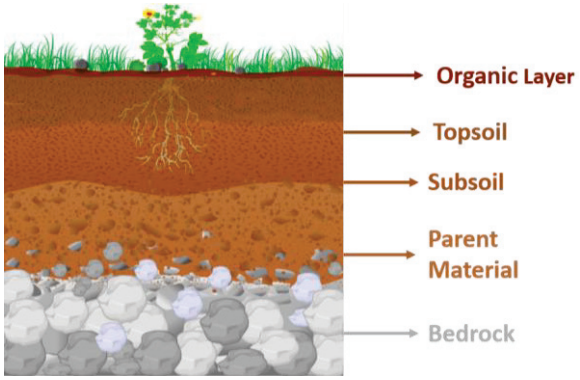

Fig. 20 Example of the different phases of a soil. Organic layer and topsoil are constituted of organic components, clay and iron oxides, the subsoil contains inorganic matter such as silicates, carbonates and soluble salts while the parent material and the bed rock are mostly constituted of limestone, granite and unweathered rocks.

It is important to define the term "polluted", which covers soils containing organic pollutants or heavy metals. The latter usually includes Hg, Cd, Cu, Ti, Pb, Ni, Mn, Mo and Zn[117-118].

Polluted sites can also be subdivided into seriously polluted sites, i.e. where the pollutants have penetrated rather far into the soil (30 cm depth from the top soil), and sites where the pollution is mainly present at the surface[119] (within 10 cm from the top soil)[117].

Pollutants themselves can be subdivided according to their physical state, as they can be found absorbed within the soil, in the liquid or solid state, around or inside soil particles. Knowing the state and distribution of the pollutant facilitates the depollution task, which can be based on biological or chemical methods[118-119].

3.1 Biological depollution techniques

Several strategies of soil depollution can be executed through *in situ* biological techniques, aiming to depollute the soil without removing it from its site. A few of those strategies are listed hereafter:

- Bio-restoration or bio-extraction, wherein organic compounds are decomposed using microbial degradation (fungi, bacteria) and the products pumped up via special wells.
- *In situ* extraction, in which an aqueous extractant is introduced in the contaminated site. The soluble pollutants are then dissolved and pumped up from the site.

- Phytoremediation, wherein the inherent abilities of living plants to remove pollutants from the environment is used to reduce the volume, mobility, or toxicity of contaminants within soil, groundwater, or other contaminated media[120].

Phytoremediation, gathers different pathways such as phytoextraction, or phytoaccumulation. Through this strategy, the metal contaminants initially present in the soil are transferred from the roots to the upper compartments of the plants. It is primarily used for the removal of Ni, Co and Zn from contaminated soils[104].

3.2 Chemical depollution techniques

There are different chemical depollution techniques developed for industrial use. It is possible to divide them in two subcategories: *in situ* and *ex situ*. The former includes:

- Solidification/stabilization. Building agents or chemical reactants are used to immobilize the pollutant in static mass or in a stabilized chemical form to inhibit the leaching process[121].
- Extraction using supercritical CO_2 ($SCCO_2$). Charged metal species are converted into neutral metal complexes by organic ligands, which are soluble in $SCCO_2$[122].

Supercritical carbon dioxide ($SCCO_2$) is a good solvent for soil cleaning, since it is safe and has a good penetration into pores. Unfortunately, further specifications about pore sizes is not easily accessible in the literature.

In situ operations have lower implementation costs[121] but are not always applicable, especially if the contamination is deep (30 cm under the surface) or the surface too extended[119]. *Ex situ* operations on the other hand are expensive, due to the step of polluted soil excavation, but is compatible with broader range of treatments.

Within those can be found[119, 123]:

- Thermal decontamination, where pollutants are evaporated to a gas phase at temperatures between 150 and 700 °C and then destructed and completely removed.
- Extraction/wet classification, where the soil is washed with water/acid treatments, followed by separation of clean soil particles and treatment of the extractant.

- Soil washing with chelating agents, same principle as extraction but with the use of organic chelating agent with high potential extraction efficiency and a specificity for heavy metals.

There are several studies involving this last technique, which benchmark the variety of organic chelating agent eligible for soil decontamination.

For metals such as lead, zinc and copper, studies showed high extraction performance by **EDTA**, citric acid (Fig.15), **DPTA** (diethylenetriamine pentaacetic acid) and **ADA** (N-2-(acetamido)iminodiacetic acid) (Fig.21)[123].

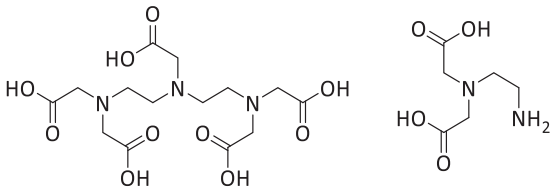

DPTA **ADA**

Fig. 21 Chemical structure of **DPTA** (diethylenetriamine pentaacetic acid) and **ADA** (N-2-(acetamido)iminodiacetic acid).

It must be noted that all the conventional soil washing mentioned above produce large amounts of secondary wastes. The use of acidic solutions, or organic synthetic chelatant results in an extraction of polluting metals, while simultaneously polluting the environment. The addition of extracting solution *ex situ* demand further treatments of separation and purification, resulting in expensive and usually tainting steps.

Since soil plays a crucial and strategic life-supporting role, there is a need for an environmentally friendly technology for soil decontamination, while preferably creating resources rather than wastes and by-products.

4 Objective of this thesis

The objective of this thesis is to design and optimize a sustainable technology which simultaneously captures CO_2, stores it into a soil and extracts its metal contaminants. To tackle this challenge, the work was divided into two main tasks:

1. The study of carbon capture and mineralization by amino acid-based solvents in aqueous media
2. The use of such sorbents on soil samples, to investigate their extraction efficiency as well as their capacity to carbonate its alkaline metal matrix

This work is the first brick of a wider project developed in collaboration with ADEME and the Vicat cement industry (France). The prospect is to use carbon emissions from cement industries to depollute, and concomitantly carbonate soils of industrial sites, which may be subsequently reintegrated in the cement production chain.

The outline of the manuscript will follow the order proposed in the introduction: first, we will summarize the state of the art and detail the results gathered for amine-based sorbents; then we will investigate the efficiency of CO_2-loaded amine sorbents for mineral carbonation on monometallic substrates. Finally, we will analyze the extraction/carbonation efficiency of loaded and unloaded sorbents on a real system, such as a sample of polluted soil.

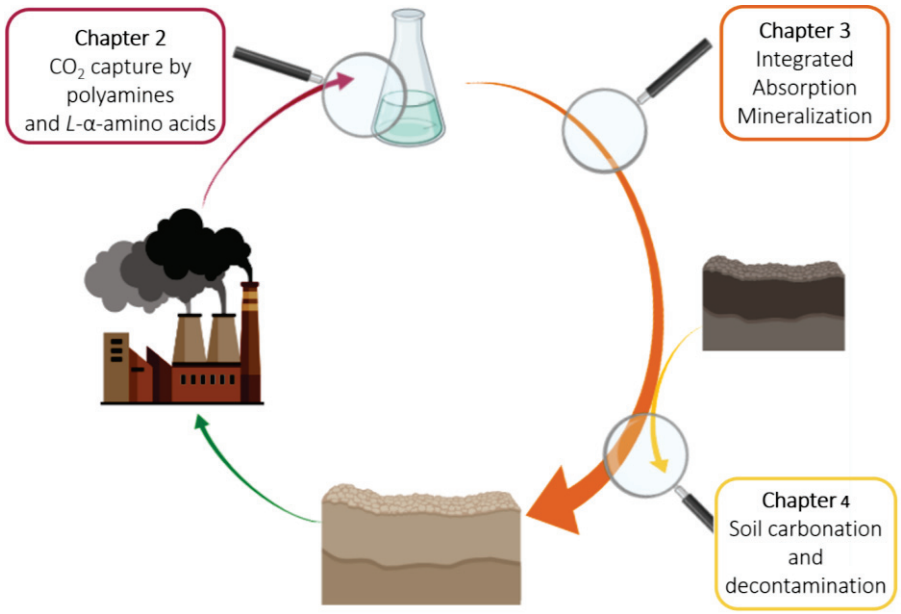

Chapter II
CO_2 capture by polyamines and *L*-α-amino acids

Chapter 2

Objective

The second chapter of this thesis will focus on polyamines and AAs as CO_2 capture agents. A thorough investigation of the literature will be depicted, focusing on the characteristics of the chosen amines, as well as their CO_2 capture properties in water. At current times, the discussion present in the literature on new possible carbon capture absorber revolves on the regeneration energy, loading capacity and cyclic capacity of an amine. The studies present discordant calculations and methods as well as incomplete investigations, especially for amino acids. The nature of the CO_2 adducts formed by a capture solvent (carbamate/carbonate) is rarely discussed in the literature, although the type of the CO_2 loaded products plays a crucial role in carbon capture strategies.

The investigation performed and reported in this chapter analyzes the capture process on a deeper molecular level, qualifying and quantifying the amine-CO_2 adducts formed in aqueous meanings by industrial polyamines and amino acids (monocarbamates, polycarbamates, carbonates). Those data will furtherly allow a general comprehension of the efficiency and suitability of each amine in the field of carbon capture.

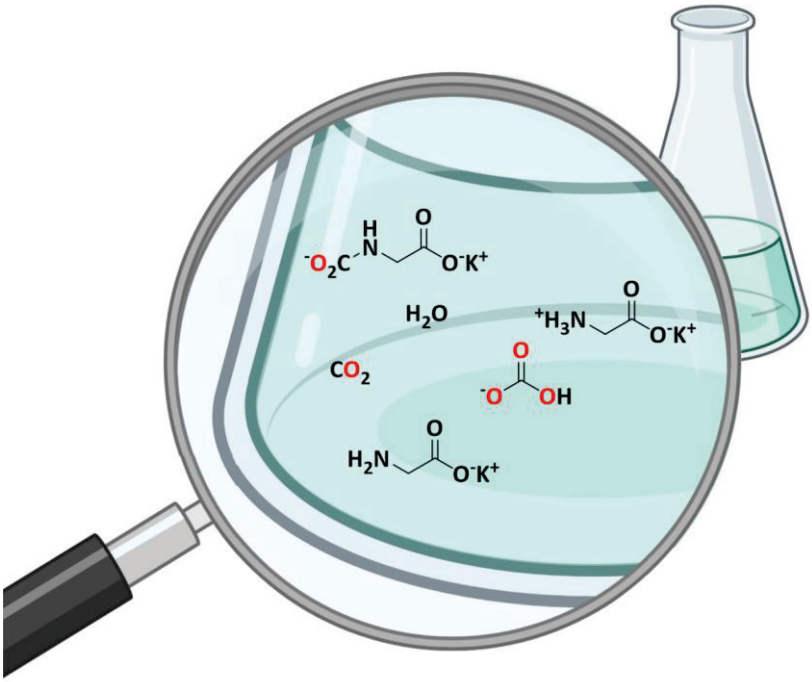

Chapter 2

1 State of the art

1.1 General properties of polyamines and α-amino acids

In this section will be presented the general properties of various amines: five industrial polyamines, monoethanolamine (**MEA**), piperazine (**PZ**), triethylenetetramine (**TETA**), diethylenetriamine (**DETA**) and ethylendiamine (**EDA**), and six natural alpha amino acids potassium salts, *L*-lysine (***L*-Lys**), *L*-cysteine (***L*-Cys**), glycine (**Gly**), sarcosine (**Sar**), *L*-arginine (***L*-Arg**) and *L*-aspartic acid (***L*-Asp**), as presented in Fig.22.

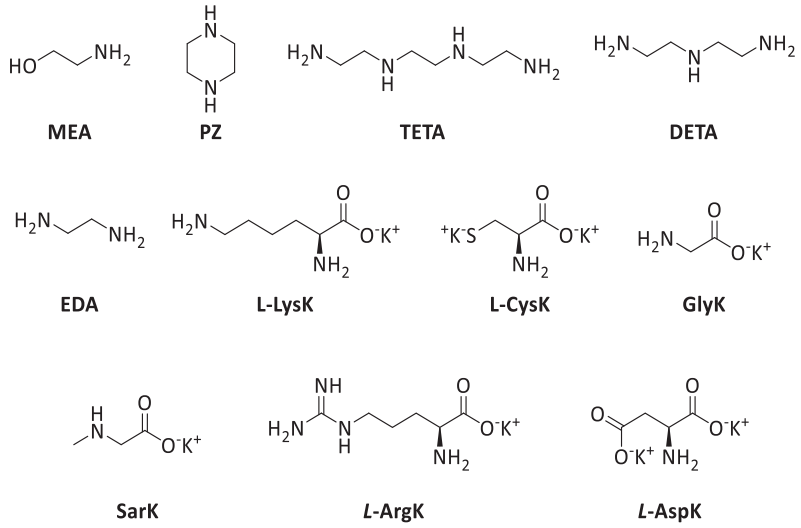

Fig. 22 Industrial polyamines and alpha amino acids investigated in this chapter.

Physical and chemical properties of polyamines such as viscosity, degradation, cost and volatility are listed in Table 8. These factors have to be considered when evaluating solvents for carbon capture, since they play a crucial role in the overall functioning of capture plants.

For instance, as discussed in Chapter 1 page 30, the absorption step in Post Combustion Amine Scrubbing Capture Plants is performed at 40 °C, while desorption is achieved at 120 °C. For this reason, amines with high boiling point (**DETA** > **MEA** > **PZ** > **EDA**) are investigated for their resistance to thermal degradation. A study published in 2012 by Rochelle[72] listed the temperatures at which thermal degradation was first observable for different amines. A sorbent with higher degradation temperature is preferred, because it accounts for better energy performance throughout the thermal swing cycle. In Table 8 is possible to notice that

PZ is more thermally stable compared to the other polyamines, while **DETA** presents the lowest degradation temperature; the degradation order can then be defined as **DETA** > **EDA** > **MEA** > **PZ.** The different tendency between boiling point and temperature of degradation indicate that other factors, such as oxidation, can play an important role on the degradation of an amine. Experiments of oxidative degradation proved that at stripper conditions (120/125 °C) a solution of 7 M **MEA** oxidates almost 7 times faster compared to an 8M solution of **PZ**[124].

Table 8 General information on **MEA, PZ, TETA**, **DETA** and **EDA**, provided by the literature. *Value at 60 °C. **Value for reagent at technical grade, 60% purity.

Amine	€/kg	Viscosity(cP)		Density (mg/mL)	Vapor Pressure (mm Hg) at 25 °C	Boiling Point (°C)	Degradation T (°C)[72]
MEA	42	18.95[125]	5.06 *	1.02	0.404	170[126]	111-125
PZ	83	/		1.1	0.16[127]	146[125]	162
TETA	74**	8.59[128]		0.98	$4.12\ 10^{-4}$[128]	266[126]	/
DETA	60	7.14[129]		0.96	0.23[93]	207[126]	108-118
EDA	39	1.5[129]		0.9	12.1[130-131]	116[125]	117

In CO_2 capture, the environmental impact generated during the production and use of the solvent have to be considered; thus using bio sourced[132] solvents, such as amino acid, is essential. In 2003 more than 2 million tons of amino acids were produced per year, with a market growth of 10% and higher each year[133]. The most common production is the application of coryneform bacteria in bioprocesses[133], while other techniques are extraction from protein hydrolysates[89], enzymatic processes and chemical synthesis[134]. While evaluating amino acids as carbon capture agents it must be considered that a large-scale production, like the one needed for CO_2 capture, could constitute a competition for the food industry, which consumes the largest part of the amino acid productions to this day[135].

General properties of the amino acids in their free form can be found in Table 9. An aspect to consider in the evaluation of an amine for carbon capture is its vapor pressure, or volatility (Table 8 and 9). An amine with low volatility will present fewer losses throughout the process and will be more profitable; unfortunately, the literature is not complete for the volatility of amino acids.

Other properties, such as viscosity, play an important role when working at high concentration (30wt%, 5M for **MEA**) like in PCC units. A chemical absorbent with low viscosity can result in less mass-transfer resistance between gas and liquid phases, thereby increasing the CO_2 absorption rate[136], while higher viscosity lowers carbon dioxide solubilization[137], therefore

inhibiting its capture. Another effect of higher viscosity is consequent increased corrosion of the absorption tank, which weighs on the maintenance costs of the capture units. A study performed with ***L*-LysK** on carbon steel confirmed this tendency. At 33 °C, it was observed that a 2.5M solution of ***L*-LysK** presented a viscosity 2.7 times higher than a 0.5M solution, and the corrosion rate resulted to be 12 times higher than the corrosion provoked by a 0.5M ***L*-LysK** solution[136].

Table 9 General information on amino acids. Values of pKa_1, pKa_2, pKa_3 correspond respectively to the carboxyl group, the alpha amine group and the side chain of the amino acid. * Value for *L*-Lys*HCl. **Value at 20 °C.

Amine	*L*-Lysine	*L*-Cysteine	Glycine	*L*-Arginine	*L*-Aspartic Acid
€/kg	119*	470	80	281	107
R-chain	basic	neutral	non-polar	basic	acidic
pKa_1	2.18	1.71	2.34	2.17	2.09
pKa_2	8.95	8.33	9.60	9.04	9.82
pKa_3	10.79	10.78	/	12.48	3.86
PI	9.87	5.02	5.97	10.76	2.98
Solubility in water (g/L) at 25 °C	1000*	25	253.1	87.1	5.3
Melting Point (°C)	224[126]	260[126]	290[125-126]	244[126]	270[125]
Vapor Pressure (mm Hg) at 25 °C	5.28**10^{-9} [94]	6.73 * 10^{-7} [94]	/	/	2.6 *10^{-7} [94]
Market size (ton/year)	600,000*[135]	1,500[132]	22,000[132]	1,200[132]	/
Production process	Fermentation	Extraction/ Enzymatic method	Chemical Synthesis	Fermentation	/

A study performed by Veawab[138] observed the corrosion effect of concentrated solution of **MEA** and 2-amino-2methyl-1-propanol (**AMP**). Experiments were performed with **MEA** and **AMP** at 3M, 80 °C and 0.2 moles of CO_2 per mole of amine; it was noticed that the corrosion rate of **AMP** was 1.5 times faster than **MEA**[138]. This phenomenon was attributed to a higher presence of bicarbonates in an **AMP** solution, considered an iron corroding agent[138-139].

1.2 Properties of polyamines and α-amino acids as CO_2 capture agents

The amines presented above will be investigated in this section for their carbon capture properties. As mentioned in the general introduction, several factors determine an amine potential for CO_2 absorption; within those can be listed capture efficiency (maximum

experimental loading, eq. 31, page 35), cyclic capacity (eq. 32 page 35), and regeneration energy (reaction enthalpy).

DETA has been investigated in the literature[58, 71, 140-142] and is presented as a potential absorber for CO_2[79] for its high absorption rate[65], higher boiling point and lower vapor pressure compared to **MEA**[140]. The presence of three amine groups, two primary and one secondary, enable a higher carbamation loading of CO_2 up to 1.5 moles of carbon dioxide per moles of amine, compared to 0.5 for carbamated **MEA**. This means that a 1M solution of **DETA** is as efficient as a 3M solution of **MEA**, from a carbamation point of view. Experiments determining the heat of absorption of **DETA** in industrial conditions (3M, 40 °C) gave a value of enthalpy of around -80kJ/mol of CO_2[143]. The value, even if lower than **MEA**, is higher than the ideal binding enthalpy (between -70 and -60)[144] for industrial costs. Considering that Diethylenetriamine is highly degradable, it doesn't represent an ideal solvent for post combustion capture[60].

Ethylenediamine (**EDA**) is a shorter amine studied since 1955 for CO_2 capture[86, 145-148]. It presents a maximum carbamation loading of 1 mole of CO_2 per mole of amine, low thermal degradation and low viscosity. On the other hand, **EDA** presents a heat of absorption of -87 kJ/mol and is 30 times more volatile than **MEA**[86, 130-131]. The higher number of binding sites present on **EDA** would allow it to reach the same capture efficiency as **PZ**, and double the capture efficiency of **MEA** while working at half concentrations. Working with a 5M solution of **EDA** would double the capture efficiency compared to **MEA**'s capture units, but the solvent regeneration costs will be higher. **EDA** presents higher enthalpy of absorption than **MEA**, since its intramolecular ammonium-carbamate salt bridge is more stable than an intermolecular salt bridge by 6kJ/mol[85], which means that more energy will be required to strip CO_2 and regenerate the amine.

Furthermore, 8M **EDA** showed lower viscosity compared to an 8M solution of **PZ**, , because of its smaller molecular weight[86]. An experiment run on an 8M solution of **EDA** loaded at 0.4 mol of CO_2/mol of amine showed a 10% lost in **EDA** after 16 weeks at 100 °C, proving a slow thermal degradation at said temperature. The stripper could therefore be operated at 100-110 °C to avoid thermal degradation [86].

An investigation conducted on Triethylenetetramine (**TETA**), showed that a 1.2M solution of **TETA** reached the same overall CO_2 loading of a 4.9M solution of **MEA**, coherently with its higher number of binding sites[149]. For all polyamines with more binding site than **MEA** (**DETA**, **EDA**, **TETA**) working at 5M in amine concentration would enhance the CO_2 uptake and offer

the possibility of reducing the solvent flow rate in the scrubbing process. Further studies are necessary to confirm that properties such as viscosity, vapor pressure and CO_2 solubility of those amines are suited at industrial operation conditions for both the absorption and the desorption step.

Table 10 Data on amino acid-CO_2 systems from literature[150-153]. Initial absorption/desorption rate expressed in mol CO_2/ (mol amine*min), maximum/minimum experimental loading and cyclic capacity expressed in mol CO_2/mol amine.

R_2NH	T °C	C (mol/L)	α_{min}	α_{max}	Cyclic capacity	Initial absorption rate	Initial desorption rate
***L*-LysK**[152]	60	2.27	0.88	1.22	0.34	/	/
GlyK[150]	/	1	0.27	0.74	0.47	$3.93\ 10^{-2}$	$1.84\ 10^{-2}$
***L*-Cysk**[150]	/	1	0	0.49	0.49	$3.18\ 10^{-2}$	$2.46\ 10^{-2}$
***L*-ArgK**[150]	/	1	0.54	1.11	0.57	$3.56\ 10^{-2}$	$2.19\ 10^{-2}$
***L*-SarK**[151]	80	4	0.1	0.95	0.85	/	/

The amino acids discussed in this section present a variety of different R-groups: hydrogen, primary amines, guanidinium groups, carboxylic acid and thiols. The nature of the R-group, which determines whether an amino acid is classified as non-polar (hydrophobic), polar or charged (acid or basic), plays a key role in CO_2 capture, either as the nucleophile or as the base necessary for the reaction (Ch.1, section 1.5).

Several studies present in literature[154-156] examined which inorganic bases are best suited for the deprotonation of amino acid, furtherly used in carbon capture processes. An investigation on NaOH, LiOH and KOH observed that KOH has higher solubility limit at 25 °C (121 g/100 mL of H_2O), compared to NaOH (109 g/100 mL of H_2O) and LiOH (12.8 g/100 mL of H_2O)[154-155]. Furthermore, amino acid neutralized with NaOH showed in general lower absorption rate than those neutralized with KOH[156]. For these reasons, KOH is considered the most suitable inorganic base for the deprotonation of amino acids in carbon capture.

When working with amino acids at high loading and concentration, the precipitation of bicarbonate may be observed, as reported by a study performed on 5 M Potassium Sarcosinate (**SarK**)[63, 156]. The precipitation could have a positive effect in displacing the equilibrium towards higher production of bicarbonate, although it may also lead to severe operating difficulties, since the system would have to be adjusted to handle slurries[134].

Within the amino acids chosen for this investigation, salts of ***L*-LysK** have proven to have higher absorption capacity than **MEA**, since the presence of two primary amine groups allows a maximal carbamation loading of 1 mole of CO_2 per mole of amine. Upon CO_2 capture, *L*-lysine

can yield two regioisomers for ammonium monocarbamates (on α-NH_2, and ε-NH_2) and a dicarbamate, coupled with diammonium (Fig.23).

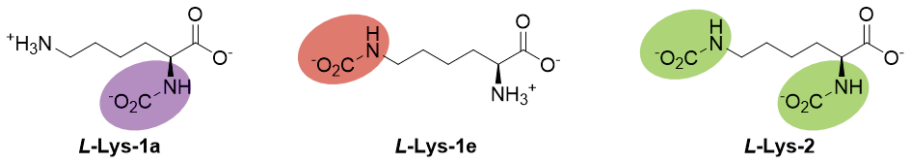

Fig. 23 *L*-Lysine ammonium carbamates on the α-NH_2 (***L*-Lys-1a**, purple) and ε-NH_2 (***L*-Lys-1e**, red). For the *L*-lysine dicarbamate ***L*-Lys-2** (green) the correspondent diammonium counterion is omitted for clarity.

A study conducted by Al-Terkawi *et al.*[157] in 2020, reported a solvent-free method for the regioselective production of *L*-lysine ammonium carbamate ***L*-Lys-1e**. The reaction performed by mechanochemistry with pure *L*-lysine, for 5 minutes of grinding at 500 rpm under 5 bars of pure CO_2 flux, yielded a complete conversion of *L*-lysine in epsilon ammonium carbamate[157], confirmed by ^{13}C NMR (δ_{N-CO_2}= 164.8 ppm). In Table 11 are reported the experimental conditions tested in the study, with the respective monocarbamate products (α, ε).

Table 11 Experimental conditions reported by Al-Terkawi et al.[157] for CO_2 capture by *L*-lysine in different reaction set-ups. α, ε indicate the *L*-lysine ammonium carbamate regioisomers yielded in those specific operating conditions and LAG indicates Liquid Assisted Grinding.

Method	C (M)	m (g)	pCO_2 (bar)	rpm	H_2O (mL)	t (min, h)	Reactor	Product
Solution	0.7	0.5	/	/	5	4h	/	α, ε
LAG	/	0.5	5	800	0.05	5h	ZrO_2	α, ε
Neat Grinding	/	0.5	5	500	/	5min	ZrO_2	ε

The authors justify the regioselectivity of the neat-grinding reaction by the crystalline structure of *L*-lysine. Since the latter was determined to be in its zwitterionic form[158], with α-NH_2 protonated (α-NH_3), ε-NH_2 is consequently more reactive towards CO_2, yielding ε-monocarbamates. The investigation also reports experiment of CO_2 capture by *L*-lysine in aqueous solutions and by Liquid Assisted Grinding (LAG). The latter presents a reactive grinding in which both solid and liquid reactants are used, the specific technique and parameters will be furtherly discussed in Chapter 3. It can be noticed that both pathways yield a mixture of alpha (δ_{N-CO_2}= 163.7 ppm) and epsilon ammonium carbamates. When the CO_2 capture experiment was performed in water, a considerable fraction of bicarbonate was observed (δ_{HCO_3}= 160.6 ppm), yielding ammonium-bicarbonate salts in solution[157].

The results reported by Al-Terkawi's study show that the operating conditions in which CO_2 is captured by *L*-lysine have a great influence on the regioselectivity of the ammonium carbamate. Furthermore, studies[152, 159] also show fast kinetics of absorption[159] and high CO_2 loading, indicating that ***L*-LysK** can act as a good absorbent alternative for CO_2 capture[160]. Although, it must be considered that studies for ***L*-Lys/*L*-LysK** were performed at a maximum concentration of 3M[161] due to its limited solubility, which can represent an important industrial drawback.

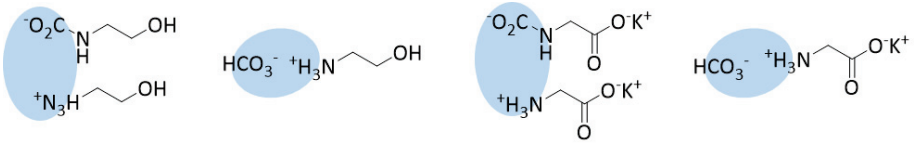

Fig. 24 Carbamate and carbonate adducts for **MEA** and **GlyK** with relative protonated ammonium counterion. The intermolecular salt bridge is indicated with a blue circle.

Glycine presents a short carbon chain and a single amine group, with a maximal carbamation loading of 0.5, hence comparable to **MEA**. In Fig.24 are reported the ammonium carbamate and carbonate adducts for **MEA** and **GlyK**. For both amines the carbamate-ammonium salt and the bicarbonate-ammonium salt have to be formed through intermolecular interactions. The molecular structure of carbamate **GlyK-1**, though, forces in close proximity two negative charges (carbamate and carboxylate), which can lower the stability of the adduct.

This last affirmation can be explained taking dicarboxylic acids as an example (Fig.25). If the nitrogen of **GlyK-1** is virtually substituted by a $-CH_2-$, succinic acid is obtained. In such a backbone the carboxylic acids present a $pka_1 = 4.2$ and $pka_2 = 5.6$, compared to 2.34 for glycine. The difference between the pKas of succinic acid indicate the difficulty encountered for the deprotonation of both carboxylic acids, giving a qualitative indication of the repulsion between two carboxylates in such proximity. This reasoning gives a perception of the repulsion present in the **GlyK-1** carbamate structure, which will influence its stability.

Fig. 25 Structures of **GlyK-1** carbamate and Potassium Succinate.

At present times there are no quantitative studies on the repartition between glycine carbamate/carbonate, while it presents a fundamental point for the overall knowledge of glycine capture mechanism. This aspect will be investigated in section 4 of this chapter. Furthermore, studies on potassium glycinate have shown lower oxidative degradation than **MEA**[162], but faster thermal degradation rates[90]. It must be considered that investigation of glycine as a carbon capture agent were only developed for a maximal concentration of 3M[96], while **MEA** is used at 5M in PCC units. Glycine's high absorption kinetics, solubility and availability enables it to be a frequently used solvent[96, 109].

Cysteine is considered a neutral amino acid and presents a thiol group on its R-chain. ***L*-Cys** shows a high initial absorption rate (3.18 E−02 mol CO_2/(mol amine*min)), although it is lower than the one of glycine, coherently with studies which show that amino acids with bulkier substituent group have slower absorption rate and faster desorption rate[150]. Currently the only example of a nucleophilic attack of the thiol group on CO_2 is limited to the formation of thiocarbonates via electrochemical reduction of disulfides[163-164].

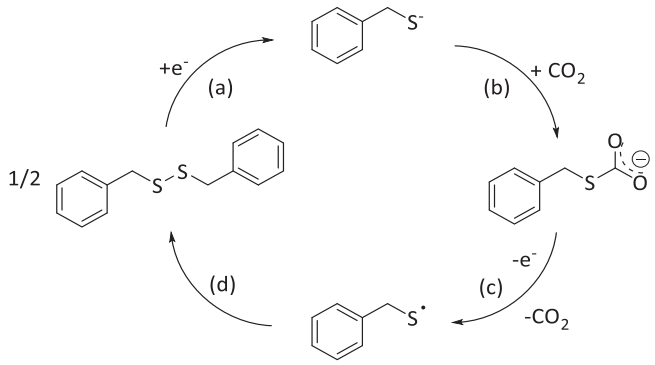

Fig. 26 Principle of carbon capture by benzyl disulfide by Singh[163] and Harris[164]; a) Electrochemical reduction of benzyl disulfide into benzyl thiolate (RS^-); b) CO_2 capture and formation of thiocarbonate ($R\text{-}S\text{-}CO_2^-$); c) oxidation of the latter, release of CO_2 and d) regeneration of the precursor benzyl disulfide.

In a study published in 2017 by Singh *et al.*[163], benzyl disulfide was electrochemically reduced (Fig.26a) to benzyl thiolate (RS^-) in ionic liquid medium and used as an *in situ* capture agent (Fig.26b) for CO_2. The generated S-benzylthiocarbonate[165] ($RS\text{-}CO_2^-$) was characterized by ^1H, ^{13}C NMR, FT-IR and electrochemical analysis and quantum chemical calculations gave a binding energy of -66.3 kJ/mol, resulting in a stable adduct. The thiocarbonate is then oxidized, releasing CO_2 and regenerating the sulfide precursor[163] (Fig.26c,d). This process demonstrates that capture/release can be conducted by electrochemical means. This same concept was also

extended to water, with no apparent gain in reduction potential or reaction energy[164]. The formation and stability of cysteine carbamates have not been investigated in literature, but will be furtherly discussed in this chapter.

Arginine (***L*-Arg**) contains a basic guanidinium side chain (pKa= 12.48), and presents low solubility at 298K (Table 9, page 61). Studies have confirmed a comparable absorption rate of 0.5M ***L*-ArgK** to 0.5M **MEA**[166]. The high alkalinity of the guanidinium group could promote the formation of carbamates and bicarbonates, acting as a base for both the zwitterion and termolecular mechanisms[166].

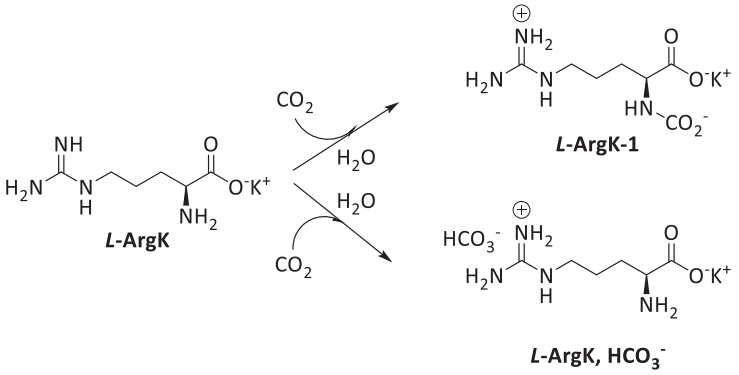

Fig. 27 CO_2 capture by ***L*-ArgK**. Both ammonium carbamate ***L*-ArgK-1** and ammonium bicarbonate ***L*-ArgK, HCO_3^-** structures were observed and characterized by Shen et al.[166].

Both ***L*-ArgK-1** ammonium carbamate and ***L*-ArgK** bicarbonate salt were observed by ^{13}C NMR with chemical shift of δ_{N-CO_2}= 163.7 ppm and δ_{HCO_3}= 160.4 ppm[166]. Furthermore, arginine has a relatively low cyclic capacity (Table 10, page 63), which may be attributed to the stability of the carbamate/carbonate ammonium salt[150]. Qualitative and quantitative studies on ***L*-ArgK**-CO_2 adducts will be furtherly discussed in the results section.

Aspartic Acid (***L*-Asp**) is the only acidic αAA investigated in this work, although it is not often considered a suitable solvent for CO_2 capture. In the literature, aspartic acid is studied in the formation of carbon dioxide hydrates.

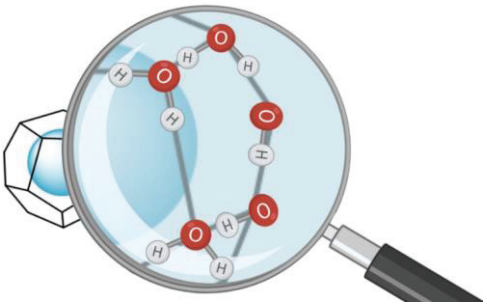

Fig. 28 Example of gas-hydrate with a gas molecule (blue circle) trapped in a water-molecule cage[167-168] linked by hydrogen bonds.

Gas hydrates are ice-like crystalline compounds formed by trapping gas molecules in hydrogen bonded water molecules at high pressure (25-40 atm) and low temperature conditions (2-8 °C), and are being investigated for their use in CO_2 capture and transportation. Aspartic acid has proven to have an inhibitory effect on gas hydrate formation at low concentrations (0.01M). A study performed by Sa *et al.* in 2014[169] affirmed than this tendency is correlated to the hydropathy index of the amino acid. The latter indicates the hydrophobic or hydrophilic character of an amino acid, where the most hydrophobic is isoleucine (4.5) and the most hydrophilic is arginine (-4.5). Aspartic acid is an hydrophilic amino acid and presents an hydropathy index of -3.5[169]. Furthermore, is was observed that the inhibition impact of aspartic acid can be reduced by increasing working concentrations from 0.01 and 0.1M. Due to the low solubility of the AA, an increase in concentration leaves unreacted aspartic acid in the system, which promotes hydrate formation, hence reducing the inhibitory effect [168]. At present times there are no specific studies on aspartic acid for its role as CO_2 capture agent, as well as possible carbamate and carbonate formation. Those aspects will be discussed in section 4 of this chapter.

Chapter 2

2 Dynamic Combinatorial Chemistry

In this investigation carbon capture by various amines is tackled via a Dynamic Combinatorial Chemistry approach (DCC). DCC has been developed in the 90's and it is defined as combinatorial chemistry under thermodynamic control. While combinatorial chemistry consists in creating extensive libraries of prefabricated molecules, DCC uses the reversible interaction between basic components to create a mixture of all possible combinations, also known as Dynamic Combinatorial Libraries (DCLs)[170].The reaction between an amine and carbon dioxide can give rise to a DCL with a variety of ammonium carbamates/carbonates adducts, all in equilibrium one with the other at mild conditions.

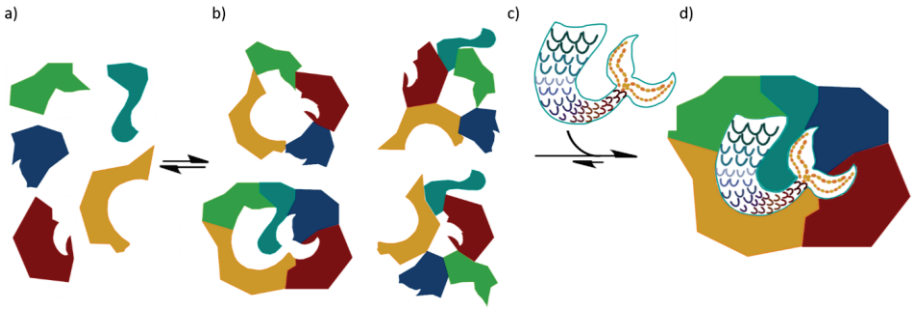

Fig. 29 Dynamic Combinatorial Chemistry (DCC). a) building blocks, b) dynamic combinatorial library (DCL) in equilibrium, c) addition of a template, d) optimal combination of host, thermodynamically favored [170].

Library members of DCLs are all in equilibrium, and they have the ability to interconvert into one another through reversible chemical processes, involving covalent bonds, noncovalent interactions or metal-ligand coordination (Fig. 29)[171].

Through this approach it is possible to create all combinations, which relative proportion is directly dependent on their stability. As observable in Fig.30, when an external stimulus (i.e. chemical stimulus) is introduced in the system, the stability of the components varies and consequently so does the distribution of species in the library.

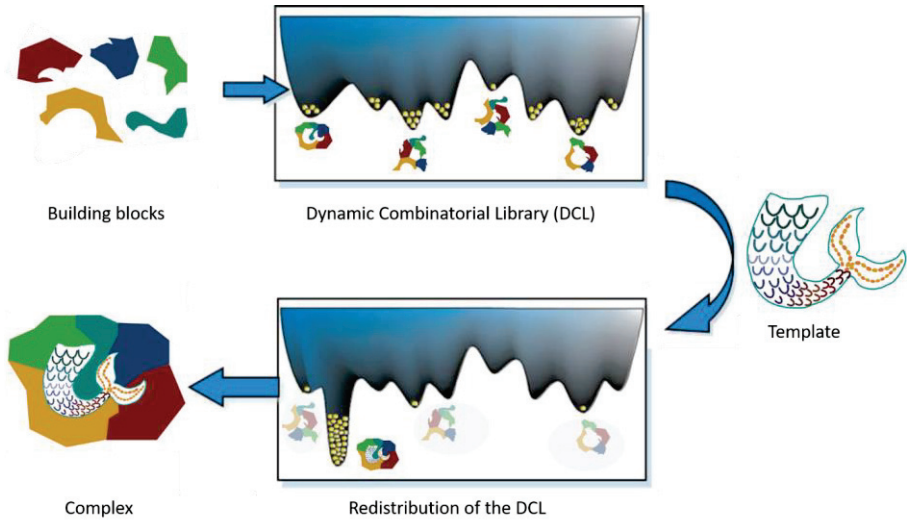

Fig. 30 Redistribution of a Dynamic Combinatorial Library (DCL) after introduction of a chemical stimuli (template) in the dynamic system [171].

DCC is commonly used in host-guest recognition chemistry, in which the library is modified driven by the thermodynamic control of the host-guest interaction.

In the context of this thesis, two aspects of DCC are explored. The first will be discussed in this chapter, and it concerns the dynamic combinatorial libraries developed between carbon dioxide and polyamines/amino acids. The focus will be on determining which carbamate/carbonate adducts are more abundant and what properties characterize their stability.

The second aspect will be discussed in Chapter 3, where a three-level dynamic combinatorial chemistry will be developed by introducing a metal chloride salt in the DCL. The metal salt may act as a template, showing preferential affinity towards one or multiple ligands, therefore impacting the distribution of the CO_2-loaded adducts. This effect will be investigated in homogeneous and heterogeneous systems with $MgCl_2$ and $CaCl_2$, for the identification and understanding of the affinities between those alkaline metals and carbamates/carbonates adducts in aqueous meanings.

Chapter 2

3 General methods

A series of experiments was performed on polyamines and amino acids to collect comprehensive knowledge on the repartition of carbamates/carbonates with increased CO_2 loading and correlate these molecular data to performances indicators such as cyclic capacity and reaction enthalpy.

In this section the objective and general methods of those experiments will be presented; further information on materials, reagents and reactors can be found in the experimental section.

3.1 Speciation by ^{1}H, ^{13}C quantitative NMR

A speciation analysis is defined as the qualitative identification and quantitative measurement of chemical species in a system. It can be performed by NMR[141], potentiometric[172] or conductimetric analysis[173]. In this work, speciation experiments were used to computationally analyze a R_2NH-CO_2-H_2O library.

Speciation experiments were done by means of quantitative ^{13}C Nuclear Magnetic Resonance (qNMR) and ^{1}H qNMR on a 500MHz Advance Bruker (^{1}H, ^{13}C nuclei 125MHz), using an internal reference whose initial concentration was accurately measured. ^{13}C qNMR has been approved as a valid method for this purpose, although this type of experiment is not widely used in literature[141, 172, 174].

The set-up used in this study involves the preparation of a 10 mL 0.5 M solution of amine at 25 °C in D_2O, furtherly divided into 10 aliquots of 1 mL each. Increasing quantities of pure CO_2 are introduced in the aliquots and measured by continuous gravimetric analysis. It is considered that maximum $\alpha(CO_2)$ is reached when the weight of the sample does not increase upon continuous loading. The possible evaporation of the solvent throughout the experiment, although minimal for water at 25 °C, renders the gravimetric measurement inaccurate. For this reason, CO_2 loading is precisely attested by qNMR analysis.

This technique provides information on the carbamation state of various adducts, while the protonation degree of the amines can be assessed by potentiometric techniques, or extrapolated from the experimental data, but not observable by NMR. This is due to the fast exchange of protons between protonated and unprotonated amines, which is not detectable

through NMR analysis[175]. In this study ^{13}C quantitative NMR was chosen as the most suitable technique, compared to ^{1}H qNMR, since it enabled the integration of the carbonate signal (δ= 160 ppm) and since less overlapping between the NMR peaks was generally observed in the spectrum. The corresponding aliphatic carbon peaks of each species were integrated with respect to an internal reference, and the molar fraction of such species was calculated for each $\alpha(CO_2)$ loading; the same method was applied to the integration of HCO_3^-.

A graph representing the evolution of the adducts abundance was then obtained by plotting the molar fraction of each species vs $\alpha(CO_2)$, and the experimental points were fitted with a 3rd degree polynomial.

It must be noted that in this work, from this point on, CO_2 loading will be calculated as:

$$\alpha(CO_2) = \frac{\sum n_i * \#_{(CO_2)i}}{moles_{R_2NH} * \#N} \quad (31)$$

Where $n_i * \#_{(CO_2)_i}$ corresponds to the number of moles of the species "i" multiplied by the number of CO_2 molecules bound to it and #N is the number of nitrogen sites present on the molecule backbone. The overall experimental loading is therefore defined as normalized $\alpha(CO_2)$ and it is expressed as moles of CO_2 per mole of nitrogen.

3.2 Cyclic Capacity

As defined in Chapter 1, the cyclic capacity of CO_2 absorption/desorption of an amine is given by the difference between the rich and the lean loadings in CO_2 (eq. 32, page 35). To experimentally determine this parameter amines were loaded with a continuous flow of pure CO_2 at 25 °C, the signals corresponding to carbamate and carbonate species were followed *in situ* by a FT-IR probe. At the end of the absorption step, the system was flushed by continuous flow of pure N_2 at 100 °C to induce desorption. At the end of each absorption/desorption step an aliquot of solution was taken for ^{13}C qNMR analysis, which allowed a precise quantification of the reached CO_2 loading. The absorption/desorption cycles were performed between 2 and 5 times on the amines solutions to test their regeneration/degradation properties. For industrial use, new carbon absorbing solvents with high cyclic capacity are more suitable than solvents with low cyclic capacity, as it allows reducing solvent circulation flow rate, size of the amine plant and overall costs[59].

3.3 Power Compensated Calorimetry (PCC).

In addition to α(CO_2) and cyclic capacity, another determining parameter for the choice of new potential CO_2 absorbing solvent is the reaction enthalpy (Δ_rH° kJ/mol of CO_2). The latter can be determined by calorimetric measurements such as Power Compensated Calorimetry (PCC). In those experiments a solution of amine is introduced in a thermostatic and stirred calorimetry reactor (Fig.31) and loaded with a continuous flow of CO_2/N_2. In this work PCC experiments are run under "industrial type conditions"[143], for an amine concentration of 0.5-3M, above room temperature (40 °C) and with a mixture of gases (CO_2/N_2 at ratios 15:85).

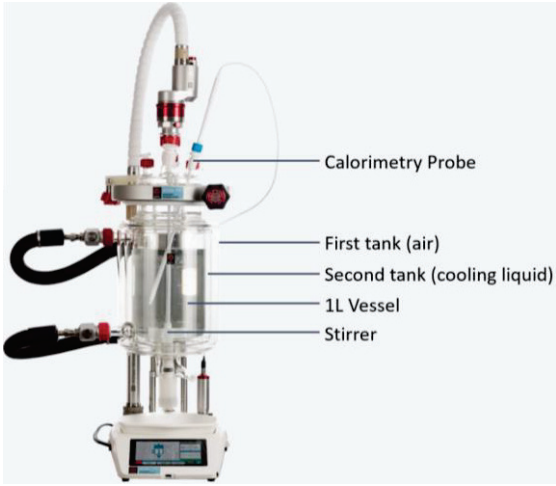

Fig. 31 Power Compensated Calorimetry (PCC) reactor set-up. The solution is introduced in the vessel and the system is brought at 40 °C by heating the liquid present in the second tank. Gases are introduced by mass flowmeter (non-present in the picture) and the heat liberated by the exothermic reaction is compensated by a 50 W calorimetry probe.

To maintain the system at 40 °C, the heat dissipated by the exothermic reaction is compensated by a 50 W probe. The enthalpy of reaction (Δ_rH°(kJ)) is then measured and calculated by a software. A ^{13}C qNMR analysis is performed at the end of the reaction to quantify the CO_2 moles absorbed by the amine solvent, necessary to determine Δ_rH° (kJ/mol of CO_2). In this way it is possible to collect important information about the regeneration energy needed for each potential absorber in future industrial applications. Given that higher recovery energy means higher operational costs, PCC experiments give a perception of the suitability of the solvent as a carbon dioxide absorber.

Chapter 2

4 Results and discussion

In this section will be presented the results obtained via ^{1}H and ^{13}C quantitative NMR speciation, cyclic capacity and power compensated calorimetry experiments performed over two industrial polyamines and five amino acids.

4.1 Ethylenediamine (EDA)

An aqueous solution of Ethylenediamine loaded with CO_2 yields a mixture of monocarbamate, dicarbamate and bicarbonate. As shown in Fig.32 two categories of equilibria, involving the carbamate bond, can take place:

- C-N formation or cleavage (eq.56-57)
- Disproportionation, which can occur at fixed CO_2 through intermolecular reaction (eq.58)

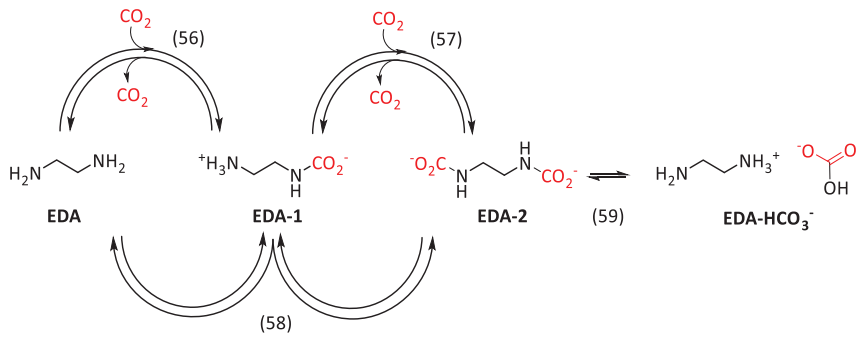

Fig. 32 Summary of absorption/desorption by Ethylendiamine in water. Formation of monocarbamate **EDA-1** (eq.56), dicarbamate **EDA-2** (eq.57), concomitant protonation phenomena omitted for clarity. Disproportionation of monocarbamate and bicarbonate into free amine and dicarbamate (eq.58). Formation of bicarbonate salt **EDA-HCO_3^-** (eq.59).

As mentioned in Ch.1, carbonates enthalpy of formation is 15-30 kJ[41, 47-50] lower compared to carbamates, for this reason the cleavage of an ammonium-bicarbonate salt will require less energy compared to the cleavage of a carbamate. As previously mentioned, structural characteristics of the amine (distance between amine groups, steric hindrance) will determine which route (carbamation/carbonation) will predominate. Parameters such as initial pH, concentration, ionic strength and temperature can also influence this repartition, although their screening was not investigated in this thesis.

The resulting adducts of the **EDA**-CO_2 dynamic system are shown, with a color code, in Fig.33. In the quantitative ^{13}C NMR speciation of a 1M aqueous solution of **EDA**, four magnetically distinct species can be observed: **EDA**, monocarbamate **EDA-1**, dicarbamate **EDA-2** and bicarbonate.

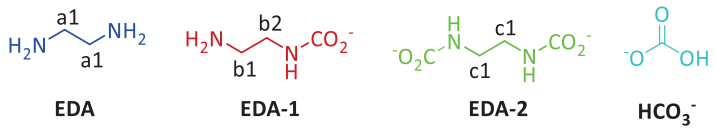

Fig. 33 **EDA**-CO_2 adducts color coded for clarity. **EDA** (blue), monocarbamate **EDA-1** (red), dicarbamate **EDA-2** (green), bicarbonate HCO_3^- (light blue). Carbons with different NMR signals are denominated on each adduct.

4.1.1 ^{1}H and ^{13}C quantitative NMR speciation

The **EDA**-CO_2 library was investigated by both ^{13}C qNMR and ^{1}H qNMR. The presence of few adducts with limited peak overlap, enabled an accurate interpretation and quantification of the ^{1}H spectra, while ^{13}C qNMR spectra were analyzed to quantify the amount of bicarbonate. Colored stacked ^{13}C spectra presenting the evolution of each species upon CO_2 loading can be found in the Annexes (page 207).

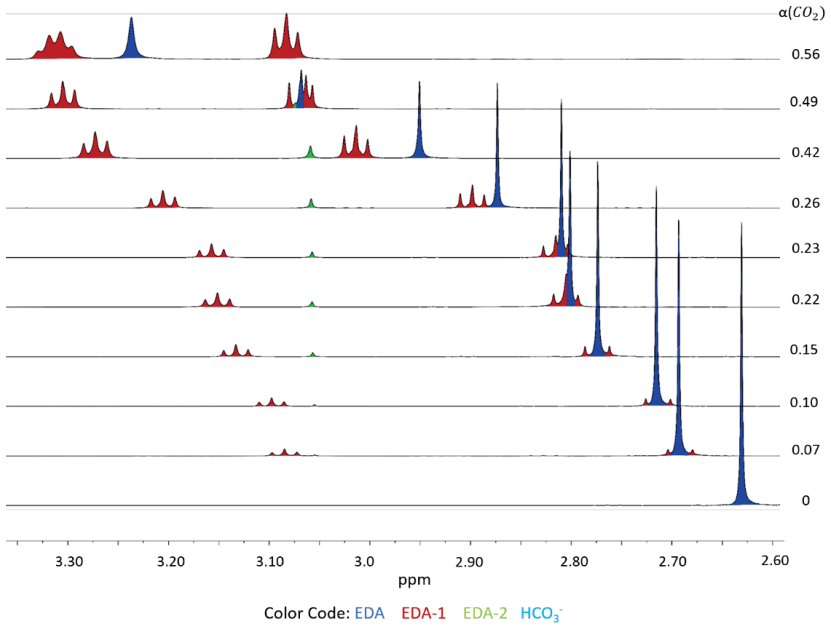

Fig. 34 Stacked ^{1}H qNMR spectra of **EDA** 1M in water upon increasing α(CO_2). Color code: **EDA** (blue), monocarbamate **EDA-1** (red), dicarbamate **EDA-2** (green), bicarbonate (light blue).

Ethylenediamine presents a symmetrical structure, for which it is possible to observe a singlet ^{1}H NMR signal at δ= 2.62 ppm. The formation of the asymmetric monocarbamate **EDA-1** is represented by the formation of two triplets with different chemical shifts (δ= 2.70 ppm and δ= 3.10 ppm for a CO_2 loading of 0.07). The different chemical shift of the two triplets is justified by the relative proximity of the protons to the carbamate group. Further on, the formation of dicarbamate **EDA-2** can be observed by the evolution of a singlet at δ= 3.05 ppm, where the multiplicity of the signal is justified by the symmetrical structure of the CO_2-loaded adduct. The variation in chemical shift observable in both figures is due to the pH variation of the solution, which decreases with CO_2 loading.

In Fig.35 is reported the chemical speciation obtained by plotting the molar fraction (X_i) of the species with the total α(CO_2) loading. Monocarbamate **EDA-1** is the most abundant species, only partially transformed in dicarbamate **EDA-2** upon CO_2 loading. At α(CO_2) = 0.35 dicarbamate is hydrolyzed to yield **EDA-1** and HCO_3^-; the dicarbamate low abundance can be explained by the instability caused by the proximity of the two anionic groups, as discussed for **GlyK** on page 65. Moreover, the dicarbamates require intermolecular pairing with one diammonium or two monoammoniums, which are unfavored respectively enthalpically and entropically.

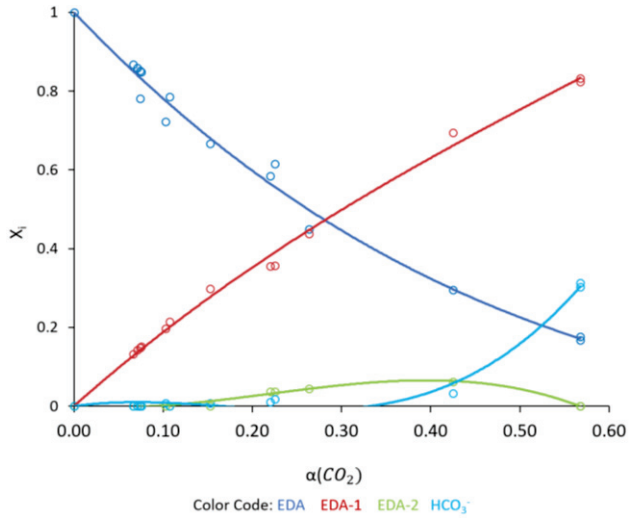

Fig. 35 Chemical speciation of 1M **EDA**-CO_2 in deuterated water. The graph is expressed in molar fraction (X_i) vs loading (α(CO_2)). The experimental data (circles) are fitted with a 3rd degree polynomial. Color code: **EDA** (blue), monocarbamate **EDA-1** (red), dicarbamate **EDA-2** (green), bicarbonate HCO_3^- (light blue).

At the experimental maximal loading ($\alpha(CO_2) = 0.57$), the **EDA**-CO_2 library is composed of 73% of monocarbamate and 27% of bicarbonates. From the ^{13}C qNMR data it was possible to extrapolate the molar fraction of carbamates and carbonates groups per moles of nitrogen, defined as the normalized molar fraction (X_i^N):

$$X^N{}_{(-N-CO_2^-)} = \frac{\sum n_{N-CO_2^-} * \#_{CO_2}}{moles_{R_2NH} * \#N} \quad (60)$$

$$X^N{}_{(HCO_3^-)} = \frac{n_{HCO_3^-}}{moles_{R_2NH} * \#N} \quad (61)$$

The normalized molar fraction of ammonium groups (eq.62) is obtained as the sum of eq.60 and eq.61, therefore equal to the $\alpha(CO)_2$ (eq. 31):

$$X^N{}_{NH_3^+} = \frac{\sum n_i * \#_{CO_2}}{moles_{R_2NH} * \#N} = \alpha(CO_2) \quad (62)$$

Consequently, the molar fraction of free -NH_2 groups was obtained by subtraction of ammonium (eq.62) and carbamate (eq.60) from the initial molar fraction of the free amine group (eq.63):

$$X^N{}_{NH_2} = 1 - X_{NH_3^+} - X_{(N-CO_2^-)} \quad (63)$$

An extrapolation of the ammonium and the residual non-protonated amine was executed, calculating also the normalized molar fractions of carbonate and carbamate (Fig.36).

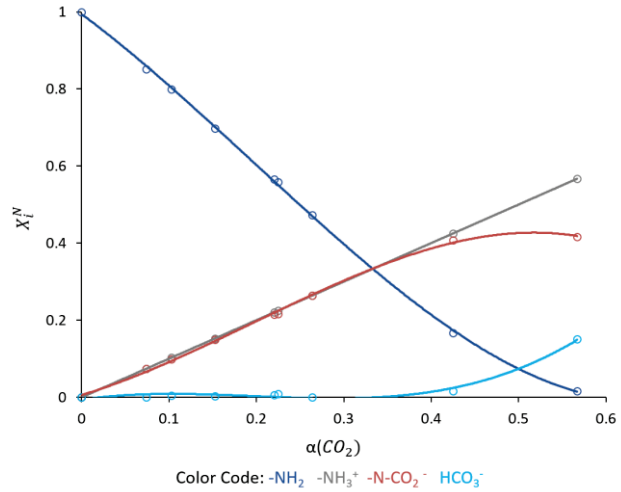

Fig. 36 Evolution of the normalized molar fraction (X_i^N) of deprotonated amine (blue), ammonium (gray), total carbamate (red) and bicarbonate (light blue) plotted against increasing CO_2 loading ($\alpha(CO_2)$) for a 1M solution of **EDA** in D_2O.

From Fig.35 and Fig.36 it is possible to conclude that, at high loading, the system presents ammonium salts of monocarbamates and carbonates, with no residual free -NH_2 in solution.

4.1.2 Cyclic capacity

To complement this analysis, an aqueous solution of **EDA** 0.26M was investigated for cyclic capacity, which was determined by following the loading of the solution via *in situ* FT-IR and ^{13}C qNMR.

Table 12 IR absorption frequencies for **EDA**-CO_2[176, 177].

Group	Vibration mode	This work (cm^{-1})	Literature (cm^{-1})
CO_3^{2-}	doubly degenerate stretching	1388	1388
HCO_3^-:	C–OH bending	1301	1298
C-O	stretching HCO_3^-	1360	1360
COO-	primary asymm. stretching	1560	1568
COO-	primary symm. stretching	1486	1486
N-COO	stretching	1322	1322
COO-	secondary asymm. stretching	1478	1481
N-COO	secondary stretching	1296	1296

The FT-IR probe enabled to record full spectra on the range of 650-4000 cm^{-1}, in particular wavelengths specific to carbamates and carbonates, permitting to detect saturation corresponding to equilibriums or steady states (Fig.37).

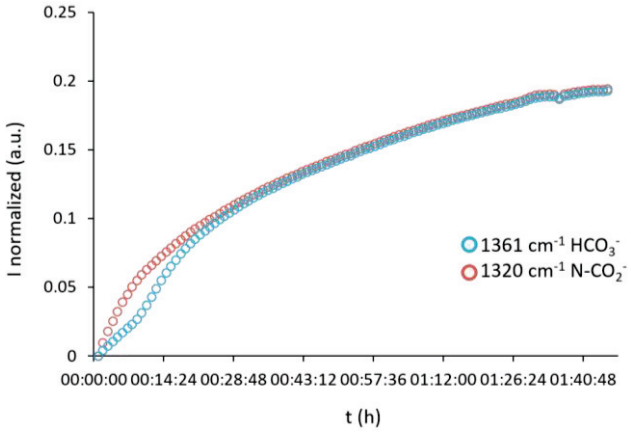

Fig. 37 Evolution of IR frequencies in the first absorption step for a 0.26M **EDA** aqueous solution loaded with a pure flux of CO_2 at 200 mL/min. The normalized intensities of wavelengths corresponding to carbamate (1320 cm^{-1}, red) and bicarbonate (1361 cm^{-1}, light blue) are plotted against reaction time (h).

The FT-IR analysis confirmed a higher kinetics for the formation of ammonium carbamate compared to ammonium carbonate, coherently with the kinetics information reported by the literature[102].

A maximal CO_2 loading of 0.58 ± 0.01 (same as **EDA** 1M, $\alpha(CO_2)$ = 0.57) was reached for the absorption steps at 25 °C, while loading for the desorption steps at 100 °C was calculated at 0.08 ± 0.02 (Fig.38). From those data it was possible to obtain the mean cyclic capacity of 0.26M **EDA** in water, calculated as reported in Ch.1, eq.32, for a total cyclic capacity value of 0.5 ± 0.03.

$$\Delta\alpha = \alpha_{rich} - \alpha_{lean} \quad (32)$$

It must be mentioned that even in industrial conditions (120 °C) the amine sorbents never reach a full desorption state, since the required energy supply would be too high.

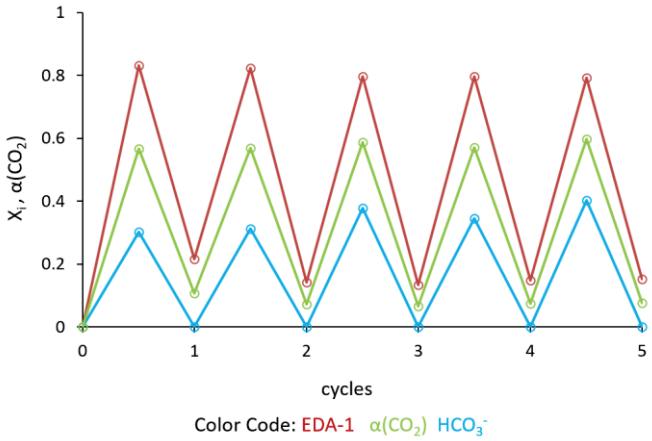

Fig. 38 Cyclic capacity of **EDA** 0.26M in D_2O. Color code: $\alpha(CO_2)$ for absorption and desorption steps (green), molar fraction of carbamate **EDA-1** (red) and molar fraction of HCO_3^- (blue). The $\alpha(CO_2)$ and the molar fractions are plotted with the number of cycles performed in the cyclic capacity experiment (n = 5).

Since the 0.26M solution was not investigated by ^{13}C qNMR speciation, it is not possible to determine the evolution and abundance of the adducts upon increasing CO_2 loading. Nevertheless, through the ^{13}C qNMR analysis performed for the cyclic capacity, it is possible to determine the repartition between molar fractions of $N\text{-}CO_2^-/HCO_3^-$ in the lean and rich state. It can be observed that monocarbamate **EDA-1** is the most abundant species in the rich state, representing 77% ± 2% of the CO_2-loaded adducts, while carbonate accounts for 23% ± 2%. There is no visible trace of dicarbamate **EDA-2**, probably due to the lower working concentration. Overall, the carbamate/carbonate repartition of 0.26M **EDA** is similar to that of 1M **EDA** (73% carbamates, 27% carbonates), which allows us to compare the two systems, despite the different operating conditions.

4.1.3 Power Compensated Calorimetry

A PCC experiment was run at 40 °C on 500 mL of a 1 M aqueous solution of **EDA**, loaded with a continuous flow of pure CO_2, fixed at 0.4 ln/min. The overall reaction enthalpy was measured to be -89.03 kJ/mol of CO_2.

Overall, **EDA** presents high CO_2 loading and high cyclic capacity, which must be considered positive features for carbona capture, nevertheless, its synthetic origin, corrosivity and enthalpy value do not favor it as the preferred carbon dioxide sorbent.

4.2 Diethylenetriamine (DETA)

When working on a longer polyamine the system may present a wider variety of ammonium monocarbamates, polycarbamates and bicarbonate adducts. As for **EDA**, different categories of equilibria, involving the carbamate bond, can take place:

- C-N formation or cleavage (eq.64-67)
- Disproportionation of monocarbamates into dicarbamates and uncarbamated amine (eq.68, 69).
- C-N bond exchange, which can occur at fixed CO_2 loading through *inter*- and/or *intra*molecular substitution reactions (transcarbamation) (eq. 70, 71).

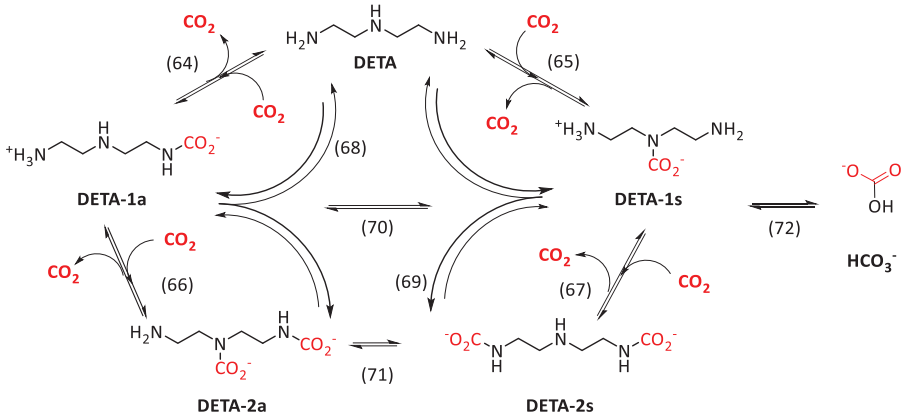

Fig. 39 Reactions of CO_2 absorption by diethylenetriamine. Reversible C-N bond formation/cleavage (eq.64-69,), disproportionation (eq.68, 69) transcarbamation (eq.70, 71) (concomitant protonation phenomena omitted for clarity), and bicarbonate formation (eq.72).

A study performed on **DETA** 0.5M in MeOH demonstrated that transcarbamation exchanges (eq.70, 71) are almost isoenergetic, promoting this phenomenon in the library[41].

In an aqueous solution of loaded **DETA**, both carbamation and carbonation occur, albeit in different proportions. In Fig.39 monocarbamate **DETA-1a** and **DETA-1s** are represented as intramolecular zwitterion, although, they may also form a less stable intermolecular salt bridges with an ammonium counterion at low loading. For dicarbamates the formation of intermolecular salt bridges is inevitable. Considering equilibrium (66), the disproportionation of 2 molecules of **DETA-1a** yield **DETA-2a** and its correspondent diammonium counterion, with the hypothesis that dimeric adducts (**DETA-2a**, **DETA-2H**) are entropically more favored than trimeric adducts (**DETA-2a**, 2 **DETA-H**) (Fig. 41).

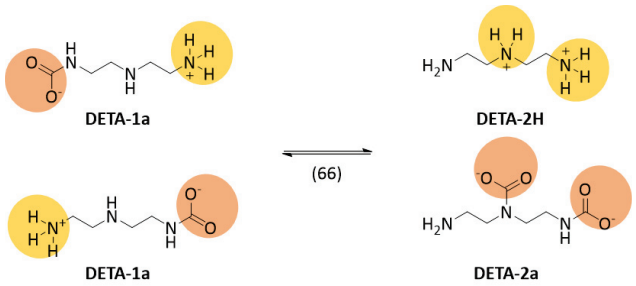

Fig. 40 Transcarbamation of **DETA-1a** (intramolecular zwitterion) to **DETA-2a**, represented with its diammonium counterion. Yellow circles indicate a potential protonation exchange, while red circles indicate the transcarbamation observable by ^{1}H, ^{13}C qNMR analysis.

4.2.1 ^{13}C quantitative NMR speciation

In the quantitative ^{13}C NMR speciation of a 0.5M aqueous solution of **DETA**, six magnetically distinct species can be observed: **DETA**, asymmetrical monocarbamate **DETA-1a**, symmetrical monocarbamate **DETA-1s**, symmetrical dicarbamate **DETA-2s**, asymmetrical dicarbamate **DETA-2a** and **HCO_3^-**. In Fig.41 are reported the different species already shown in Fig.39, with a color code differentiation for further clarity and a labeling of carbons which will be carried throughout the thesis.

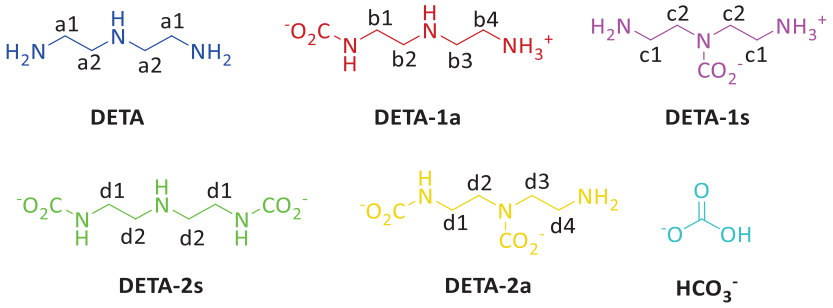

Fig. 41 **DETA**-CO_2 adducts color coded. Carbons with different signals are denominated on each adduct and the corresponding intermolecular ammonium counterion is omitted for clarity.

Diethylentriamine, having a symmetrical structure, shows only two aliphatic NMR signals at δ_{a1} = 39.83 ppm and δ_{a2} = 50.58 ppm. The proximity of carbon a1 and carbon a2 to, respectively, a primary and a secondary amine explains the difference in chemical shift. The chemical shift of each species with increasing quantities of CO_2 can be found in the Annexes (page 208). The stacked spectra of aliphatic and carbonyl signals of **DETA** upon increasing loading are displayed in Fig.42 and Fig.43, respectively. The variation in chemical shift

observable in both figures is due to the pH variation of the solution, which decreases with CO_2 loading.

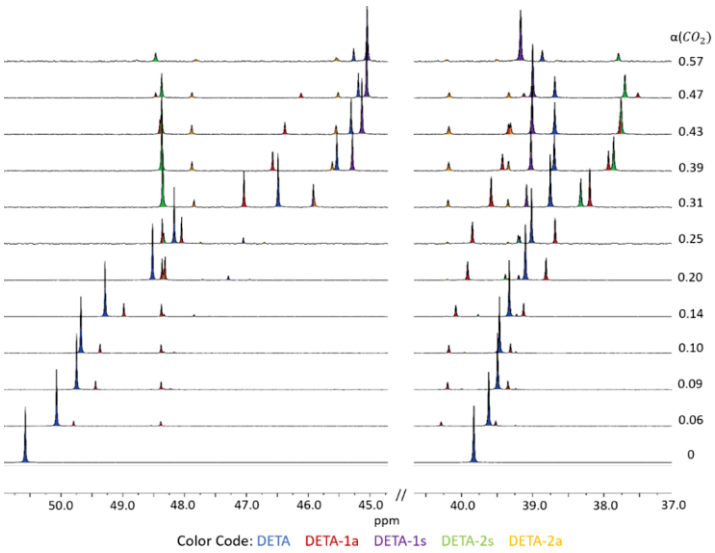

Fig. 42 ^{13}C qNMR speciation of **DETA** 0.5M in D_2O. The abscissa axis presents a zoom on two aliphatic regions: from 37 to 41 ppm for carbon atoms in proximity of the primary amine groups and from 45 to 51 ppm, for carbon atoms adjacent to the secondary amine. On the ordinate axis are reported the increasing values of CO_2 loading. Legend of color code below.

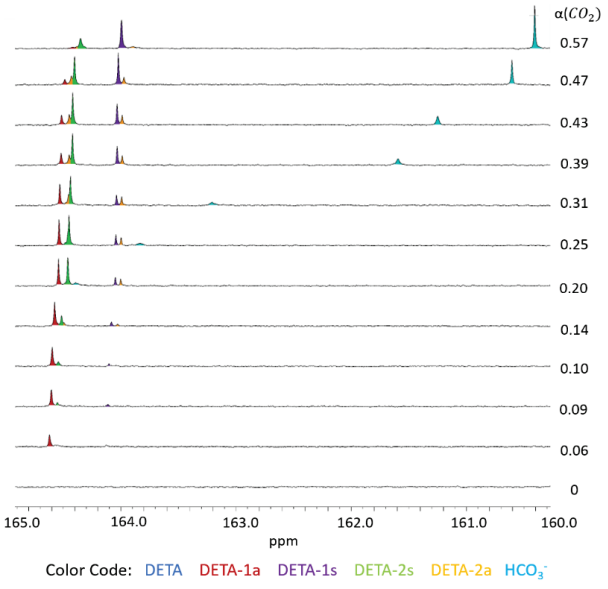

Fig. 43 ^{13}C qNMR speciation of **DETA** 0.5M in D_2O. Zoom on the carbonyl zone from 160 to 165 ppm. On the ordinate axis are reported the increasing values of CO_2 loading. Legend of the color code below.

In Fig.44 is reported the speciation of **DETA** 0.5M in D_2O, analyzed via ^{13}C qNMR. The molar fraction of uncarbamated **DETA** decreases upon increasing CO_2 loading, yielding asymmetrical monocarbamate **DETA-1a**. The symmetrical monocarbamate **DETA-1s** can be observed starting from $\alpha(CO_2)$ = 0.10. At higher loading is possible to observe the formation of symmetrical dicarbamate **DETA-2s** and asymmetrical dicarbamate **DETA-2a**. The latter is destabilized by the two negative charges in close proximity, as previously discussed for **GlyK**, which may explain its low abundance.

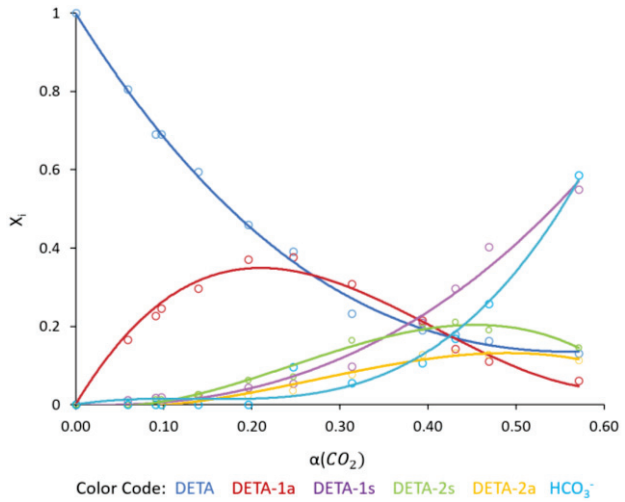

Fig. 44 Chemical speciation of a 0.5M solution of **DETA** in deuterated water. The graph is expressed in molar fraction (X_i) vs loading ($\alpha(CO_2)$). Experimental data fitted with 3rd degree polynomial. Color code: **DETA** (blue), asymmetrical monocarbamate **DETA-1a** (red), symmetrical monocarbamate **DETA-1s** (purple), symmetrical dicarbamate **DETA-2s** (green), asymmetrical dicarbamate **DETA-2a** (yellow), bicarbonate **HCO_3^-** (light blue).

Up until a loading of $\alpha(CO_2)$ = 0.2, the most abundant CO_2-loaded species is the asymmetric monocarbamate **DETA-1a**, which could lead to **DETA-1s** through intramolecular transcarbamation (eq.70). At higher loading, the formation of dicarbamates must occur by intermolecular abstraction of a proton from the zwitterionic monocarbamate **DETA-1a**, where the base role can be played either by **DETA** or **DETA-1a** itself. At higher $\alpha(CO_2)$ loading (0.4/0.45) dicarbamates disproportionate to yield symmetric monocarbamate **DETA-1s** and bicarbonates HCO_3^-. From the general profile of the chemical speciation is possible to conclude that monocarbamate **DETA-1a** and dicarbamates act as CO_2-transient species. At high loading the **DETA**-CO_2 library presents 34% of ammonium bicarbonates and 66% of ammonium carbamates, calculated with respect to the total amount of CO_2-loaded species.

As for **EDA**, alternative quantification of the ammoniums and the residual non-protonated amine was expressed by calculating the normalized molar fractions of carbonate and carbamate (eq.60-63) (Fig.45).

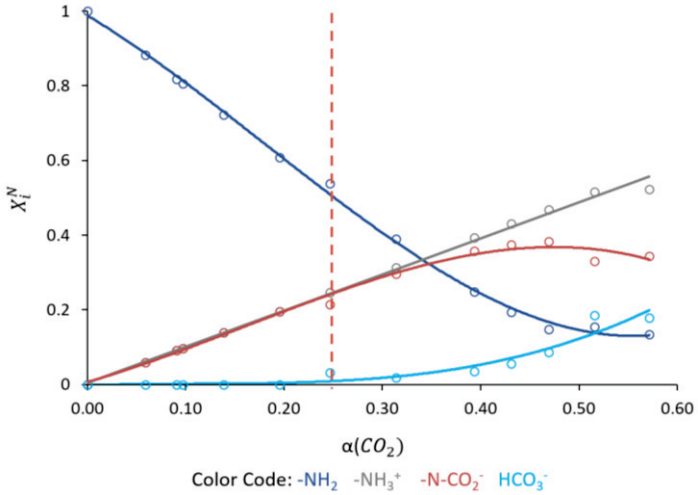

Fig. 45 Evolution of the normalized molar fraction (X_i^N) for **DETA** 0.5M in D_2O, plotted against increasing CO_2 loading ($\alpha(CO_2)$). Color-code: deprotonated amine (blue), ammonium (gray), total carbamate (red) and bicarbonate (light blue). The dotted red line indicates $\alpha(CO_2)$ = 0.25.

Until $\alpha(CO_2)$ = 0.25 (red dotted line) the increase in molar fraction for ammonium and carbamate are overlapping, indicating the exclusive formation of *intra* and *inter* molecular ammonium-carbamates adducts. From loading 0.25 the ammonium growth follows that of bicarbonate. At high loading, the ammonium normalized molar fraction reaches X_i^N = 0.6, which indicate the presence of diammoniums in solution. In fact, since **DETA** presents three nitrogen atoms, the maximum molar fraction of mono-ammonium **DETA** is X_i^N = 0.33. It is then possible to calculate the diammonium minimal normalized fraction ($X_{2-NH_3^+}^N$) as follows:

$$X_{2-NH_3^+}^N = \frac{(X_{NH_3^+}^N - 0.33)}{2} \quad (73)$$

Where ($X_{NH_3^+}^N$) is the ammonium normalized fraction (eq.62, page 76). From eq.73 is possible to determine that at $\alpha(CO_2)$ = 0.4 the diammonium represents 10% of the ammonium groups, while at maximum experimental loading ($\alpha(CO_2)$ = 0.58), the diammonium fraction increases to 20%. Those calculations strengthen the hypothesis discussed at page 81, for which it was considered that dicarbamate **DETA-2a** formed a dimeric adduct with diammonium **DETA-2H** counterion, and not a trimeric adduct with two ammoniums **DETA-H** (Fig.41).

The protonation state of the bicarbonate was verified *a posteriori*. The overall pH of a 0.5M solution of **DETA** was followed upon increasing CO_2 loading with a potentiometric probe. The data allowed to establish a correlation between the pH value of the solution and $\alpha(CO_2)$ (Fig. 46).

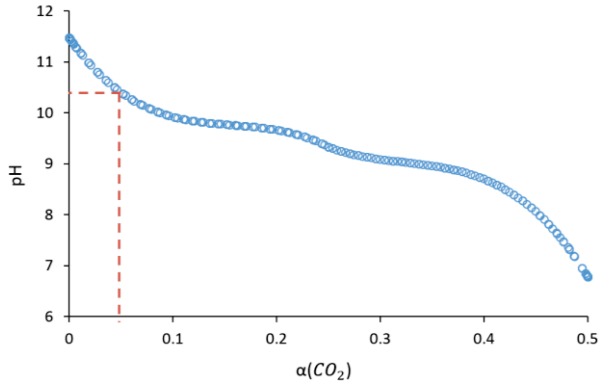

Fig. 46 Evolution of the overall pH of a 0.5M aqueous solution of **DETA** upon increasing CO_2 loading, pH values are plotted against $\alpha(CO_2)$.

Considering that H_2CO_3 presents a pKa_1 = 6.37 and pKa_2 = 10.32, it can be confirmed that carbonates CO_3^{2-} are present in the solution until loading 0.05 (pH 10.32); after which bicarbonates will be formed in the system. Therefore, the hypothesis of a 1:1 stoichiometry between ammoniums and bicarbonates showed in Fig.45 is confirmed *a posteriori*.

The results obtained by chemical speciation and potentiometric analysis show that, compared to **EDA**, which CO_2 capture is mostly driven by carbamation, **DETA** presents both carbonation and carbamation pathways. This could lead to favorable kinetics and thermodynamic features, as fast absorption rate, high cyclic capacity and low reaction enthalpy.

4.2.2 Cyclic capacity

The cyclic capacity of **DETA**-CO_2 was determined by following the loading of the solution via FT-IR and ^{13}C qNMR. The solution of amine was studied at 0.5M, and the experiment proceeded as described in section 3.2.

In Fig.47a are shown the wavelengths corresponding to the stretching band of the ammonium bicarbonate (1361 cm^{-1}) and ammonium carbamate (1320 cm^{-1}). As observed for **EDA** and as reported in the literature[102], the kinetics of ammonium carbonates is slower compared to that of ammonium carbamates.

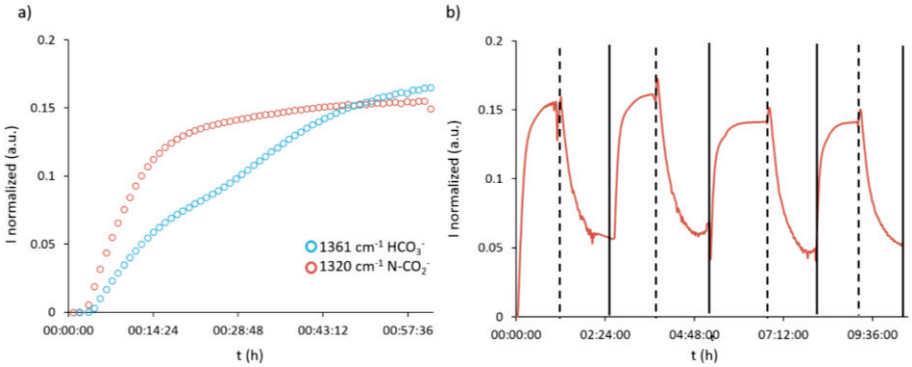

Fig. 47 a) Evolution of IR frequencies in the first absorption step for a 0.5M **DETA** aqueous solution loaded with a pure flux of CO_2 at 200 mL/min. The normalized intensities of wavelengths corresponding to carbamate (1320 cm^{-1}, red) and bicarbonate (1361 cm^{-1}, light blue) are plotted against reaction time (h); b) Evolution of carbamate frequency (1320 cm^{-1}) for all five cycles of absorption/desorption, plotted against time. The end of the absorption step is indicated by a dotted black line, while the continuous black line indicates the end of the desorption step.

In Fig. 47b, is represented the evolution of wavelength 1320 cm^{-1} throughout the whole cyclic capacity experiment. The intensity of the signal decreases during the desorption, although never reaching the same intensity corresponding to full stripping, meaning that CO_2 is never completely desorbed from the system. The experiment was performed over five consecutives absorption/desorption cycles, although only four are reported in Fig.26 due to an acquisition error of the FT-IR probe. To precisely quantify the CO_2 loading of each rich/lean phase, ^{13}C qNMR analysis was performed at the end of each absorption/desorption step. Fig.48 shows the rich and lean loading values for five consequent cycles. Coherently with FT-IR analysis the system never reaches desorption, for a lean loading of 0.11 ± 0.01.

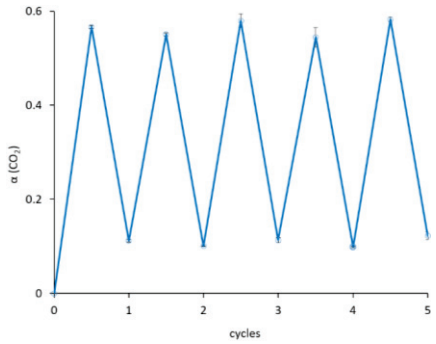

Fig. 48 Cyclic capacity of an aqueous solution of **DETA** 0.5M. Values of $\alpha(CO_2)$ for each absorption/desorption phase vs number of cycles (n = 5).

An aqueous solution of **DETA** 0.5M loaded with a pure CO_2 flow at 200 mL/min, at 25 °C, and stripped with a pure N_2 flow at 200 mL/min at 100 °C, shows a cyclic capacity of 0.46 ± 0.01; confirming a high absorption and desorption capacity. The cyclic capacity of **EDA** 0.26 M is slightly higher than the one of **DETA** 0.5 M (CC = 0.5 ± 0.03 and CC = 0.46 ± 0.01, respectively), despite presenting higher concentration of carbamates in solution (77% ± 2% for **EDA** and 64% for **DETA**). Overall the two polyamines show a similar chemistry for CO_2 capture, although the direct comparison between the systems should be performed at same operational conditions.

4.2.3 Power Compensated Calorimetry

The PCC experiment was run at 40 °C on 500 mL of a 0.5 M aqueous solution of diethylenetriamine, loaded with a continuous flow of pure CO_2, fixed at 0.25 L/min. The overall reaction enthalpy was measured to be -82.42 kJ/mol of CO_2. The profile of the PCC experiment can be found in the Annexes, page 209.

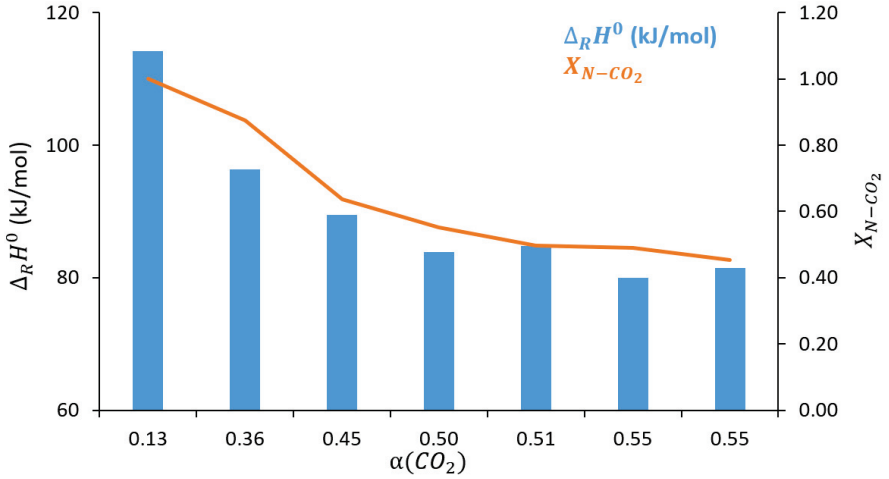

Fig. 49 Correlation between reaction enthalpy of **DETA** 0.5M(aq) and carbamate molar fraction upon increasing CO_2 loading. Reaction enthalpy $\Delta_r H^\circ$ expressed in kJ/mol (blue columns) and molar fraction of carbamates $X_{N-CO_2^-}$ (orange line) calculated with respect to total moles of captured CO_2, plotted against increasing $\alpha(CO_2)$.

To investigate the contribution of carbamation and carbonation on the reaction enthalpy, aliquots of the solution were collected and analyzed via ^{13}C qNMR throughout the experiment, enabling to determine the molar fraction of ammonium carbamates and carbonates upon increasing CO_2 loading.

Fig.49 highlights a linear correlation between the reaction enthalpy $\Delta_r H^\circ$ (kJ/mol) and molar fraction of carbamates. The reaction enthalpy for **DETA** can then be expressed as the sum of the reaction enthalpy of carbamates and carbonates, each multiplied by their respective molar fractions (eq.74):

$$\Delta_r H^\circ = x_{N-CO_2^-} \Delta_r H^\circ(N - CO_2^-) + x_{HCO_3^-} \Delta_r H^\circ(HCO_3^-) \quad (74)$$

$$\Delta_r H^\circ = x\Delta_r H^\circ(N - C) + (1 - x)\, \Delta_r H^\circ(O - C) \quad (75)$$

$$\Delta_r H^\circ = x(\Delta_r H^\circ(N - C) - \Delta_r H^\circ(O - C)) + \Delta_r H^\circ(O - C) \quad (76)$$

$$\Delta_r H^\circ = x\Delta\Delta_r H^\circ + \Delta_r H^\circ(O - C) \quad (77)$$

Where $\Delta\Delta_r H^\circ$ in eq.77 represents the difference between carbamation enthalpy and carbonation enthalpy (eq.76).

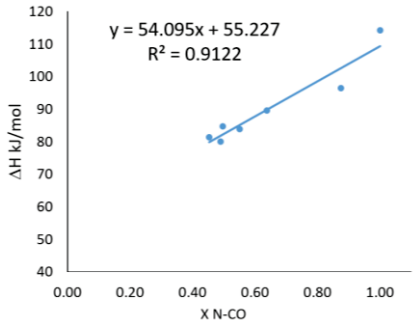

Fig. 50 Linear regression between $\Delta_r H^\circ$ (kJ/mol) and carbamate molar fraction.

Although the model is an approximation and would need further studies and investigations, Fig.50 reports the linear regression expressed by eq.76. The equation delivers a carbonation enthalpy of -55.2kJ/mol and a carbamation enthalpy of -109kJ/mol. The difference between these two values suggest that solvents which yield more carbonates than carbamates require less regeneration energy and are therefore more suited for carbon capture.

Overall, **DETA** presents interesting features for carbon capture, such as high CO_2 loading and high cyclic capacity over five cycles. At the same time, its corrosivity, thermal degradation, enthalpy value and synthetic origin do not favor it as the ideal carbon dioxide sorbent.

4.3 Glycine

Glycine is the only non-polar and not chiral amino acid investigated in this work. Frequently used in carbon capture[92, 96, 109, 178], as mentioned in section 1.2, it is commonly compared to **MEA** for its capture capacity, although its carbamate/carbonate repartition is not investigated in literature. The glycine-CO_2 library encompasses two types of adducts, a monocarbamate **GlyK-1**, and an ammonium/bicarbonate salt (Fig.51).

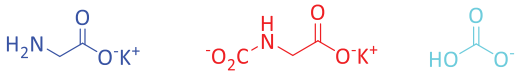

GlyK GlyK-1 HCO_3^-

Fig. 51 Adducts of **GlyK** upon CO_2 loading.

A 0.5M aqueous solution of **GlyK** was produced neutralizing the amino acid with one equivalent of KOH. The initial pH of the solution was measured at 10.57 and enabled the determination of the protonated/deprotonated proportion of the amino acid via the Henderson-Hasselbach relation:

$$pH = pKa + \log\frac{[A^-]}{[AH]} \quad (78)$$

Since the pKa of the glycine amine group is 9.60, at the given initial pH 90% of the NH_2 groups are deprotonated.

4.3.1 ^{13}C quantitative NMR speciation

The ^{13}C qNMR speciation of a 0.5M aqueous solution of **GlyK** is shown in Fig.52 (corresponding ^{13}C qNMR spectra can be found in the Annexes, page 209).

The investigation revealed a maximum experimental loading of $\alpha(CO_2)$ = 0.8, higher than 1M **EDA** and 0.5M **DETA** (0.57 and 0.58, respectively), with a rapid growth of monocarbamate **GlyK-1** at low loading. At loading $\alpha(CO_2)$ = 0.40 the monocarbamate is hydrolyzed to yield carbonates, with a sequential increase in free amine. At high loading the CO_2-loaded system is composed of 9% of monocarbamate and 91% of bicarbonate.

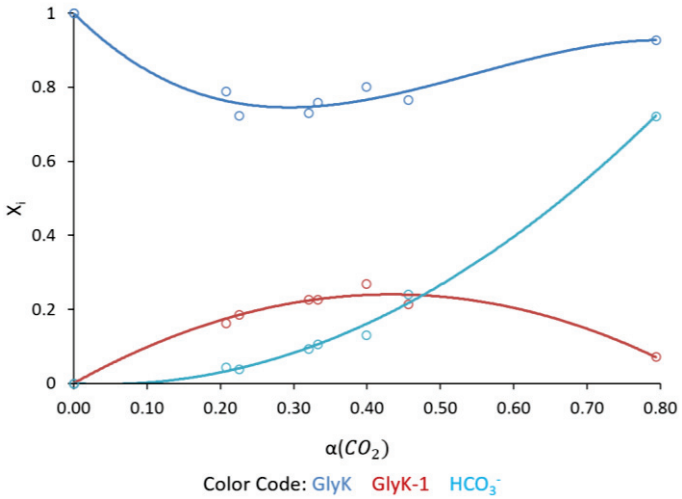

Fig. 52 Chemical speciation of a 0.5M solution of **GlyK** in deuterated water. The graph is expressed in molar fraction (X_i) vs loading ($\alpha(CO_2)$). Experimental data fitted with 3rd degree polynomial. Color code: **GlyK** (blue), monocarbamate **GlyK-1** (red), bicarbonate HCO_3^- (light blue).

The normalized molar fraction of ammonium and free amine in solution were calculated from the data obtained by the ^{13}C qNMR speciation (Fig.53a). Glycine was then compared to **EDA** to analyze the influence of the second amine/carboxylate substituent on CO_2 capture.

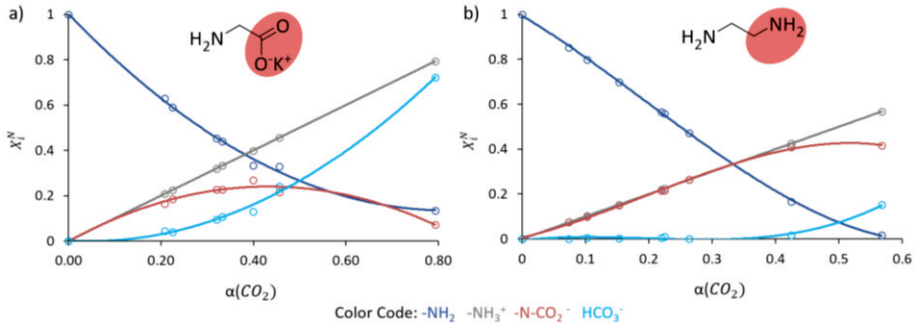

Fig. 53 Normalized molar (X_i^N) fraction of amine (blue), ammonium (gray), carbamates (red) and bicarbonate (light blue) for a) 0.5M solution of **GlyK**-CO_2 in D_2O and b) 1M aqueous solution of **EDA**-CO_2.

For **EDA** (Fig.53b) the presence of two primary amine groups expectedly favors the formation of carbamates, yielding mostly zwitterionic monocarbamate **EDA-1**. Glycine on the other hand can only form intermolecular ammonium-carbamate adducts, which can thus be considered as a transient species for the formation of bicarbonate-ammonium salts. Thermodynamically, this could enable higher cyclic capacity upon bicarbonate desorption.

4.3.2 Cyclic capacity

To verify this hypothesis a cyclic capacity experiment was conducted on a 0.5M aqueous solution of **GlyK**-CO_2. The solution was loaded with a pure flow of CO_2 at 200 mL/min, at 25 °C and desorption was performed with a pure flux of N_2 at 200 mL/min at 100 °C. The evolution of the species was analyzed by *in situ* FT-IR and ^{13}C qNMR. The results showed a rich loading of 0.78 ± 0.02, and a lean loading of 0.13 ± 0.07 (Fig.54). Overall **GlyK** presents a cyclic capacity of 0.65 ± 0.04, higher than **DETA** and **EDA**, for a more efficient CO_2 desorption and amine regeneration.

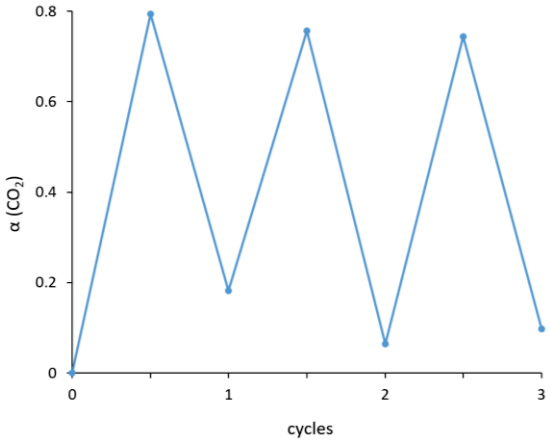

Fig. 54 Cyclic capacity of an aqueous solution of 0.5M of **GlyK**. Value of CO_2 loading versus number of absorption/desorption cycles (n = 3).

Furthermore, the FT-IR evolution for the first absorption step of 0.26M **EDA** and 0.5M **GlyK** were compared, to investigate the influence of glycine carbonation chemistry on the overall kinetics of absorption (Fig.55). It can be noticed that while **EDA** presents fast kinetics of carbamation and slow kinetics of carbonation, glycine shows the opposite trends. It can be hypothesized that, given the instability of ammonium monocarbamate **GyK-1**, the formation of ammonium bicarbonate is enhanced.

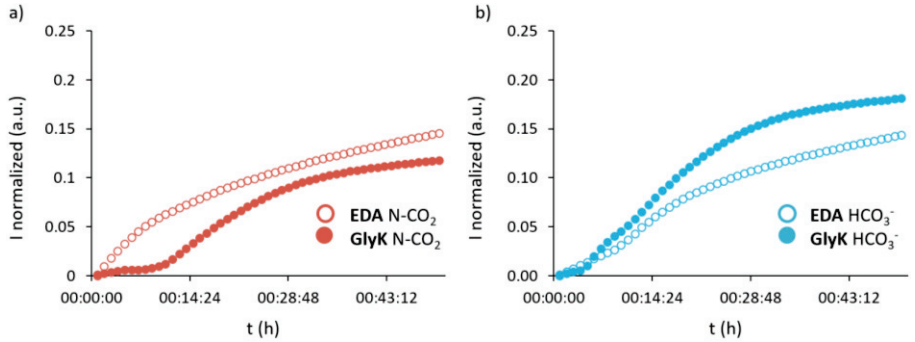

Fig. 55 Evolution of the normalized intensities of wavelengths corresponding to a) carbamate (1320 cm^{-1}, red); b) bicarbonate (1361 cm^{-1}, light blue) for a 0.26M aqueous solution of **EDA** (empty circles) and a 0.5M aqueous solution of **GlyK** (full circles). Both solutions were loaded with a pure flux of CO_2 at 200 mL/min at 25 °C.

4.3.3 Power Compensated Calorimetry

To assess the energetic impact of the fixation pathway, a PCC experiment was performed on a 3 M aqueous solution of **GlyK**, in industrial conditions. The reaction enthalpy for carbon dioxide absorption by glycine was measured at $-\Delta H_{abs} = 68.61$ kJ/mol of CO_2, which falls in the ideal zone[27] of enthalpy values for an efficient CO_2 capture process.

Overall, the carbonation chemistry of glycine provides a higher maximal loading compared to **MEA** (0.8 vs 0.5 mol CO_2/mol of nitrogen), fast kinetics of absorption, high cyclic capacity and low enthalpy of reaction. Based on the data obtained in this work and on the already existing studies and applications of **GlyK** in carbon capture technologies and researches[92, 96, 109, 178], glycine can be considered an efficient carbon capture solvent.

4.4 *L*-Lysine

A 0.5 M aqueous solution of *L*-lysine was produced from chloride salt (***L*-LysCl**) neutralized with two equivalents of KOH. The resulting 0.5 M ***L*-LysK** solution presented an overall pH of 11.79, from which was possible to calculate the protonated/deprotonated proportion of the amino acid, via the Henderson-Hasselbach relation. The alpha amine group resulted completely deprotonated, while the epsilon amine group presented a deprotonated fraction of 91%.

A CO_2 loaded ***L*-LysK** solution can potentially yield carbonates, carbamates and dicarbamates. The negative charges of the latter should be stable, compared to **EDA**, due to the C_5 carbon chain between the two amine groups, as in **DETA-2s**.

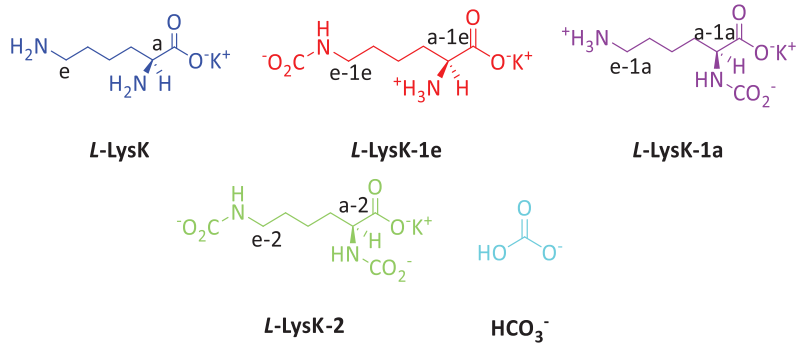

Fig. 56 Adducts of potassium lysinate with carbon dioxide. ***L*-LysK** (blue), epsilon monocarbamate ***L*-LysK-1e** (red), alpha monocarbamate ***L*-LysK-1a** (purple), dicarbamate ***L*-LysK-2** (green), bicarbonate HCO_3^- (light blue).

4.4.1 ^{13}C quantitative NMR speciation

Colored spectra of the ^{13}C qNMR speciation of an aqueous solution of ***L*-LysK** 0.5M can be found in the Annexes (page 214). The results obtained by ^{13}C qNMR speciation are showed in Fig. 57, wherein molar fractions of CO_2-loaded adducts are plotted against increasing $\alpha(CO_2)$. It is possible to observe that until $\alpha(CO_2)$ = 0.4 free amine is consumed to yield exclusively monocarbamates ***L*-LysK-1e** and ***L*-Lysk-1a**, the latter being more abundant.

The low formation of the epsilon carbamate ***L*-LysK-1e** (red), whose maximum abundance is 20%, can be due to the partial protonation of the epsilon-NH_2. Consequently, the dicarbamate ***L*-Lysk-2** (green) is hardly formed, resulting in the least abundant species in the library. Once the solution reaches loading of 0.4, monocarbamates are hydrolyzed to yield carbonates and uncarbamated amine in solution. At high loading the ***L*-LysK**-CO_2 library presents an overall percentage of carbamates of only 7%, while bicarbonates represent a total of 93%.

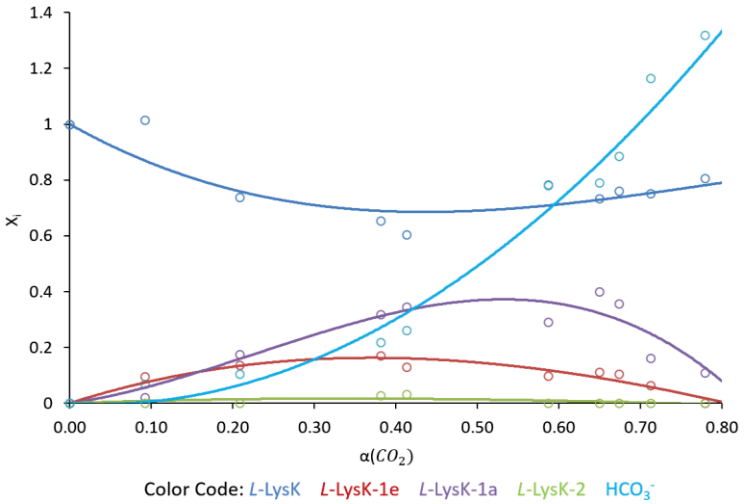

Fig. 57 Chemical speciation of a 0.5M solution of ***L*-LysK**-CO_2 in D_2O. The graph is expressed in molar fraction (X_i) vs loading ($\alpha(CO_2)$). Color code: ***L*-LysK** (blue), epsilon monocarbamate ***L*-LysK-1e** (red), alpha monocarbamate ***L*-LysK-1a** (purple), dicarbamate ***L*-LysK-2** (green), bicarbonate HCO_3^- (light blue). The experimental values (dots) are fitted with 3rd degree polynomial (curve).

To assess the protonation state of the amine upon increasing CO_2 loading, the same 0.5M aqueous solution of ***L*-LysK** was followed with a pH probe throughout the reaction. The potentiometric analysis showed that at $\alpha(CO_2) = 0.5$ the solution presents an overall pH of 8.5 (graph in Annexes, page 210). Consequently, only 26% of α-NH_2 and 0.5% of ε-NH_2 are deprotonated, which explains the low abundance of ammonium carbamates at high loading.

To assess the influence of the substituents on the α,ω-diamine backbone on carbon capture, the ammonium/free amine evolution of ***L*-LysK** and **DETA** were compared. The common feature between *L*-lysine and Diethylenetriamine is the α,ω-diamine backbone, the basic groups are highlighted with red circles in Fig.58. It can be observed that while **DETA**-CO_2 capture is undergoing carbamation, *L*-lysine capture is mainly reacting by carbonation. At loading 0.7 *L*-lysine-monocarbamates are almost completely hydrolyzed to yield carbonates, thereby increasing free amine in solution. It is also observable that the tendency of **DETA** to form carbamates limits its absorption at loading 0.6, while ***L*-LysK** shows higher absorption capacity reaching a maximum experimental loading of 0.8, due to carbonates.

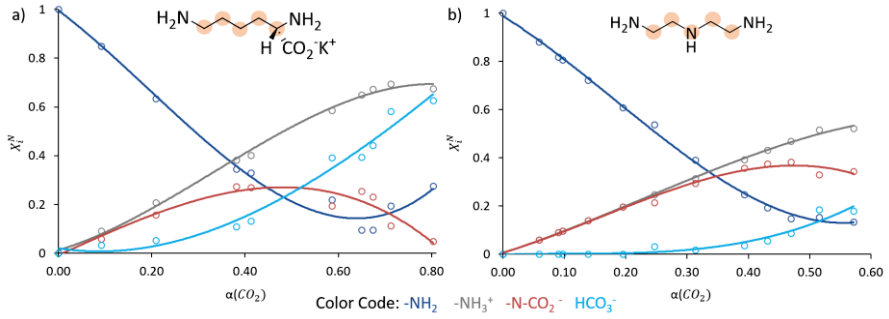

Fig. 58 Molar fraction of free amine (blue), ammonium (gray), (carbamates (red) and carbonates (light blue) versus total CO_2 loading for a) ***L*-LysK** 0.5M, b) **DETA** 0.5M. Red circles highlight the 5 atoms separating the primary amine groups on both amine structures.

4.4.2 Cyclic capacity

Cyclic capacity was measured on the same 0.5M aqueous solution of ***L*-LysK** over three absorption/desorption cycles (Fig.59). *L*-Lysine showed a rich loading of 0.76 ± 0.05 within the three cycles, while desorption reached 0.17 ± 0.09. An experimental error encountered during the second desorption cycle impeded the solution to reach 100 °C, which justifies the different profile of the second cycle as well as the high lean-loading.

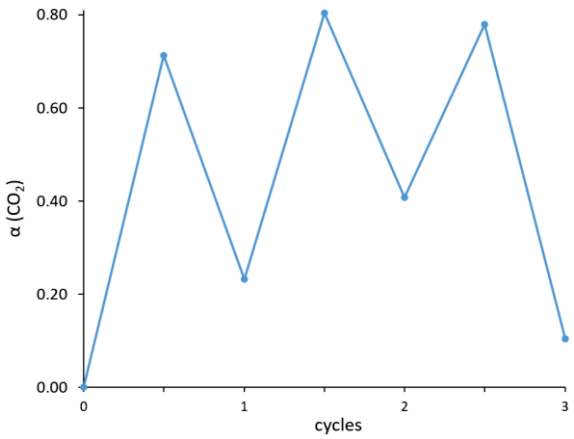

Fig. 59 Cyclic capacity of an aqueous solution of 0.5M of ***L*-LysK**. Rich and lean values of CO_2 loading versus number of absorption/desorption cycles (n = 3).

Overall, ***L*-LysK** presents a cyclic capacity of 0.60 ± 0.14. Coherently with what observed for glycine, the higher cyclic capacity of *L*-lysine could be explained by the higher percentage of bicarbonates in solution (93% at high loading) compared to **EDA** (23% bicarbonates) and **DETA** (34% bicarbonates).

The evolution of carbamates and carbonates wavelengths followed by *in situ* FT-IR of ***L*-LysK** and **DETA** were confronted, to assess the influence of the α,ω-diamine backbone on the kinetics of absorption.

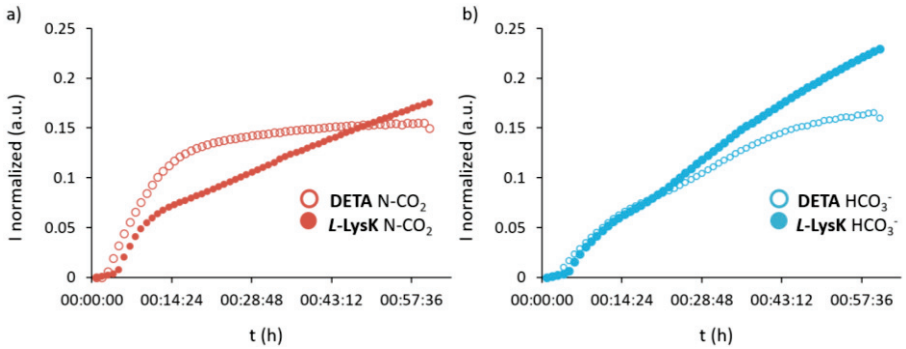

Fig. 60 Evolution of the normalized intensities of wavelengths corresponding to a) carbamate (1320 cm^{-1}, red); b) bicarbonate (1361 cm^{-1}, light blue) for a 0.5M aqueous solution of **DETA** (empty circles) and a 0.5M aqueous solution of ***L*-LysK** (full circles). Both solutions were loaded with a pure flux of CO_2 at 200 mL/min at 25 °C.

It can be observed that the carbamation of *L*-lysine is slower compared to **DETA**, with the same behavior observed for glycine vs **EDA**. Carbonation on the other hand evolves simultaneously at the beginning of the absorption step and grows steeper for *L*-lysine.

Finally, a PCC experiment was run on a 3M aqueous solution of *L*-lysine neutralized with one equivalent of KOH, at 40 °C with a combined flow of CO_2/N_2 at respectively 15% and 85%. The operating parameters were chosen to reflect industrial conditions. The reaction enthalpy for ***L*-LysK** with $\alpha(CO_2) = 0.8$ was measured to be $\Delta_r H^0 = -72.9$ kJ/mol of CO_2, which is close to the optimal absorption enthalpy of sorbents (-70 to -60 kJ/mol of CO_2)[27].

L-lysine appears to be a good potential new sorbent for CO_2 capture, showing maximum experimental loading of 0.8, absorption by carbonation, 0.60 ± 0.14 of cyclic capacity and low enthalpy of absorption.

4.5 *L*-Cysteine

The expertise of the CSAp groups on thiol chemistry, the potential formation of thiocarbonates in water and the metal-binding character of *L*-cysteine were the main factors which lead to the investigation of the neutral amino acid as a CO_2 sorbent.

The thiol group on its side chain gives rise to the possible formation of a disulfide bond in oxidative conditions, forming *L*-cystine, dimer of *L*-cysteine (Fig.61).

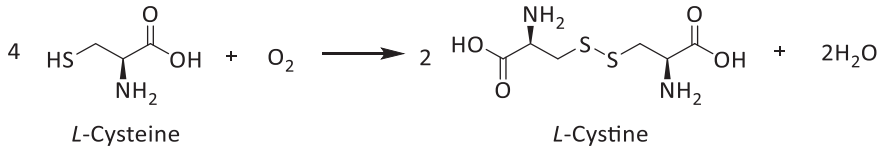

Fig. 61 Oxidation of *L*-cysteine into its dimer *L*-cystine.

There are several ways to prevent the formation of disulfide bonds in solution, for instance degassing water to remove oxygen or prepare the solution and the solvent through a series of freeze-pump steps. Such precaution steps may hamper the industrial process, so it was decided to work in the simplest conditions and investigate the *L*-cysteine-CO_2 system without any preliminary processing.

An aqueous solution of ***L*-CysK** loaded with CO_2 gives rise to two main adducts: monocarbamate ***L*-CysK-1** and bicarbonate HCO_3^- (Fig.62).

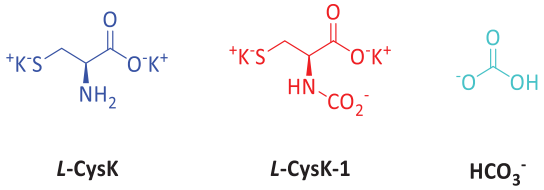

Fig. 62 Adducts of potassium cysteinate loaded with CO_2. Free amine ***L*-CysK** (blue), monocarbamate ***L*-CysK-1** (red), bicarbonate (light blue).

4.5.1 ^{13}C quantitative NMR speciation

To perform a ^{13}C qNMR speciation experiment, a 0.5M aqueous solution of ***L*-CysK** was prepared, neutralizing the amino acid with two equivalents of KOH. The resulting pH of the solution was measured to be 11.63. For the Henderson-Hasselbach relation it was calculated that 99% of the amine was in its deprotonated form and 88% of the thiol was in its sulfide form.

Although sulfides may not act as nucleophiles for carbon capture, in water they can act as a Bronsted base. To take this reactivity into account, the $\alpha(CO_2)$ loading was redefined to moles of carbon dioxide per moles of nitrogen and sulfur moieties (eq.79):

$$\alpha(CO_2)_{S,N} = \frac{moles_{CO_2}}{moles_{R_2NH} * \#\,S,N} = \frac{moles_{CO_2}}{moles_{S,N}} \quad (79)$$

The colored spectra obtained by ^{13}C qNMR speciation can be found in the Annexes, page 212. The speciation of ***L*-CysK** (Fig.63a) shows a fast growth of monocarbamate ***L*-CysK-1** (red) versus bicarbonate (light blue) at low loading. It can be observed that the molar fraction of monocarbamate decreases starting from $\alpha(CO_2)_{S,N}$ = 0.4, indicating its hydrolysis into HCO^-_3. The ammonium bicarbonate (light blue) increases rapidly, and at high loading its species dominate the system. At the end of the speciation the ***L*-CysK-CO₂** library is composed of 21% of monocarbamate and 79% of bicarbonate for a maximal $\alpha(CO_2)_{S,N}$ of 0.7.

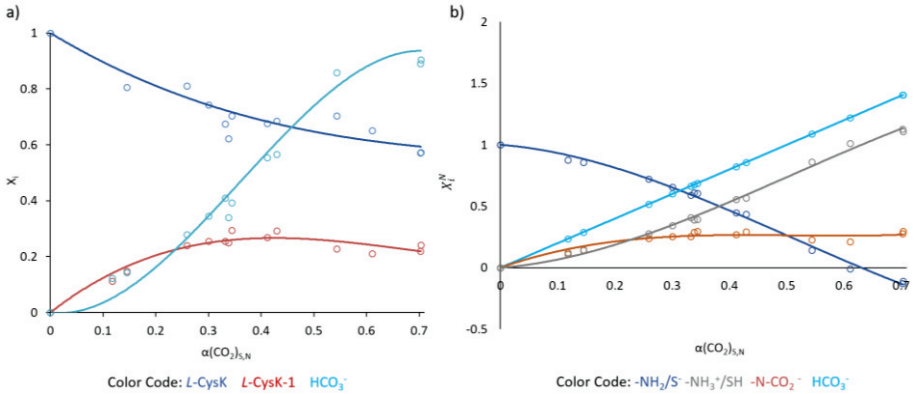

Fig. 63 a) ***L*-CysK**-CO_2 speciation in water. The graph is expressed in molar fraction (X_i) vs loading ($\alpha(CO_2)_{S,N}$). Polynomial fit color code: ***L*-CysK** (blue), monocarbamate ***L*-CysK-1** (red), bicarbonate HCO_3^- (light blue); b) Normalized molar fraction (X_i^N) of amine/thiolate (blue), ammonium/thiol (gray), carbamates (red) and bicarbonates (light blue) for a 0.5M aqueous solution of ***L*-CysK** -CO_2.

In Fig.63b is represented the repartition between amine/thiolate and ammonium/thiol, carbonates and carbamates. It can be observed that, at maximal loading, the amine/thiolate fraction is completely consumed to yield carbamates and ammonium/thiol. The observed tendency was confirmed by a potentiometric analysis. The latter was performed on a 0.5M aqueous solution of ***L*-CysK**, which showed a pH shift from 11.63 to 8.6 upon $\alpha(CO_2)$ loading (graph in Annexes, page 211). Since the thiol group presents a pKa of 10.78, at high $\alpha(CO_2)$ it will be completely protonated into R-SH.

4.5.2 Cyclic capacity

A 0.5M solution of ***L*-CysK** was investigated at 25-100 °C to determine the cyclic capacity of the system. Fig.64 shows two consecutives cycles of CO_2 absorption/desorption from which was obtained an overall value of cyclic capacity of 0.36 ± 0.004. Despite the high

concentration of carbonates, the lean CO_2 loading reaches a minimum of 0.34 ± 0.004, resulting in a poor regeneration of ***L*-CysK**.

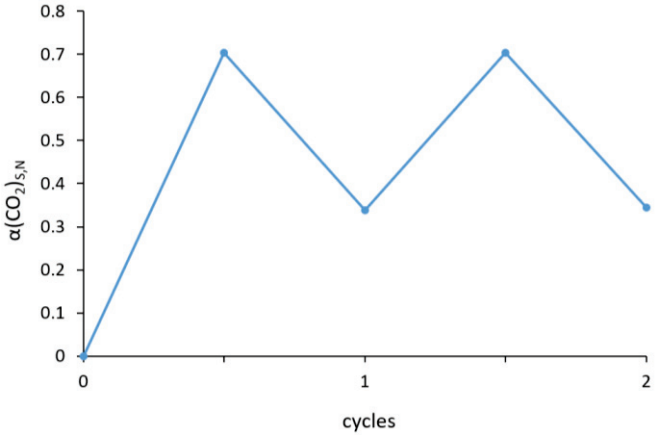

Fig. 64 Cyclic capacity of an aqueous solution of 0.5M of ***L*-CysK**. Value of $\alpha(CO_2)_{S,N}$ loading are plotted against the number of absorption/desorption cycles.

Generally, ***L*-CysK**-CO_2 system shows high maximal $\alpha(CO_2)_{S,N}$ loading with a prevalent carbonation chemistry, although the ineffectiveness of desorption indicates that *L*-cysteine does not represent an ideal solvent for CO_2 capture.

4.6 *L*-Arginine

L-Arginine was chosen for this study as a basic amino acid with a guanidinium group, in order to investigate the influence played by the latter on the amino acid carbon capture thermodynamics, kinetics and chemistry.

A 0.5M aqueous solution of Potassium Argininate was prepared neutralizing the amino acid with one equivalent of KOH. The solution reached a pH of 13.71, which resulted in 99% of deprotonated amine and 94% of deprotonated guanidine group, according to the Henderson-Hasselbach relation.

A qualitative ^{13}C NMR investigation was performed on the resulting 0.5M solution of ***L*-ArgK**, loaded with a pure flux of CO_2 at 25 °C. ^{13}C NMR analysis showed the presence of ammonium carbamate (***L*-ArgK-1**) on the alpha amino group, and bicarbonates. The presence of a guanidinium group enables the formation of single and double bicarbonate salts, ***L*-ArgK**-HCO_3^- and ***L*-ArgK**-$(HCO_3^-)_2$ respectively.

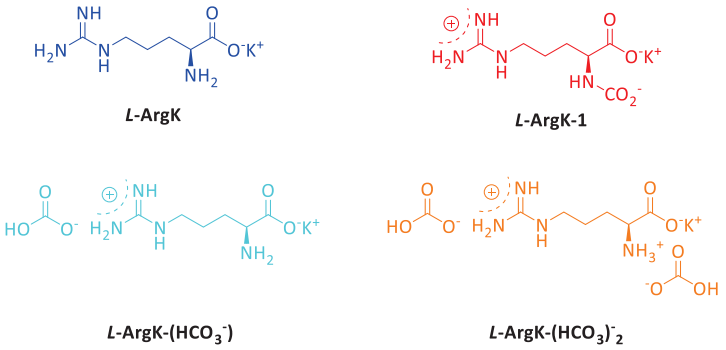

Fig. 65 Potential adducts of ***L*-ArgK**-CO_2 dynamic system. Free amine ***L*-ArgK** (blue), monocarbamate ***L*-Argk-1** (red), guanidinium bicarbonate salt ***L*-ArgK**-HCO_3^- (light blue), ammonium and guanidinium bicarbonate salt (***L*-ArgK**-$(HCO_3^-)_2$) (orange).

L-Arginine was not investigated via a quantitative ^{13}C NMR speciation, although the maximum experimental loading and the carbamate/bicarbonate composition was explored via a cyclic capacity experiment.

4.6.1 Cyclic capacity

A 0.5M aqueous solution of ***L*-ArgK** loaded with CO_2 at 25 °C showed a maximum rich-loading of 0.45 for both absorption cycles. After the desorption step, achieved by flushing N_2 in the solution at 100 °C, the lowest lean-loading was determined at 0.23±0.03, for a final value of 0.21±0.06 of cyclic capacity (Fig.66).

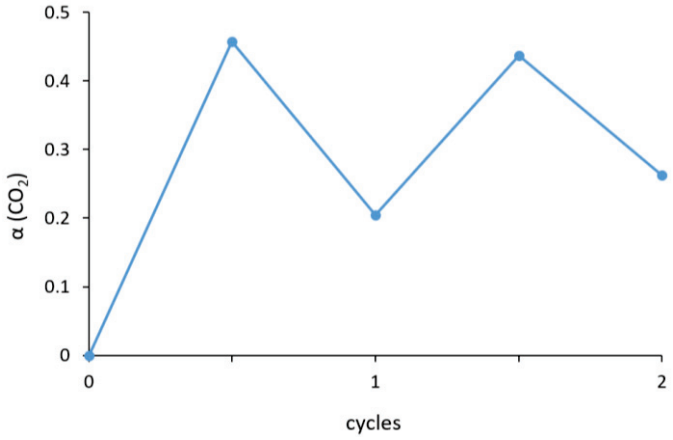

Fig. 66 Cyclic capacity of a 0.5M aqueous solution of ***L*-ArgK** loaded with carbon dioxide. CO_2 loading is fitted with the number of cycles of absorption/desorption performed on the system (n = 2).

From the ^{13}C qNMR spectra obtained for the cyclic capacity of ***L*-ArgK** (Annexes, page 215), it was possible to quantify the molar fraction of free amine, ammonium, carbamate and carbonate for each absorption/desorption step.

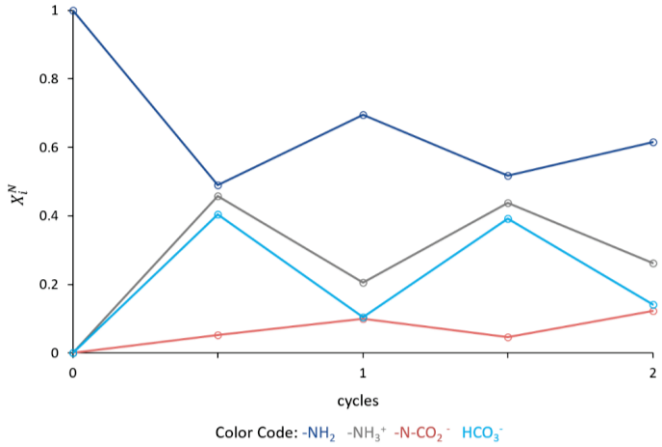

Fig. 67 Repartition of free amine (blue), ammonium (gray), carbamates (red) and bicarbonates (light blue) in a cyclic capacity experiment of ***L*-ArgK** 0.5M. Molar fraction is plotted against the number of absorption/desorption cycle (n = 2).

In Fig.67 the normalized molar fractions are plotted against the cyclic capacity cycles. Monocarbamate ***L*-ArgK-1** presents low abundance throughout the experiments, while bicarbonate is the most abundant CO_2-loaded species for each absorption cycle. At high loading 50% of the amine is in a protonated form, suggesting the formation of a double bicarbonate-ammonium salt upon CO_2 loading (***L*-ArgK**-$(HCO_3^-)_2$).

The ***L*-ArgK**-CO_2 system presented an affinity for bicarbonates, coherently with the guanidinium group nature, and the general set-up showed a low cyclic capacity, compared to other amines investigated in this work, which does not promote its suitability for carbon capture.

4.7 *L*-Aspartic Acid

L-Aspartic Acid is the only αAA with an acid R-chain investigated in this thesis. As for the other AAs, ***L*-Asp** was neutralized with two equivalents of KOH; the 0.5M ***L*-AspK** aqueous solution presented a pH of 10.6, for an overall 85% of deprotonated amine.

Upon CO_2 loading, ***L*-AspK** can yield monocarbamate **L-AspK-1** and bicarbonate (Fig. 68).

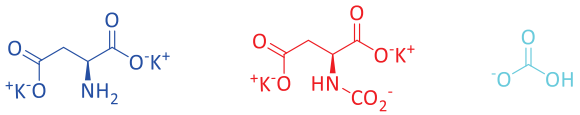

Fig. 68 CO_2 loaded adducts of ***L*-AspK**, free amino acid (blue), monocarbamate ***L*-AspK-1** (red), bicarbonate HCO_3^- (light blue).

4.7.1 Cyclic capacity

As for ***L*-ArgK**, no complete speciation was performed on this αAA. A cyclic capacity was run in the same conditions described in section 3.2: 0.5M aqueous solution followed by *in situ* FT-IR and at 25-100 °C and followed by ^{13}C qNMR analysis (spectra can be found in the Annexes, page 216). Throughout the absorption phases potassium aspartate reached loadings of 0.67 ± 0.004 moles of CO_2 per mole of nitrogen, while during desorption phases the minimum loading is reached at 0.27 ± 0.002 moles of CO_2 per mole of nitrogen, for a final value of cyclic capacity for ***L*-AspK** of 0.4 ± 0.002.

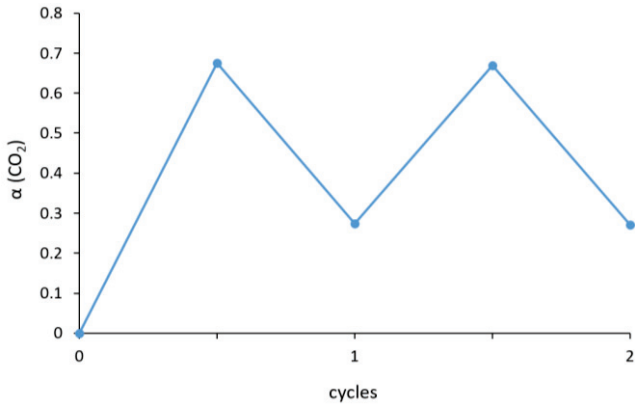

Fig. 69 Cyclic capacity of a 0.5M solution of ***L*-AspK**. The value of CO2 loading is fitted with the number of absorption/desorption cycles (n = 2).

Results from a ^{13}C qNMR analysis were used to gain further information about the composition of the system in both the absorption and the desorption phases. The normalized molar fractions of free amine, ammonium, carbamate and carbonate are plotted in Fig.70 versus the number of absorption/desorption cycles.

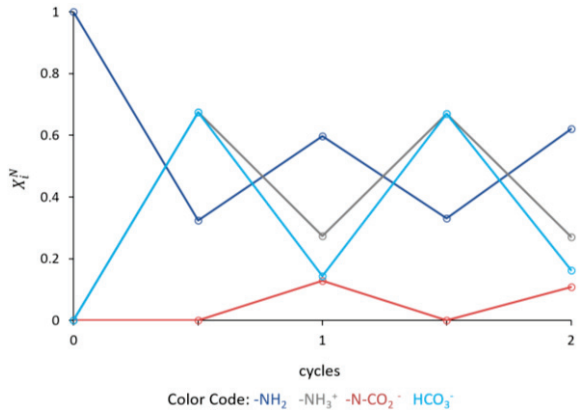

Fig. 70 Normalized molar fractions of free amine (blue), ammonium (gray), carbamates (red) and bicarbonates (light blue) in a cyclic capacity experiment of a 0.5M aqueous solution of ***L*-AspK**, plotted against the number of absorption/desorption cycle (n = 2).

Visibly, at high loading the system is driven by carbonation, while at low values of $\alpha(CO_2)$ both carbamate and carbonate are present in solution. The formation of monocarbamates at low loading could explain the limited CO_2 desorption and the lower cyclic capacity of ***L*-AspK** compared to *L*-lysine and glycine. As observed for arginine, these characteristics do not promote the suitability of aspartic acid salts for carbon capture.

5 Conclusions to chapter 2

Throughout this second chapter, properties for carbon capture such as maximum experimental loading, cyclic capacity and enthalpy of absorption were investigated for seven different amines. The investigation was performed via a molecular approach as new CO_2 loaded adducts were identified and quantified for each dynamic combinatorial library. In Table 13 are reported the experimental results discussed in this chapter.

Table 13 Values of maximum experimental CO_2 loading, bicarbonate/carbamate composition of the systems at maximum loading, cyclic capacity and enthalpy of absorption for 0.5M aqueous solutions of **DETA**, **EDA**, ***L*-LysK**, ***L* -CysK**, **GlyK**, ***L*-ArgK**, ***L*-AspK** determined by experiments performed in this work. * value at 20 °C.

Amine	Solubility in water (g/L) at 25 °C	α_{exp}^{max}	HCO_3^-	N-CO_2^-	CC	-$\Delta_r H^0$ (kJ/mol of CO_2)
EDA		0.6	27%	73%	0.5 ± 0.03	89.03
DETA		0.57	34%	66%	0.46 ± 0.01	82.42
GlyK	253.1	0.8	91%	9%	0.65 ± 0.04	68.61
***L*-LysK**	1000*	0.8	93%	7%	0.60 ± 0.14	72.9
***L*-CysK**	25	0.7	79%	21%	0.36 ± 0.04	/
***L*-ArgK**	87.1	0.45	90%	10%	0.21 ± 0.06	/
***L*-AspK**	5.3	0.7	100%	/	0.4 ± 0.002	/

It can be observed that at high loading industrial polyamines such as **DETA** and **EDA** present a chemistry of carbamation with relatively high cyclic capacity, comprised between 0.46 and 0.5. For the literature, the enthalpy of absorption of **EDA** and **DETA** (correspondingly -89.03 kJ/mol of CO_2 and -82.42 kJ/mol of CO_2) is considered too high, which indicates that these polyamines are not the most suited solvents for carbon capture. Contrary to industrial polyamines, the five amino acids show a chemistry of bicarbonates. The highest cyclic capacity values were obtained with *L*-lysine and glycine (respectively 0.52 and 0.65), which also reported the lowest enthalpy of absorption (correspondingly -72.9 kJ/mol of CO_2 and -68.61 kJ/mol of CO_2).

Those characteristics led to the conclusion that, within the seven amine systems observed in this chapter, glycine and *L*-lysine present the most promising properties for further carbon capture applications.

In the context of carbon capture utilization and storage, determining an efficient carbon sorbent is fundamental, although not sufficient. The integrated carbonation of metals is also a critical aspect, which will be furtherly illustrated and discussed in the next chapter.

Chapter 3
Integrated Absorption Mineralization (IAM)

Chapter 3

Objective

The third chapter of this thesis will focus on Integrated Absorption Mineralization (IAM) as a CCUS strategy combining amine-based CO_2 capture and mineral carbonation. The state of the art will present recent examples of IAM with various industrial amines and amino acids, applied to calcium and magnesium-based salts. The chemical regeneration of the amine sorbent will be discussed, as well as cyclic IAM processes and present applications for CO_2 capture from flue gases.

In this chapter, **DETA**, **EDA**, ***L*-LysK**, ***L*-CysK** and **GlyK**, previously explored for their carbon capture properties, will be investigated for the integrated carbonation of metals. The study will be divided into two model-substrates systems: chlorides and oxides. In the first system the amines will be tested for their ability to carbonate $MgCl_2$ and $CaCl_2$, in both homogeneous and heterogeneous conditions. In the second system, alkaline and transition metal oxides will be treated via mechanochemistry by CO_2-loaded amines.

These two model systems were chosen as intermediary to the CO_2 metal-free amine libraries presented in Chapter 1 and real and complex system, which will be presented in Chapter 4. For both models the study will be focused on the carbonation yield of metals, carbon capture efficiency and chemically assisted amine regeneration.

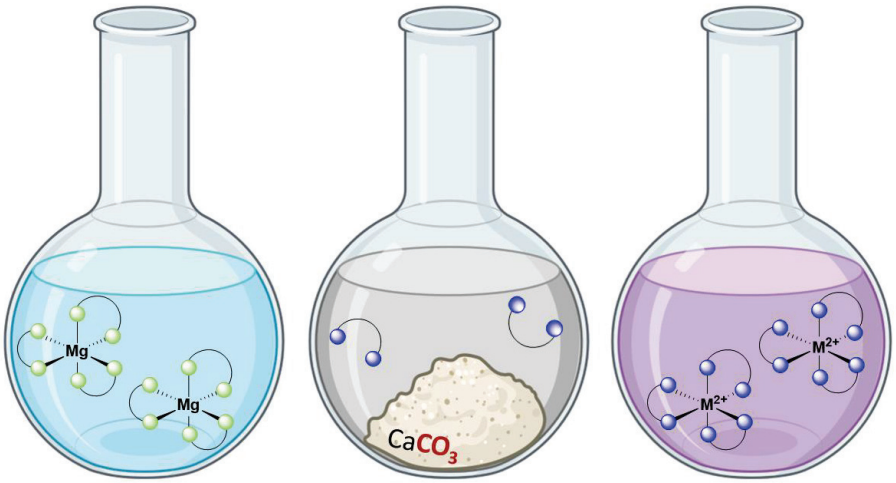

Chapter 3

1 State of the art

The concept of Integrated Absorption Mineralization was previously introduced in Chapter 1 section 2.3, as an alternative strategy to conventional amine scrubbing and *ex situ* mineral carbonation. The IAM technique couples the CO_2 absorption properties of amine solvents with the downhill[115] reaction of mineral carbonation, in a single CCUS process[179].

The interest of creating such innovative routes relies on the need to decrease the energetic expenditures of amine scrubbing, specifically the thermal desorption and solvent regeneration step. The formation of mineral carbonates can be performed at 40 °C[180-181], like for the CO_2 absorption step, enabling chemical regeneration[182] of the amine sorbent and eliminating thermal desorption. At the same time, IAM proposes an alternative for conventional *ex situ* mineral carbonation, as it removes the need of pH-swings necessary[24] to yield $CaCO_3$ and $MgCO_3$ from Ca, Mg-based minerals.

Hereafter are summarized the IAM processes reported in the literature[99, 180-181], divided in two alternative approaches: one-pot and two-pots.

The first strategy consists in a one-pot IAM reaction, wherein an aqueous solution of amine is mixed with solid calcium or magnesium-containing salts, forming a reactive slurry (Fig.71a). The mixture is then loaded with carbon dioxide, which is introduced in the reactor as a pure gas or as a CO_2/N_2 mixture.

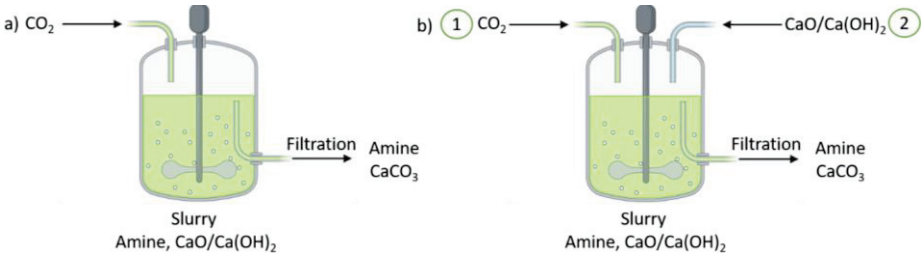

Fig. 71 One-pot IAM reaction. a) CO_2 is directly introduced into a slurry of aqueous amine and Ca^{2+} salts. Once the mineralization reaction is complete the mixture is filtered yielding $CaCO_3$ and the regenerated lean amine solution; b) CO_2 is introduced into an aqueous solution of amine until it reaches saturation (step 1), solid Ca^{2+} salts are added to the solution (step 2); the resulting slurry yields $CaCO_3$ and regenerated amine, which are separated upon filtration. Adapted from Liu *et al.*[99].

Carbon dioxide is captured by the amine, yielding ammonium carbamates and carbonates (eq.53 and 49)[7]. Simultaneously, the metal oxide salts are hydrolyzed into metal hydroxides (eq.50), which can then react with bicarbonates ion present in solution (eq.51). Ammonium

carbamates can then act as CO_2 transient species, and $Ca(OH)_2$ and $Mg(OH)_2$ can enhance their hydrolysis leading to the formation of carbonate salts (eq.54) and amine regeneration (eq.55).

$$2\,R_2NH + CO_2 \longrightarrow R_2NH_2^+ + R_2NCO_2^- \quad (53)$$

$$R_3N + H_2O + CO_2 \longrightarrow R_3NH^+ + HCO_3^- \quad (49)$$

$$CaO + H_2O \longrightarrow Ca(OH)_2 \quad (50)$$

$$HCO_3^- + Ca(OH)_2 \longrightarrow CaCO_3 + H_2O + OH^- \quad (51)$$

$$R_2NCO_2^- + Ca(OH)_2 \longrightarrow R_2NH + CaCO_3 + OH^- \quad (54)$$

$$R_2NH_2^+ + OH^- \longrightarrow R_2NH + H_2O \quad (55)$$

Once the metal feedstock is totally converted into metal carbonates, the slurry is filtered, enabling the simultaneous recovery of the solid product and the lean amine solution. One-pot IAM can also take place in two consecutives steps (Fig.71b). In this case a solid metal salt is introduced into an amine solution after its saturation with carbon dioxide. The mixture is then filtered and $CaCO_3$ and amine are recovered separately.

The reaction can also be performed in a two-pots set-up (Fig.72). First, the amine solution is introduced into an absorber tank and loaded with carbon dioxide[99, 182], yielding ammonium carbamates and carbonates (eq.53 and 49).

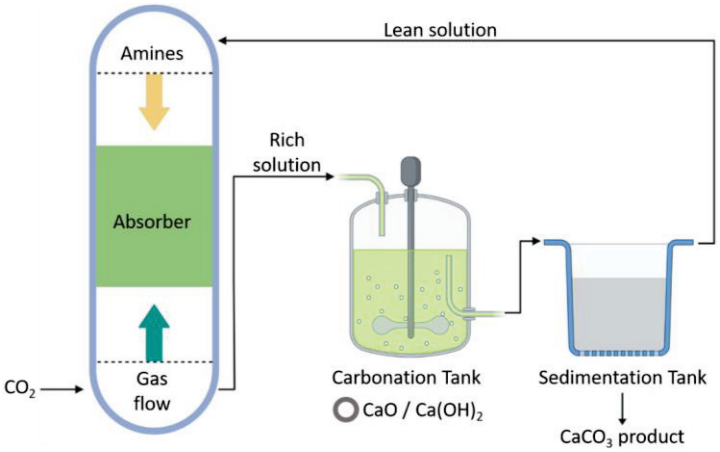

Fig. 72 Two-steps IAM reaction. Carbon dioxide is captured from flue gases in an amine absorber, yielding a CO_2 rich solution, which is introduced in a carbonation tank containing Ca^{2+}-bearing salts. Once the reaction is complete, the slurry is transported in a sedimentation tank from which are recovered the solid $CaCO_3$ product and the lean amine solution. The latter can be then reintroduced in the absorption tank and reused for further carbonation cycles. Adapted from Zhang *et al.*[182].

The CO_2-rich solution is then poured into a reactor containing the metal salt, where metal hydrolysis (eq.50) and CO_2 transfer reactions, from ammonium carbamates and carbonates to metal carbonates, take place (eq.51, 54). The resulting slurry is stirred until complete conversion of metal oxides into carbonates. The mixture can then be transferred to a sedimentation tank to separate the solid from the lean amine solution. The chemically regenerated amine obtained during one-pot and two-steps IAM processes, can potentially be reused for further capture and mineralization cycles[115].

1.1 IAM with industrial amines

The literature presents several examples of IAM with a variety of industrial amines and mineral substrates. The most investigated amines are **MEA**, **DEA**, **MDEA**, **AMP** and **PZ**, for their high CO_2 absorption capacity and fast absorption rates, previously discussed in Chapter 2[65, 71, 183].

In a study published in 2017, Arti *et al.*[180] compared the efficiency of mineral and thermal regeneration of a CO_2-saturated solution of **AMP**. Thermal stripping was accomplished by heating the solution at 90 °C for 70 min, achieving 68% of CO_2 desorption. Mineral regeneration on the other hand was performed by introducing $CaCl_2$ in a 1:1 ratio with captured CO_2, converting 97.4% of ammonium carbamate/carbonate into calcium carbonate within 30 min. Arti *et al.* also investigated the IAM process on **MEA**, **DEA** and **MDEA.** The results are reported in Table 14. It can be observed that all four amines present higher desorption rates via mineral desorption compared to thermal desorption. In addition, the cyclic capacity is 1.3−3 times higher, providing an example of efficient amine regeneration with no thermal degradation drawback[180].

Table 14 Comparison between thermal and mineral desorption on an IAM process with CO_2-loaded amines and $CaCl_2$. Values extracted from the study of Arti *et al.*[180]; cyclic capacity (CC) expressed in mol of CO_2 per mol of amine, absorption and desorption rate expressed in mmol/(mol*s), mass yield expressed as $CaCO_3$(g)/$CaCl_2$ (g).

R_2NH	Thermal desorption			Mineral desorption					
	CC	Abs rate	Des rate	CC	Abs. rate	Des. rate	Initial pH	Final pH	Mass yield $CaCO_3$
MEA	0.22	0.204	0.054	0.64	0.204	0.355	8.10	6.8	0.24
DEA	0.49	0.200	0.108	0.66	0.200	0.383	8.09	6.6	0.63
MDEA	0.50	0.163	0.138	0.65	0.163	0.526	8.50	6.7	0.62
AMP	0.52	0.192	0.083	0.73	0.192	0.352	8.60	5.9	0.75

Arti *et al.* also reported a noticeable pH shift of the amine/Ca solution during CO_2 capture. In a conventional mineral carbonation process, the formation of MCO_3 is obtained first by adding a strong acid (i.e. HCl) to mineralize the metal-bearing mineral, followed by a strong base to induce carbonate precipitation, and this represents a pH swing. In an IAM system both pH changes are spontaneous: first the addition of a metal salt decreases the overall pH of the system, inducing the hydrolysis of ammonium carbamates into bicarbonates and carbonates ions, second the formation of $CaCO_3$ induces the regeneration of the amine, causing a final pH increase (eq.51 and 54).

In 2021, Liu and Gadikota[115] proposed an IAM process with either **MEA** or **AMP** to mineralize CaO, $CaSiO_3$, and MgO, which are abundant constituents of fly ash, an alkaline industrial residue. The experiments were performed on a slurry at 75 °C, with a partial pressure of CO_2 (p_{CO_2}) of 1 atm, a 15wt% solid and a 300 rpm stirring rate for a reaction time of 3h.

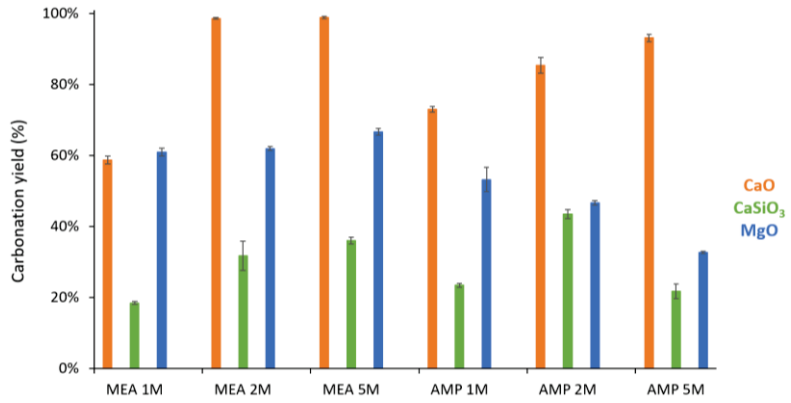

Fig. 73 Carbonation yield (%) of CaO (orange), $CaSiO_3$ (green) and MgO (blue). Reactions performed with **MEA** and **AMP** at 1M, 2M and 5M at 75 °C, p_{CO_2} 1 atm, 3h, 300 rpm. Results reported by Liu *et al.*[115].

It can be observed that $CaSiO_3$ is the least reactive metal salt with a maximum carbonation yield of 42% with 2M **AMP**. This phenomenon is due to the lower dissolution rates of calcium silicates, compared to CaO, and to the formation of passivating silica layers which inhibit the carbonation reaction (eq.80, 81)[99, 184-185].

$$CaSiO_3 + H_2O \longrightarrow Ca(OH)_2 + SiO_2 \quad (80)$$

$$Ca(OH)_2 + CO_2 \longrightarrow CaCO_3 + H_2O \quad (81)$$

Calcium oxide proves to be the most reactive substrate, with a carbonation yield of 98.9% with 5M **MEA**, while in the same operating conditions MgO attains a maximum carbonation yield of 66.6%. The higher solubility product (pKs) of $Mg(OH)_2$, compared to $Ca(OH)_2$ (pKs = 11.15 and 5.19, respectively) can affect its reactivity, resulting in a lower carbonation yield compared to CaO[186]. Coherently with the IAM chemical desorption principle, the amine regeneration yield parallels the yield of mineral carbonation, which means that the CaO system enables higher amine recovery yields compared to $CaSiO_3$ and MgO.

A study published in 2021 by Ji *et al.*[181] proposed two IAM reactions, **MEA**/$Ca(OH)_2$ and **PZ**/ $Ca(OH)_2$, in a one-pot, one-step set-up. 600 mL of a 0.5 M aqueous solution of amine were mixed with 2 equivalents of $Ca(OH)_2$, and the slurry was set at 55 °C under constant stirring. Contrary to previous reports, in which CO_2 was introduced as a pure gas, Ji *et al.* introduced a CO_2/N_2 (40:60 ratio) mixture into the slurry. This was chosen to check the efficiency of mineral carbonation for carbon capture from industrial-type flue gases.

Overall, $CaCO_3$ was obtained with an 87% purity with both amines, while CO_2 capture was observed to be more efficient with Piperazine than with **MEA** (97% and 90% removal, respectively). Mineral carbonation can entail potential amine loss, due to the absorption of the latter within carbonated products. To assess the extent of **MEA** and **PZ** loss, two samples of $CaCO_3$ were tested by TGA (Thermogravimetric Analysis) experiments. One sample was collected after filtration while the other was collected and washed with ultrapure water. Both solids were then dried at 60 °C overnight. TGA results showed that 0.65 mmol/g of **MEA** were lost in the unwashed sample, while no amine could be detected in the washed solid. In the case of **PZ**, no amine was detected in either solid, a phenomenon which could be explained by the higher pKa value of **PZ** compared to **MEA** (9.73 and 9.5, respectively). The higher affinity of PZ towards H^+ ions reduces the concentration in free amine in solution, reducing its retention in the solid[181].

In 2020, Zhang *et al.* investigated a cyclic experiment with a mixture of **MEA**/**MDEA** and $Ca(OH)_2$[182] (Fig.74). Following the two-steps set-up showed in Fig.72, a 2M aqueous solution of **MEA**/**MDEA** was loaded with a pure flux of CO_2 at 20 °C and then poured in a reactor containing $Ca(OH)_2$. In order to promote CO_2 stripping and chemical regeneration of the amine, the calcium hydroxide amount was calculated to reach a CO_2/Ca molar ratio of 1:1.

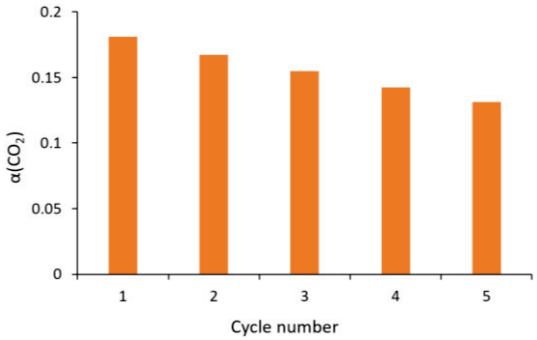

Fig. 74 CO_2 loading (α(CO_2), expressed in moles of CO_2 per moles of nitrogen on the amine backbone) of a 2M **MDEA**/**MEA** solution in five cycles of CO_2 absorption and chemical regeneration. Experiments performed with CO_2/Ca ratio of 1:1 at 20 °C, stirring rate 600 rpm, reaction time of 30min. Results reported from Zhang *et al.* [182].

The carbonation reaction was then performed at 20-60 °C for 30 minutes, stirred at 600 rpm. After the solid carbonate was collected, the amine lean solution was reused for four consecutive absorption/mineralization cycles, showing an average cyclic capacity of 0.537 (α(CO_2) = mol(CO_2)/moles of N) and a constant absorption decrease of 5% throughout the five consecutives cycles.

By the examples reported in the literature is possible to affirm that Integrated absorption mineralization is an extremely versatile strategy applicable to various amine sorbents and metal feedstocks. It is also possible to observe that, despite the use of different operating conditions, the carbonation yields and amine recovery are generally satisfactory.

1.2 IAM with αAA

IAM reactions were also tested with glycine, as a potential natural substitute for industrial amines. CO_2-capture efficiency and mechanism of glycine was investigated in this work and discussed in Chapter 2, where it was observed that the αAA forms both ammonium-carbamate (eq.82) and carbonate (eq.83) adducts upon CO_2 capture, with a majority of the latter (91%) (Fig 52, page 90, glycine speciation).

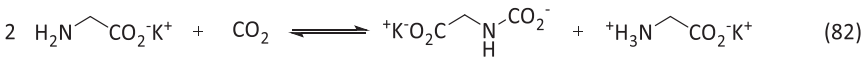

(82)

(83)

In 2020 Liu *et al.*[109] reported a series of experiments performed with 1M **GlyNa** and 15wt% of CaO, $CaSiO_3$. The reactions were performed in a one-pot set-up, for 3h, at a stirring rate of 300 rpm and at temperatures between 25 °C and 90 °C.

The results obtained Liu and Gadikota are reported in Fig.75. As previously observed, calcium silicate presents low carbonation yield compared to CaO, with a slight increase for experiments performed at 75 °C ($CaCO_3$ < 40%), compared to experiments performed at 25 °C and 55 °C. Coherently with its higher reactivity, calcium oxide presents elevated carbonation yields, comprised between 77% and 97%[109]. In the IAM pathway, lower temperatures favor the thermodynamics of carbon capture, while higher temperatures favor the kinetics of mineral dissolution and carbonate precipitation. For this reason, higher carbonation yield is reached at higher temperatures.

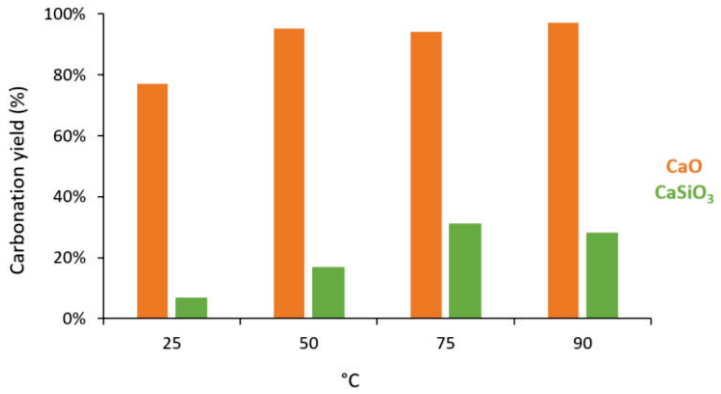

Fig. 75 Carbonation yield (%) of CaO (orange) and $CaSiO_3$ (green) for IAM experiments with 1M **GlyNa**, 15wt% solid, for 3h at 300 rpm at different temperatures (25 °C, 50 °C, 75 °C and 90 °C). Results reported from Liu *et al.*[109].

In the same operating conditions (1M amine, 75 °C, 3h, 15wt% CaO), CaO carbonation is more efficient with glycine (97%)[109], than with **MEA** (60%)[115]; this phenomenon could be explained by the different CO_2-capture mechanism of **MEA** and **GlyNa**. While monoethanolamine yields mainly ammonium carbamates[68-69], required to hydrolyze into bicarbonates, **GlyNa** directly yields bicarbonates ions in solution, enhancing the mineral carbonation reaction.

A mineral carbonation reaction involving MgO and **GlyNa** was performed by Liu *et al.* at 0.5 M, 1 M and 2.5 M amine concentrations[115], yielding 67%, 88% and 74% of $MgCO_3$, respectively.

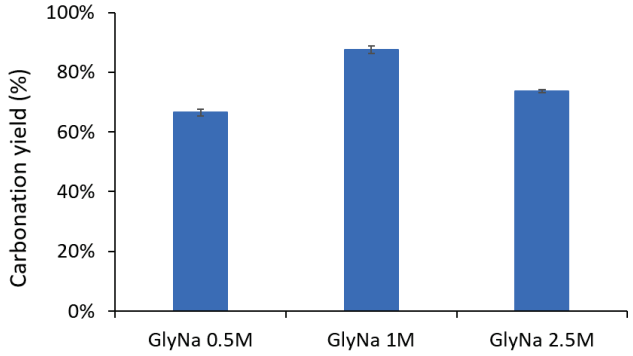

Fig. 76 Carbonation yield (%) of MgO (blue). Reaction performed with **GlyNa** at 0.5M, 1M and 2.5 M at 75 °C, p_{CO_2}1 atm, 3h, 300 rpm. Results reported by Liu *et al.*[115].

As previously observed with CaO, the carbonation extent of MgO is higher when treated with a 1M solution of Sodium glycinate (88%) at 75 °C, compared to 1M **MEA** (61%). Again, the different carbonation yield can be attributed to the higher concentration of bicarbonate salts in a **GlyNa** solution.

When magnesium oxide is treated with a 2.5M solution of **GlyNa**, its carbonation decreases (74%). The phenomenon can be due to the higher viscosity of the solution, which inhibits mineral dissolution and, consecutively, mineral carbonation[115].

Overall, Integrated Absorption Mineralization proves to be an efficient and valid alternative strategy to conventional amine scrubbing and *ex situ* mineral carbonation. The chemical regeneration of amine solvents could drastically reduce the energy penalty and costs of amine scrubbing[7, 27, 44], while generating mineral carbonates which are valuable products in various markets[42, 187]. Furthermore, the lower operational temperature could prevent amine degradation and tank corrosion [188-189], avoiding potential environmental issues.

In the next sections will be presented a variety of IAM processes performed with two industrial polyamines (**DETA** and **EDA**) and three αAA (**GlyK**, ***L*-LysK** and ***L*-CysK**).

First, the influence of the amines on mineral carbonation will be investigated in solution with metal chloride salts in both homogeneous and heterogeneous conditions. Then, IAM reactions will be performed via mechanochemical reactions for the carbonation of metal oxides. The investigation of both chloride and oxide salts will help gain fundamental knowledge over reactivity, carbonation efficiency and amine regeneration of two model systems.

1.3 Metal leaching and carbonation by mechanochemistry

In this thesis, mechanochemistry was chosen as a greener technique [190], since it has proven to be an efficient alternative to solution reactions, while involving considerably lower amounts of solvents[191].

Mechanochemistry is defined as the chemical and physicochemical transformation of compounds during the aggregation caused by the mechanical energy[192]. It presents several advantages, such as simplicity, lower reaction time and solvent waste reduction [193,194]. During a mechanochemical process, the solid reagents can undergo particle size reduction[24], crystalline structure decomposition, specific surface area expansion, and bond breakage[195]. In complement, this mechanical activation can lower the activation energy required for the reaction, increasing reactivity[194-195].

Mechanochemistry is applied in numerous fields, such as chemical engineering, organic synthesis, building and coal industry, pharmacy and extractive metallurgy. For the latter, mechanochemistry has proven to be a useful tool for metal lixiviation and recovery from industrial wastes[194-195].

There are two types of mechanochemical set-ups for metal lixiviation: dry grinding and wet grinding. In the former the metal-bearing material is grinded to reduce size particles and increase the reactive surface area, then the material is mixed in a separate reactor with a leaching solution, usually containing acids or chelating agents[196-197]. The latter consists in a one-pot process in which the material is mixed with the leaching solution directly in a grinding reactor[194].

An example of metal recovery was provided by the extraction of Lithium and Cobalt contained in Lithium batteries with PVC (polyvinyl chloride). After 30h of grinding the reaction reported in eq.84 yielded 100% and 90% of cobalt and lithium chlorides, respectively[198].

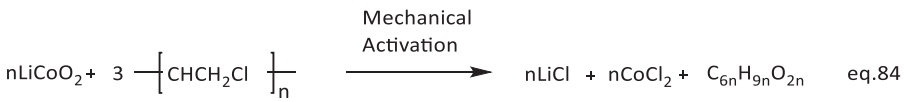

$$nLiCoO_2 + 3\left[CHCH_2Cl\right]_n \xrightarrow{\text{Mechanical Activation}} nLiCl + nCoCl_2 + C_{6n}H_{9n}O_{2n} \qquad \text{eq.84}$$

In 2000, Zhang *et al.* proposed a dry-grinding process to extract lithium and cobalt from lithium batteries[199]. $LiCo_{0.2}Ni_{0.8}O_2$ was grinded with Al_2O_3 for 60 minutes and then the resulting solid was introduced in a leaching solution of HNO_3 1N, obtaining 90% extraction of Co, Ni and Li.

Another example is the extraction of lead from Cathode-Ray tube (CRT) glass. While conventional leaching processes enabled the extraction of 5% of Pb, a wet grinding reaction with 5M NaOH at 70 °C reached 97% of metal extraction[200].

In the early 2000's Zhang *et al*.[201] and Wang *et al.*[202] proposed the transformation of waste metal oxides into sulfides via mechanochemical reactions. The use of an additive such as iron or aluminum triggered the transformation of metal oxides into sulfides (eq.85, 86 respectively), the reaction has proven applicable also to lead and copper oxides.

$$4ZnO + 4S + 3Fe \xrightarrow[3h,\ 500rpm]{} 4ZnS + Fe_3O_4 \qquad \text{eq.85}$$

$$3ZnO + 3S + 2Al \xrightarrow[3h,\ 500rpm]{} 4ZnS + Al_2O_3 \qquad \text{eq.86}$$

In this thesis mechanochemistry was chosen as an innovative tool for the carbonation and leaching of pure metal oxides by CO_2-loaded amines, i.e. via IAM reactions. Considering the applications of dry and wet grinding depicted in the literature, the concomitant leaching of each metal will be investigated and discussed. This will allow to obtain a general overview on the carbonation/leaching behavior of metals in H_2O/amine/CO_2 ternary systems.

2 Methods

The experiments presented in this chapter can be divided into three main classes: speciations, carbonation, and mechanical grinding. The studies were performed to assess the amine catalytic effect on metal carbonation, to quantify the potential modification of carbamate/carbonate repartition in the amine libraries induced by the metal salts and to identify the conditions promoting metal carbonation.

In this section, will be presented the objective and the general methods followed in the experiments, while further information on materials and reagents can be found in the experimental section, page 198.

2.1 Study of metal-amine-CO_2 homogeneous system by NMR speciation

In this chapter, the speciation experiments are performed in ternary mixtures of CO_2-amines-$MgCl_2$. The objective, as for the amine-CO_2 speciation experiment reported in Chapter 2, is to analyze the evolution of the CO_2-amine dynamic combinatorial library (DCL) induced by the presence of soluble metal salts.

Unless otherwise stated, the speciation experiments were performed on a 0.5M solution of amines in D_2O, with an internal reference fixed at 0.05M and 0.25 equivalents of metal chloride salt with respect to the amine. The solution was divided in 10 aliquots and loaded with increasing quantities of CO_2, determined by gravimetric analysis. Each sample was then analyzed by ^{1}H and ^{13}C quantitative NMR (qNMR) to identify and quantify the amine-CO_2 adducts within the DCL.

The evolution of the library is then monitored by plotting the molar fraction of each species vs $\alpha(CO_2)$, the CO_2 loading is defined as eq.31:

$$\alpha(CO_2) = \frac{\sum n_i * \#_{(CO_2)i}}{moles_{R_2NH} * \#N} \quad (31)$$

As a reminder, $\#_{CO_2}$ is the number of CO_2 molecules bound to the specie "i" and N the number of nitrogen atoms in the amine structure. This experimental loading is therefore expressed as moles of CO_2 per mole of nitrogen sites on the absorbent.

2.1.1 Amplification Factors

The binding of each metal salt with either monocarbamates, polycarbamates or bicarbonates should modify the repartition of the species in the amine-CO_2 library.

The metal can therefore act as a template. Its effect can be quantified by calculating the amplification factors, defined as the difference between the molar fraction of a species "i" in the templated library (X_i^M) and the molar fraction of the same species in the untemplated library (X_i^0), divided by the molar fraction of the metal template itself (X_M^0) (eq.87):

$$AF_i^M(\alpha) = \frac{X_i^M(\alpha) - X_i^0(\alpha)}{X_M^0} \quad (87)$$

By construction, the sum of the amplification factors should equal zero:

Where "M" indicates the system in presence of metal template. The X_i used in those calculations are provided by the polynomial model. If the model deviates, it can entail a concomitant deviation of the mass balance of the CO_2-loaded species (eq.88). For this reason, the evolution of eq.88 is calculated for each $\alpha(CO_2)$ and used as an indicator of the accuracy of the model. Only values over this indicator were considered significant in this work.

2.2 Study of metal-amine-CO_2 heterogeneous system

The procedure of the investigation of heterogeneous systems is similar to the speciation. First, a 0.5M solution of amine is prepared in deionized H_2O with 0.25 equivalents of a metal chloride salt, then the solution is divided in aliquots of 4 mL and loaded with increasing quantities of CO_2, assessed by gravimetry. At low loading ($\alpha < 0.15$) the precipitation starts after 20/30 minutes, while it is faster (< 15 min) at high loading ($\alpha > 0.30$). The precipitate is then left to stabilize for 6-12 h. Afterwards, the samples are centrifuged at 500 rpm for 10 minutes and the solid is washed with 1 mL of deionized water. All liquid and solid phases are then gathered and lyophilized.

In order to analyse the repartition of each building block (CO_2, amine, metal) in each phase, three different analyses are performed: ^{1}H qNMR to quantify the amine, volumetric analysis to quantify the amount of CO_2 and ICP-OES analysis for the quantification of the metal. Finally, the stoichiometry between amine, metal and CO_2 in both liquid and solid phase, provides an indication on the nature of the precipitate which could be either a metal carbonate or an insoluble metal carbamate complex. Additional analysis such as TGA-MS and XRD would be required to define the exact composition of the solid and liquid phases.

2.3 IAM by mechanochemistry

In this chapter, metal leaching and carbonation experiments were performed on metal oxides with both Liquid Assisted Grinding (LAG)[203] and neat grinding techniques. The simple distinction between neat grinding and liquid assisted grinding depends on the amount of solvent employed. The critical parameter is “eta”, η, expressed in µL of solvent per mg of solid reactant. For neat grinding, η = 0, while for LAG experiments η can be between 0 and 2 µL/mg.

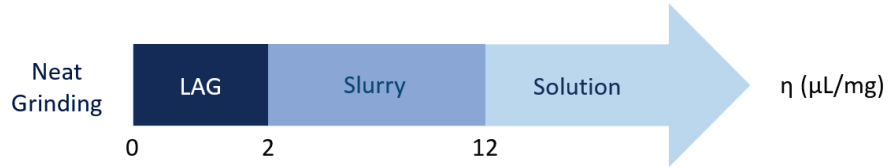

Fig. 77 Mechanochemical techniques for increasing volume of solvent added to the reaction. The parameter η indicates the volume of solvents (µL) added per mass of solid reagent (mg).

While the affecting parameters of neat grinding are mainly temperature, reaction time and speed, LAG is a more versatile approach[204]. The catalytic amount of liquid added in the reaction promotes the mobility of the reagents and can therefore accelerate or enable

reactions, that would not proceed as easily in neat grinding[205]. A study performed by Friščić *et al.*[206] on crystallization by mechanical grinding, claimed that in LAG conditions the solubility of reactants did not affect the reaction outcome. On the contrary, the solubility of the reagents/products has to be considered for slurry and solution reactions.

To perform an IAM reaction an amine sorbent is first loaded with CO_2 and then introduced in a grinding reactor containing a metal oxides salt. Both LAG and neat-grinding reactions can then be considered IAM experiments performed in a two-steps set-up.

2.3.1 Liquid Assisted Grinding (LAG)

The LAG experiments were performed on metal oxides as the solid reagent, with a precise amount of CO_2-loaded amine solution. The objective of the experiments was to determine if the presence of a liquid CO_2 carrier (CO_2-loaded amine) would enhance the CO_2 transfer from the amine to the metal, therefore increasing the carbonation kinetics and yield.

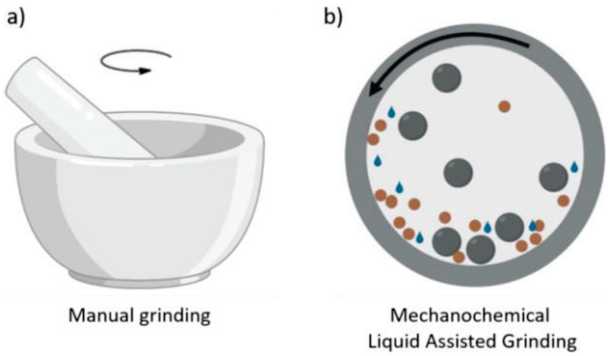

Fig. 78 Mechanical activation of chemical reactions; a) manual grinding with mortar and pestle; b) mechanochemical LAG in a planetarium reactor, the blue drops represent the added solution, brown circles indicate the solid reagent, and the gray spheres represent the grinding marbles in the reactor.

Once the grinding reaction is completed (3 cycles of 10 minutes at 500 rpm) the resulting mixture is recovered with water or methanol, centrifuged, and separated into liquid and solid phases. As for experiments in heterogeneous systems, both phases were studied by ICP-OES, ^{1}H qNMR and volumetric analysis, to determine the solid/liquid repartition of metal, carbon dioxide and amine. The final objective was to determine the behavior of various metals towards mineral carbonation and attritive leaching, while at the same time quantify the potential amine loss into the solid phase for each experiment.

2.3.2 Neat Grinding

To perform neat grinding experiments, it was necessary to obtain a solid CO_2 carrier which would react with solid metal oxides. For this reason, solid adducts of CO_2-loaded amino acids were prepared (the preparation procedure can be found on page 203 of the experimental section). The solid αAA-CO_2 were investigated by solid-state NMR and ^{13}C qNMR, to quantify the bicarbonate/carbamate composition of the library and assess the global CO_2 loading of the sample. A neat grinding experiment was then performed with equivalent quantities of metal oxide with respect to CO_2.

The absence of a liquid binder, such as water or concentrated amine solution, could have either positive or negative physical effect on the overall carbonation reaction, by influencing the phase transfer kinetics. In fact, it may lower CO_2 transfer from the amine to the metal, hence inhibiting carbonation, or it might prevent the leaching of the metal in the liquid phase, hence promoting carbonation.

As for carbonation and LAG experiment, the goal of these investigations was to determine which operating condition would provide the highest metal carbonation yield with minimum amine loss. Compared to the IAM strategies discussed in the previous section, neat and LAG grinding would significantly reduce the waste production of IAM reactions, i.e. water volumes, as well as the energy expenses, considering that a 30 minutes reaction at ambient temperature and pressure would require less energy compared to hours of reactions at 75-90 °C.

Chapter 3

3 Results and discussion

3.1 Influence of the metal on CO_2-amines systems by speciation

3.1.1 Polyamines-$MgCl_2$: homogeneous system

A one-pot IAM experiment was performed by introducing pure CO_2 in an aqueous solution of **EDA** 0.5M, in presence of sub-stoichiometric amounts of $MgCl_2$ (0.125 M). The presence of a metal template may modify the distribution of the CO_2-loaded adducts (carbamates and carbonates) in the Dynamic Combinatorial Library, as mentioned in Chapter 2, section 2, page 69. Fig.79a presents the comparison between the ^{13}C qNMR chemical speciation of the templated and untemplated library, represented by continuous and dotted line respectively. The ^{13}C qNMR stacked spectra can be found in the Annexes, page 217.

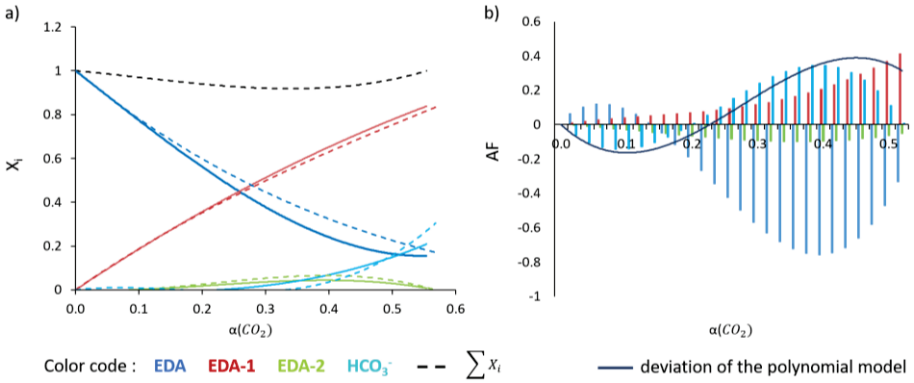

Fig. 79 a) Chemical speciation of **EDA**-CO_2 0.5M with 0.25 equivalents of $MgCl_2$ compared to the chemical speciation of **EDA**-CO_2 1M in D_2O expressed in molar fraction (X_i) vs loading ($\alpha(CO_2)$). The evolution of the species in the templated library are represented by continuous lines, while the evolution of the untemplated library is indicated by dotted lines. The black dotted line in graph a indicates the mass balance of the amine in the templated library. b) Amplification factors upon increasing CO_2 loading of the **EDA**-CO_2 DCL in presence of 0.25 eq. of $MgCl_2$, the blue line indicates the deviation of the polynomial model, calculated as the sum of the AF. Color code: **EDA** (blue), monocarbamate **EDA-1** (red), dicarbamate **EDA-2** (green), bicarbonate **HCO_3^-** (light blue).

It can be observed that the presence of the metal template entails a slight, yet not significant, increase of monocarbamate **EDA-1** and bicarbonate HCO_3^- and a concomitant decrease of dicarbamate **EDA-2** and free amine **EDA**. The equilibrium displacement can be quantified by the amplification factors, presented in Fig.79b, wherein the blue line indicates the sum of the amplification factors (eq.88), which should be equal to zero. The deviation of this mass balance

indicates that the visible fluctuation of the populations can be mostly attributed to the polynomial model, rather than to template effects.

In absence of CO_2, the amine-metal solution displays a pH of 10.5 and presents the formation of a white suspension, which can be justified by the formation of $Mg(OH)_2$. Given the concentration of magnesium and OH^- ions in solution it was possible to calculate the moles of $Mg(OH)_2$ formed in solution ($1.6*10^{-7}$), and given the solubility of $Mg(OH)_2$ ($Ks = 10^{-11.15}$, table 6), it is possible to confirm that the white precipitate observed in the amine-metal solution is in fact the metal hydroxide.

Table 15 Metal carbonate and hydroxide pKs at 25 °C and ionic strength 0. *Value for calcite.

Metal	pKs MCO_3 $M^{n+}(CO_3^{2-})_m$	pKs $M^{n+}(OH)_n$
Mg	7.46	11.15
Ca	8.35*	5.19

The introduction of increasing quantities of carbon dioxide increases the solution pH, dissolving the suspension and yielding a transparent and colorless solution. It can be hypothesized that Magnesium forms soluble complexes with free **EDA** or monocarbamate **EDA-1**[207] (Fig.80a,b). Since the capture equilibrium is not driven to the precipitation of $MgCO_3$, the final IAM step is inhibited and there cannot be any chemical regeneration of the amine solvent.

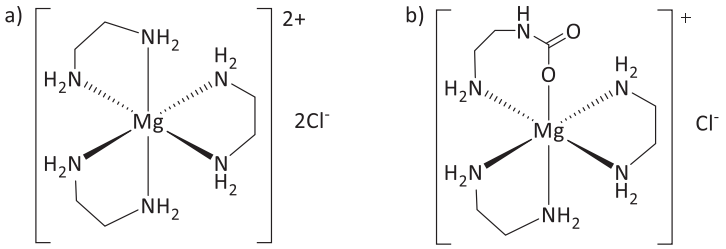

Fig. 80 Potential soluble complex present in the **EDA**-CO_2 templated library with chloride counterion. a) Mg(**EDA**)$_3$Cl$_2$ and b) Mg(**EDA**)$_2$(**EDA-1**)Cl.

The introduction of $MgCl_2$ as a metal template in a 0.5M **DETA** solution yielded similar results. In Fig.81a the chemical speciations of the templated and untemplated libraries are put in comparison. The ^{13}C qNMR stacked spectra can be found in the Annexes, page 218.

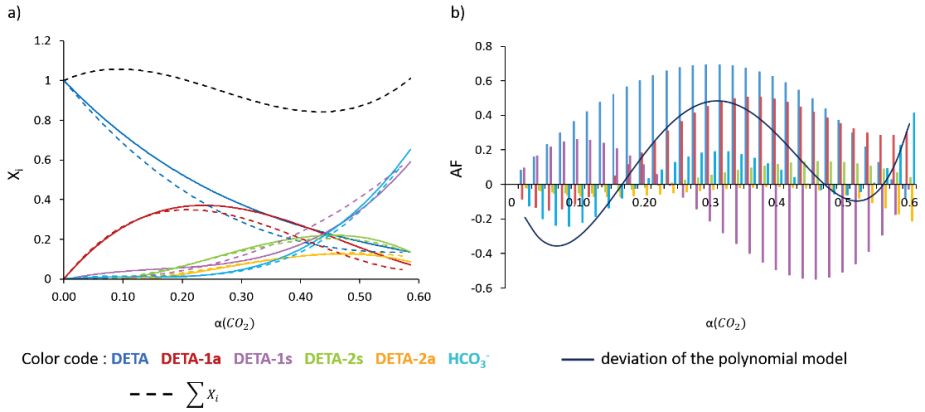

Fig. 81 a) Chemical speciation of **DETA**-CO_2 0.5M with 0.25 equivalents of $MgCl_2$ (continuous line) compared to the chemical speciation of **DETA**-CO_2 0.5M in D_2O (dotted line) expressed in molar fraction (X_i) vs loading ($\alpha(CO_2)$). The black dotted line in graph a indicates the mass balance of the amine in the templated library. b) Amplification factors upon increasing CO_2 loading of the **DETA**-CO_2 DCL in presence of 0.25 eq. of $MgCl_2$. Color code: **DETA** (blue), asymmetric monocarbamate **DETA-1s** (red), symmetric monocarbamate **DETA-1a** (purple), symmetric dicarbamate **DETA-2s** (green), asymmetric dicarbamate **DETA-2a** (orange), bicarbonate **HCO_3^-** (light blue).

To determine the pH variation caused by the presence of the metal salt, a potentiometric titration of the solution was recorded upon increasing CO_2 loading. The pH of the starting solution resulted to be 10.44, instead of 11.5 for untemplated **DETA** 0.5M, and the overall pH decreased until reaching a final value of 8.3 instead of 6.8 observed for **DETA**-CO_2 at $\alpha(CO_2)$ = 0.5. The two potentiometric analyses can be found in the Annexes, page 219. Once again the initial basic pH of the solution lead to the formation of $Mg(OH)_2$ (pKs = 11.15, Table 15, page 122), which was dissolved once CO_2 loading reached $\alpha(CO_2)$ = 0.25 (pH = 9.74).

At higher loading ($\alpha(CO_2)$=0.5) the asymmetric monocarbamate **DETA-1a** and free amine **DETA** present a slight increase, with consequent decrease of symmetric monocarbamate **DETA-1s**. It can be hypothesized that once the metal is dissolved from its hydroxide salt, it forms soluble complexes with free and loaded amine (Fig.82).

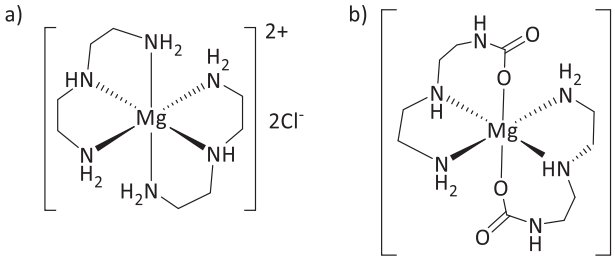

Fig. 82 Potential soluble complex present in the **DETA**-CO_2 template library with chloride counterion. a) Mg(**DETA**)$_2Cl_2$; b) Mg(**DETA**)(**DETA-2s**).

The amplification factors, calculated by eq.87, are presented in Fig.81b. As for **EDA**, the mass balance is not optimal (oscillating blue line), indicating that most variation observed in the AF graph seems to derive from the polynomial model.

At $\alpha(CO_2)$ = 0.57 (maximal experimental loading), the concentration of HCO_3^- ions in solution is 0.31M. From this data it was possible to calculate the maximum potential concentration of $MgCO_3$ in the system, which resulted to be $1.26*10^{-7}$. In those conditions, and given a Ks of $10^{-7.46}$ (Table 15, page 122), the magnesium carbonate should precipitate. Since no precipitation was observed in the aliquots, it is possible to conclude that $MgCO_3$ is not the main Mg-bearing species in solution, which strengthen the hypothesis of the formation of magnesium-amine soluble complexes in the library.

In the chosen operating conditions, the introduction of Magnesium did not entail any significant amplification in the **DETA**-CO_2 dynamic library, although it is not excluded that at higher amine concentration the system could yield insoluble $MgCO_3$, completing the IAM process.

3.1.2 α-Amino acids-$MgCl_2$: homogeneous system

Glycine, *L*-lysine and *L*-cysteine were investigated for IAM experiments in presence of $MgCl_2$, in the previously described operating conditions. In Fig.83a is reported the chemical speciations of **GlyK** 0.5M, analyzed by ^{13}C qNMR, in presence and in absence of the metal template (spectra in Annexes, page 219). The curves present very similar profiles, with slight variations between the templated and untemplated libraries until a CO_2 loading of 0.3.

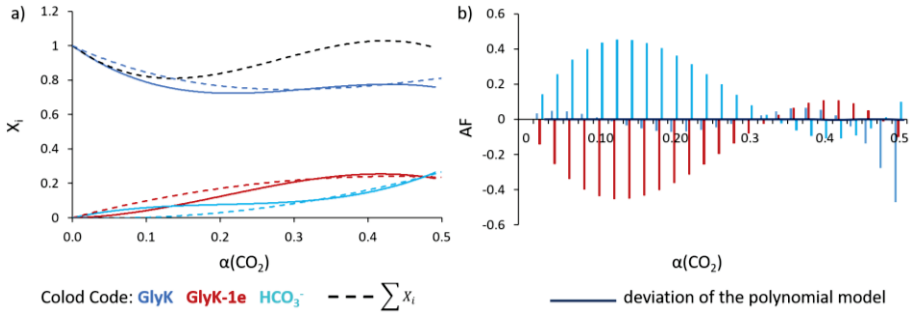

Fig. 83 a) Chemical speciation of **GlyK**-CO_2 0.5M with 0.25 equivalents of $MgCl_2$ in D_2O (continuous line), compared to the chemical speciation of **GlyK**-CO_2 0.5M in D_2O (dotted line), expressed in molar fraction (X_i) vs loading ($\alpha(CO_2)$). The mass balance of the amine species is indicated by a black dotted line in graph a. b) Amplification factors upon increasing CO_2 loading of the **GlyK**-CO_2 DCL in presence of 0.25 eq. of $MgCl_2$. The blue continuous line indicates the mass balance of the AF. Color code: **GlyK** (blue), monocarbamate **GlyK-1** (red), bicarbonate HCO_3^- (light blue).

At low loading, the AF calculated by eq.87 reveal an increase of bicarbonate, counterbalanced by an equivalent decrease of monocarbamate **GlyK-1**. In the case of glycine, the sum of all AF (eq.88) is equal to zero for all values of $\alpha(CO_2)$, which indicates that all variations are significant, and do not derive from the polynomial model.

Contrary to **EDA** and **DETA** and despite an initial pH of 10.98, the glycine/magnesium solution did not present any visible formation of $Mg(OH)_2$. The stability constant between glycine and Mg is logK = 2.22 for a ML stoichiometry, it is therefore possible to form amine-metal soluble complexes in the templated library. Nevertheless, based on the amplification factors, magnesium seems more prone to form bicarbonates salts in solution. The presence of the metal could entail the hydrolysis of the monocarbamate **GlyK-1** (eq.89), or a counterion exchange with **GlyK-HCO₃** (eq.90).

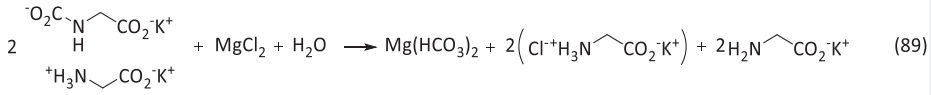

(89)

(90)

Similarly, a 0.5 M solution of ***L*-LysK** was investigated in presence of 0.25 equivalents of $MgCl_2$ and compared to the speciation of untemplated ***L*-LysK** in D_2O (Fig.84a). The stacked ^{13}C qNMR spectra can be found in the Annexes, page 220.

The solution presented an initial pH of 11.18 and formation of $Mg(OH)_2$ in absence of CO_2, until $\alpha(CO_2)$ = 0.1. Compared to **EDA**, **DETA** and **GlyK**, lysine induces the most significant variations within the library. The molar fractions of monocarbamates ***L*-LysK-1e** and ***L*-LysK-1a** decrease by an AF of -0.5 and -1 respectively. In parallel, bicarbonate HCO_3^- is amplified throughout the reaction, reaching an AF of 1.5 at maximum CO_2 loading.

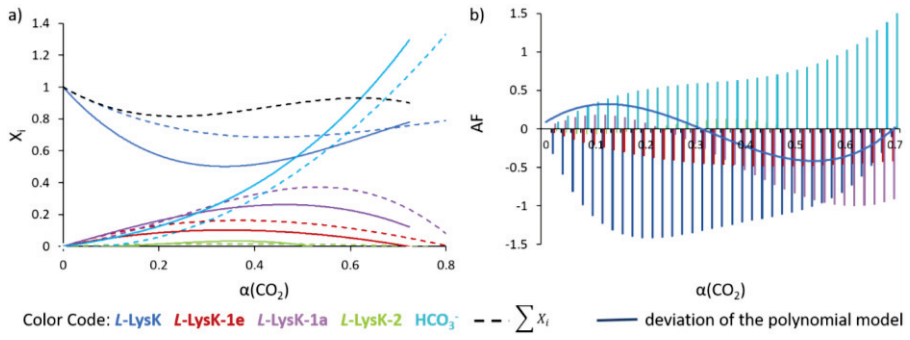

Fig. 84 a) Chemical speciation of ***L*-LysK**-CO_2 0.5M with 0.25 equivalents of $MgCl_2$ in D_2O (continuous line), compared to the chemical speciation of ***L*-LysK**-CO_2 0.5M in D_2O (dotted line), expressed in molar fraction (X_i) vs loading ($\alpha(CO_2)$). The mass balance of the amine species in the templated library is indicated by a black dotted line in graph a. b) Amplification factors upon increasing CO_2 loading of the ***L*-LysK**-CO_2 DCL in presence of 0.25 eq. of $MgCl_2$. Color code: ***L*-LysK** (blue), epsilon monocarbamate ***L*-LysK-1e** (red), alpha monocarbamate ***L*-LysK-1a** (purple), dicarbamate ***L*-LysK-2** (green), bicarbonate HCO_3^- (light blue).

It must be mentioned that the drastic variation observed for free lysine (Fig.84b, dark blue columns) is due to an analysis or polynomial error, since the decrease of mono and dicarbamates should entail the increase of free amine in solution, and not its loss. Duplicates of these experiments could provide further data to verify those trends and reduce the experimental error.

Nevertheless, the amplification of bicarbonate can be attributed to the presence of metal, although it is not possible to determine whether there is formation of $MgCO_3$, $Mg(HCO_3)_2$ or of a mixture between protonated amine, bicarbonate and metal. The significant amplification of bicarbonate reported for **GlyK** and ***L*-LysK** was observed in less extent in the templated libraries of **EDA** and **DETA**. It can be hypothesized that the limited formation of $Mg(CO_3)_2$ does not affect the carbamate-driven CO_2 capture of industrial polyamines, while it influences the carbonate-driven amino acids libraries. Further experiments at higher metal concentrations could entail the precipitation of $Mg(CO_3)_2$ and potentially modify the CO_2 capture chemistry of polyamines from carbamation to carbonation.

Contrary to the other amines, ***L*-CysK** was not studied via a complete speciation. Two solutions of ***L*-CysK** 0.5M in D_2O and ***L*-CysK** 0.5M with 0.25 eq. of $MgCl_2$ in D_2O were investigated at loading $\alpha(CO_2) = 0.43$ to compare the carbamate/carbonate repartition in the templated and untemplated library, although the results did not show any variation in the system. The ^{13}C qNMR spectra of the ***L*-CysK**-Mg system can be found in the Annexes, page 221.

Although none of the experiments presented above resulted in the precipitation of $MgCO_3$ enhanced by amine-capture, the results showed that amino acids can act as potential absorber for metal carbonation. These preliminary results call for further the investigation of the optimal operating conditions for an efficient IAM process with amino acids.

3.2 IAM of $CaCl_2$ in solution

3.2.1 DETA-$CaCl_2$: heterogeneous system

To investigate the influence of $CaCl_2$ on a **DETA**-CO_2 library, a 0.5M aqueous solution of amine was prepared with 0.083 equivalents of $CaCl_2$ and loaded with increasing amounts of CO_2. The amine:metal ratio (6:1) is different from the previous **DETA**/Mg system (ratio 4:1). It was initially chosen based on the hypothesis that calcium could enhance the formation of **DETA-2s**, by yielding a dicarbamate-metal complex shown in Fig.85.

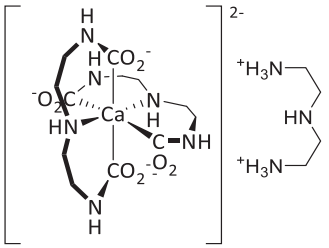

Fig. 85 Hypothetical Ca(**DETA-2s**)$_2$(**DETA-H**) complex yielded by the introduction of CO_2 into a 0.5M solution of **DETA** with 0.083 equivalents of $CaCl_2$: the dicarbamate species act as ligand for the metal cation while the overall negative charge of the complex is counterbalanced by a molecule of protonated amine in the second coordination sphere.

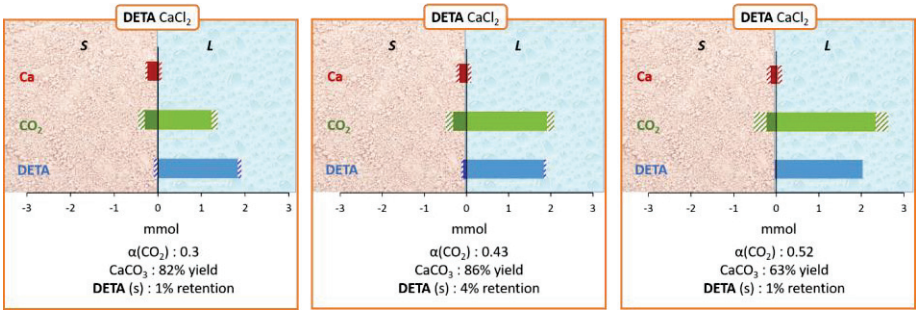

Fig. 86 Carbonation via an IAM experiment of an aqueous solution of 0.083M $CaCl_2$ with 0.5M **DETA**, loaded with pure CO_2 at 25 °C. a) Loading $\alpha(CO_2)$ = 0.3, calcium carbonation yield 82% and amine retention in the solid 1%; b) loading $\alpha(CO_2)$ = 0.43, calcium carbonation yield 86% and amine retention 4%; c) loading $\alpha(CO_2)$ = 0.52, calcium carbonation yield 63% and amine retention in the solid 1%. Color code: metal (red), CO_2 (green), amine (blue). The graphs are divided into solid fraction (negative values) and liquid fraction (positive values).

The experimental results showed no amplification of the symmetric dicarbamate **DETA-2s**, instead they revealed an efficient carbonation of calcium. In Fig.86a, b, c are reported the results obtained by loading the amine-metal solution with an increase in $\alpha(CO_2)$ of 0.3, 0.43 and 0.52, respectively. Each graph displays the partition between solid and liquid phase of calcium cation (red), carbon dioxide (green) and **DETA** (blue).

As depicted in section 2.2, page 118, the experimental set up requires the solid to be washed and separated from the liquid phase. These steps could entail the partial loss of the sample. When the mass balance of the components does not reach 100%, the lost fraction is represented by a lined pattern. This percentage is calculated as the difference between the initial moles of a component and the sum of the moles in the solid and liquid phase, determined by experimental analysis. The loss is graphically arbitrarily displayed between solid and liquid.

$$\%\, loss = \; n^i - (n^S + n^L) \quad (91)$$

It can be noticed that regardless the CO_2 loadings, calcium is mostly retained in the solid and displays elevated carbonation yields. The latter were calculated as the ratio between the moles of CO_2 in the solid phase and the initial moles of metal (eq.92), while the amine retention in the solid was determined as the ratio between the moles of **DETA** in the solid versus the initial moles of amine (eq.93).

$$MCO_3(\%) = \frac{n_{CO_2}^S}{n_{Ca}^i} \quad (92)$$

$$R_2NH_{(s)}(\%) = \frac{n_{R_2NH}^S}{n_{R_2NH}^i} \quad (93)$$

The highest calcium carbonation extent, 82% and 86%, are obtained with α(CO_2) = 0.3 and 0.43 respectively, while higher loading yields only 63% of $CaCO_3$. The phenomenon could be explained by the lower pH reached with higher CO_2 loading, which could inhibit carbonate formation.

Overall, the three examples show a rather low amine retention in the solid (1%-4%) and an efficient mineral carbonation yield obtained at room temperature with an amine:metal ratio of 6:1. Furthermore, the remaining fraction of amine and CO_2 in the liquid could potentially be reused for further calcium carbonation cycles, thus improving the chemical regeneration of **DETA**.

3.2.2 α-Amino acids-$CaCl_2$: heterogeneous system

Integrated absorption mineralization of $CaCl_2$ was then investigated with a 0.5M aqueous solutions of glycine, *L*-lysine and *L*-cysteine. The solutions were prepared with 0.125M $CaCl_2$, for a final amine:metal ratio of 4:1 and were loaded with pure CO_2 at 25 °C, for a one-pot IAM experiment.

Fig.87a, b, c reports the results obtained for the three amino acids, glycine, *L*-lysine and *L*-cysteine respectively, with a total CO_2 loading between 0.44 and 0.49. The three experiments present a general pattern in which the majority of calcium is found in the solid with medium/high carbonation yields, while the αAA is nearly all transferred to the liquid phase. This indicates that the solid does not contain calcium-amino acid complexes.

The quantification of the amine residue in the solid was measured at 1, 2% which indicates a high chemical regeneration of the amine and a low contamination of the solid. Contrary to **DETA**, the formation of a white precipitate was immediate upon CO_2 introduction, nevertheless the samples were left to stabilize for 12h.

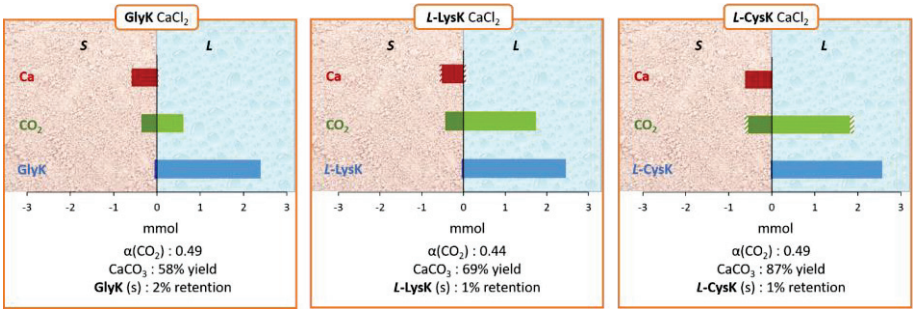

Fig. 87 Carbonation via an IAM experiment of an aqueous solution of 0.083M $CaCl_2$ with 0.5M solution of amino acids loaded with pure CO_2 at 25 °C. a) **GlyK**, $\alpha(CO_2)$ = 0.49; b) ***L*-LysK**, $\alpha(CO_2)$ = 0.44; c) ***L*-CysK**, $\alpha(CO_2)$ = 0.49. Color code: metal (red), CO_2 (green), amine (blue). The graphs are divided into solid fraction (negative values) and liquid fraction (positive values).

Glycine, Fig.87a, shows a carbonation yield of 58%, which indicates that 30% of the introduced CO_2 is transformed in $CaCO_3$. Consequently, the recovered amine presents a loading of 0.25, compared to the initial 0.49, which indicate an efficient, yet unoptimized, amine regeneration. Lysine and cysteine (Fig.87b,c) display a calcium carbonation yield of 69% and 87%, respectively, which corresponds to 20% of the introduced CO_2 . For both amino acids, the $\alpha(CO_2)$ loading after carbonation is 0.25, compared to the initial 0.44 and 0.49 for lysine and cysteine.

The last IAM experiment with $CaCl_2$ was performed with ***L*-LysK** 0.5M with increasing concentrations of metal and final ***L*-LysK**:Ca ratios of 1:1 and 2:1. A higher metal concentration could have a greater impact in displacing the reaction equilibrium towards the carbonate formation, thus promoting CO_2 stripping.

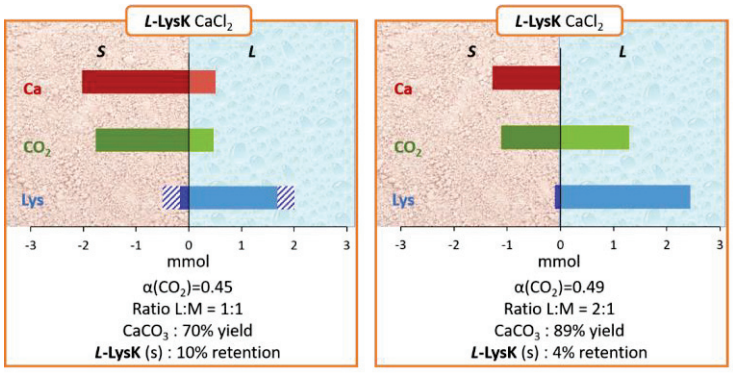

Fig. 88 IAM experiment of an aqueous solution of 0.5M ***L*-LysK** loaded with pure CO_2 at 25 °C, with different quantities of $CaCl_2$. a) ***L*-LysK**:Ca ratio 1:1, $\alpha(CO_2)$ = 0.45; b) ***L*-LysK**:Ca ratio 2:1, $\alpha(CO_2)$ = 0.49. Color code: metal (red), CO_2 (green), amine (blue). The graphs are divided into solid fraction (negative values) and liquid fraction (positive values).

Fig.88a reports the results obtained via an IAM experiment with an amine:metal ratio of 1:1. It can be observed that, while the carbonation yield is elevated (70%), the amine retention increased from 1% (Fig.88b, lysine:calcium ratio of 4:1) to 10% and 20% of the metal is leached in the solution. On the contrary, increasing the metal concentration for a final amine:metal ratio of 2:1 seems to improve the metal carbonation yield (89% compared to 69%) with a less significant amine retention (4% instead of 10%).

The lower carbonation yield in presence of higher concentration of $CaCl_2$ (0.5M) could be explained by a study performed by Arti *et al.*[180]. Arti *et al.* noticed an important pH drop when $CaCl_2$ was introduced in a CO_2-loaded solution of **MEA**, for which the overall pH changed from 8 to 6[180]. The author hypothesized that a higher concentration of metal decreases the pH of the solution, resulting in partial protonation of the primary amine groups thus inhibiting CO_2 capture via carbamate formation.

Concerning the higher retention of ***L*-LysK** in the precipitate, it is likely that the formation of $CaCO_3$ is obtained faster at higher calcium concentrations, causing the amine to be accidentally trapped into the solid matrix, thus affecting its recovery.

Finally, from the results reported in Table 16, it can be concluded that the IAM of $CaCl_2$ by **DETA** is efficient, although the retention of the industrial amine can represent an additional form of pollution of the carbonated product. Glycine seems to be the least efficient amino acid in the chosen operating conditions, while *L*-cysteine presents carbonation yields comparable to **DETA**, with lower amine retention. Finally, *L*-lysine provided the highest calcium carbonation yield (89%) and a higher optimization of the operating parameters could provide higher metal carbonation extents and higher amine recovery.

Table 16 Results of the carbonation of $CaCl_2$, with a 0.5M amine solution in H_2O, loaded with pure CO_2.

R_2NH	R_2NH:Ca	$\alpha(CO_2)$	$CaCO_3$(s) yield	R_2NH(s) loss
DETA	6:1	0.30	82%	1%
		0.43	86%	4%
		0.52	63%	1%
***L*-LysK**	4:1	0.44	69%	1%
	2:1	0.49	89%	4%
	1:1	0.45	70%	10%
***L*-CysK**	4:1	0.49	87%	1%
GlyK	4:1	0.49	58%	2%

3.3 Mechanochemistry

3.3.1 LAG: DETA and MOx

The LAG experiments were performed using a variety of metal oxides as the solid reagent, and 1 mL of CO_2-loaded **DETA** as solvent. It was decided to work in equivalent conditions between the metal and CO_2, to incite complete metal carbonation. To provide a higher concentration of carbon dioxide in the reaction, the amine solutions were prepared with a final concentration of 5M in deionized water, instead of 0.5M. The solutions were then loaded with CO_2 and analyzed by ^{13}C qNMR to determine the precise value of $\alpha(CO_2)$.

Two possible reactions are shown in eq.94 and eq.95. In the first example, CO_2 can be transferred from an ammonium carbamate to the metal carbonate, or there can be complexation between the metal and the CO_2-loaded amine. In eq.95, on the other hand, is reported the case in which the metal binds preferably the amine, resulting in a soluble complex which can then be leached from the reactive mixture.

$$MO + R_2N\text{-}CO_2^- + R_2NH_2^+ \rightleftharpoons 2R_2NH + MCO_3 \quad (94)$$

$$M'O + 2R_2NH + H_2O \rightleftharpoons M'^{2+}(R_2NH)_2, 2OH^- \quad (95)$$

The LAG experiments were performed in duplicate. For each **DETA**-metal system one sample was recovered and washed with purified water and the other with methanol, then the solid/liquid phases were separated. Methanol was chosen as a polar and less dissociative solvent, compared to water, to investigate the influence of the solvent during washing. It was assumed that the carbonate is insoluble in MeOH, while the amine-CO_2 libraries are not, which would provide a higher separation of the organic/inorganic components, as well as a higher amine recovery.

The Liquid Assisted Grinding experiments with **DETA** were performed on 11 metal oxides and the specific experimental conditions of each amine/metal system can be found in Table 17.

The parameter η (μL/mg) was introduced in Section 2.3, page 118, and indicates the ratio between the liquid solvent and the solid reagents in the reaction. For LAG experiments η values should be between 0 and 2 μL/mg. From Table 17 it can be noticed that some experiments were performed a higher liquid/solid ratio which bring them in a slurry category

rather than LAG. Since the priority was given to the control of metal/CO_2 stoichiometric ratios, the η factor resulted to be outside the ideal range.

Table 17 Experimental conditions for LAG experiments with a 5M aqueous solution of **DETA** and MOx; grindings were performed in a tungsten carbide reactor (WC) for 3 cycles of 10 minutes at 500 rpm. MCO_3 (%) indicates the carbonation yield and R_2NH(s)% indicated the amine retention in the solid. *Ti, Al, Ni and Fe experiments could not be exploited, as the ICP-OES quantification failed, the metal carbonation yield reported for these metals has to be considered an approximation.

R_2NH	M (mol/L)	α(CO_2)	η (µL/mg)	MOx	M:CO_2	Solvent	MCO_3 (%)	R_2NH(s) %
DETA	5.03	0.45	4.68	Li_2O	1:0.47	H_2O	31%	6%
			4.96		1:0.50	MeOH	40%	39%
	5.30	0.39	3.89	MgO	1:0.97	H_2O	17%	6%
			3.97		1:0.98	MeOH	66%	29%
	5.11	0.46	4.48	*Al_2O_3	1:1.6	H_2O	16%	0%
			4.16		1:1.5	MeOH	14%	1%
	5.03	0.45	2.56	CaO	1:0.98	H_2O	51%	7%
			2.63		1:1	MeOH	100%	41%
	5.03	0.45	3.51	*TiO_2	1:1.91	H_2O	12%	0%
			3.59		1:1.95	MeOH	6%	0%
	5.03	0.45	2.21	MnO	1:1.07	H_2O	28%	2%
			2.28		1:1.10	MeOH	34%	0%
	5.30	0.39	2.96	*Fe_2O_3	1:1.47	H_2O	12%	0%
			2.89		1:1.59	MeOH	13%	0%
	5.00	0.34	2.29	CoO	1:0.99	H_2O	6%	0%
			2.33		1:1.01	MeOH	3%	0%
	5.00	0.34	2.27	*NiO	1:0.98	H_2O	4%	0%
			2.29		1:0.99	MeOH	3%	0%
	5.03	0.45	1.86	CuO	1:1	H_2O	8%	0%
			1.89		1:1.02	MeOH	10%	0%
	5.03	0.45	1.79	ZnO	1:0.99	H_2O	43%	56%
			1.80		1:1	MeOH	63%	72%

Table 18 Stability constant of different metal cations with DETA for ML and ML_2 complexes and pKs of metal hydroxides/carbonates at 25 °C[126, 208]. * Value at 18 °C, **value at 20 °C.

M^{X+}	LogK (25 °C)		pKs (25 °C)	
	DETA (ML_1/M.L^1)	DETA (ML_2/M.L^2)	Hydroxide	Carbonate
Li^+	/	/	/	/
Mg^{2+}	/	/	11.15	7.46
Al^{3+}	/	/	33.5	/
Ca^{2+}	/	/	5.19	8.35
Mn^{2+}	3.99	6.91	12.8	9.3
Fe^{3+}	/	/	/	/
Co^{2+}	8.57	14.77	14.9	9.98
Ni^{2+}	10.96	19.27	15.2	6.87
Cu^{2+}	16.1	21.2	19.32	9.63
Zn^{2+}	8.62	12.4	15.52	10

Considering the equilibrium showed in eq.94, a series of calculations were made for the MO-DETA systems. In order to calculate the equilibrium constant of eq.96, the latter was divided into separate equilibriums with known constants (eq.97-103). The formation of the carbonate ion (eq.100) is divided into three additional equilibriums indicating the carbonic acid dissociation (eq.101-103).

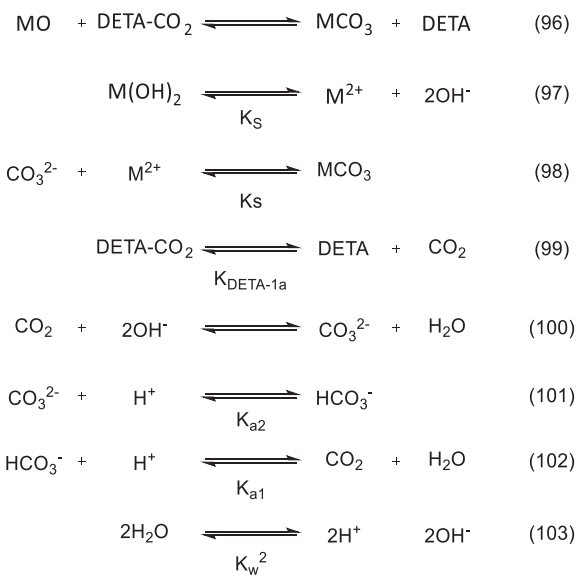

Starting from these equilibriums, eq.96 can be calculated as:

$$(eq.96) = (-eq.97) * (eq.98) * (-eq.99) * (eq.100)$$

$$(eq.96) = (-eq.97) * (eq.98) * (-eq.99) * [(-eq.101) * (-eq.102) * (eq.103)^2]$$

$$K_{(eq.96)} = \frac{1}{Ks_{OH}} * K_{co_3} * \frac{1}{K_{DETA-1a}} * \frac{1}{K_{a2}} * \frac{1}{K_{a1}} * K_w^2$$

The assumption was made for which $Ks_{(MO)} = Ks_{(M(OH)_2)}$. A previous investigation conducted by our group allowed the determination of the equilibrium constant of eq.99, in which the asymmetric monocarbamate **DETA-1a** is dissociated into uncarbamated amine and CO_2. This value was estimated at 48 L/mol[41]. Finally, for the pKs listed in table 18 and for a value of Kw = 10^{-14}, K_{a1} = $10^{-6.37}$ and K_{a2} = $10^{-10.32}$ it was possible to calculate the equilibrium constants of eq.96 for Mg, Ca, Mn, Co, Ni, Cu and Zn (Table 19).

Table 19 Equilibrium constants of eq.96 for Mg, Ca, Mn, Co, Ni, Cu and Zn, calculated via eq.97-101.

M^{2+}	$K_{(eq.96)}$
Mg^{2+}	$5.00\ 10^{-10}$
Ca^{2+}	$7.06\ 10^{-17}$
Mn^{2+}	$3.23\ 10^{-10}$
Co^{2+}	$8.49\ 10^{-09}$
Ni^{2+}	$2.18\ 10^{-05}$
Cu^{2+}	$5.00\ 10^{-04}$
Zn^{2+}	$3.38\ 10^{-08}$

These calculations indicate that calcium is more prone to precipitate as carbonate, compared to nickel and copper, which on the contrary could be leached in solution via the formation of a soluble **DETA**-metal complex.

In Fig.89 are presented the results obtained with Li_2O (a, b), MgO (c, d) and CaO (e, f) after water and methanol treatment. It can be observed that the amine retention in the solid after MeOH washing (Fig.89b, d and f) is 7 times higher than with water (Fig.89a, c and e).

At the same time, the dissolution of carbonates and carbamates decreases, which entails a higher percentage of CO_2 in the solid. In the case of CaO, when the solid is washed with Methanol (Fig.89f), carbon dioxide is completely retained in the solid, showing a potential mineral carbonation of 100%.

Unfortunately, the mass balance for calcium is not complete, as shown by the red lined patterned bars. Potentially, a significant fraction of the sample was lost during the recovery of the mixture from the grinding reactor.

Furthermore, the solid cannot be considered pure since it presents 41% of **DETA**. The high presence of amine in the solid could also indicate the formation of a Ca-**DETA**-CO_2 complex. Based on the literature and on the $CaCl_2$ carbonation results, the hypothesis of a stable metal/amine complex seems unlikely. Additional XRD and TGA-MS analysis could reveal the nature of the solid, confirming the presence of metal carbonate or of a metalorganic complex.

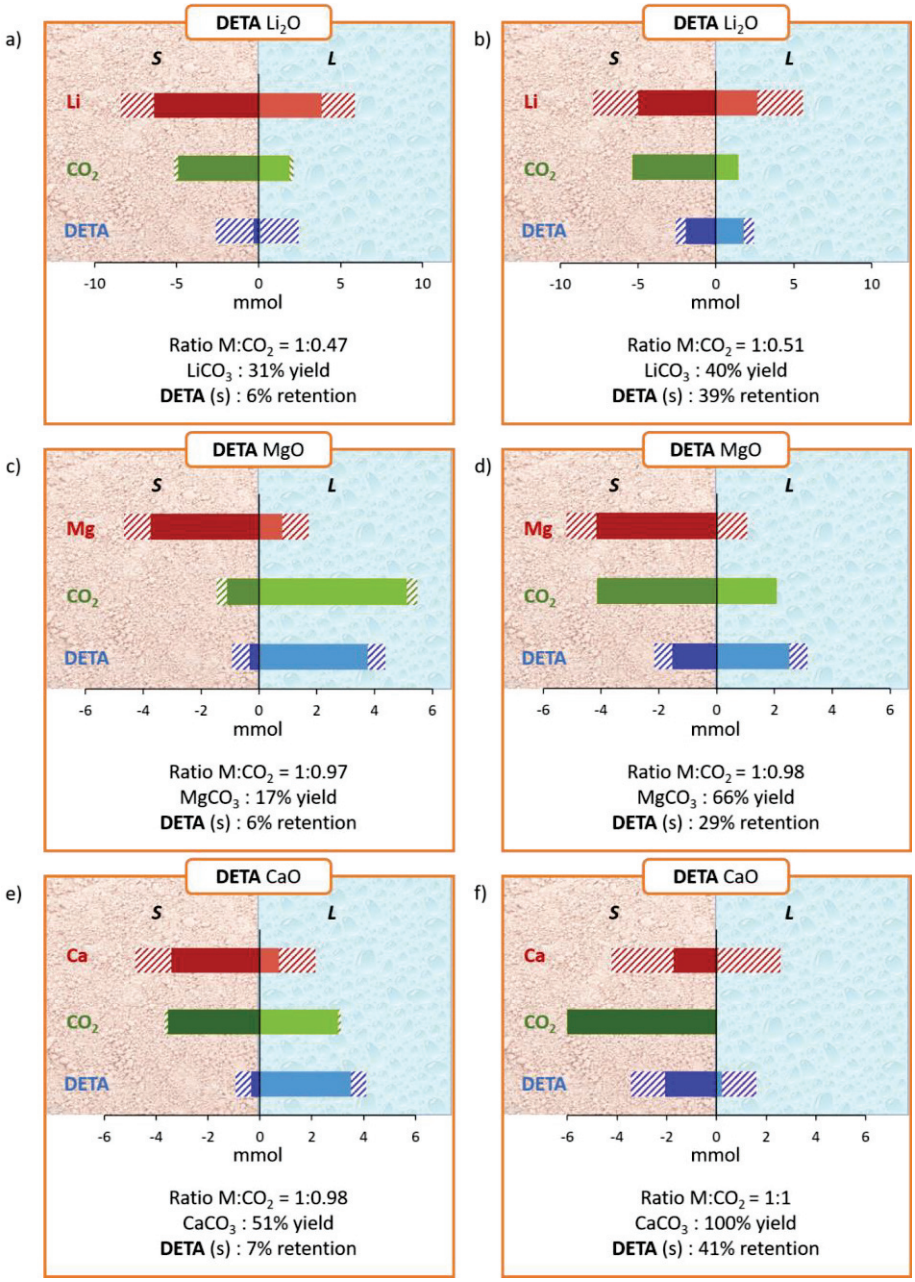

Fig. 89 Results obtained by LAG with a 5M solution of **DETA** in H_2O; grindings performed for 3 cycles of 10 minutes at 500 rpm. a) Li_2O, $Li:CO_2$ = 1:0.47, water washing; b) Li_2O, $Li:CO_2$ = 1:0.5, MeOH washing; c) MgO, $Mg:CO_2$ = 1:0.97, water washing; d) MgO, $Mg:CO_2$ = 1:0.99, MeOH washing; e) CaO, $Ca:CO_2$ = 1:0.98, water washing; f) CaO, $Ca:CO_2$ = 1:1, MeOH washing. Color code: metal (red), CO_2 (green), amine (blue). The graphs are divided into solid fraction (negative values) and liquid fraction (positive values).

The results obtained with manganese are showed in Fig.90a, b. The stochiometric amount of CO_2 present in the soil enables only partial carbonation of MnO, yielding 28%-34% of $MnCO_3$. The solvent influence appears to be the same as for Li_2O, MgO and CaO: MeOH inhibits metal lixiviation, increasing carbonation. Furthermore, no amine is detected in the solid, although the significant amine loss in case of MeOH calls for additional experiments and analysis to confirm that no amine is actually retained in the solid phase.

Titanium, aluminum, nickel and Iron experiments could not be exploited, as the ICP-OES quantification failed. The graphs are omitted from the discussion but can be found in the Annexes, page 222.

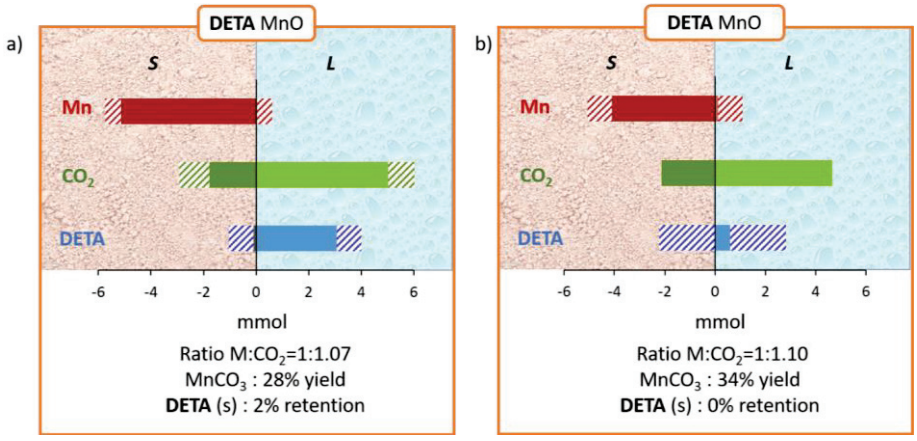

Fig. 90 Results obtained by LAG with a 5M solution of **DETA** in H_2O; grindings performed for 3 cycles of 10 minutes at 500 rpm. a) MnO, Mn:CO_2 = 1:1.07, water washing; b) MnO, Mn:CO_2 = 1:1.10, MeOH washing. The graphs are divided into solid fraction (negative values) and liquid fraction (positive values).

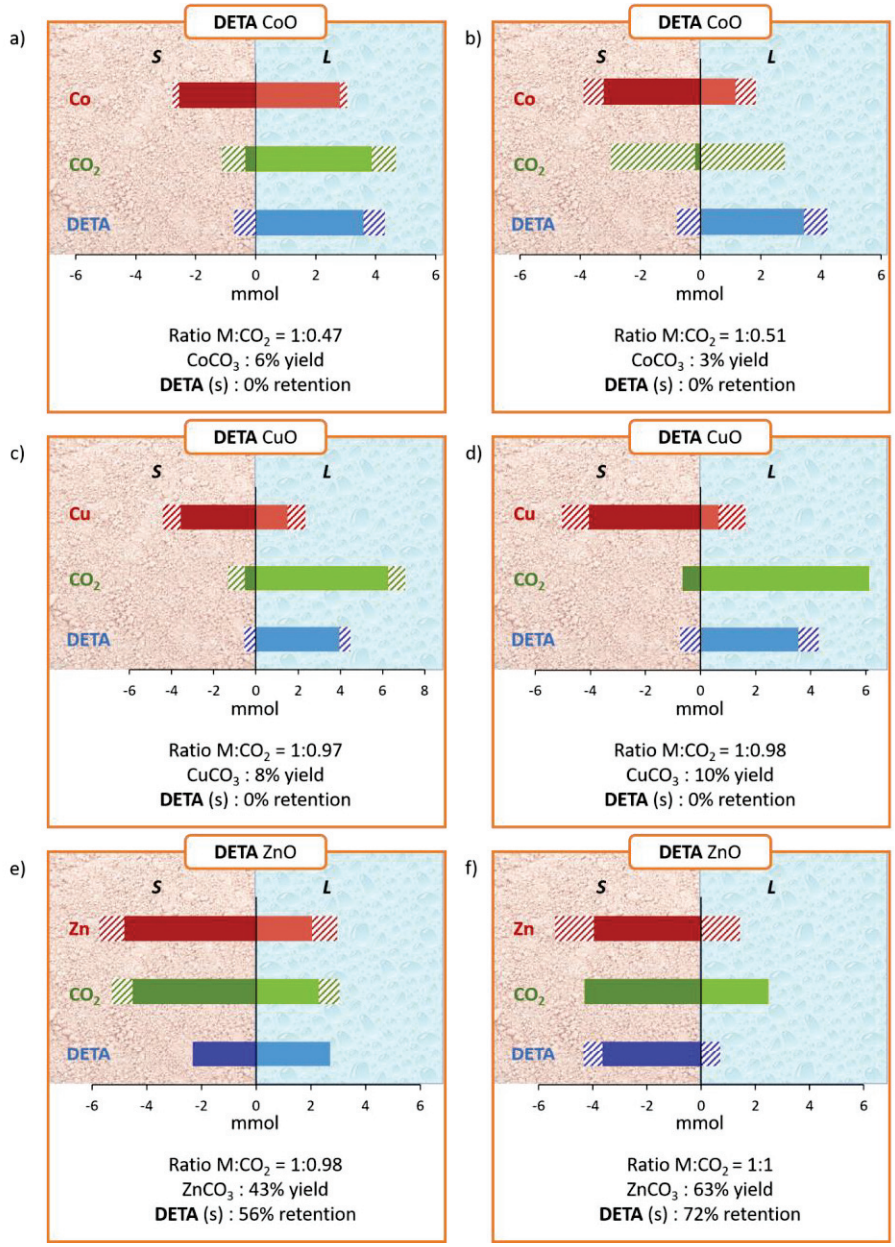

Fig. 91 Results obtained by LAG with a 5M solution of **DETA** in H_2O; grindings performed for 3 cycles of 10 minutes at 500 rpm. a) CoO, Co:CO_2 = 1:0.99, water washing; b) CoO, Co:CO_2 = 1:1.01, MeOH washing; c) CuO, Cu:CO_2 = 1:1.1, water washing; d) CuO, Cu:CO_2 = 1:1.02, MeOH washing; e) ZnO, Zn:CO_2 = 1:0.99, water washing; f) ZnO, Zn:CO_2 = 1:1.1, MeOH washing. Color code: metal (red), CO_2 (green), amine (blue). The graphs are divided into solid fraction (negative values) and liquid fraction (positive values).

In Fig.91 are reported the results of the LAG experiments run on cobalt (Fig.91a, b), copper (Fig.91c, d) and zinc oxides (Fig.91e, f). It can be observed that cobalt and copper present very low carbonation extent (3%-10%), with no retention of the amine in the solid. At the same time, a metal leaching effect is observable for both systems in water and methanol.

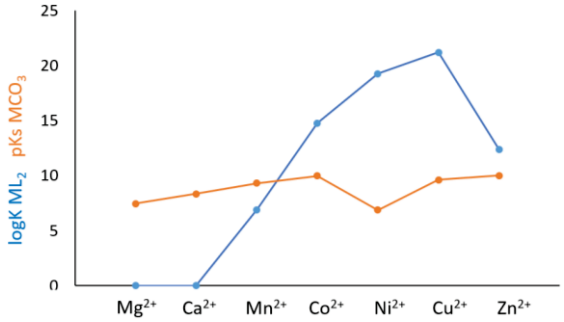

Fig. 92 pKs of MCO_3 (orange) and logK of ML_2 metal-**DETA** complexes (blue) at 25 °C, ionic strength 0. Values listed for Mg^{2+}, Ca^{2+}, Mn^{2+}, Co^{2+}, Cu^{2+} and Zn^{2+}.

In Fig.92 are shown the pKs of MCO_3 (orange) and the logK for ML_2 metal-**DETA** complexes (blue) for each metal. Cobalt and copper both display a higher affinity for **DETA** complexation (logK = 14.77 and 21.1, respectively) than carbonate formation (pKs = 9.98 and 9.63, respectively), confirmed by the low carbonation extent and high fraction of metal and amine in the liquid phase. The formation of Werner complexes is a driving force toward metal leaching, as illustrated by the presence of 50% of Co^{2+} in the liquid phase (Fig.91a). From Fig.92 it can be observed that nickel presents a logK = 19.27 for a ML_2 complex with **DETA**, and a pKs of 6.87 for $NiCO_3$. Although the results obtained with nickel are not discussed in this chapter, it could be expected to follow the same tendencies as cobalt and copper, resulting in high metal leaching and low metal carbonation. Finally, the residual metal in the solid phase could be attributed to an unreacted fraction of metal oxide.

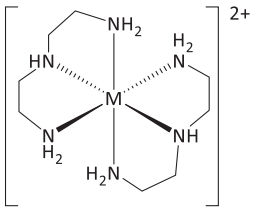

M = Co^{2+}, Cu^{2+}, Ni^{2+}

Fig. 93 Potential structure of **DETA**-Metal Werner complex with a ML_2 stoichiometry.

The results obtained by LAG of ZnO with **DETA** show a different behavior (Fig.91e, f). The calculated carbonation extent reaches 43% with water, and 63% with MeOH, although in the same conditions the amine retention rises from 56% in water to 72% in Methanol.

As shown in Fig.94, Zinc presents close values for both carbonation (pKs = 10) and **DETA** complexation (logK = 12.4). Given these constants and the elevated presence of **DETA** in the solid, the potential formation of a Zn-**DETA**-CO_2 must be considered. This hypothesis is strengthened by the several examples of Zn-carboxylate and Zn-carbamate complexes[209-213] reported in the literature.

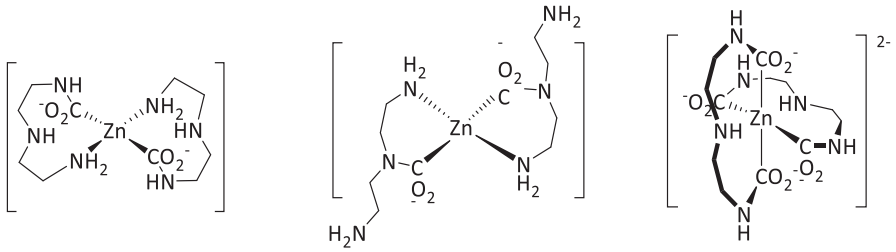

Fig. 94 Potential structures for a Zn(**DETA**-CO_2)$_2$ complex for different carbamate adducts. From the left: Zn(**DETA-1a**)$_2$, Zn(**DETA-1s**)$_2$, Zn(**DETA-2s**)$_2$.

Table 20 Stoichiometry between **DETA**/Zn and CO_2/**DETA** for the solid and liquid phases of LAG experiments between **DETA** 5M and ZnO.

	H_2O washing		**MeOH washing**	
	S	L	S	L
DETA/Zn	0.48	1.32	0.92	0.00
CO_2/DETA	1.94	0.84	1.19	0.00

The stoichiometries between zinc, amine and CO_2 for water and methanol (Fig.91g, h) reported in Table 20 indicate the potential formation of a Zinc/**DETA-**CO_2 complex in both solid and liquid phases, although it is not possible to determine with certainty if there is only the formation of complexes or if there is presence of zinc carbonate in the solid. Further information could be obtained by additional TGA-MS analysis on the solid phase, since the CO_2 desorption from an organic adduct takes place at 200 °C, while the desorption of CO_2 from metal carbonates takes place at around 800 °C.

Furthermore, an additional ^{13}C qNMR speciation can provide useful information of the evolution of carbamated species, by which it could be possible to determine any potential amplification of monocarbamates or dicarbamates, as discussed in section 3.1 of this chapter.

3.3.2 LAG: *L*-LysK and MgO

The LAG experiments between lysine and MgO were performed using a solid adduct of CO_2-loaded ***L*-LysK**. The latter was characterized by ^{13}C qNMR, which revealed a total loading of $\alpha(CO_2) = 0.79$ (moles of CO_2/moles of N) for a library composed by 79% of bicarbonate and 21% of carbamates (Annexes, page 224).

The amount of MgO necessary for the reaction was then calculated to fit a stochiometric ratio of 1:1 between Mg^{2+} and CO_2. Three experiments were performed with the same quantities of solid reagents (***L*-LysK**, MgO), to which were added increasing quantities of water in order to investigate the influence of a liquid binder on the reaction outcome.

The reactions were performed in a Tungsten Carbide (WC) reactor for 30 minutes at 500 rpm. In Table 21 are reported all the experimental conditions, while the results are shown in Fig.95a, b, c.

Table 21 Experimental conditions for LAG experiments between ***L*-LysK**-CO_2(s), MgO and H_2O. The reactions were performed in a WC reactor with 30min grinding at 500 rpm.

R_2NH	$\alpha(CO_2)$	η (µL/mg)	M:CO_2	MCO_3(s)	R_2NH(s)
***L*-LysK**	0.8	0.5	1:1	41%	8%
		1.0	1:0.99	37%	13%
		2.0	1:0.97	31%	6%

It can be noticed that for η = 0.5, 1 and 2, the lixiviation extent of magnesium stays constant at around 5%, indicating that the increasing volume of water does not have a direct impact on the metal dissolution[206].

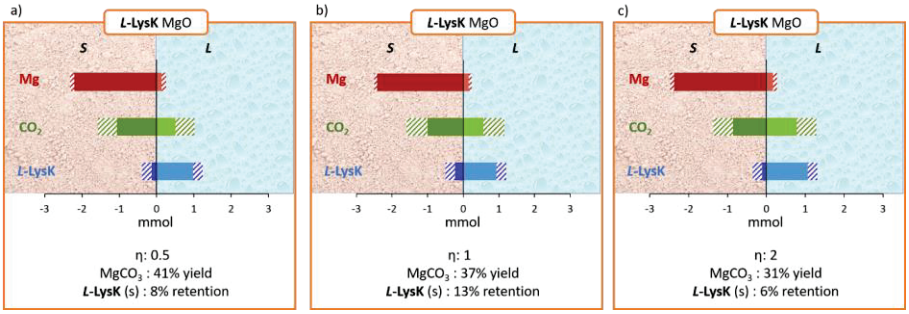

Fig. 95 LAG experiments with 0.3g of ***L*-LysK**-CO_2(s) at $\alpha(CO_2) = 0.8$. Grinding reactions performed at 500 rpm for 30 minutes a) MgO:CO_2 1:1, η = 0.5; b) MgO:CO_2 1:0.99, η = 1; c) MgO:CO_2 1:0.97, η = 2. Color code: metal (red), CO_2 (green), amine (blue). The graphs are divided into solid fraction (negative values) and liquid fraction (positive values).

The amine retention shows no specific tendencies correlated to the increasing η factor, and oscillates between 6% and 13%.

The literature reported a reaction between **GlyNa** 1M and MgO, performed at 75 °C under continuous flow of CO_2 which reached 88% of metal carbonation[115]. The LAG experiments reported above do not reach the same results, although it must be considered that the proposed experimental set-up provides lower water waste, shorter reaction times (30 minutes compared to 3h) and lower reaction temperature (25-35 °C compared to 75 °C)[115].

Overall, the efficiency of the unoptimized process shows a potential alternative pathway for the carbonation of MgO.

3.3.3 Neat grinding: αAA and MgO

The neat grinding experiments were performed with solid CO_2-loaded amino acid adducts and metal salts, to observe the potential carbonation yield of alkaline-earth metal oxides in a solvent-free set-up.

Table 22 Experimental conditions for the neat grinding of MgO with solid **GlyK**-CO_2. The grinding reactions were performed in a WC reactor for increasing grinding times (30 minutes, 1h, 2h) at 500 rpm. The α(CO_2) loading, HCO_3^- and N-CO_2^- percentage are referred to the solid amino acid and were determined by ^{13}C qNMR. MCO_3(s) indicate the carbonation yield while R_2NH(s) indicates the amine retention in the solid.

R_2NH	α(CO_2)	%HCO_3^-	%N-CO_2^-	Grinding Time	Mg:CO_2	MCO_3(s)	R_2NH(s)
GlyK	0.61	100%	0%	30min	1:0.94	8.9%	0.1%
				1h	1:0.76	6.8%	0.2%
				2h	1:0.81	0.9%	0.2%

The solid CO_2-loaded **GlyK** is previously characterized by ^{13}C qNMR in the absence of metal salt, determining a total loading of α(CO_2) = 0.61 for a library composed by 100% of bicarbonate (Annexes, page 224). The reactions were then run with a Mg:CO_2 ratio of 1:1 at three different grinding times, 30 minutes, 1 hour and 2 hours (Table 22). The resulting reaction mixture was then washed three times with 5 mL of water. The solid and liquid phases were separated and analyzed by ^1H qNMR, volumetric analysis and ICP-OES to quantify the repartition of amine, CO_2 and metal, respectively.

From the results reported in Fig.96a, b, c is possible to notice that the carbonation yields decrease with increasing reaction time (8.9%, 6.8% and 0.9% for 30 minutes, 1h and 2h of grinding, respectively). Almost 50% of magnesium is leached in the liquid phase, while the remaining metal fraction in the solid can be attributed to unreacted MgO.

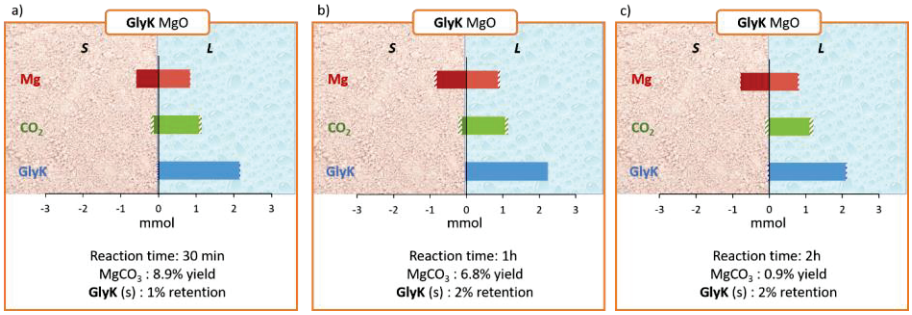

Fig. 96 Neat grinding experiments with 0.3g of **GlyK**-CO_2(s) at $\alpha(CO_2)$ = 0.61. Grinding reactions performed at 500 rpm for a) 30 minutes, MgO:CO_2 1:0.94; b) 1h, MgO:CO_2 1:0.76; c) 2h, MgO:CO_2 1:0.81. Color code: metal (red), CO_2 (green), amine (blue). The graphs are divided into solid fraction (negative values) and liquid fraction (positive values).

GlyK is mainly recovered in the liquid phase, with an amine retention in the solid of maximum 1-2%. At the same time the majority of CO_2 is transferred to the liquid. These preliminary results could indicate the formation of organic and metal-based carbonates, which are dissolved in the liquid phase. This hypothesis is strengthened by what was previously discussed for a chemical speciation of **GlyK** in presence of $MgCl_2$, where it was observed an amplification of bicarbonates in solution with no consequent precipitation of $MgCO_3$.

The lysine-magnesium experiments were performed with a solid αAA-CO_2 adduct loaded at $\alpha(CO_2)$ = 0.57, composed by 6% of ***L*-LysK-1e**, 16% of ***L*-LysK-1a** and 78% of HCO_3^- (^{13}C qNMR analysis in the Annexes, page 225). The operating conditions are reported in Table 23.

Table 23 Experimental conditions for the neat grinding of MgO with solid ***L*-LysK**-CO_2. The grinding reactions were performed in a WC reactor for increasing grinding times (30 minutes, 1h, 2h) at 500 rpm. The $\alpha(CO_2)$ loading, HCO_3^- and N-CO_2^- percentage are referred to the solid amino acid and were determined by ^{13}C qNMR. MCO_3(s) indicate the carbonation yield while R_2NH(s) indicates the amine retention in the solid.

R_2NH	$\alpha(CO_2)$	%HCO_3^-	%N-CO_2^-	Grinding Time	Mg:CO_2	MCO_3(s)	R_2NH(s)
***L*-LysK**	0.57	78%	22%	30min	1:1.02	21%	2%
				1h	1:0.96	13%	2%
				2h	1:0.99	12%	2%

The data revealed higher carbonation yields in the solid state (12%-21%) (Fig.97a, b, c) compared to **GlyK** (1%-9%). It can also be observed that a lower amount of magnesium is leached in presence of *L*-lysine, while once again the remaining metal fraction in the solid can be attributed to unreacted MgO.

The majority of *L*-lysine can be found in the liquid phase, with a constant amine retention in the solid of 2%. It can be observed that the CO_2 lost fraction is more significant with increasing reaction times. This could indicate partial desorption of carbon dioxide, which would also justify the lower carbonation yields. Additional experiments at shorter reaction times are needed to confirm this hypothesis.

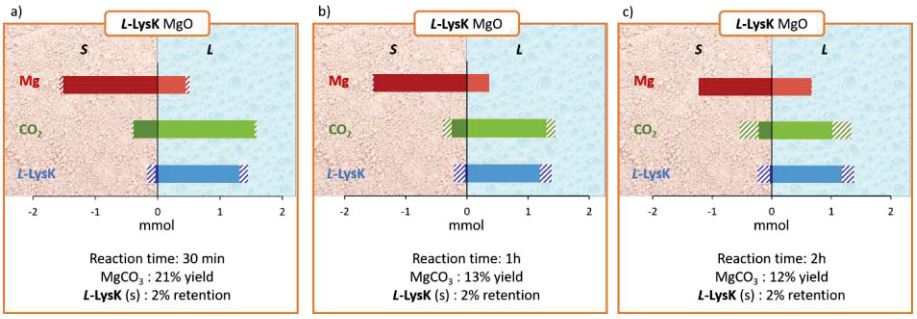

Fig. 97 Neat grinding experiments with 0.3g of ***L*-LysK**-CO_2(s) at $\alpha(CO_2)$ = 0.57. Grinding reactions performed at 500 rpm for a) 30 minutes, MgO:CO_2 = 1:1.02; b) 1h, MgO:CO_2 = 1:0.96; c) 2h, MgO:CO_2 = 1:0.99. Color code: metal (red), CO_2 (green), amine (blue). The graphs are divided into solid fraction (negative values) and liquid fraction (positive values).

In similar operating conditions, 30 minutes of grinding at 500 rpm, the LAG and neat grinding of ***L*-LysK**-MgO showed very different results, for the LAG provided a carbonation yield of 41%, compared to 21% for the neat grinding. These results could be due to the higher concentration of CO_2 in the LAG experiment ($\alpha(CO_2)$ = 0.8), compared to the neat experiment ($\alpha(CO_2)$ = 0.57) but also to the presence of water. As reported by the literature, the presence of a liquid binder can improve the reaction outcome, compared to neat grinding. In order to determine the impact of those factors on the overall carbonating efficiency of the set-up, additional experiments are needed.

Finally, the neat grinding reactions were performed with ***L*-CysK**-CO_2(s) (Fig.98a, b, c). The solid presented a loading of $\alpha(CO_2)$ = 0.61, with only ***L*-CysK-HCO_3^-** adduct (Annexes, page 227).

Table 24 Experimental conditions for the neat grinding of MgO with solid ***L*-CysK**-CO_2. The grinding reactions were performed in a WC reactor for increasing grinding times (30 minutes, 1h, 2h) at 500 rpm. The $\alpha(CO_2)$ loading, HCO_3^- and N-CO_2^- percentage are referred to the solid amino acid and were determined by ^{13}C qNMR. MCO_3(s) indicate the carbonation yield while R_2NH(s) indicates the amine retention in the solid.

R_2NH	$\alpha(CO_2)$	%HCO_3^-	% N-CO_2^-	Grinding Time	Mg:CO_2	MCO_3(s)	R_2NH(s)
***L*-CysK**	0.61	100%	0%	30min	1:0.94	16%	0%
				1h	1:1.05	18%	0%
				2h	1:1.01	29%	4%

Mineral carbonation of MgO assisted by CO_2-loaded *L*-cysteine increases with increasing grinding reaction times, for an $MgCO_3$ extent of 16%, 18% and 29% for 30min, 1h, 2h of grinding, respectively. *L*-Cysteine presents similar trends to glycine and *L*-lysine, with low amine retention in the solid (0-4%) for a significant amine recovery.

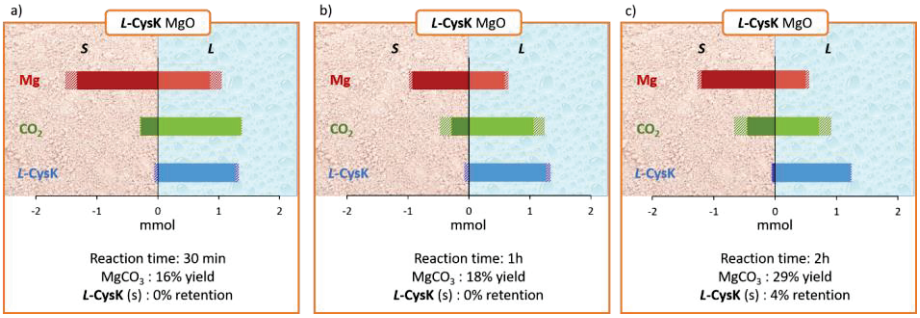

Fig. 98 Neat grinding experiments with 0.3g of ***L*-CysK**-CO_2(s) at α(CO_2) = 0.61. Grinding reactions performed at 500 rpm for a) 30 minutes, MgO:CO_2 = 1:0.94; b) 1h, MgO:CO_2 = 1:1.05; c) 2h, MgO:CO_2 = 1:1.01. Color code: metal (red), CO_2 (green), amine (blue). The graphs are divided into solid fraction (negative values) and liquid fraction (positive values).

For all the experiments described above, additional TGA-MS, NMR and XRD analysis could provide more information about the state of the metal (MgO, $MgCO_3$, $Mg(OH)_2$, $Mg(HCO_3)_2$ or $Mg(R_2NH)(CO_2)$) in the solid phase.

Overall, the neat grinding experiences with solid αAA-CO_2 and MgO showed low amine retention in the solid and lower yield of mineral carbonation, compared to the literature. Nevertheless, the unoptimized experimental set-up showed that both *L*-lysine and *L*-cysteine can be considered for further investigation of the mineral carbonation of MgO.

Table 25 Metal carbonation and amine retention in the solid obtained by neat grinding experiments of MgO with solid αAA-CO_2 adducts. Reactions were performed in a WC reactor at 500 rpm for 30min, 1h, and 2h.

R_2NH	**Grinding time**	**MgO**	
		MCO_3(s)	R_2NH (s)
GlyK	30'	8.9%	0.1%
	1H	6.8%	0.2%
	2H	0.9%	0.2%
***L*-LysK**	30'	25%	2%
	1H	16%	2%
	2H	18%	2%
***L*-CysK**	30'	16%	0%
	1H	18%	0%
	2H	29%	4%

3.3.4 Neat grinding: αAA and CaO

Finally, the two-pots IAM experiment via neat-grinding was performed with solid αAA-CO_2 and CaO. As for MgO, the mechanochemistry experiments were executed in a reactor of tungsten carbide at 500 rpm for a grinding time of 30 minutes, 1 hour and 2 hours.

Table 26 Experimental conditions for the neat grinding of CaO with solid **GlyK**-CO_2. The grinding reactions were performed in a WC reactor at 500 rpm. Carbonation yield and amine retention are indicated as MCO_3(s) and R_2NH(s).

R_2NH	α(CO_2)	%HCO_3^-	% N-CO_2^-	Grinding Time	Ca:CO_2	MCO_3(s)	R_2NH (s)
GlyK	0.61	100%	0%	30min	1:0.98	45%	5%
				1h	1:1.03	50%	10%
				2h	1:1.01	47%	6%

The solid **GlyK**-CO_2(s), analyzed via ^{13}C qNMR, displayed an α(CO_2) of 0.61, with a library composed of 100% of bicarbonate (Annexes, page 221). The grinding was performed with a Ca:CO_2 stoichiometry of 1:1. The results reported in Fig.99a, b, c, show that the mineral carbonation extent varies from 47% to 50%, which is significantly higher than the results obtained by neat-grinding of MgO (< 9%). Although the 1:1 stoichiometric condition could enable in theory complete carbonation, optimization may be required to reach 100% of $CaCO_3$.The majority of the amine is recovered in the liquid phase, with an amine retention in the solid of 5-10%. After the carbonation reaction, the amine recovered in the liquid phase presents a CO_2 loading of 0.56, 0.43 and 0.42, compared to the initial α(CO_2) = 0.61. These preliminary results indicate that the amine is partially regenerated by chemical stripping of carbon dioxide, although additional experiences are needed to determine if the liquid phase could be reused for further carbonation cycles.

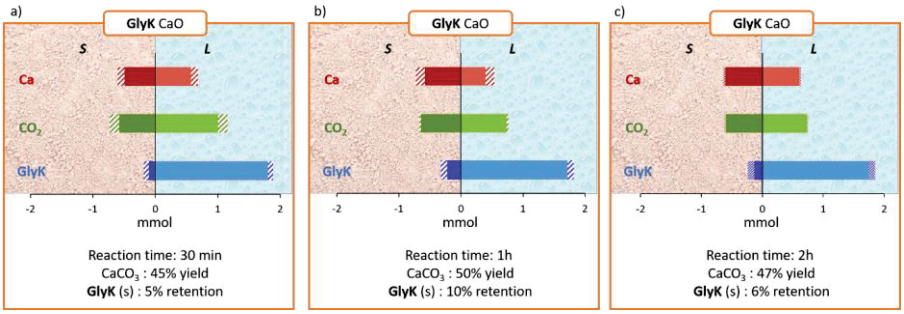

Fig. 99 Neat grinding experiments with 0.3g of **GlyK**-CO_2(s) at α(CO_2) = 0.61. Grinding reactions performed at 500 rpm for a) 30 minutes, CaO:CO_2 = 1:0.98; b) 1h, CaO:CO_2 = 1:1.03; c) 2h, CaO:CO_2 = 1:1.01. Color code: metal (red), CO_2 (green), amine (blue). The graphs are divided into solid fraction (negative values) and liquid fraction (positive values).

Chapter 3

The integrated mineral carbonation of CaO with ***L*-LysK**-CO_2(s) was performed with a new batch of ***L*-LysK** (s), and an excess of CO_2 with respect to the metal (Table 27). The loading of the solid amino acid adduct was determined by ^{13}C NMR, which displayed an $\alpha(CO_2)$ of 0.77 and a library mainly composed of bicarbonates (77%). The ^{13}C NMR spectra can be found in the Annexes, page 223.

Table 27 Experimental conditions for the neat grinding of CaO with solid ***L*-LysK**-CO_2. Carbonation yield and amine retention are indicated as MCO_3(s) and R_2NH(s). The grinding reactions were performed in a WC reactor at 500 rpm.

R_2NH	$\alpha(CO_2)$	$\%HCO_3^-$	% N-CO_2^-	Grinding Time	Ca:CO_2	MCO_3(s)	R_2NH(s)
***L*-LysK**	0.77	77%	23%	30min	1:1.47	82%	5%
				1h	1:1.54	75%	2%
				2h	1:1.74	86%	1%

Fig.100a,b, c reports the results obtained with increasing Ca:CO_2 stoichiometry, 1:1.47, 1:1.54 and 1:1.74, respectively. Although $CaCO_3$ yield does not increase proportionally to the CO_2 stoichiometry, the reaction performed with a 1:1.74 Ca:CO_2 ratio presents the maximum carbonation yield at 86% (Fig.100c). Those results indicate that a non-stochiometric supply of CO_2 may be a way to drive the reaction towards complete carbonation.

The amine retained in the solid is comprised between 1% and 5% for a high purity of the solid and high potential amine recovery. Although no metal was detected in the liquid phase, additional duplicates of these experiments are needed to confirm these preliminary results.

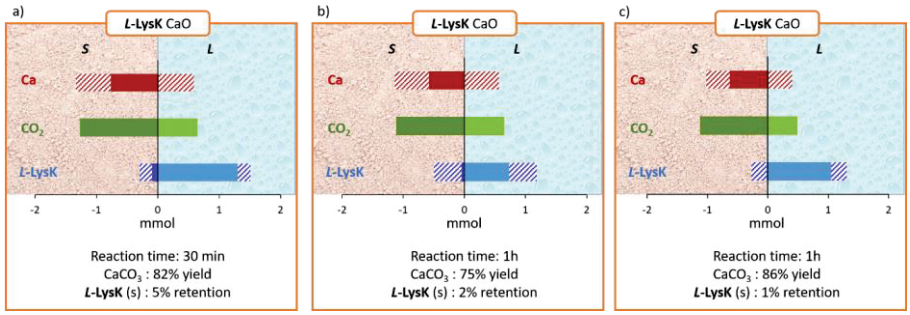

Fig. 100 Neat grinding experiments with 0.3g of ***L*-LysK**-CO_2(s) at $\alpha(CO_2)$ = 0.77. Grinding reactions performed at 500 rpm for a) 30 minutes, CaO:CO_2 = 1:1.47; b) 1h, CaO:CO_2 = 1:1.54; c) 2h, CaO:CO_2 = 1:1.74. Color code: metal (red), CO_2 (green), amine (blue). The graphs are divided into solid fraction (negative values) and liquid fraction (positive values).

Lastly, three IAM neat grinding experiments were performed with CaO ***L*-CysK**-CO_2(s) and loaded at $\alpha(CO_2)$ = 0.52. The ^{13}C qNMR spectra performed to calculate the CO_2 loading can be found in the Annexes, page 224. As for glycine, the solid presents 100% of ***L*-CysK**-HCO_3 adduct.

Table 28 Experimental conditions for the neat grinding of CaO with solid ***L*-CysK**-CO_2. The grinding reactions were performed in a WC reactor at 500 rpm at increasing reaction times (30 minutes, 1h, 2h). Carbonation yield and amine retention are indicated as MCO_3(s) and R_2NH(s).

R_2NH	α(CO_2)	%HCO_3^-	% N-CO_2^-	Grinding Time	Ca:CO_2	MCO_3(s)	R_2NH(s)
***L*-CysK**	0.52	100%	0%	30min	1:1.08	52%	0%
				1h	1:1.11	49%	1%
				2h	1:1.04	45%	1%

As previously observed for the IAM experiment of MgO, *L*-cysteine presents less amine retention in solid (0-1%). The mineral carbonation yield is similar to that of glycine, around 50%, coherently with the hypothesis that a stochiometric quantity of CO_2 does not enable full carbonation of CaO.

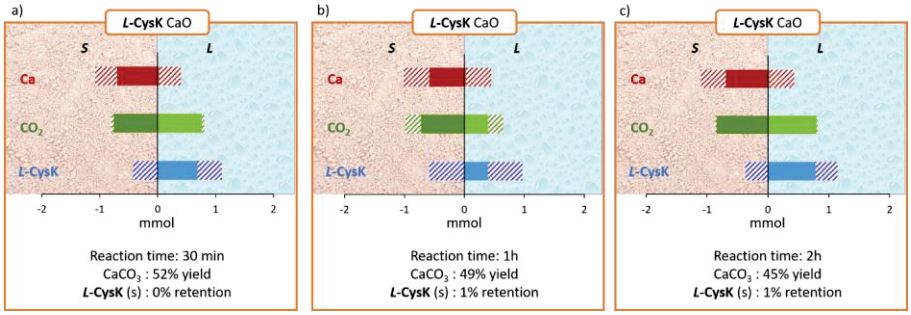

Fig. 101 Neat grinding experiments with 0.3g of ***L*-CysK**-CO_2(s) at α(CO_2) = 0.52. Grinding reactions performed at 500 rpm for a) 30 minutes, CaO:CO_2 = 1:1.08; b) 1h, CaO:CO_2 = 1:1.11; c) 2h, CaO:CO_2 =1:1.04. Color code: metal (red), CO_2 (green), amine (blue). The graphs are divided into solid fraction (negative values) and liquid fraction (positive values).

Overall, the Integrated Absorption Mineralization experiments performed on CaO with solid αAA-CO_2 showed efficient carbonation performances with low amine pollution of the solid. CaO proved to be more reactive compared to MgO, coherently with the results brought by the literature. This phenomenon could be due to the higher solubility of the hydroxide (pKs = 5.19 for $Ca(OH)_2$, compared to 11.15 for $Mg(OH)_2$) and to a lower solubility of the carbonate (pKs = 8.35 for $CaCO_3$, compared to 7.46 for $MgCO_3$).

The neat-grinding pathway was chosen as a greener alternative to IAM processes in solution, although the limited quantities of CO_2 introduced in the reaction could have prevented the obtention of higher carbonate yields.

Table 29 Metal carbonation and amine pollution in the solid obtained by neat grinding experiments of CaO with solid αAA-CO_2 adducts. Reactions were performed in a WC reactor at 500 rpm for 30min, 1h, and 2h.

R_2NH	Grinding time	CaO	
		MCO3(s)	R2NH(s)
GlyK	30’	45%	5%
	1H	50%	10%
	2H	47%	6%
L-LysK	30’	82%	5%
	1H	75%	2%
	2H	86%	1%
L-CysK	30’	52%	0%
	1H	49%	1%
	2H	55%	1%

Commenté [ct1]:

4 Conclusions to chapter 3

In this chapter were presented several Integrated Absorption Mineralization experiments for various amine-metal systems. The investigation of a homogeneous system, such as R_2NH-$MgCl_2$, showed the influence of a metal template on a dynamic combinatorial library, although it displayed no efficient carbonation of the metal.

The analysis of a heterogeneous R_2NH-$CaCl_2$ system proved the efficiency of amino acids for IAM experiments. ***L*-LysK**, for instance, provided a carbonation yield of 89% with 4% of amine retention in the solid. The amine recovery by chemical CO_2 stripping was achieved at room temperature and for short reaction times, providing a less energetic alternative to the current methods proposed in the literature.

Finally, the liquid assisted grinding and neat grinding of both transition metal oxides and alkaline/alkaline earth oxides proved mechanochemistry a useful tool for both mineral carbonation and metal lixiviation. MgO showed limited reactivity compared to CaO, coherently with the literature. The comparison between neat grinding and LAG for a ***L*-LysK** MgO system showed that the introduction of a limited volume of a liquid binder can improve mineral carbonation whilst keeping a low amine retention in the solid.

L-Lysine proved to be the most efficient amine for CaO carbonation, reaching 86% conversion after 30 minutes of neat grinding at 500 rpm. Further studies are required to simultaneously optimize metal carbonation and amine regeneration.

Chapter 4
Soil carbonation and decontamination

Chapter 4

Objective

The fourth chapter of the thesis focuses on the depollution of a metal-contaminated soil, provided by the cement industry Vicat, using CO_2-loaded amines as chelating and leaching agents.

The state or the art will present a general overview of synthetic chelating agents and possible natural substitutes. Although amino acids have been widely discussed as ligands for metal complexes, the literature reports scarce studies on their role as chelating agents for soil remediation. Nevertheless, their efficiency and suitability will be exploited. In this chapter, CO_2-loaded solutions of **DETA**, ***L*-LysK**, ***L*-CysK** and **GlyK** will be used as lixiviants for soil depollution via Liquid Assisted Grinding experiments. Each system will be investigated for its efficiency and selectivity towards metal extraction and soil remediation, and the recycling potential of chelating agents will be analyzed. Finally, the possible carbonation of the soil matrix upon CO_2 introduction will be explored and discussed. The approach proposed in this chapter could provide an example of simultaneous metal remediation and mineral carbonation of soils.

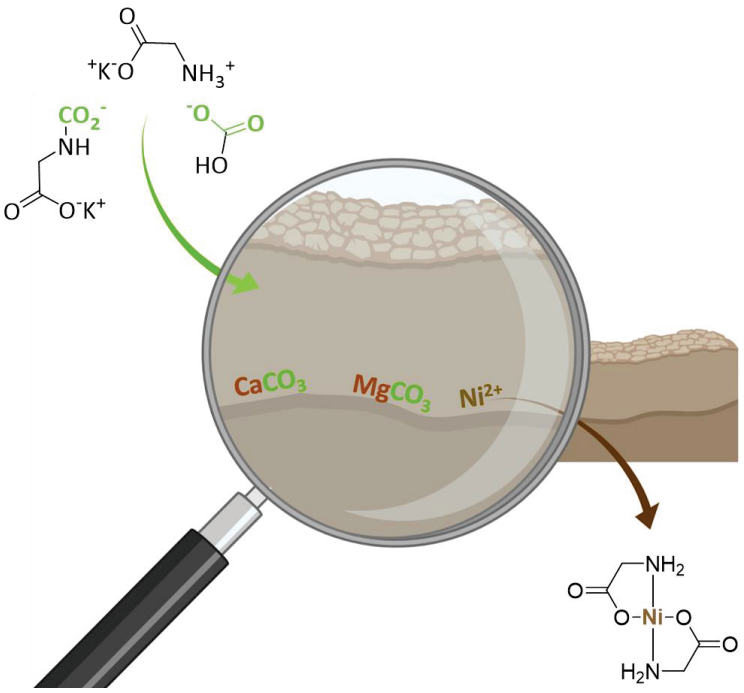

Chapter 4

1 State of the art

In the general introduction (Chapter 1, section 3, page 53) were presented several techniques for soil depollution, including soil washing with metal chelating agents[214], which can be applied for *ex situ* treatments of soils contaminated by heavy metals (Hg, Cd, Cu, Ti, Pb, Ni, Mn, Mo and Zn[117-118]).

Heavy metals (HMs) such as lead, zinc, cadmium, chromium and mercury[107], can be retained in the soil matrix in different forms and phases, depending on the nature of the soil. The binding mechanisms between soils and metals can consist in metal absorption on Fe/Mn oxides, clay particles, organic matter and carbonates. Heavy metals can also be retained as exchangeable ions[215] adsorbed on the surface of clay and humus, or in the insoluble fraction of the soil, denominated the "residual fraction".

The latter is composed of primary minerals, formed from primary igneous rocks, and secondary minerals, formed from weathering of primary rocks (i.e. aluminum silicates). The metals fixed in this fraction are usually recovered using a mixture of HF/HNO_3 and cannot be liberated via natural weathering[216].

Soil washing, or chemical leaching, was introduced in Chapter 1, section 3.2, page 54, and is a technique which consists in extracting metals via the use of acid solutions or via chelating agents. Via this technique the heavy metals are transferred from the solid matrix to the liquid phase, and then recovered from the leachate.

In literature there are numerous examples[119, 214] of soil washing procedures with strong acids solutions such as HCl, HNO_3, H_3PO_4 and H_2SO_4. These are very effective for the disruption of the soil matrix, liberating heavy metals in solution and thus yielding high metal recovery rates[214]. The use of acids, though, can alter the physical, chemical and biological features of the soil[215, 217] such as its texture, porosity and pH. These modifications influence the habitat of microorganisms, bacteria and fungi, which limits the suitability of strong acid for sustainable soil remediation[107]. For this reason, despite their high extraction efficiency, mineral acids are often substituted with organic chelating agents.

Chapter 4

1.1 Synthetical organic chelating agents

Chelating agents present an efficient soil remediation method[196], for they desorb trace metals from soil by forming stable and water-soluble metal complexes.

In Fig.102 is represented an example of *ex situ* process for soil washing with chelating agents. The contaminated soil is introduced in a soil scrubbing unit, wherein it is contacted with an aqueous stream of chelating agent; the washing solution is then recovered and treated to regenerate the chelating agent which can then be reused for other soil washing steps.

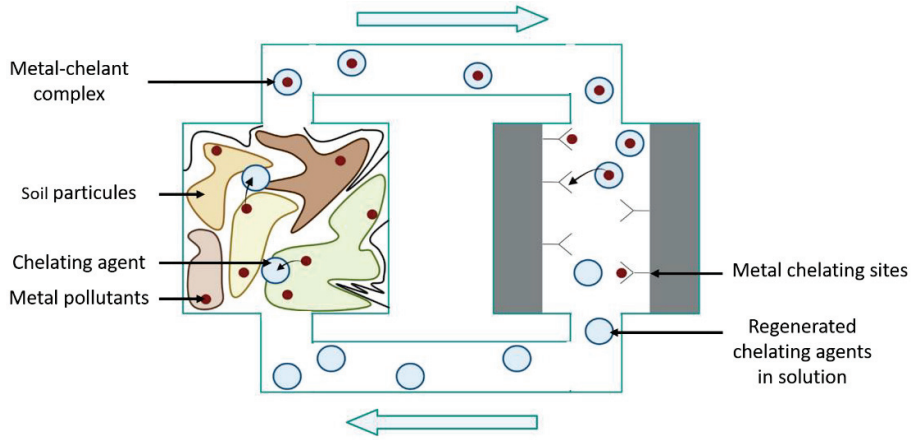

Fig. 102 Example of *ex situ* process for soil washing by chelating agent. Overall view of the extraction route with consequent regeneration and recycle of the chelants. Modified from a study published by Mohamed *et al.* [218]

A different example for *ex situ* soil washing can be introducing the soil in a stirred vessel with the washing solution for several hours, and then filtering the mixture to recover the leachate and the depolluted soil. Specific operating conditions such as washing time, concentration of the extracting agent, temperature and stirring rate depend on the type of pollution and depolluting agent in involved.

According to the literature, the choice of a suitable chelating agent is based on many factors[196-197, 219-220], reported hereafter:

- Extraction selectivity towards target metals.
- Extraction strength: the newly formed chelant-metal complexes should be stable over a wide pH range.

- The chelant should form metal complexes with low adsorption affinity towards solid soil surfaces.
- Recycling potential and low biodegradability in the soil, meaning that it should not be degraded by the microorganisms, bacteria and fungi present in the soil.
- Low toxicity and a low potential to harm the environment.
- Cost-effective.

It must be considered that polluted soils may present different properties based on their phase composition; for instance, the carbonate percentage of a soil can have a great influence on the soil pH. For this reason chelants should display a constant extraction strength over a wide pH range[221].

The most employed class of synthetical chelating agents for soil decontamination are amino polycarboxylates (APCs) [107, 220, 222]. They are chosen for their high affinity towards HMs and because they are cost effective. A few structures are represented in Fig.103.

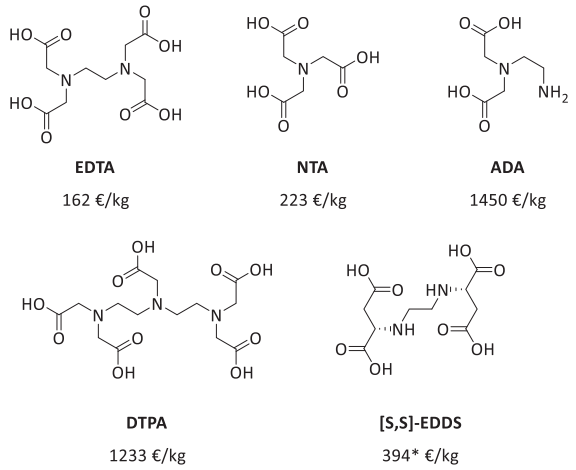

Fig. 103 Structure of APCs chelating agents: ethylenediaminetetraacetic acid (**EDTA**), nitrile triacetic acid (**NTA**), N-2-(acetamido)iminodiacetic acid (**ADA**), diethylenetriamine pentaacetic acid (**DTPA**) and ethylenediamine-disuccinic acid [S,S]-**EDDS**. Price in euros/kg by Sigma Aldrich at reagent pure grade 98%. * value for 1L of **EDDS** trisodium salt solution.

A study published in 2005 reported that the biodegradability of APCs increases when the number of tertiary amines in the ligand structure decreases (order of biodegradability **NTA/ADA > EDTA > DTPA**)[223]. In addition, the presence of primary and secondary amines

results in an increased susceptibility of APCs to biodegradation [223-224]. Therefore, **EDDS**, **NTA** and **ADA** will be more readily biodegraded compared to **DTPA** and **EDTA**. In the study, the author reported that the biodegradability of a chelant-metal complex would be influenced by the stability of said complex, although the correlation is not linear and it cannot be considered the only affecting factor.

The most investigated APC is **EDTA**, prevalently chosen for its ability to increase the solubility of heavy metals in the soil[225]. The chelating agent is usually employed as its disodium salt **Na_2EDTA** and presents high complexation constants with metals such as Pb, Zn, Cu, Cd and Fe, (for which the logK is, respectively, 18, 17.5, 19.7, 17.4 and 25)[226]. In the field of soil depollution process based on **EDTA** washing, several researches focused on the development of the most efficient operating conditions for metal recovery and chelant regeneration. A study published in 2016 showed that adding Na_2S or $Na_2S/Ca(OH)_2$ to a leachate solution of **EDTA** with Pb, Cd and Zn allowed a metal recovery of, respectively 99.32%, 99.61%, and 99.55%[221], with simultaneous regeneration of the ligand (eq.104).

$$\textbf{EDTA}\text{-Pb} \xrightarrow[0.5M\ Na_2S]{} \textbf{Na}_2\textbf{EDTA} + PbS \qquad (104)$$

In 2012, Udovic *et al.*, investigated the environmental impact of **EDTA** compared to HCl. Solutions of Na_2**EDTA** and HCl at different concentrations (3.75–45 mM for **EDTA** and 0.5–4M for HCl) were introduced on a Pb-polluted calcareous soil ($CaCO_3$ > 44%), displaying near to neutral pH (6.76-6.89). A 30mM solution of **EDTA** and a 4M solution of HCl showed similar HMs removal efficiency, measured by ICP-AES (Inductively Coupled Plasma Atomic Emission Spectroscopy). Nevertheless, the solutions displayed different impacts on soil properties. To determine the environmental impact of both washing agents, Udovic *et al.* tested the soil with enzyme activity assays. The latter consisted in comparing the substrate (glucose)-induced respiration (SIR), Phosphatase activity and Dehydrogenase activity of an untreated soil sample versus samples treated with **EDTA** and HCl. The test confirmed that HCl had a greater negative impact on soil enzyme activity[215], compared to **EDTA** leaching [107]. However, **EDTA** increased the soil pH (7.33-7.5 compared to 6.76-6.89), which could cause further repercussions on the soil microorganisms.

Furthermore, in 2016 Jez *et al.* investigated the extent of **EDTA** retention in a Pb-contaminated soil by mixing 10 mL of **EDTA** (120 mmol/kg of soil) with 10 grams of dried soil for 2h and 24h at 200 rpm, 25 °C. The chelating agent was used as a disodium salt (**Na_2H_2EDTA**) and as

calcium-disodium salt (**$CaNa_2$EDTA**). in free acid form (**H_4EDTA**), and it was observed that 20% of **EDTA** can be retained in calcareous soils, while acidic soil can retain 64% of the chelating agent[227]. This means that **EDTA** can represent an additional pollution source for the treated soils. Although low toxicity and low environmental harm are fundamental points in the choice of a chelating agent, the literature presents scarce and discording studies about the long-term effect of **EDTA** soil washing[228].

In a study published in 2009, Udovic and Lestan[229] stated that metal remediation experiments with **EDTA** increased metal mobility in the soil exchangeable fraction, which caused higher natural weathering of heavy metals from the soil. In 2014, Jelusic *et al.*[228] reported opposite results, claiming that soil treatment with **EDTA** did not influence a metal shift between soil fractions. Consequently, Jelusic *et al.*[228] state that **EDTA** soil washing did not cause undesirable long-term metal lixiviation phenomena.

Although the literature presents incomplete and incoherent results about the long-term effect of soil remediation with **EDTA**, researches are investigating other potential new chelating agents which could substitute the use of synthetical APCs.

1.2 αAA as chelating agents

Amino acids may represent a viable alternative to synthetic amino polycarboxylates; nevertheless, they have hardly been explored as soil remediation chelators.

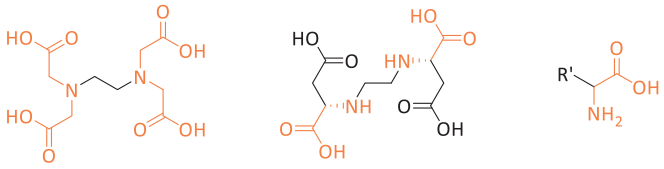

Fig. 104 Structures of **EDTA**, **EDDS** and general amino α acid with highlighted common binding sites.

Natural amino acids are known as metal complexing agents[230-232], they present the same fundamental binding sites of APCs (carboxylates/amines), plus a variety of structures and binding sites present on the R-chain, which could enable high selectivity towards metals (i.e. Pb, Cd, Zn, Ni)[230, 233]. Since amino acids play an important role in agriculture as fertilizers[234] and nitrogen source for plant growth[235], the potential retention of αAA in the soil during the washing treatment could stand as a benefic advantage, rather than a drawback.

In 2020, Dolev *et al.*[236] evaluated several amino acids as chelating agents for soil remediation. Solutions of free αAA, including glycine, *L*-cysteine and *L*-aspartic acid, were introduced in soil samples polluted with Cu, Pb, Zn, Cd and Ni. Except for aspartic acid, which was adjusted at pH 7 with NaOH, the amino acids solutions were buffered by the soil, which displayed a pH of 6.8[236]. The metal-leaching experiments were performed by mixing 20 mL of a 0.25 M solution of free amino acids with 3g of soil and stirring the mixture at 60 °C for 2 h. In Table 30 are reported the initial concentrations of metals in the soil and the amino acid/metal ratio.

Table 30 Metal concentration of the soil as reported by Dolev *et al.*[236], and amine/metal ratio calculated for the mixture of 20 mL of a 0.25 M solution of amino acid with 3 grams of soil.

Metal	ppm (mg/kg)	aAA/M
Cd	1105 ± 19	169
Cu	367 ± 4	289
Ni	612 ± 2	160
Zn	665 ± 33	164
Ca	72.067 ± 0.4	930

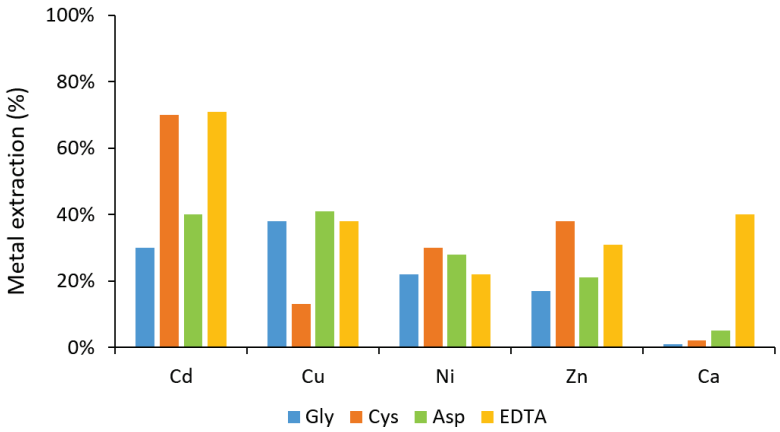

Fig. 105 Metal extraction yield (%) obtained from the lixiviation of polluted soil with 0.25M aqueous solutions of glycine, cysteine and aspartic acid compared to **EDTA**; the reactions were performed stirring the mixture at 60 °C for 2 h. Data extrapolated by Dolev *et al.* 2020[236].

The extraction results obtained by αAA in the article are compared to those of **EDTA**, and are showed in Fig.105.It can be noted that amino acids present similar efficiency to **EDTA**, except for calcium: 70% of cadmium is extracted by both *L*-cysteine and **EDTA** and around 40% of copper is extracted by glycine, *L*-aspartic acid and **EDTA**. Amino acids do not show a strong selectivity towards one metal, but rather a general high extraction efficiency.

Fig.105 also shows that the highest extraction of calcium is obtained by **EDTA** (40%), which can have a negative impact on the soil, altering its physical and chemical properties. On the contrary, amino acids extract a maximum of 5% of Ca^{2+}, therefore can be considered soil-friendly washing agents. Furthermore, the low extraction of Ca^{2+} suggests a low selectivity of amino acids towards matrix cations, which enhances the AAs efficiency for metal recovery.

Table 31 Stability constant (logK) of metal complexes for a ML^{-}_{2} metal:ligand stoichiometry at 25 °C by Dolev 2020[236]. * Value for L^{2-}. ** Value $M(HL)_2$[208].

L^{-}	**Cd^{2+}**	**Cu^{2+}**	**Ni^{2+}**	**Pb^{2+}**	**Zn^{2+}**
Gly	7.7	15.1	11.1	8.1	9.2
L*-Cys	16.9	/	20.2	16.9	17.9
L*-Asp	7.5	15.9	12.3	8.5	10.2
***L*-Lys**	/	15.05[237]	9,15**	/	/

The extraction efficiency of amino acids can be justified by the stability constant of αAA-metal complexes stated in Table 31; the structures of said metal-amino acid complexes are shown in Fig.106, as reported by the literature:

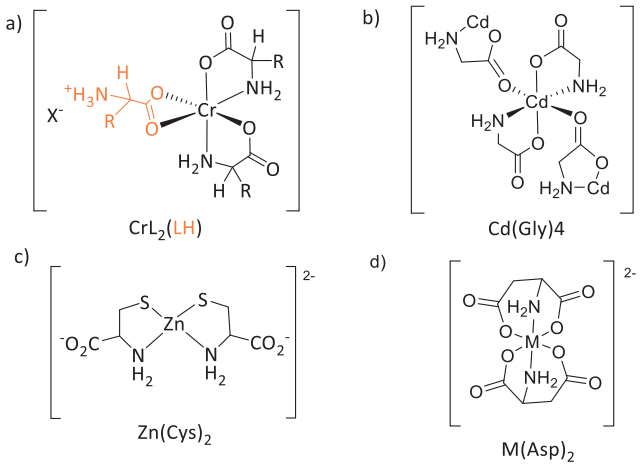

Fig. 106 Metal complexes present in literature; a) Cr(III) complex with αAA[231]; b) Cadmium (II) complex with glycine[238]; c) Zn(II) complex with *L*-cysteine[239]; d) *L*-aspartic acid tridentate metal complex[236].

The metal complexes reported in Fig.106 reveal the variety of binding sites which can be involved in metal-binding of chelating amino acids. The chromium (II)[231] and cadmium (II)[238] complexes involve a carboxyl/ammine chelation pattern, while zinc[239] is chelated by the sulfhydryl and amine groups of *L*-cysteine. *L*-Aspartic acid can form stable complexes as a trident ligand, due to the carboxyl group on the side chain[236].

Although *L*-lysine was not directly investigated as a soil remediation agent, it represents an amino acid of interest in this work. In 1963, Busch[240] investigated the Ni(**Lys**)$_3$ complexes for which it was noticed that carboxyl and alpha amine groups are the metal binding sites, while the amino butyl chain remains free (Fig.107a). In the same study it was observed that basic amino acids with shorter chains (n(CH_2) = 2, 2,4-diaminobutyric acid; n(CH_2) = 3, ornithine) can form either bidentate or tridentate complexes (Fig.107b,c).

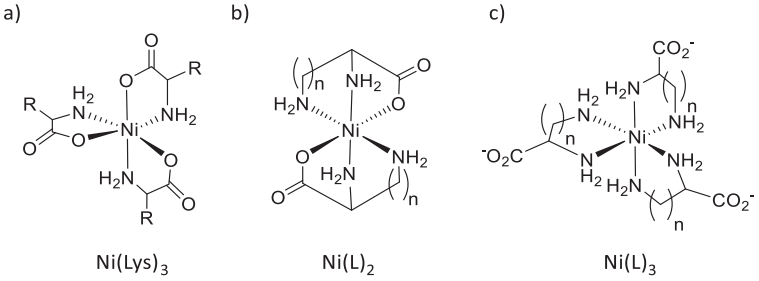

Fig. 107 Diamine-nickel metal complexes; a) ML_3 Ni(II) complex with lysine [240]; b) ML_2 Ni(II) complexes with diamine tridentate amino acids[240], logK = 15.97 for ML_2 diaminobutyric acid complex at 25 °C, 0.1 ionic strength; c) ML_3 Ni(II) complexes with bidentate diamine amino acids with n(CH_2) = 3, ornithine, logK = 10.17 at 25 °C, ionic strength 0.

The efficient metal extraction, high stability constant and versatility structures of amino acid/metal complexes obtained by the literature, support the choice of amino acids as potential chelating agents for soil remediation.

Another important aspect studied by Dolev *et al.* was the influence of pH on metal remediation by amino acids. Samples of contaminated soil were treated with two solutions of Aspartic Acid, one at pH 2.3 and the other at pH 7, adjusted with NaOH.

It is expected that at low pH the amino acid solution will dissolve the matrix carbonates liberating trace metals, while its chelating effect towards the metal will lower. On the other hand, at a neutral pH, ***L*-AspNa** is deprotonated (pKa_1 = 2.09, pKa_3 = 3.86), its chelating effect is increased, thus the amino acid is more efficient towards metal complexation[236]. The results reported by Dolev *et al*. confirmed these tendencies, demonstrating that amino acids are efficient chelating agents for soil remediation even at neutral pH. The discussion reported by the authors focuses on the pKas in absence of metals, while it should be considered that the formation of stable metal complexes could alter the pKa of the amino acids[241].

1.3 Metal separation and recovery

In section 1.1 of this chapter, was mentioned that chelating agents such as **EDTA** can be regenerated inducing metal precipitation. If the metals extracted from a polluted soil could be recovered with high purity, this step would provide an economic benefit which accompanies the soil remediation.

In 2016, our group investigated a new method for simultaneous CO_2 capture and metal separation via a supramolecular approach[242], focusing on the use of polycarbamates as potential metal chelating agents. Polycarbamates were considered as potential metal ligands as they are analogues of polycarboxylates, which are widely used metal chelating agents. In our preliminary investigations a solution of 0.5M **DETA** was studied in presence of two bimetallic systems Fe^{3+}/Nd^{3+} and Co^{2+}/Sm^{3+}, in MeOH and with an amine:metal stoichiometry of 12:1. The study, performed with trifluoroacetate metal salts ($Fe(CF_3CO_2)_3$, $Nd(CF_3CO_2)_3$) yielded soluble amine-metal complexes. Carbon dioxide was then added in the solution, causing the formation of a white precipitate, identified as a polycarbamate complex of Nd^{III}. The Co^{2+}/Sm^{3+} metallic couple showed similar results for the same operating conditions.

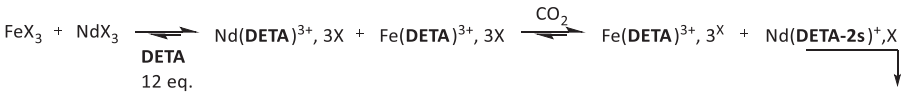

$X=CF_3CO_2^-$

In this way, the CO_2 introduced into the **DETA**/bimetallic solution induces phase and metal separation, proving a spontaneous separation between transition and rare earth metals via formation of soluble amine complexes and insoluble polycarbamate complexes[242].

Furthermore, in 2020, our group proposed a CO_2-capture based process to recycle metals contained in batteries[41]. The investigation was conducted on an aqueous bimetallic system prepared from $LaCl_3$ and $NiCl_2$ (Fig. 108a) wherein the introduction of 12 equivalents of **DETA** yielded soluble amine-Nickel complexes and solubilized $LaCl_3$ (Fig.108b).

A pure stream of CO_2 was then introduced in the solution where it is captured by **DETA** as symmetric dicarbamate **DETA-2s**. Lanthanum is then complexed by the polycarbamate yielding La(**DETA-2s**)$_2$H. The latter is then hydrolyzed causing the precipitation of $La_2(CO_3)_3$. After full precipitation was reached, the solid and liquid phases were separated enabling the recovery of both Ni(**DETA**)$_2Cl_2$ and $La_2(CO_3)_3$ (Fig.108c).

In addition, this metal separation process was tested with exhaust fumes of an internal combustion engine as CO_2 source, instead of a pure gas flux. Even in those conditions the metals were successfully recovered, with yield and purity of 99% for both metals.

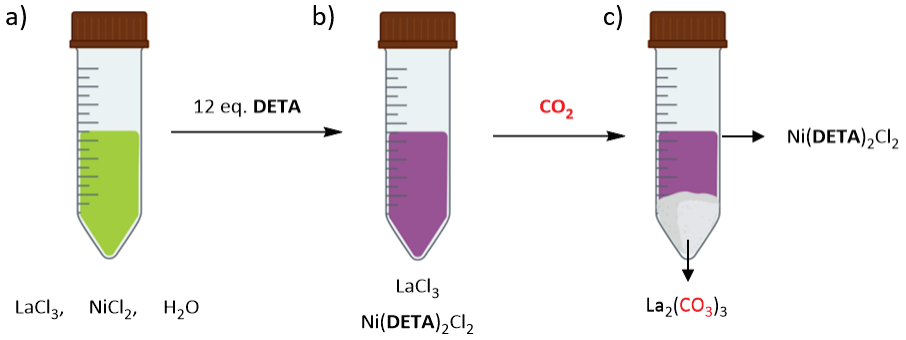

Fig. 108 Separation of $LaCl_3$ and $NiCl_2$ via supramolecular approach by addition of **DETA** and CO_2; a) aqueous solution of $LaCl_3$ and $NiCl_2$; b) introduction of 12 eq. of **DETA** and formation of soluble Ni(**DETA**)$_2Cl_2$ complexes; c) introduction of CO_2 and precipitation of $La_2(CO_3)_3$.

Furthermore, the same metal separating method was applied to a trimetallic La_2CoNi_9 alloys. The first step of the process saw the introduction of CO_2 in a **DETA**-metals solution, which caused selective separation of $La_2(CO_3)_3$ from the trimetallic system, with a 99.4% yield and a 99.8% purity.

The resulting bimetallic (Co,Ni) solution was treated via two additional CO_2 loading steps and two EtOH/*i*-PrOH washing steps, after which it was possible to collect 55% of Cobalt as a complex of **DETA**-CO_2 at 97% purity and 95% of Ni as Ni(**DETA**)$_2Cl_2$ with 98% purity. The efficiency of those proposed separation processes is based on the intrinsic affinity of each metal towards CO_2 and NH_2 ligands, resulting in a versatile tool which can be applied to a variety of substrates.

In this chapter several amines will be investigated for their efficiency and selectivity towards metal extraction and remediation both in presence and in absence of CO_2. Despite being an industrial polyamine, **DETA** will be exploited as a potential chelating agent for soil remediation and used as reference to which other natural chelating agents (glycine, *L*-lysine and *L*-cysteine) will be compared. Furthermore, the amine capacity to capture CO_2 will be exploited to introduce carbon dioxide in the soil, potentially allowing mineral carbonation and stable CO_2 storage.

Chapter 4

2 Description of the soil used in this study

The soil investigated in his work was brought from St. Jean d'Illac, near Bordeaux. The soil is a waste product of an industrial site and was chosen for its elevated concentration of heavy metal. Before starting the investigation, the soil was analyzed by several techniques to gain maximum knowledge about its composition.

In order to collect a representative sample of the soil, two kilos of the matter were dried at 40 °C and grinded in an industrial mechanochemistry reactor until reaching a particle diameter of < 2mm. The sample was then separated by the quartering technique, which consist in creating four equal sections, two of which will be chosen to form a final reduced sample, representative of the whole soil (Fig.109).

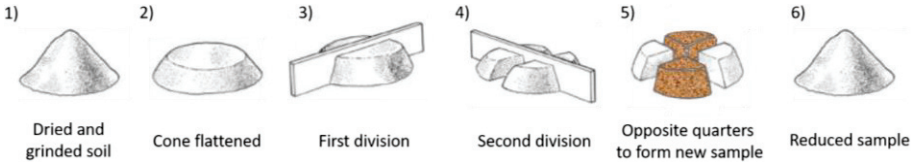

Fig. 109 The six steps of the quartering technique: 1) Drying and grinding, 2) flattened cone form, 3) first division, 4) second division, 5) collection of two opposite quarters (colored in brown), 6) obtention of a reduced and quartered sample.

An X-Ray Diffraction (XRD) analysis provided a general comprehension of the abundance of the different phases in the soil. In Fig.110 is showed a simplified representation of the soil in which the different major components are divided in layers, although this does not represent the actual distribution of the components in the soil. It can be observed that Quartz and Aluminosilicates are the major components, accounting for 46% and 39% of the soil, respectively.

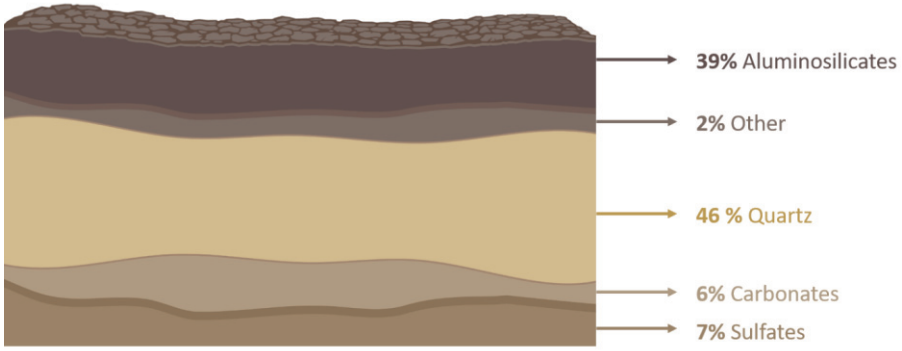

Fig. 110 Simplified representation of the phases of the soil, expressed in weight percentage obtained by an XRD analysis. Phases in order of abundance: Quartz (46%), Aluminosilicates (39%), Sulfates (7%), Carbonates (6%), Others (2%).

Apart from Quartz and Aluminosilicates it is possible to observe the presence of carbonates, sulfates and other minerals such as Anglesite ($PbSO_4$), which is symptomatic of a lead pollution. It is also possible to notice that calcium carbonates and sulfates represent 9% of the overall composition (Table 32).

Table 32 Detailed composition of the soil, divided in principal major phases: silicates, carbonates, sulfates, alumino-silicates and other.

Phase	Mineral	Composition	Percentage
Silicates	Quartz	SiO_2	46%
Carbonates	Calcite	$CaCO_3$	4%
	Aragonite		2%
Sulfates	Gypsum	$CaSO_4*2H_2O$	5%
	Arcanite	K_2SO_4	2%
Alumino-silicates	Clinochlore	$(Mg, Fe^{2+})_5Al(Si_3Al)O_{10}(OH)_8$	5%
	Chlorite IIb	$(Fe, Mg, Al)_6(Si,Al)_4O_{10}(OH)_8$	2%
	Kaolinite	$Al_2Si_2O_5(OH)_4$	4%
	Orthoclase	$KAlSi_3O_8$	10%
	Albite	$NaAlSi_3O_8$	9%
	Muscovite 2M2	$KAl_2(Si_3Al)O_{10}(OH, F)_2$	9%
Other	Hematite	Fe_2O_3	1%
	Anglesite	$PbSO_4$	1%

In order to qualify and quantify the metallic components of the soil, three external laboratories were charged to perform a complete ICP-OES analysis following an acid mineralization using HF/HNO_3. From the results obtained by the three laboratories was calculated the average initial concentration of each metal and its standard deviation. In Fig. 111 are reported the parts per million of each metal in the soil, also defined as

milligrams of metal per kilogram of dried soil (DS); metal concentrations expressed in mmols per gram of soil can be found in the annexes, page 227.

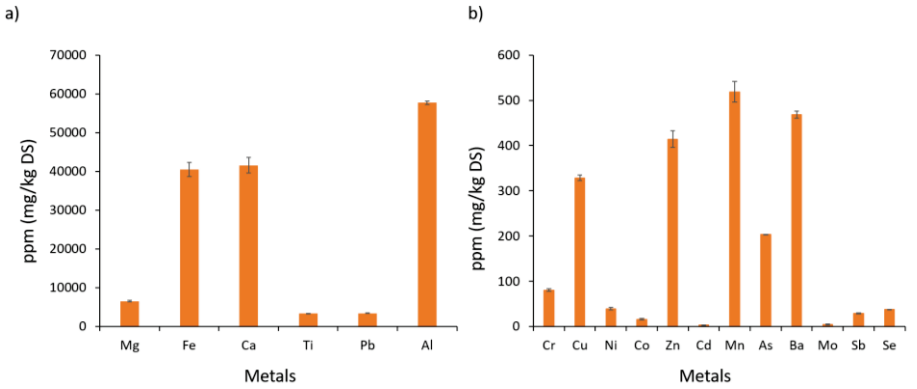

Fig. 111 Concentration of metals expressed in parts per million (ppm) also defined as milligram of metal per kilogram of dried soil (mg/kg DS) and its relative error. a) concentration of most abundant metals in the soil (majors), b) concentration of less abundant metals in the soil (minors).

The soil presents two groups of metals, those showing the highest concentrations (up to 60000 ppm) are defined as major metals (Fig. 111a) and include magnesium, iron, calcium, titanium, lead and aluminum, in agreement with the phases identified by XRD. The remaining metals, whose concentration varies from several ppm to 500 ppm are defined as minor metals and include chromium, copper, nickel, cobalt, zinc, cadmium, manganese, arsenic, barium, molybdenum, antimony and selenium (Fig. 111b).

In 2012, a French prefectural decree imposed specific leaching limits for metals in materials used for the cement production. The leaching limit indicates how many ppm of a certain metal can be leached from a material by natural weathering.

To determine the natural leaching extent of metals in the investigated soil, a simple water extraction was performed by an external laboratory. The experimental procedure consisted in introducing a sample of 111 g of soil in 900 mL of distilled water, stirred for 24 h. Afterwards the solution was tested for leached metals and the results are reported in Table 33, together with the leaching limit per metal permitted by law.

Table 33 Concentration of metals in the soil, metal leaching and limit given by a French law of 2012.

Element	Soil (ppm)	Leaching (ppm)	2012 Law (ppm)
Cr	80.3	< 0.01	0.5
Cu	328.3	0.03	2
Ni	39.2	0.04	0.4
Zn	414.0	0.1	4
Cd	3.1	0.0002	0.04
As	203.0	0.57	0.5
Ba	468.9	0.26	20
Sb	28.5	0.49	0.06
Se	38.0	0.19	0.1
Pb	3400.8	0.08	0.5

Table 33 indicates that arsenic (As), antimony (Sb) and selenium (Se) exceed the legal lixiviation limit, presenting therefore a source of pollution, while lead is contained in the matrix in its stable form of $PbSO_4$. Once the information about phase composition, mineral percentage, metal presence and limitations were gathered, a sequential extraction of the soil was investigated.

Sequential extraction is a tool to determine the mobility of trace metals based on their mineral phase (carbonates, oxides, etc.). First used around the 1970's[216] the protocol was modified[243-245] throughout the years until it was officially standardized. It is divided into four steps: the first is the extraction via acetic acid to leach the acid-soluble fraction (carbonates); second is the treatment with Hydroxylammonium Chloride ($NH_3OH^+Cl^-$) to leach the reduceable fraction (oxides); third is the reaction with Hydrogen Peroxide (H_2O_2) and Ammonium Acetate ($CH_3CO_2^-NH_4^+$) to lixiviate the oxidable fraction (organic matter); finally, any metal which was not leached in the first three steps is considered as contained in the residual section.

The protocol can be found in the experimental section (section 2.9, page 202) and the results are reported in Table 34. The sequential extraction reveals a higher percentage of carbonate for cadmium (Cd 69%), copper (Cu 37%) and manganese (Mn 47%); selenium is contained completely in the organic portion, while the rest of the metals is mainly contained in the residual fraction. It must be mentioned though, that the metal distribution determined by sequential extraction does not directly reflect the metal association with the different soil phases[246]. In Table 35 can be found the pKs values for metal carbonates and metal hydroxides at 25 °C.

Table 34 Extraction rate divided in the four steps of the sequential extraction performed on the polluted soil. First extraction concerns the carbonate fraction, second the oxides, third the organic matter and fourth the residual fraction.

Element	Sequential extraction							
	Extraction 1 Carbonates		Extraction 2 Oxides Fe		Extraction 3 Organic matter		Extraction 4 Residual fraction	
	mg/kg	%	mg/kg	%	mg/kg	%	mg/kg	%
As	1.5	1%	9	4%	4	2%	185	93%
Cd	1.3	69%	0	17%	0	9%	0	5%
Co	3.9	23%	1	8%	1	6%	11	63%
Cr	12	14%	1	1%	17	21%	52	64%
Cu	122	37%	19	6%	87	26%	102	31%
Mn	256	47%	65	12%	57	11%	161	30%
Ni	9	21%	4	10%	5	13%	23	56%
Pb	50	2%	103	3%	16	1%	3029	95%
Sb	1	2%	1	3%	1	3%	26	92%
Se	0	1%	1	1%	39	101%	-1	-3%
Sn	0	0%	0	0%	2	4%	37	95%
Zn	133	35%	66	17%	40	11%	140	37%
Ba	6	1%	21	4%	97	21%	346	74%

Table 35 Metal carbonate and hydroxide pKs at 25 °C and ionic strength 0. * ML_3, ionic strength 0.5. ** value for ML_2/MO. ***Value for $Ba(OH)_2$*8 H_2O.

Metal	pKs MCO_3 $M^{n+}(CO_3^{2-})_m$	pKs $M^{n+}(OH)_n$
As^{3+}	/	/
Cd^{2+}	13.74	14.35
Co^{2+}	9.98	14.9
Cr^{3+}	/	29.08*
Cu^{2+}	9.63	19.32
Mn^{2+}	9.3	12.8
Ni^{2+}	6.87	15.2
Pb^{2+}	11	15.1**
Sb^{3+}	/	/
Se^{2+}	/	/
Zn^{2+}	10	15.52
Ba^{2+}	8.3	3.6***
Al^{3+}	/	33.5
Fe^{3+}	/	38.8
Mg^{2+}	7.46	11.15
Ca^{2+}	8.35	5.19

Furthermore, the soil was analyzed by GC-MS and CNHS to determine the nature of the organic components as well as the overall concentration of carbon, nitrogen and hydrogen. The most abundant organic materials are reported in Fig.112, while the complete list can be found in the Annexes, page 228.

a)

Organic materials	ppm
Naphthalene	0.2
Acenaphthene	0.14
Fluorene	0.17
Phenanthrene	2.21
Anthracene	0.44
Fluoranthene	3.33
Pyrene	2.58
Benzo (a) anthracene	1.47
Benzo fluoranthene	2.04
Benzo pyrenes	1.37

b)

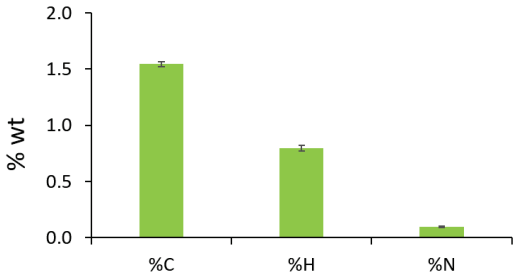

Fig. 112 a) Organic components analyzed by GC-MS with the respective concentrations expressed in ppm; b) initial presence of Carbon, Hydrogen and Nitrogen in the soil, determined by CHNS analysis represented in weight percentage (% wt).

Comprehending the starting material, both in terms of structure and composition, is fundamental for further treatment and investigation. It allows to determine the efficiency of the extraction treatments, as well as an understanding of the process at a molecular level.

3 CO_2Met Strategy

As previously mentioned, the final application of this thesis is to use CO_2-loaded amine-based solvents for metal carbonation and depollution of contaminated soils. The hypothetical principle behind this process is depicted in Fig.113.

The first step follows the red arrow (1), wherein an aqueous amine solvent, $\mathbf{L_0}$, is loaded with CO_2 yielding monocarbamates $\mathbf{L_1}$; the ligands structure is simplified using blue, grey and red circles to represent the amine, the ammonium and the carbamate, respectively.

Equation 2 indicates the potential disproportionation of monocarbamates $\mathbf{L_1}$ into diammonium ($\mathbf{L_0}$-**H**) and dicarbamates ($\mathbf{L_2}$) ligands, which was previously discussed in Chapter 2. The library of ligands ($\mathbf{L_0}$-**H**, $\mathbf{L_2}$) is then introduced as a reactive solution in the soil, represented by a solid matrix of alkaline metal silicates ($MgSiO_3$), (green arrow).

In this step the ligands dissolve the matrix and form complexes with its components ($\mathbf{L_0X}$, $\mathbf{L_2M}$) (3). The new-formed complexes between carbamates and matrix metals ($\mathbf{L_2M}$) can then undergo hydrolysis in a mineral carbonation step (4) yielding metal carbonates and simultaneously releasing free amine in the system. At the same time the disruption of the matrix discharges trace metals in solution, where they can form complexes with the previously liberated amines ($\mathbf{L_0M}$) (5), facilitating metal extraction from the soil.

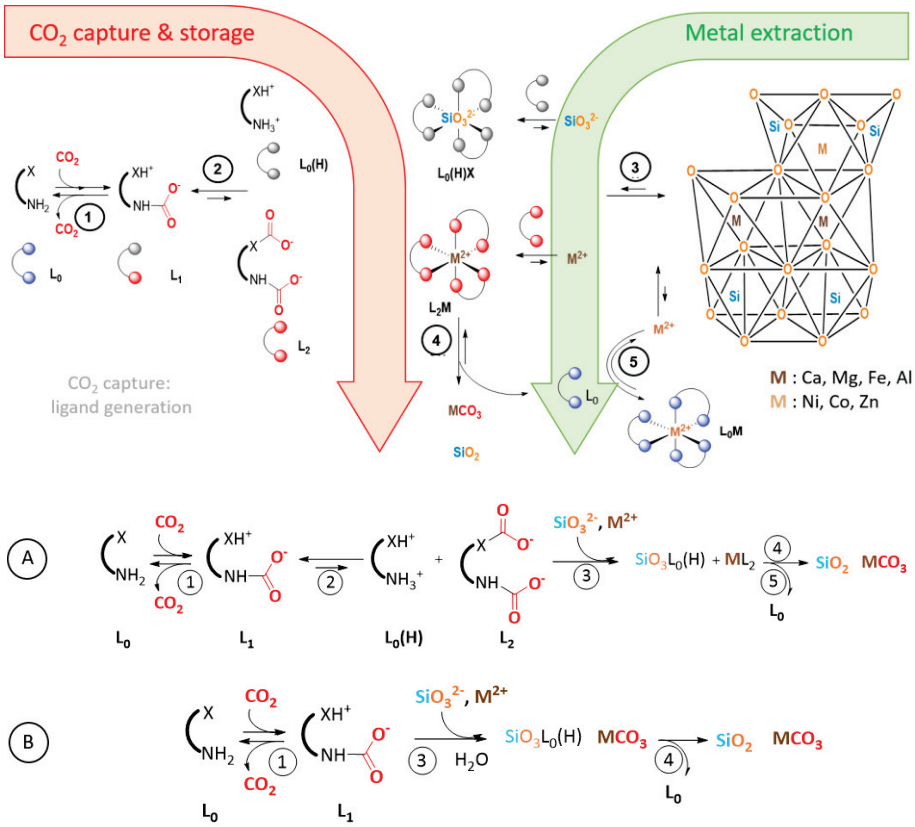

Fig. 113 Hypothetical CO_2Met Strategy. 1) Ligand generation of CO_2 loaded amines, 2) Disproportionation of monocarbamates L_1 into diammonium (L_0H) dicarbamates (L_2); 3) disruption of soil matrix through formation of complexes between alkaline metal silicates and CO_2 loaded ligands, 4) mineral carbonation with concomitant release of free amine, 5) liberation of metals from the soil matrix and further complexation. Courtesy of Prof. Julien Leclaire. A) First hypothetical pathway via disproportionation of ligands; B) second hypothetical pathway with direct hydrolysis of monocarbamated ligand.

The potential pathways A, with disproportionation of the ligand, is supported by previous investigations conducted by our group. In a study performed with **DETA** and $LaCl_3$, it was in fact observed that the metal template could enhance the disproportionation of monocarbamates into dicarbamates by forming stable ML_2 complexes[41]. Since alkaline earth and lanthanides present similar behaviors towards metal complexation[247-248], it could be assumed that matrix cations (Mg^{2+}, Ca^{2+}) could also promote the formation of dicarbamates and thus follow the previously illustrated path.

The second potential pathway is reported in equilibrium B. In this case the monocarbamates L_1 undergo hydrolysis, yielding diammoniums (L_0-H) and carbonates. The matrix could then be

dissolved via the formation of $SiO_3(L_0H)$ complexes, liberating matrix cations (Mg^{2+}, Ca^{2+}) which can then precipitate as carbonates. Once again, the uncarbamated amine would be released in the soil enabling trace-metal complexation. This second pathway is supported by the results reported in Chapter 3, where the introduction of $MgCl_2$ and $CaCl_2$ in an CO_2-loaded amine system did not show an amplification of polycarbamates, but rather an enhancement in bicarbonates and carbonate formation.

4 General methods

Samples of soils were treated with 0.5M aqueous amine solutions either CO_2-loaded and unloaded, whose composition is presented in chapter 2. Experiments were performed by Liquid Assisted Grinding (LAG) using a planetarium grinding reactor. Further information about material and methods can be found in the experimental section (page 197).

The soil was mixed with the leaching solution in the reactor (Fig.114a), where it was grinded for 30 minutes at 500 rpm. Then the mixture was collected with the help of a specific volume of water (Fig.114b), centrifuged (Fig.114c) and finally separated into solid and liquid phase (Fig.114d).

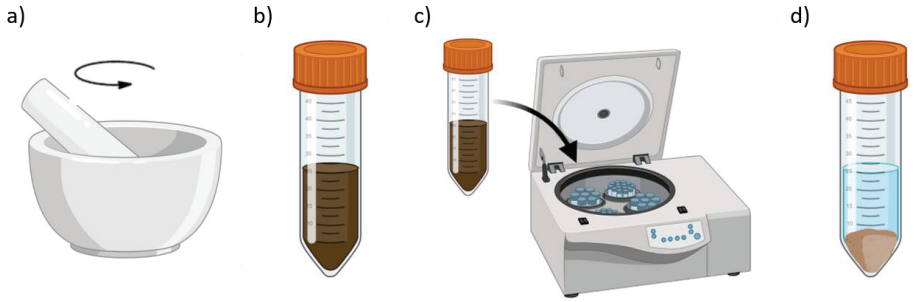

Fig. 114 Liquid Assisted Grinding of soils, general procedure: a) mechanical grinding of soil with extractive solution at 500 rpm for 30 minutes; b) collection of the sample; c) centrifugation; d) separation of solid and liquid phase.

The leachate was then mineralized with an aqueous solution of HNO_3 5% and analyzed with ICP-OES, to identify and quantify the extracted metals.

Those results allowed to determine the extraction rate of a metal (ER_M %), calculated as the number of moles of a leached metal over its initial number of moles in the soil sample (eq.105):

$$ER_M\ \% = \frac{n_M^{liquid}}{n_M^{initial}} \quad (105)$$

The treated soil, on the other hand, was not analyzed by ICP-OES, since the complete dissolution of the solid matrix would have required an acid digestion with HF/HNO_3 which was not performable in our laboratories.

However, the solid was lyophilized and analyzed via CHNS elementary analysis to quantify the amount of carbon and nitrogen present in the soil after the treatment. To those results were subtracted the initial amounts of Carbon and Nitrogen found in the soil matrix (Fig.112), enabling the quantification of amine and CO_2 fixation in the soil.

The fixation rate of the amines (FR_{R_2NH}%) and the fixation rate of carbon dioxide (FR_{CO_2}%) are calculated as the number of moles of amine and CO_2 in the solid fraction over their initial number of moles (eq.106, 107):

$$FR_{R_2NH}\ \% = \frac{n_{R_2NH}^{solid}}{n_{R_2NH}^{initial}} \quad (106)$$

$$FR_{CO_2}\ \% = \frac{n_{CO_2}^{solid}}{n_{CO_2}^{initial}} \quad (107)$$

The experiments were run under specific conditions of liquid to solid ratio, amine concentration, α(CO_2) loading, volume and number of washes, washing solution, nature of the reactor, duration and speed of grinding, all listed in Table 36.

Table 36 Conditions of grinding, liquid to solid ratio (L/S), concentration of amine solution expressed in Molarity (C(M)), α(CO_2) loading, volume and number of aqueous washes expressed in milliliters (V(mL)), material of the reactor (stainless steel (SS) or tungsten carbide (WC)), time expressed in minutes (min) and calculated as the number of cycles times the duration of the cycle and speed of grinding (rpm).

L/S	C_{R_2NH} (M)	α(CO_2)	V (mL)	Washes	Reactor		t(min)	rpm
1:1	0.5	0.5	8	3	Stainless Steel	WC	3*10′	500

From these operating conditions it was possible to calculate the ratio between the moles of amine (Ligand/M) the moles of nitrogen/sulfur binding sites (N, S/M), the moles of CO_2 and the major metals (CO_2/M), reported in Table 37.

Table 37 Ratios between moles of ligand/moles of metal (Ligand/M), moles of N, S binding sites/ moles of metal (N, S/M), and moles of CO_2/moles of metal (CO_2/M). The ratios were determined for the operating conditions of 1 gram of soil treated with 1 mL of a 0.5M solution of amine loaded at $\alpha(CO_2) = 0.5$.

M	$n_M(1g)$	Ligand/M	n(N, S)/n(M)			n(CO_2)/n(M)		
			DETA	Lys/Cys	Gly	DETA	Lys/Cys	Gly
Mg	0.00028	1.81	5.44	3.62	1.81	2.72	1.81	0.91
Fe	0.00070	0.71	2.13	1.42	0.71	1.07	0.71	0.36
Ca	0.00115	0.44	1.31	0.87	0.44	0.65	0.44	0.22
Al	0.00220	0.23	0.68	0.45	0.23	0.34	0.23	0.11
$\sum_M$	0.00433	0.12	0.35	0.23	0.12	0.17	0.12	0.06

In addition, to investigate whether the hardness of the material enhanced metal extraction and/or the mineral carbonation, it was decided to test two reactors, the first made of stainless steel and the second made of tungsten carbide (WC). The latter also presented the possibility of following the evolution of temperature and pressure inside the reactor throughout the grinding experiment. All experiments performed in a stainless-steel reactor were run in triplicates. The ICP-OES results are reported as the average value, and the associated standard deviation (σ_{SS}) is calculated as follows:

$$\sigma_{SS} = \sigma_T + \sigma_i \quad (108)$$

Where σ_T is relative to the triplicates experiments and σ_i to the metal initial concentration. On the other hand, the experiments performed in a tungsten carbide reactor were only executed once, therefore the standard deviation associated with the data will be $\sigma = \sigma_i$.

For some experiments the ICP results for Cobalt and Molybdenum showed an extraction rate ER > 100%. This error can be due to different factors: the preparation of the sample, analysis perturbation, or malfunction of the device. For clarity, those metals were omitted from the discussion, although the values can be found in the annexes, page 229.

Chapter 4

5 Results and discussion

In this section will be presented the results obtained by Liquid Assisted Grinding of the soil with amine-based leaching. Each leaching agent will be examined separately for clarity.

5.1 LAG: Water Leaching

The first experiment performed on the dried soil was an extraction with water, to identify which metals were extracted in simple aqueous meaning. A liquid assisted grinding reaction was performed by grinding 1 g of dried soil with 1 mL of deionized water, at 500 rpm, for 3 cycles of 10 minutes of grinding in a stainless-steel reactor. The ICP-OES analysis results are displayed in Fig.115.

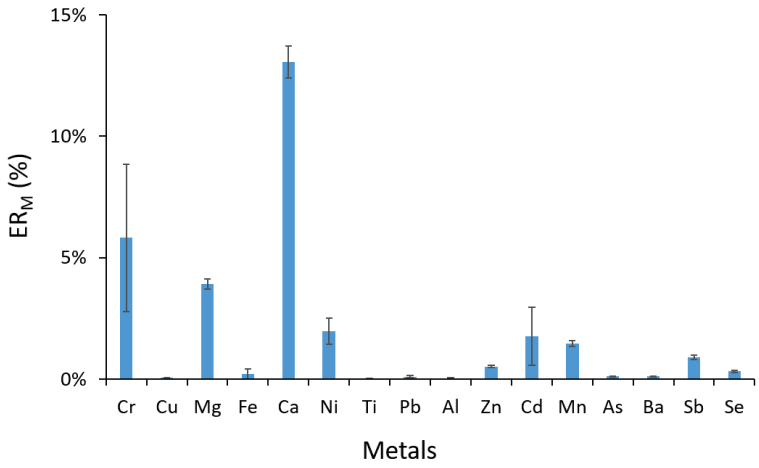

Fig. 115 Extraction rate of metals (ER_M %) obtained by grinding 1 g of dried soil with 1 mL of deionized water; the reaction was performed at 500 rpm for 3 cycles of 10 minutes of grinding in a stainless-steel reactor. The experiments were performed in triplicate and in the graph is reported the average ER_M % and the relative standard deviation.

It can be observed that the overall extraction rate is low (ER < 15%). Calcium, as one of the major matrix components, presents the highest extraction rate (ER = 13%) while all other metals are poorly lixiviated (ER < 6%). Those results are coherent with the sequential extraction performed on the soil (section 2, page 167), which shows that Cd and Mn are mostly present as carbonates, therefore leached in acid solutions, while Ni and Cr are contained in the residual fraction, displaying low accessibility.

5.2 LAG: DETA-CO_2

The first amine sorbent tested for the soil was Diethylenetriamine. A 5 mL stock solution of aqueous 0.5M **DETA** was prepared and a 2.5 mL aliquot of the solution was loaded with $\alpha(CO_2) = 0.33$ expressed in moles of CO_2 per mole of nitrogen. The lixiviants were then used for LAG experiments on one gram of dried soil, with the following operating conditions:

Table 38 Reaction conditions for **DETA**/dried soil (blue) and **DETA**-CO_2/dried soil (red) liquid assisted grinding in a stainless-steel reactor. Liquid to solid ratio (L/S), concentration of amine solution expressed in Molarity (C(M)), $\alpha(CO_2)$ loading, volume and number of aqueous washes expressed in milliliters (V(mL)), material of the reactor, time expressed in minutes (min) and speed of grinding (rpm).

R_2NH	L/S	C_{R_2NH} (M)	$\alpha(CO_2)$	pH	Washes	Reactor	t(min)	rpm
DETA	1:1	0.5	/	11.47	8 mL*3	Stainless Steel	3*10’	500
DETA	1:1	0.5	0.33	9	8 mL*3	Stainless Steel	3*10’	500

After the attritive leaching, or grinding, the leachate solutions were analyzed by ICP-OES, which permitted to calculate the extraction rate of each metal. In Fig.116 are reported the results obtained via **DETA** treatment (blue), compared to those obtained via leaching with **DETA**-CO_2 (red).

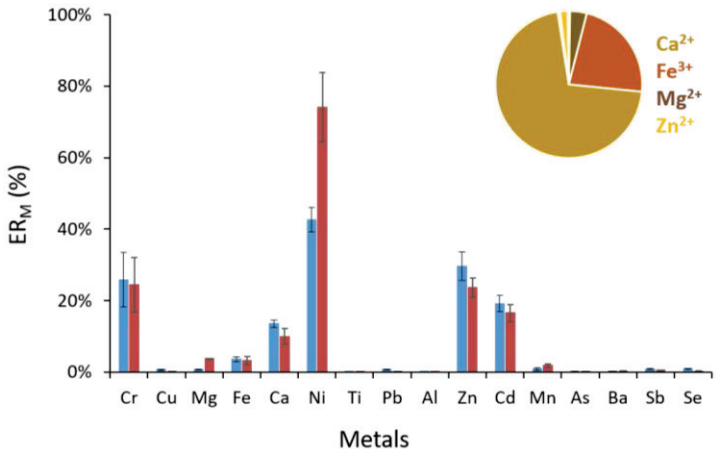

Fig. 116 Extraction rate of metals obtained by lixiviation of 1 g of dried soil with 1 mL of an aqueous solution of **DETA** 0.5M (blue), and **DETA** 0.5M loaded with 0.33 equivalents of CO_2 (red). Reaction performed in a stainless-steel reactor. The pie chart reports the ratio between the concentration of each metal and the sum of metals concentrations in the leachate obtained by **DETA**-CO_2 treatment. Color code: calcium (beige), iron (red), magnesium (brown, zinc (yellow).

The pie chart shown in Fig.116 reports the metal composition of the leachate, calculated as the relative concentration of the metal “i” over the total metal concentrations in solution.

It shows that even though the extraction rate of calcium is only 8%, the alkaline earth metal presents the highest concentration in the leachate solution.

Table 39 LogK of **DETA**-metal complexes of ML_2 stoichiometry[208].

R_2NH	Cd^{2+}	Cu^{2+}	Ni^{2+}	Pb^{2+}	Zn^{2+}	Cr^{2+}	Mn^{2+}	Fe^{3+}
DETA	13.84	20.9	18.6	10.37	14.3	9.34	6.91	/

Soil treatment with **DETA** 0.5M shows no extraction of As, Ba, Ti, Pb and Al, low-medium extraction rates for chromium, zinc and cadmium (ER≤20%), and an extraction rate of over 40% for nickel. The extraction of nickel can be explained by the formation of a Werner-like[249] complex Ni(**DETA**)$_2$[41] (Fig.117), which presents a high stability constant (logK = 18.6, Table 39).

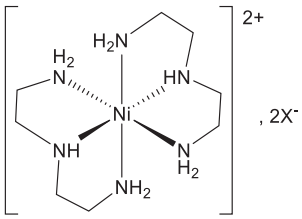

Fig. 117 Structure of the Werner-like complex of $[Ni(DETA)_2]^{2+}$ $2X^-$.

On the other hand, the attritive leaching performed using **DETA**-CO_2 as leaching agent shows lower extraction rates for calcium, chromium, zinc and cadmium, and higher for nickel with an ER of 74% (Fig.116). As shown in Fig.44, page 83 (chemical speciation of **DETA**), for a solution of diethylenetriamine loaded with 0.33 equivalents of CO_2 in the absence of metal salt, the most abundant species are free **DETA** and asymmetric monocarbamate **DETA-1a**. A study published by our group in 2020[41], demonstrated that the presence of a $NiCl_2$ salt in a CO_2-loaded diethylenetriamine solution can enhance the hydrolysis of carbamates into carbonates[41], freeing the amine and forming a (Ni(**DETA**)$_2$ complex [250](eq.109):

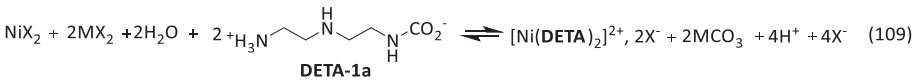

It was hypothesized that the higher metal extraction obtained with **DETA**-CO_2 could be due to the higher acidity of the solution, for which the pH is 9, compared to 11.47 of **DETA** 0.5M. To verify this hypothesis, the extraction rate of each metal was plotted against the pH values of the different leaching solutions (**DETA**, **GlyK**, ***L*-LysK** and ***L*-CysK** in their CO_2 loaded and unloaded state).

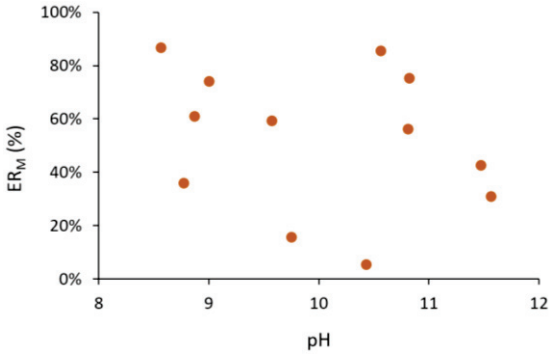

Fig. 118 Extraction rate of nickel (%) plotted against the pH value of the different leaching solutions **DETA**, **GlyK**, ***L*-LysK** and ***L*-CysK,** in their CO_2-loaded and unloaded state.

Fig.118 shows no direct correlation between the extraction yield of nickel and the pH of the reactive solution, therefore it must be concluded that all leaching effects must be attributed to the reactivity between the metals and the leaching solution. For the other metals the correlation between the extraction yield and the working pH can be found in the Annexes, page 229.

Furthermore, it must be mentioned that, based on the stability constants in Table 39, the most stable complex would have been Cu(**DETA**)$_2$, with a logK of 20.9. In theory, copper should be more readily accessible than nickel, since 37% of Cu^{2+} can be found in the carbonates fraction and 31% in the residual fraction, compared to 21% and 56% respectively for nickel. Nevertheless, $Ni(OH)_2$ and $NiCO_3$ (pKs = 15.2 and 6.87, respectively) are more soluble than $Cu(OH)_2$ and $CuCO_3$ (pKs = 19.32 and 9.63), therefore more easily leached from the solid matrix.

In presence of **DETA**-CO_2, the Calcium extraction is lower compared to the aqueous extraction showed in section 5.1 (ER 8% vs 13%); this can be explained by the formation of calcium carbonate in the soil which is highly insoluble, therefore poorly leached.

To justify this hypothesis, a CHN elementary analysis was performed on the soil sample to determine what fraction of carbon dioxide and organic lixiviant was fixed on the solid matrix (Fig.119a,b).

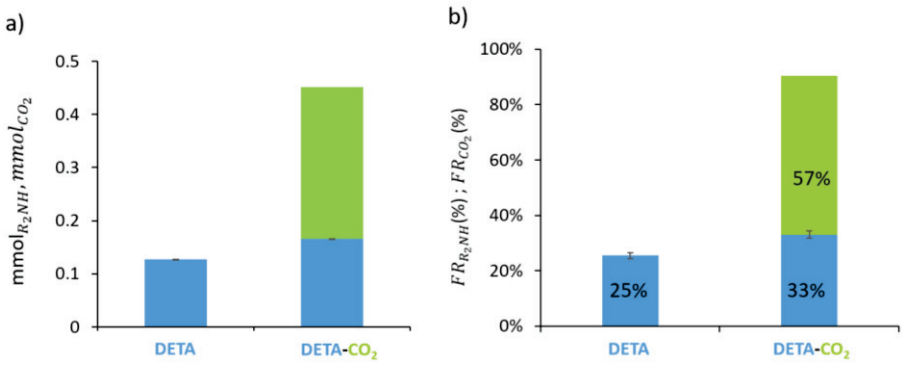

Fig. 119 CHN results obtained on a sample of soil treated by LAG with **DETA** and **DETA**-CO_2 in a stainless-steel reactor. a) mmols of **DETA** (blue) and CO_2 (green) fixed in the soil; b) fixation rate of Diethylenetriamine (blue) and CO_2 (green) in the solid matrix.

When the soil was treated with unloaded aqueous **DETA**, the fixation rate of the latter reached 25%; whereas after an attritive leaching with **DETA**-CO_2 the fixation rate for the amine rose to 33% and the fixation rate of carbon dioxide reached 57%. Via the CHNS analysis is not possible to determine what kind of adduct is present in the soil, i.e. carbamates or carbonates, but the high fixation rate of CO_2 could validate our previous hypothesis of mineral carbonation. Additional TGA and TGA-MS analysis could depict whether CO_2 is fixed as a mineral carbonate or an ammonium carbamate in the soil.

The same experiment was performed in a tungsten carbide reactor, with the following operating conditions:

Table 40 Reaction conditions for **DETA**/dried soil (blue) and **DETA**-CO_2/dried soil (red) liquid assisted grinding in a tungsten carbide reactor.

R_2NH	L/S	C_{R_2NH} (M)	α(CO_2)	pH	Washes	Reactor	t(min)	rpm
DETA	1:1	0.5	/	11.47	8 mL*3	WC	3*10’	500
DETA	1:1	0.5	0.41	8.59	8 mL*3	WC	3*10’	500

The ICP-OES results of the attritive leaching can be found in Fig.120a. Unfortunately, the extraction rate for nickel in the tungsten carbide reactor experiments is unacceptable (ER = 210% for **DETA** leaching and ER = 164% for **DETA**-CO_2 treatment, probably due to analysis errors), therefore it is not possible to compare the efficiencies of nickel extraction between stainless-steel and tungsten-carbide reactors. The values for the metals omitted in Fig.120a can be found in the Annexes, page 228.

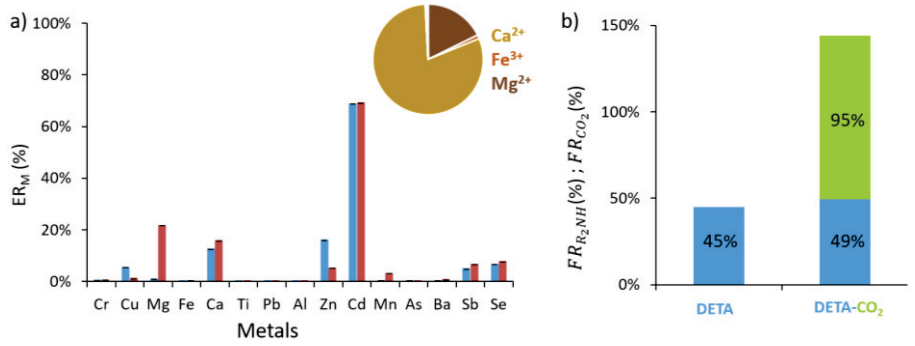

Fig. 120 a) LAG of dried soil in a WC reactor. Extraction rate of metals obtained by lixiviation of soil with an aqueous solution of **DETA** 0.5M (blue), and by an aqueous solution of **DETA** 0.5M loaded with 0.41 equivalents of CO_2 (red). The pie chart reports the relative concentration of each metal in the leachate obtained by **DETA**-CO_2 treatment. Color code: calcium (beige), iron (red), magnesium (brown); b) Fixation rates of amine (blue) and CO_2 (green) obtained by CHNS on solid phase of LAG with **DETA** and LAG with **DETA**-CO_2 expressed in %.

The **DETA**-CO_2 solution employed in this experiment presents an $\alpha(CO_2)$ of 0.41, which is higher than the loading reported for the previous experiment, $\alpha(CO_2) = 0.33$. The results of Fig.120a show that the extraction rate of cadmium is constant at 69% with and without the introduction of CO_2, this high constant seems related to the use of a WC reactor. It is hypothesized, yet not confirmed, that the hardness of the material provides a more energetic grinding, which increases the contact area between the reagents, affecting the reaction outcome. Once released, the metal can be complexed by **DETA** in a ML_2 complex stoichiometry[251] (Fig.121).

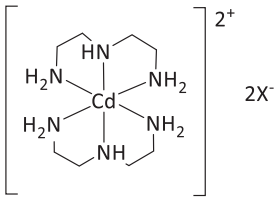

Fig. 121 $[Cd(\mathbf{DETA})_2]^{2+}$ complex with general counterion, by Lib *et al.*, 2007[251].

Furthermore, in Fig.122 are shown the evolution of both temperature (°C) and pressure (ΔP, mbar) throughout the reaction, measured by the Easy-GTM tungsten carbide reactor. It can be observed that the temperature oscillates between 21 °C and 36 °C, while the ΔP (pressure variation with respect to the atmospheric pressure) varies between 36 mbar to 253 mbar, both mild conditions for metal leaching and mineral carbonation.

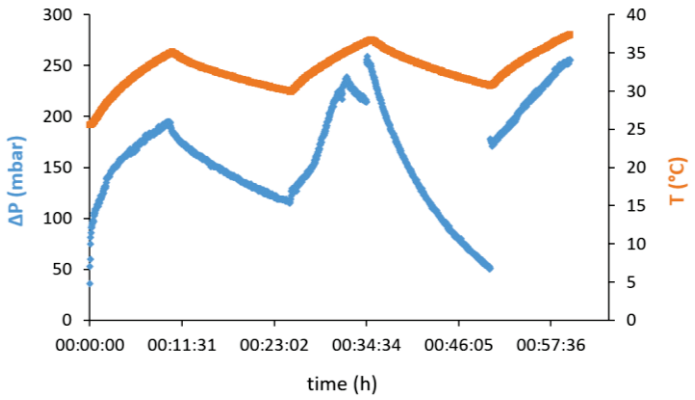

Fig. 122 Evolution of temperature (°C, orange) and pressure (mbar, blue) of the grinding reaction of 1g of dried soil with a CO_2 loaded solution of 0.5M **DETA**, for three cycles of 10 minutes of grinding at 500 rpm.

To investigate the influence of the material of the reactor on the fixation rate of amine and carbon dioxide, the treated soil was tested via CHN analysis. As shown in Fig.120b, the amine reached a fixation rate of 45% while after lixiviation with **DETA**-CO_2 the extraction rate of amine and carbon dioxide reached, respectively, 49% and 95%. From the comparison of Fig.119 and Fig.120b, is possible to conclude that the hardness of the grinding material has a significant impact not only on the metal extraction in the leachate, but also on the fixation of amine and CO_2 in the solid phase. Overall, 25 to 50% of **DETA** can be retained in the soil, and it can be considered an additional form of pollution. For this reason, our investigation moved to the use of natural αAA, which represent a more environmentally benign choice.

5.3 LAG: GlyK-CO_2

A solution of **GlyK** 0.5M, prepared by dissolving 0.005 moles of glycine with 1 equivalent of KOH in 10 mL of purified water, was used as extracting agent in LAG experiments, with the following operating conditions:

Table 41 Reaction conditions for **GlyK**/dried soil (blue) and **GlyK**-CO_2/dried soil (red) liquid assisted grinding.

R_2NH	L/S	C_{R_2NH} (M)	α(CO_2)	pH	Washes	Reactor	t(min)	rpm
GlyK	1:1	0.5	/	10.56	8 mL*3	Stainless Steel	3*10’	500
GlyK	1:1	0.5	0.5	8.56	8 mL*3	Stainless Steel	3*10’	500

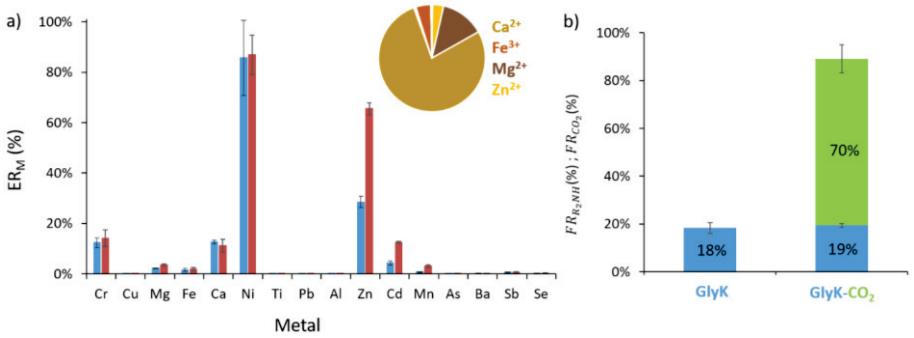

Fig. 123 a) Extraction rate of metals obtained by lixiviation of dried soil with an aqueous solution of **GlyK** 0.5M (blue), and by an aqueous solution of **GlyK** 0.5M loaded with 0.5 equivalents of CO_2 (red), the pie chart presents the relative concentration of metals in the leachate solution, color code: calcium (beige), iron (red), magnesium (brown) and zinc (yellow); b) fixation rates of amine (blue) and CO_2 (green) obtained by CHN analysis on soils after LAG treatment.

From the ICP-OES results shown in Fig.123a glycine appears to be an efficient lixiviant for nickel, with an extraction rate of 86% and 87% with both **GlyK** and **GlyK**-CO_2 leaching solutions. In presence of CO_2 the extraction of zinc increases from 29% to 65%, this effect could be due to a higher disruption of the matrix causing higher mobility of the metal in the solution.

Nickel and zinc complexes of glycine are widely discussed in literature[230, 252-255] and the higher extraction of nickel, compared to zinc, reflects the higher stability constant of the complexes. Both metals can be found in ML_2 and ML_3 stoichiometry, and in both cases Gly-Nickel complexes are more stable than Gly-Zn complexes (Fig. 124).

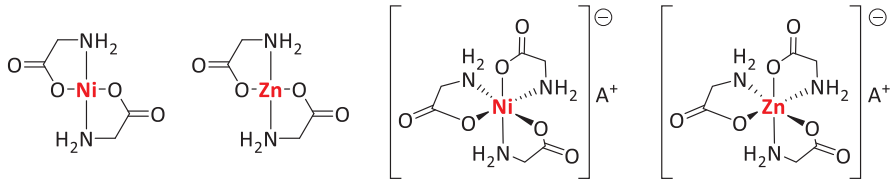

Fig. 124 Structures and stability constants of Ni^{2+}, Zn^{2+} glycine complexes in ML_2 and ML_3 stoichiometries. Values obtained from the literature[208, 236].

The ^{13}C NMR speciation of glycine, presented in Chapter 2, showed that for a loading of 0.5 the Gly-CO_2 library is composed of 50% of monocarbamate and 50% of bicarbonates. According to the CHN results in Fig.123b, 70% of CO_2 is transferred from carbamates/bicarbonates ammonium salts to metal-carbonates, while less than 20% of the

amine is retained in the soil, providing a high ratio between mineral carbonation efficiency and amine contamination.

In Table 42 are listed the operating conditions for the LAG experiments with **GlyK**/**GlyK**-CO_2 performed in a tungsten carbide reactor.

Table 42 Reaction conditions for **GlyK**/dried soil (blue) and **GlyK**-CO_2/dried soil (red) liquid assisted grinding.

R_2NH	L/S	C_{R_2NH} (M)	α(CO_2)	pH	Washes	Reactor	t(min)	rpm
GlyK	1:1	0.5	/	10.22	8 mL*3	WC	3*10'	500
GlyK	1:1	0.5	0.31	9.6	8 mL*3	WC	3*10'	500

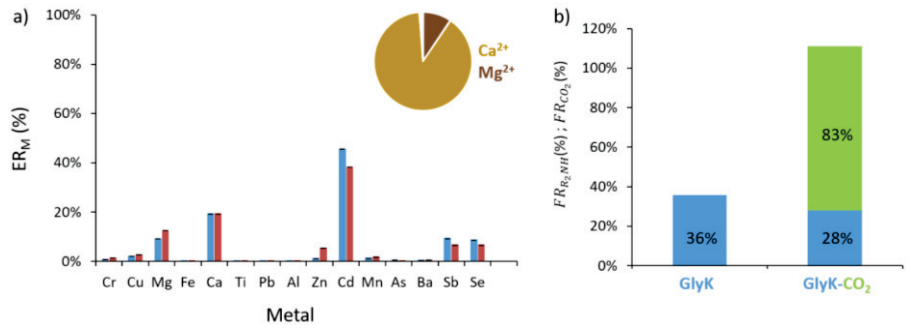

Fig. 125 a) extraction rate of metals obtained by lixiviation of dried soil with an aqueous solution of **GlyK** 0.5M (blue), and by a 0.5M aqueous solution of **GlyK** loaded with 0.31 equivalents of CO_2 (red) in a WC reactor, the pie chart presents the relative concentration of metals in the leachate solution, color code: calcium (beige), magnesium (brown); b) CHN analysis performed on the soil after lixiviation, fixation rate of **GlyK** (blue) and CO_2 (green).

Unfortunately, the extraction rate of nickel (ER = 123%) had to be omitted from the ICP-OES results reported in Fig.125a, due to an analysis error. As for **DETA**, the mobility of Cadmium is enhanced in a WC reactor, with an extraction rate of 46% and 38% with **GlyK** and **GlyK**-CO_2, respectively. The literature reports an ML_4 complex[238] for glycine and cadmium, with a stability constant of 7.7, where two glycine molecules behave as bidentate ligands, while two other glycine units are bound to the metal by the oxygen of the carbonyl group (Fig.126).

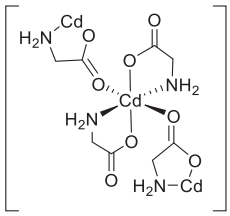

Cd(Gly)4

Fig. 126 Cadmium (II) complex with glycine[238].

In Fig.125b are reported the fixation rates of glycine and carbon dioxide on the soil, after the LAG experiment. A 10% increase in the fixation rate of both amine and carbon dioxide can be noted for **GlyK** and **GlyK**-CO_2. For both experiments (stainless steel, tungsten carbide) glycine presents high fixation rate of CO_2 with the low fixation rate of amine, indicating an efficient mineral carbonation effect with a high potential for amine recycling.

5.4 LAG: *L*-LysK-CO_2

A liquid assisted grinding experiment was performed using a 0.5M aqueous solution of ***L*-LysK** in a stainless-steel reactor, with the following operating conditions:

Table 43 Reaction conditions for ***L*-LysK**/dried soil (blue) and ***L*-LysK**-CO_2/dried soil (red) liquid assisted grinding.

R_2NH	L/S	C_{R_2NH} (M)	α(CO_2)	pH	Washes	Reactor	t(min)	rpm
***L*-LysK**	1:1	0.5	/	11.56	8 mL *3	Stainless Steel	3*10’	500
***L*-LysK**	1:1	0.5	0.46	8.87	8 mL *3	Stainless Steel	3*10’	500

The results of the ICP-OES analysis performed on the leached solution can be found in Fig.127a. In presence of free ***L*-LysK**, the highest extraction rates are reached by chromium and nickel with 18% and 37% respectively; when the soil is treated with a CO_2-loaded solution of ***L*-LysK** chromium and nickel extraction rates are increased to 25% and 65%.

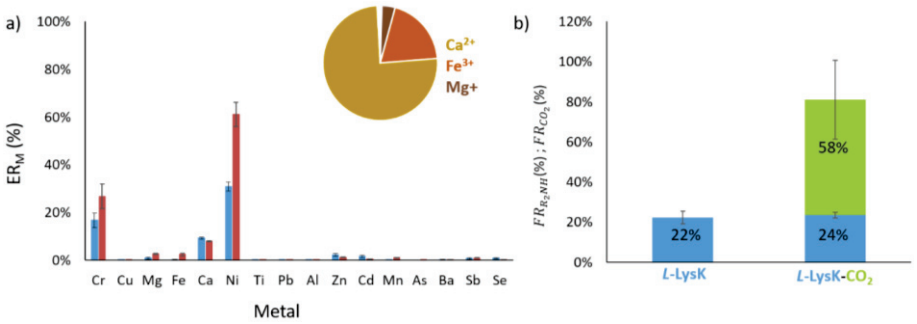

Fig. 127 a) Extraction rate of metals obtained by lixiviation of dried soil with an aqueous solution of ***L*-LysK** 0.5M (blue), and by an aqueous solution of ***L*-LysK** 0.5M loaded with 0.46 equivalents of CO_2 (red), the pie chart presents the relative concentration of metals in the leachate solution, color code: calcium (beige), iron (red), magnesium (brown). b) Fixation rate of amine (blue) and CO_2 (green) in the soil provided by CHNS analysis. Reaction performed in a stainless-steel reactor for 3 cycles of 10 minutes of grinding at 500 rpm.

The CHN elementary analysis reported in Fig.127b, show that after both treatments only 20% of ***L*-LysK** is trapped in the soil matrix, and 60% of the introduced CO_2 is fixed on the soil. The interpretation of both ICP-OES and CHN results suggest that the matrix is dissolved in presence of ***L*-LysK**-CO_2, and free amine forms chromium and nickel complexes[231, 240] (logK = 10.11[256-257] and 9,15[208], respectively), as shown in the introduction. On the other hand, matrix cations (Ca^{2+} and Mg^{2+}) are reprecipitated as carbonates. Based on the mols of Ca^{2+}, Mg^{2+} and CO_2 contained in the solid phase it was possible to calculate a maximum yield of $CaCO_3$ of 24% and a maximum carbonation yield of 96% for $MgCO_3$.

A liquid assisted grinding experiment was performed in a Tungsten carbide reactor and the experimental conditions are reported in Table 44. It must be mentioned that, due to an experimental error, the CO_2-loading of the ***L*-LysK** 0.5M solution is $\alpha(CO_2) = 0.27$, significantly lower than the loading reported for the previous experiment ($\alpha(CO_2) = 0.46$).

Table 44 Reaction conditions for liquid assisted grinding reaction of dried soil with ***L*-LysK** soil (blue) and ***L*-LysK**-CO_2 (red) in a reactor of tungsten carbide.

R_2NH	L/S	C_{R_2NH} (M)	$\alpha(CO_2)$	pH	Washes	Reactor	t(min)	rpm
***L*-LysK**	1:1	0.51	/	10.82	8 mL *3	WC	3*10’	500
***L*-LysK**	1:1	0.51	0.27	9.75	8 mL *3	WC	3*10’	500

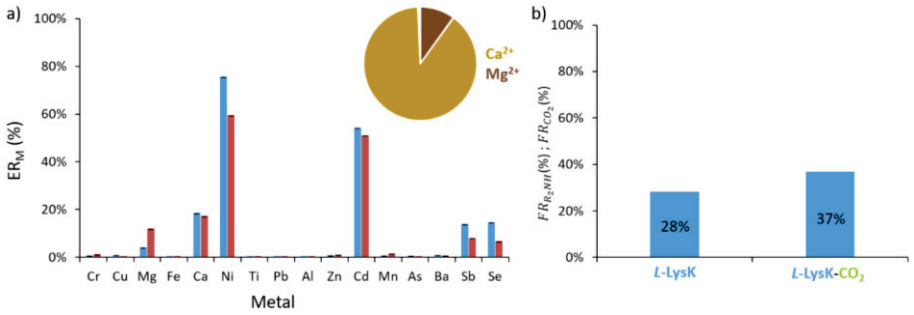

Fig. 128 Extraction rate of metals obtained by lixiviation of 1 g of dried soil with 1 mL of ***L*-LysK** 0.5M (blue), and 1 mL of ***L*-LysK** 0.5M loaded with 0.27 equivalents of CO_2 (red), the pie chart presents the relative concentration of metals in the leachate solution after treatment with ***L*-LysK-CO_2**, color code: calcium (beige), magnesium (brown); b) CHN analysis performed on the soil after lixiviation, fixation rate of ***L*-LysK** (blue). Lixiviation performed in a tungsten carbide reactor.

The ICP-OES results reported in Fig.128a are visibly different compared to those obtained with a stainless-steel reactor (Fig.127a). First of all, there is no extraction of chromium, while 14% of Sb and Se are lixiviated using ***L*-LysK** as extracting agent. Cadmium shows the same behavior observed in the **DETA** and **GlyK** experiments; the use of a WC reactor enhances its availability and 51-54% of the metal is extracted and complexed via lysine.

It can also be noted that higher extraction of nickel is obtained with ***L*-LysK** (75%) instead of ***L*-LysK-CO_2** (59%), contrary to what observed for the experiment performed in a stainless-steel reactor. This tendency could be explained by the higher amine retention in the solid, which would inhibit the complexation and extraction of metal. The CHN analysis reported in Fig.128b display a higher amine retention in the solid compared to the previous ***L*-LysK** experiment (28-37% compared to 22-24%), while the fixation rate of CO_2 was omitted as the value was unacceptable (FR = 153%). In addition, a lower CO_2 loading entails lower percentage of carbonated matrix, confirmed by a higher percentage of extracted calcium in solution for Fig.128a.

5.5 LAG: *L*-CysK-CO_2

The dried soil was tested in a liquid assisted grinding experiment with a 0.5M aqueous solution of ***L*-CysK**, with the following operating conditions:

Table 45 Reaction conditions for ***L*-CysK**/dried soil (blue) and ***L*-CysK**-CO_2/dried soil (red) liquid assisted grinding.

R_2NH	L/S	C_{R_2NH} (M)	α(CO_2)	pH	Washes	Reactor	t(min)	rpm
***L*-CysK**	1:1	0.5	/	10.81	8 mL*3	Stainless Steel	3*10’	500
***L*-CysK**	1:1	0.5	0.48	8.77	8 mL*3	Stainless Steel	3*10’	500

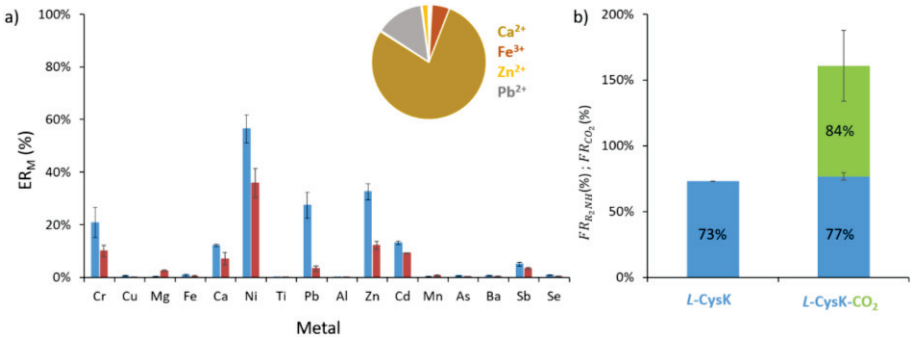

Fig. 129 Extraction rate of metals obtained by lixiviation of dried soil with an aqueous solution of ***L*-CysK** 0.5M (blue), and by an aqueous solution of ***L*-CysK** 0.5M loaded with 0.48 equivalents of CO_2 (red), the pie chart reports the relative concentration of metal in the leachate solution after treatment with ***L*-CysK**, color code: calcium (beige), iron (red), zinc (yellow), lead (gray); b) Fixation rate of ***L*-CysK** (blue) and CO_2 (green) after LAG treatment of dried soil.

The ICP-OES results in Fig.129a show a 30% extraction of Pb, obtained by lixiviation with ***L*-CysK** (blue), which corresponds to 13.5% of the leachate composition. Several studies in literature[239, 258-260] have discussed the affinity between cysteine and lead, attributing the stability of the Pb(***L*-Cys**)$_2$ complex to the trident character of the cysteinate ligand (binding sites: thiolate $-S^-$, carboxylate $-COO^-$ and amine $-NH_2$). In 2015 Jalilehvand *et al.*[258] investigated the formation of Pb(***L*-Cys**)$_2$ complexes at different pH, observing the formation of two possible ML_2 isomers at pH 9.1 to 10.4, shown in Fig.130.

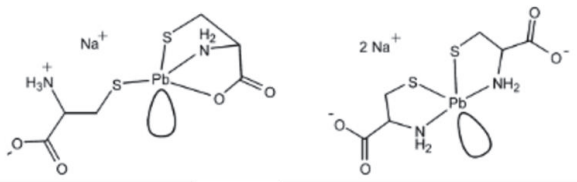

Na[Pb(S,N,O-Cys)(S-HCys)] $Na_2[Pb(S,N\text{-}Cys)_2]$

Fig. 130 Structures for Pb-Cysteinate complex with ML_2 stoichiometry at pH 9.1-10.4, reported by Jalilehvand *et al.*, 2015[258], logK (ML_2) = 18.57 at 25 °C.

Since the reaction was performed at pH 10.81, it can be assumed that *L*-cysteine forms soluble complexes with Pb^{2+} increasing its mobilization and extraction (ML_2, logK = 16.9[236]). As mentioned in the introduction, Cysteinate can also form stable ML_2 complexes with zinc, where the metal is bounded by NH_2 and S^- groups (Fig.106c).

Observing the ICP-OES results it can be noticed that ***L*-CysK**-CO_2 lixiviating solution presents a low extraction efficiency, compared to ***L*-CysK**. This trend can be attributed to the lower pH of the solution, 8.77 compared to 10.81; in those conditions both thiolate and amine binding sites are protonated, decreasing the complexation character of the amino acid.

Furthermore, the CHNS results reported in Fig.129b, show higher fixation rate for *L*-cysteine, compared to **DETA**, ***L*-LysK** and **GlyK**. 73% of the amine is retained in the soil in after lixiviation with ***L*-CysK**, while 77% of cysteine and 84% of CO_2 are fixed in the solid matrix after leaching with ***L*-CysK**-CO_2. Knowing that the ***L*-CysK**-CO_2 lixiviating solution is mostly composed of bicarbonates salts (Chapter 2, Section 4.5, page 96), is possible to assume that CO_2 is transferred from ammonium salts to metal carbonates, while the amine is trapped in the matrix. While the high fixation of CO_2 presents an interesting result for mineral carbonation, a high amine fixation rate is a grave drawback, for it impedes the recycling of the chelating agent resulting in higher process costs.

As for **DETA**, ***L*-LysK** and **GlyK** the leaching experiment was also performed in a tungsten carbide reactor, with the following operating conditions:

Table 46 Reaction conditions for liquid assisted grinding of dried soil with ***L*-CysK** (blue) and ***L*-CysK**-CO_2 (red) in a WC reactor.

R_2NH	L/S	C_{R_2NH} (M)	α(CO_2)	pH	Washes	Reactor	t(min)	rpm
***L*-CysK**	1:1	0.5	/	10.43	8 mL*3	WC	3*10’	500
***L*-CysK**	1:1	0.5	0.27	9.75	8 mL*3	WC	3*10’	500

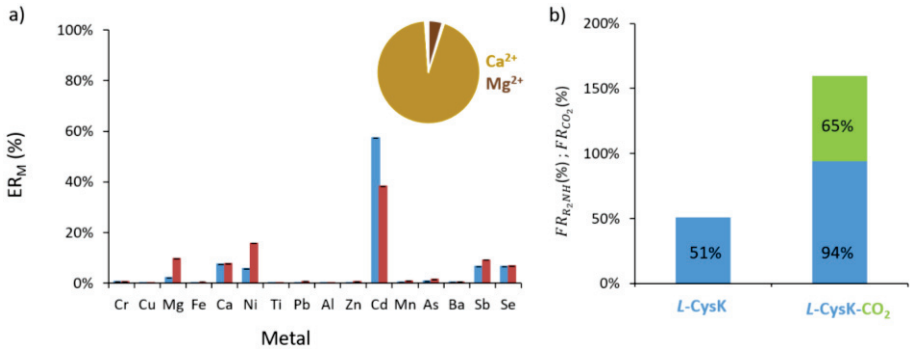

Fig. 131 a) ICP-OES results, extraction rate of metals obtained by lixiviation of dried soil with an aqueous solution of ***L*-CysK** 0.5M (blue), and ***L*-CysK** 0.5M loaded with 0.27 equivalents of CO_2 (red), the pie chart reports the relative concentration of metal in the leachate solution after treatment with ***L*-CysK**, color code: calcium (beige), magnesium,(brown) ; b) CHNS results, fixation rate of ***L*-CysK** (Blue) and CO_2 (green) in LAG treatment of dried soil. Lixiviation performed in a tungsten carbide reactor.

Compared to the LAG experiments performed in a stainless-steel reactor, the ICP-OES results reported in Fig.131a show no extraction of chromium, lead and zinc with neither ***L*-CysK** nor ***L*-CysK**-CO_2 solutions. On the other hand, cadmium extraction in visibly increased, reaching an ER of 60% and 40% with ***L*-CysK** and ***L*-CysK**-CO_2, respectively.

As for the other leaching solutions, the increased mobility of cadmium is explained by the use of a harder reactor material (WC rather than stainless steel), while the high extraction of cadmium can be due to the formation of a ML_2 complex with cysteine. ***L*-CysK** presents a high affinity for Pb^{2+} and Cd^{2+} [239, 259], and both Pb(***L*-Cys**)$_2$ and Cd(***L*-Cys**)$_2$ complexes present a stability constant of logK = 16.9[236] (Section 1.2, Table 31, page 159). The competition between the two metals in solution could therefore explain the drastic decrease in lead extraction (30% to 1%) with the simultaneous increase in cadmium recovery (10% to 60%).

Finally, the CHNS analysis performed on the soil after lixiviation with ***L*-CysK**-CO_2 solution (Fig. 131b) show a 94% fixation rate of amine and 65% fixation of CO_2. In the case of *L*-cysteine, the use of a harder reactor material has a negative impact on the fixation rate of CO_2 and amine, for it lowers the former while increasing the latter.

5.6 Screening

To conclude, a few operating conditions were screened to test a possible optimization of the process. For the experiments performed in a stainless-steel reactor, the modified conditions can be found in Table 47.

Table 47 Modified grinding cycles conditions (in red) of LAG experiments performed in a stainless-steel reactor with 0.5M ***L*-LysK**-CO_2 and **GlyK** on dried soil. The reactions underwent 1 and 2 grinding cycles of 10 minutes at 500 rpm, instead of 3 cycles as for previous experiments.

R_2NH	L/S	C(M)	α (CO_2)	pH	Cycles of grinding	
***L*-LysK-CO_2**	1:1	0.5	0.48	8.86	1*10'	2 * 10'
GlyK	1:1	0.5	/	11.09	1*10'	2 * 10'

For LAG experiments in a stainless-steel reactor the number of cycles was reduced to 1 and 2, to test whether a shorter reaction time would result as effective as a 30 minutes grinding. The test was performed with a CO_2 loaded solution of ***L*-LysK** 0.5M and a free solution of **GlyK** 0.5M, since both systems showed interesting results for basic operating conditions. The extraction rates of both systems are represented hereafter in Fig. 132, each compared to the results obtained with 3 consecutives grinding cycles.

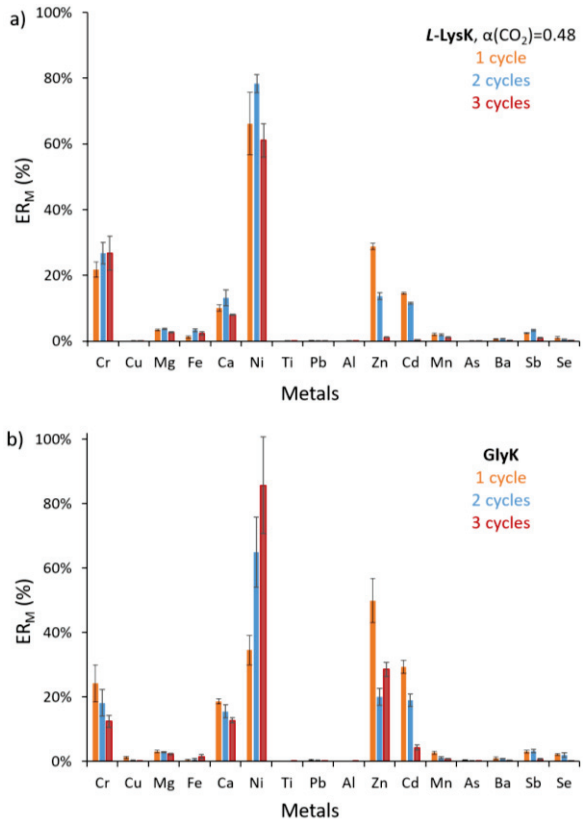

Fig. 132 Metal extraction rate (ER_M(%)) obtained by LAG of dried soil with a) 0.5M aqueous solution of ***L*-LysK** loaded with 0.48 equivalents of CO_2, and b) a 0.5M aqueous solution of **GlyK**. Color code: results obtained after 1 grinding cycle (orange), 2 grinding cycles (blue) and three grinding cycles (red).

The results reported in Fig.132 show a general metal extraction efficiency for both *L*-lysine and glycine systems. Although it is not possible to determine a linear correlation between the number of grinding cycles and the extraction rate of metals, it seems that a shorter grinding time allows a broader extraction of metals such as Zn, Cr, Ca and Cd. Overall both ***L*-LysK**-CO_2 and **GlyK** display an efficient metal extraction character, with a large spectrum of possible metal-organic complexes. Additional TGA and XRD analysis of the soil after the reactive leaching would provide the information necessary to verify this hypothesis.

The other modified parameter was the liquid to solid ratio. As previously mentioned, in Liquid Assisted Grinding experiments (LAG) the L/S ratio can vary from 0 - 2 mL/g[205]; for this reason part of the experiments were conducted with 0.1 mL of leaching solution for 1 gram of dried soil, for a final L/S ratio of 0.1.

Table 48 Modified conditions of LAG experiments (in red) performed in a Tungsten Carbide reactor with a liquid/solid ratio of 1:10 for ***L*-LysK**, ***L*-CysK** and **GlyK** on dried soil.

R_2NH	L/S (mL/g)	C(M)	α (CO_2)	pH	Cycles
***L*-LysK**	**0.1**	0.5	/	11.86	3 * 10′
			0.41	9.53	3 * 10′
***L*-CysK**	**0.1**	0.5	/	11.40	3 * 10′
			0.39	9.40	3 * 10′
GlyK	**0.1**	0.5	/	11.73	3 * 10′
			0.39	9.47	3 * 10′

The results obtained treating the dried soil with 0.1 mL of a 0.5M aqueous solution of ***L*-LysK** and **GlyK** are reported in Fig.133a,b. ***L*-CysK** presented the same trends displayed by *L*-**LysK**, it was omitted from the text to avoid repetition although the results can be found in the Annexes, page 230.

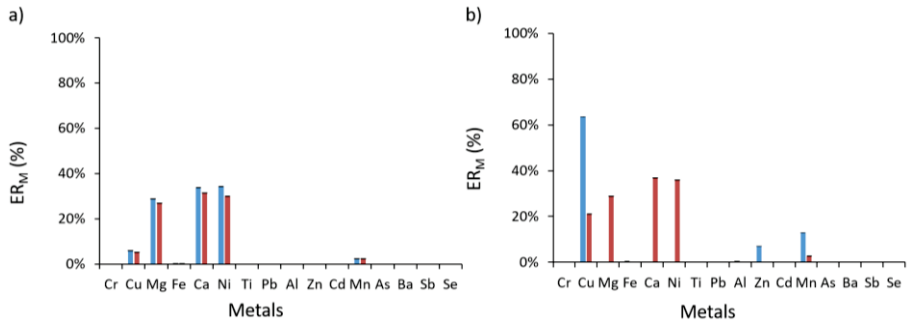

Fig. 133 ICP-OES results for LAG experiments of dried soil treated with 0.1 mL of a 0.5 M aqueous solution of a) ***L*-LysK** (blue) and ***L*-LysK-CO_2** (red); b) **GlyK** (blue) and **GlyK-CO_2** (red).

In Fig.133a, it can be noticed that calcium and magnesium present the highest extraction rates observed so far. It can be hypothesized that the CO_2 introduced in the solid was not sufficient to carbonate the matrix, which resulted in the lixiviation of major metals, while the small volume of washing solution was not enough to complexate and leach the trace metals.

Since the purpose of this investigation was to eliminate trace metals whilst carbonating the solid matrix, those results cannot be considered an optimization of our previous experiments. The same conditions were tested for a dried soil/glycine lixiviation (Fig.133b); due to analysis error the extraction values of Mg, Ca and Ni obtained by LAG with **GlyK** were not acceptable, therefore not reported in the graph. Overall, the extraction of matrix metal is coherent with the results shown for *L*-lysine. Finally, Fig.133b shows the first example of a high extraction of copper, reaching ER = 60%. The literature presents several examples of copper complexes with glycine and glycine-glycine dimers[261-262] (Fig.134).

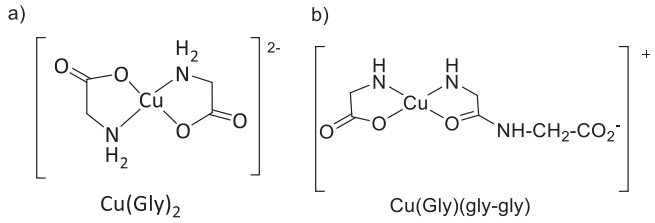

Fig. 134 a) Glycine-copper complex with ML_2 stoichiometry; b) possible structure of a ternary complex of glycine-copper-glycylglycine, reported by Martin *et al.*[261].

From the data reported in Table 31, page 159, copper presents higher stability constants for both *L*-lysine and glycine (logK = 15.05, 15.1, respectively) compared to nickel (logK = 9.15, 11.1, respectively). Despite this factor, the extraction of copper was unsuccessful throughout the previous experiments, potentially due to its low solubility. In order to determine if the extraction of copper is due to a physical or chemical effect, additional analysis should be performed with amino acids and industrial polyamines in these operating conditions.

6 Conclusion to chapter 4

In this chapter was proposed a new approach for simultaneous soil remediation and mineral carbonation. Four amines, including three natural amino acids, were investigated as chelating agents for metal recovery, exploiting their CO_2-capture properties to investigate *in situ* mineral carbonation of the soil matrix. Metal extraction and the fixation of both carbon dioxide and chelating agent were quantified for each proposed system to determine the efficiency of the approach.

Table 49 Results obtained in this work, divided in experiments performed in a stainless-steel and WC reactor. For each experiment are indicated the highest metal extraction (%), amine fixation rate (%) and CO_2 fixation rate (%).

R_2NH	Stainless Steel				WC			
	M^{n+}	ER_M %	FR_{R_2NH}%	FR_{CO_2}%	M^{n+}	ER_M %	FR_{R_2NH}%	FR_{CO_2}%
DETA	**Ni^{2+}**	40	25	/	**Cd^{2+}**	69	45	/
DETA-CO_2	**Ni^{2+}**	74	33	57	**Cd^{2+}**	69	49	95
GlyK	**Ni^{2+}**	86	18	/	**Cd^{2+}**	46	36	/
GlyK-CO_2	**Ni^{2+}**	87	19	70	**Cd^{2+}**	38	28	83
L-LysK	**Ni^{2+}**	37	22	/	**Ni^{2+}**	75	/	/
L-LysK-CO_2	**Ni^{2+}**	65	24	58	**Ni^{2+}**	59	/	/
L-CysK	**Ni^{2+}**	56	73	/	**Cd^{2+}**	57	51	/
L-CysK-CO_2	**Ni^{2+}**	35	77	84	**Cd^{2+}**	38	94	65

From the results obtained in this work, it can be concluded that nickel and cadmium are the most extracted metals, when working in a stainless steel and WC reactor. Other affinities were observed such as *L*-lysine-chromium, glycine-zinc and *L*-cysteine-lead, which could be exploited by an optimized process. Furthermore, the amines were retained in the soil with a range of 19%-94% with no specific pattern traceable to the reactor material.

Finally, the overall experiments showed a fixation rate of CO_2 higher than 57%, proving a high mineral carbonation efficiency of the process. More tests and analysis should be run on the liquid assisted grinding of heavy-metal polluted soil, to determine the operating conditions for an optimized mineral carbonation and metal extraction.

General conclusions

At present times, the economic and energetic costs of conventional amine scrubbing impede the vast application of this carbon capture technology; in addition, the use of industrial amines such as **MEA** and **PZ**, increases the footprint associated to the use and disposal of the amine sorbent. These problematics push the scientific community to find an innovative technology which could simultaneously lower the energetic and economic costs of CCS, while limiting the footprint of the technology. The objective of this thesis was therefore to design a sustainable strategy which captured CO_2 via amino acids, to store it into a heavy-metal polluted soil while extracting its metal contaminants.

The investigation of CO_2 capture by industrial polyamine (**DETA**, **EDA**) and α-amino acids (**GlyK**, ***L*-LysK**, ***L*-CysK**) on the molecular level enabled the identification and quantification of the different amine-CO_2 adducts formed in aqueous solutions. It was observed that industrial polyamines are principally reacting by carbamation, yielding mono and polycarbamates upon CO_2 capture. On the contrary, αAA undergo carbonation which enables to reach higher CO_2 loading compared to **DETA** and **EDA**. Furthermore, the thermodynamic study of carbon capture by the selected amine-based sorbent revealed a lower reaction enthalpy of amino acid compared to the benchmark amine sorbent **MEA**. This confirms the potential of amino acids as substitutes to industrial amines in the field of carbon capture.

The amine sorbents previously investigated were then explored for the integrated carbon capture and carbonation of metals. The study focused on two model-substrates: soluble metal chlorides and metal oxides. The introduction of magnesium chloride in the **DETA**-CO_2, **EDA**-CO_2 dynamic combinatorial libraries did not induce any significant amplification of either carbonates or carbamates in solution. On the contrary, $MgCl_2$ induced the amplification of bicarbonate salts in solution of αAA loaded with CO_2. In contrast, $CaCl_2$ was carbonated into insoluble $CaCO_3$ by all investigated amines. *L*-Lysine displayed the highest carbonation yield (89%) with low amine retention in the solid (4%), enabling potential recovery of the amine sorbent after chemical stripping.

Carbonation of alkaline and transition metal oxides by CO_2-loaded amine was investigated via mechanochemistry in both Liquid Assisted Grinding and neat grinding conditions. A thorough study conducted with **DETA** 5M on 11 metal oxides proved that mechanochemistry can be

considered a useful tool for both mineral carbonation and metal lixiviation. Furthermore, *L*-lysine proved to be the most efficient amine for CaO carbonation, reaching 86% conversion after 30 minutes of neat grinding at 500 rpm.

Finally, **DETA**, **GlyK**, ***L*-LysK** and ***L*-CysK** were investigated as chelating agents for soil depollution via LAG experiments, with concomitant *in situ* mineral carbonation of the soil matrix. The results reported in this chapter showed high extraction yields of both nickel and cadmium for all leaching agents, while specific affinities, such as *L*-lysine-chromium, glycine-zinc and *L*-cysteine-lead, were observed. Both *L*-lysine and glycine displayed high CO_2 sequestering yields (60% and 70%, respectively) with limited amine retention in the soil matrix (24% and 19%, respectively). These preliminary data confirmed amino acids are environmentally benign and powerful mineral carbonation and remediation agents.

Overall, this thesis paves the way toward an alternative approach to conventional amine scrubbing, metal remediation and soil depollution, via a Carbon Capture Utilization and Storage strategy.

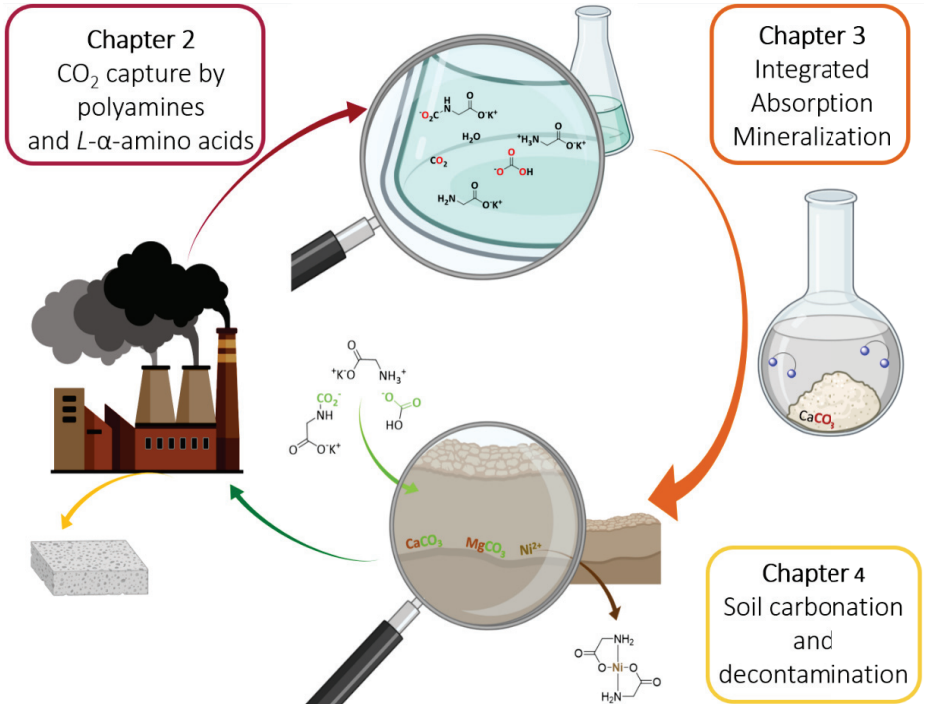

Experimental section

Experimental Section

1 Materials

1.1 Reagents and solvents

All reagents and solvents were obtained from Sigma-Aldrich and Thermo Fisher Scientific at reagent-grade purity and used as received. CO_2 (99,95%) and N_2 (> 99.9**%**) were obtained from Air Liquid. D_2O (99,90% D) and DCl (99,90% D) were purchased from Eurisotop. Ultrapure water was collected from an ACCU 20 Ultra-Pure Water from Fischer Scientific.

1.2 Gravimetric Analysis

Gravimetric analyses were conducted on a Mettler Toledo XSR high precision (± 0.01 mg) analytical balance.

1.3 NMR

1.3.1 Liquid state NMR

All experiments for liquid NMR were recorded on an Advance Bruker spectrometers Av300MHz (^{1}H, ^{13}C nuclei 70MHz) and Av500MHz (^{1}H, ^{13}C nuclei 125MHz) at the Centre Commun de RMN (CCRMN) of the University of Lyon. The chemical shifts are indicated in ppm (parts per million) in reference to Tetramethilysilane **(TMS)**. Spectra for speciation, calorimetry and cyclic capacity were recorded at 25 °C in D_2O, D_2O/H_2O (10%) on an Advance III 500MHz spectrometer with a standard BBFO probe from Bruker. T_1 relaxation time measurement of ^{1}H and ^{13}C were run with the standard inversion recovery experiment from Bruker pulse program library. Spectra were recorded at 25 °C ± 0.1, and samples were kept at 4 °C before measurement. Accuracy of the quantitative analyses was ensured by running the experiments using 90 degrees pulses and relaxation delay of 75s, therefore higher than five times T_1 (NCO_2^-, HCO_3^- $10 < T_1 < 15$ s).

1.3.2 Liquid state NMR D_2O/DCl

^{1}H qNMR spectra for capture experiments were recorded at 25 °C in D_2O/DCl (95:5) on an Av300 MHz at the CCRMN at the University of Lyon.

1.3.3 Solid state NMR

Solid-state NMR spectra were recorded at room temperature on a Bruker AVANCE III 500 WB spectrometer (11.7T, ^{13}C at 125.73 MHz) equipped with a Bruker 4mm MAS H/X/Y (magic angle spinning) probe. HPDEC (High power decoupling) spectrum was recorded at a spinning rate of 10 kHz, a $\pi/2$ pulse of 3.7µs was applied on ^{13}C and 69 kHz ^{1}H Spinal-64 decoupling was applied during acquisition. The spectral width was set to 400 ppm (50.5KHz), the recycle delay was set to 60s and 1400 scans were accumulated. For data processing, the spectrum was referenced to adamantane (38.5 ppm) and line broadening of 20Hz was applied.

1.4 Potentiometric titration

Potentiometric titrations and pH measurements in water were performed at 25 °C on a Mettler Toledo T5 titrator excellence with a DGi-102 mini probe.

1.5 *In situ* FTIR

Infrared measurements were performed with Attenuated Total Reflectance Fourier transform infrared (ATR-FTIR) technology using ReactIR 15 workstation from Mettler Toledo. The instrument was equipped with a 0.3 mm AgX DiComp probe (Wetted Materials: Alloy C22; Diamond; Gold). *In situ* IR spectra were recorded with 128 scans per-spectrum, with a 60s interval, in the optical range of 4000 – 650cm^{-1} and with a $\Delta\nu$ = 2 cm^{-1} resolution.

1.6 Volumetric titrations

Titration for the determination of the CO_2 loading in solids was performed with a Chittick apparatus using a 3 mL burette. Between 5 and 10 mg of solid were titrated with 1 mL of H_2SO_4 1 M. The calibration was performed with $NaHCO_3$ and H_2SO_4 1 M obtaining a correlation of y = 13.225 with a R^2 = 0.9943.

1.7 ICP-OES

ICP-OES analysis were performed on a Plasma Quant 9000 Elite Analytik-Jena apparatus. The vertical torch used for the analysis is composed of an aluminium-oxide injector (2 mm), a syalon outer tube and an alumina inner tube. All samples and calibrating solutions were diluted in a HNO_3 5% matrix.

a) b)

Fig. 135 a) ICP-OES instrument, b) vertical torch used for the analysis.

1.8 CHNS analysis

The elementary analysis to quantify the presence of C, H, N and S in solid samples is performed by three different analysers:

- C, H microanalyzer: the sample is burned at 1050 °C under O_2 flux. The resulting CO_2 and H_2O are quantified by IR detectors.
- N microanalyzer, DUMAS method: the sample is burned at 1050 °C under O_2 and Helium flux. Nitrogen is oxidized into NOx and then reduced in N_2, quantified by thermal conductivity detector.
- S analyser LECO SC 144: the sample is burned at 1350 °C under O_2 flux. The sulphur is transformed into SO_2 and quantified by IR detectors.

1.9 XRD

X-Ray Diffraction analysis for the identification of crystalline phases was performed on an EVA V5.0 Brucker analyzer and mineral quantification was performed with Rietveld refinement on a TOPAS V5.0 Brucker in VICAT Laboratories in L'Isle d'Abeau.

1.10 Calorimetry

Calorimetry experiments were performed on an Atlas HD Potassium reactor with a 1L vessel by Syrris using a Coated Heater 50W 500mm. The reactions were followed by pH probe 400mm with Swivel adaptor, turbidity probe 400mm. The introduction of N_2/CO_2 was controlled by mass-flowmeters EL-FLOW Select by Bronkhorst and followed by a Bronkhorst

Flowsuit program. Conductivity was followed with a Seven Compact Conductivity system by Mettler Toledo.

1.11 Mechanochemistry

All grinding experiments were performed in a Fritsch Pulverisette 7 Planetarium device. All reactors presented a volume of 20 mL and were used with 60 marbles of 5 mm of diameter. Three types of reactors were used: stainless-steel, 20 mL tungsten carbide and an Easy-GTM reactor in tungsten carbide with an integrated sensor to measure temperature and pressure.

2 Methods

2.1 qNMR Speciation

10 mL of a 0.5M solution of amine was prepared in a volumetric flask, brought to volume with D_2O. In the case of α-AA, the solutions were prepared neutralizing the amino acids with the necessary equivalents of KOH (1 equivalent for glycine and *L*-arginine, 2 equivalents for *L*-lysine, *L*-cysteine and *L*-aspartic acid). The solution was prepared including **TMPCl** as an internal reference for a concentration of 0.1 M. The solution was then divided into 10 aliquots of 1 mL using a Mettler Toledo Pipette Mann and introduced in PTFE tubes of 10 mL. The aliquots were loaded with increasing quantities of CO_2 followed by gravimetric analysis. Pure CO_2 was delivered at a fixed flow rate (5 or 10 mL/min) through a mass-flow controller. After absorption, a 550 µL aliquot of each sample was transferred into an NMR tube and stored at 4 °C before analysis to avoid CO_2 desorption. Each sample was analyzed by ^{1}H and ^{13}C qNMR. The concentration of each adduct was determined as the sum of the integration of their ^{13}C peaks, compared to the reference. The total loading of each NMR sample is calculated as the sum of the number of moles of the species, each one multiplied by the number of CO_2 moles bound, divided by the initial number of amine moles by the number of nitrogen present on its backbone:

$$\alpha = \frac{\sum n_i * \#_{(CO_2)i}}{n_{R_2NH} * \#_N} \qquad (31)$$

$\#_{(CO_2)i}$= number of bound CO_2 molecules per species.

$\#_N$ =number of nitrogen atoms on the amine backbone

The experimental molar fraction of each species was then plotted against total loading of CO_2 and fitted with a 3rd degree polynomial.

2.2 qNMR Speciation in presence of metals

A stock solution was prepared dissolving 0.005n of amine and 0.0005n of **TMPCl** in 5 mL of D_2O in a volumetric flask, obtaining a solution of 1 M in amine and 0.1 M in internal reference. A stock solution of metal chloride salt $MgCl_2$ was prepared dissolving 0.001265 n of salt in 5 mL of D_2O in a volumetric flask, obtaining a solution 0.25 M of metal. Solutions were prepared separately to prevent precipitation of $Mg(OH)_2$ in the volumetric flask. In a PTFE tube of 10 mL were introduced 0.5 mL of amine solution and 0.5 mL of metal solution. This allowed to have 10 aliquots with amine at 0.5 M, **TMPCl** at 0.05 M and $MgCl_2$ at 0.125 M, for a final amine:metal ratio of 4:1. Each aliquot was then loaded with CO_2 with a 5 mL/min flow controlled by a mass flowmeter, and the loading in CO_2 was followed by gravimetric analysis. 550 µL of each aliquot were transferred in an NMR tube and analyzed by ^{13}C qNMR and ^{1}H qNMR. The concentration of each CO_2-loaded adduct was determined as the sum of the integration of their ^{13}C qNMR peaks, compared to the integration of the reference. The molar fraction was plotted against total loading of CO_2 and fitted with a 3rd degree polynomial. The influence of the introduction of a metal template in the amine-CO_2 system was quantified using amplification factors.

2.3 Potentiometric titration

A stock solution of 100 mL was prepared dissolving 0.05 moles of amine in deionized water, for a final amine concentration of 0.5 M. An aliquot of 50 mL of said solution was loaded with CO_2 at 20 mL/min and followed by gravimetric analysis until maximum loading was reached. 550 µL of loaded solution was then introduced in an NMR tube with 50 µL of a 0.1 M solution of **TMPCl** in D_2O as an internal reference, for NMR quantification of the overall loading. 15 mL of free amine solution were then titrated with 15 mL of loaded solution, and vice versa, to obtain direct correlation between pH and $\alpha(CO_2)$. The experiments were run between one and three times and, when possible, the medium value and the relative deviation standard were calculated.

2.4 Cyclic Capacity

A 100 mL 0.5 M stock solution of the amine sorbent was prepared with deionized water in a volumetric flask and transferred to a three-neck round bottom flask with a magnetic stirrer. For further ^{1}H and ^{13}C quantitative analysis, 550 µL of the stock solution were collected and introduced in an NMR tube with 50 µL of a **TMPCl** 0.5 M solution in D_2O as internal reference. The solution was then subject of 2-5 cycles of CO_2 absorption/desorption.

2.4.1 Absorption step

The temperature and FT-IR probe were inserted in solution, the stirring rate was set to 500 rpm and the heating was set at 25 °C. The solution was then loaded with pure CO_2 at 200 mL/min, the flowrate being controlled by a mass-flowmeter. FT-IR intensities at 1320 and 1361 cm^{-1} were monitored and the absorption step was stopped once all infrared intensities had reached a plateau. After the first absorption step another ^{13}C qNMR sample was collected, as described in the previous section, allowing the quantification of the loading value in the rich state.

2.4.2 Desorption step

The loaded solution was heated at 100 °C and a 200 mL/min flow of pure N_2 was introduced by a mass-flowmeter to induce stripping. Once the FT-IR signals reached a new low plateau the desorption step was considered complete and stopped. An NMR sample was collected for further analysis and the loading value of the lean state wad calculated. The solution volume was then adjusted with deionized water before starting another absorption/desorption cycle. At the end of the different cycles the values were averaged for α_{max} and α_{min} to calculate the mean cyclic capacity with its relative error.

2.5 Power Compensated Calorimetry

A stock solution of 1L of amine 0.5M was prepared in deionized water in a volumetric flask and transferred in the calorimetry reactor. The stirrer, heating probe, pH probe (turbidity and conductivity optional) probes were introduced in the reactor as well. The system was brought at 40 °C through the system chiller and stirred at 700 rpm. The Power compensated Calorimetry step was launched after the system was stabilized at 40 °C for 5 min. PCC was run at 40 °C, the gases flow was controlled by a flowmeter and was set for a mixture of CO_2/N_2 at

respectively 0.15 L/min and 0.85 L/min; the total volume and temperature of both gases was measured by Bronkhorst Flowsuit program. The reaction was followed by *in situ* FT-IR and gas addition was stopped once the FT-IR signals reached a plateau. The system was let to stabilize for 30-40 minutes before completely stop the PCC experiment, to allow the program to accurately calculate the enthalpy of reaction. NMR samples were collected at the beginning and at the end of the reaction to assure a quantitative measure of the CO_2 loading of the solution. 550 µL of solution was introduced in an NMR tube with 50 µL of a 0.5 M **TMPCl** solution in D_2O and analysed by ^{13}C qNMR as described in previous sections. From the enthalpy of reaction (kJ) obtained by PCC and the precise value of CO_2 loading reached by the system it was possible to calculate the enthalpy of reaction in kJ/mol of CO_2.

2.6 Amine-metal heterogeneous systems: carbonation

A stock solution is prepared with 0.025 moles of amine and 0.00625 moles of metal chloride salt ($CaCl_2$) for a total amine concentration of 0.5 M and an amine/metal ratio of 4:1. The solution is prepared in deionized water in a volumetric flask and divided in aliquots of 5 mL each introduced in a PTFE tube of 10 mL. Each sample is then loaded with increasing quantities of pure CO_2 at 50 mL/min, followed by time of flux and gravimetric analysis. The tubes are closed, and the samples are left to stabilize for 12 h. After this time a white precipitate can be observed in the samples; the tubes are centrifuged at 500 rpm for 10 minutes and the solid is washed with deionized water. All liquid and solid phases are collected and lyophilized. A gravimetric measure is taken for all samples and phases after lyophilization and then each sample undergoes three analysis to determine the repartition of CO_2/amine/metal in between the phases : volumetric titration to quantify CO_2 (section 1.6); ^1H NMR for the quantification of the amine, where the solid is dissolved in a solution of D_2O/DCl (95:5) containing an internal reference (liquid NMR section 1.3.2) and finally ICP-OES analysis to determine the repartition of metal, where the sample is dissolved in a 5% solution of HNO_3 in ultrapure water.

2.7 Solid AAS

Procedure by Al-Terkawi et al., 2020[157]. 1g of amino acid and 1 equivalent of KOH were dissolved in 6 mL of deionized H_2O/MeOH in a 1/5 ratio. CO_2 was bubbled in the solution at 200 mg/min for 1 hour, with noticeable formation of a white precipitate. At the end of the reaction the precipitate is filtered, washed with a cold mixture of H_2O/MeOH ratio 1:5; the

solid is then vacuum-dried for 12h. The solid was weighted, then analysed via solid-state NMR and liquid state quantitative ^{13}C-NMR to qualify and quantify its loading state. On each solid was calculated the yield and the complete E factor (cEF), as:

$$cEF = \frac{\text{raw materials} + \text{reagents} + \text{solvents} + \text{water (g)}}{\text{final product (g)}} - 1 \quad (6)$$

2.8 Mechanical grinding

2.8.1 LAG: Metal Oxides

A stock solution of **DETA** 5M was prepared in deionized water in a volumetric flask and loaded with CO_2 via mass flowmeter, and the added CO_2 was controlled via gravimetric analysis. For each reaction was used a 1 mL of the stock solution and then one equivalent of metal oxide, in reference to CO_2, was added in the WC reactor. The Liquid assisted grinding was followed by Easy-GTM and let for 3 cycles of 10 minutes at 500 rpm. Each experiment was run twice, after the reaction the resulting material of one sample was collected with water and the other with methanol. Each sample was washed and centrifuged three times with 5 mL of the chosen solvent, and its liquid phases were gathered. Both solid and liquid phase were lyophilised (water treatment), or vacuum-dried (methanol treatment). Solid and liquid phases were then tested by ICP-OES, Volumetric titration and ^{1}H NMR (section 1.3.2) to quantify respectively the metal, CO_2 and **DETA**.

2.8.2 LAG: Soils

A 5mL stock solution of amine 0.5 M was prepared in deionized water in a volumetric flask. A 2 mL aliquot of said solution was loaded with CO_2 via mass flowmeter, and the added CO_2 was controlled via gravimetric analysis.

A 1 g sample of dried soil was introduced in a grinding reactor (stainless-steel/ WC, chapter 4), then 1 mL of the free amine/ loaded amine solution was introduced in the reactor. The grinding was performed at 500 rpm with 3 cycles of 10 minutes of grinding followed by 15 min pause, for a total reaction time of 30 minutes. The sample was then collected with 8mL of deionized water, centrifuged and washed 3 times with 8 mL of deionized water. The liquid phases were either studied separately or united; the solid phase was lyophilized and weighted after lyophilisation. The liquid phase was investigated by ICP-OES and the solid phase was investigated by CHNS.

2.8.3 Neat grinding

0.3 grams of solid αAA-CO_2 (section 2.7) were introduced in an WC reactor. The metal oxide was introduced in equivalent conditions to the introduced moles of CO_2. Grindings were performed at 500 rpm for 30 min, 1 h and 2 h; the latter was performed in an EASY-GTM reactor to follow temperature and pressure throughout the reaction. Resulting solids were collected with 5 mL of deionized water and the solid was washed 3 times. Solid and liquid phases were then separated and analysed separately as previously described.

2.9 Sequential extraction

Method of sequential extraction performed on 1 g of dried soil:

1. Extraction 1, carbonates: 1 gram of dried soil is introduced in 40 mL a 0.11M aqueous solution of acetic acid, at 25 °C and stirred for 16 h at 500 rpm. The solid is then filtered and used for the next step.
2. Extraction 2, Fe/Mn oxides: the solid is introduced in 40 mL of an aqueous solution of Hydroxylammonium Chloride ($(NH_3OH^+)Cl^-$) at concentration 0.1 M and pH 2. The mixture is stirred for 16h at 500 rpm.
3. Extraction 3, organic fraction: the solid is introduced in 2x10 mL 8.8 M H_2O_2 at 80 °C for 1 h; after which it is dried. The soil is then treated with 50 mL of a 1 M aqueous solution of Ammonium Acetate (pH 2, 16 h of stirring).

The residual fraction is obtained as the difference between the initial concentration of metals, and the sum of the first three extractions. Liquid/solid separation is performed by centrifugation and filtration of the supernatant on a 0.45 µm Whatman filter (#40).

Images in this thesis were created and modified with BioRender.

Annexes

1 Annexes Chapter 2

1.1 Ethylenediamine (EDA)

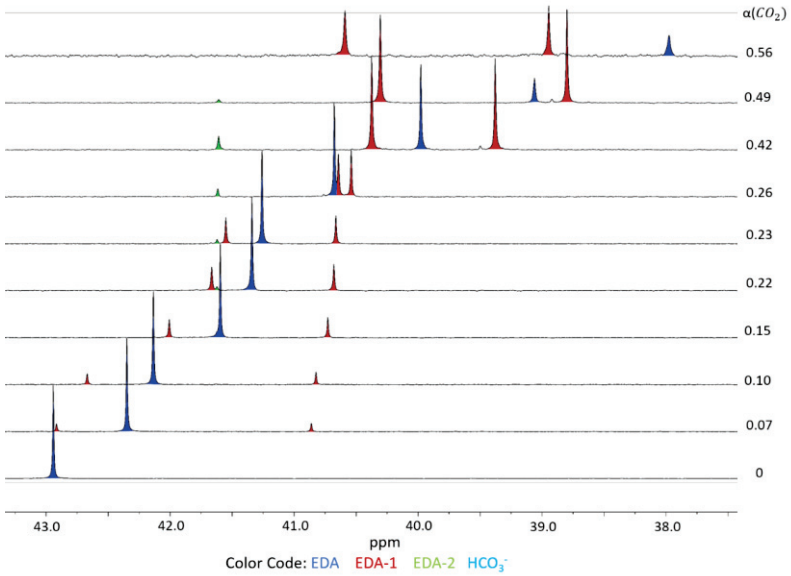

Fig. 136 ^{13}C qNMR speciation of a 1M solution of **EDA** in D_2O at 25 °C. Zoom on the aliphatic zone from 37-43 ppm. Legend of the color code on the right.

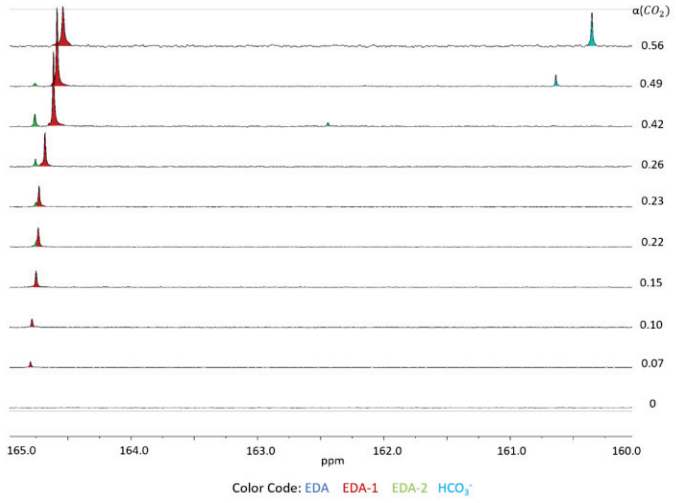

Fig. 137 ^{13}C qNMR speciation of a 1M solution of **EDA** in D_2O at 25 °C. Zoom on the carbonyl zone from 160-165. Legend of the color code on the right.

1.2 Diethylenetriamine (DETA)

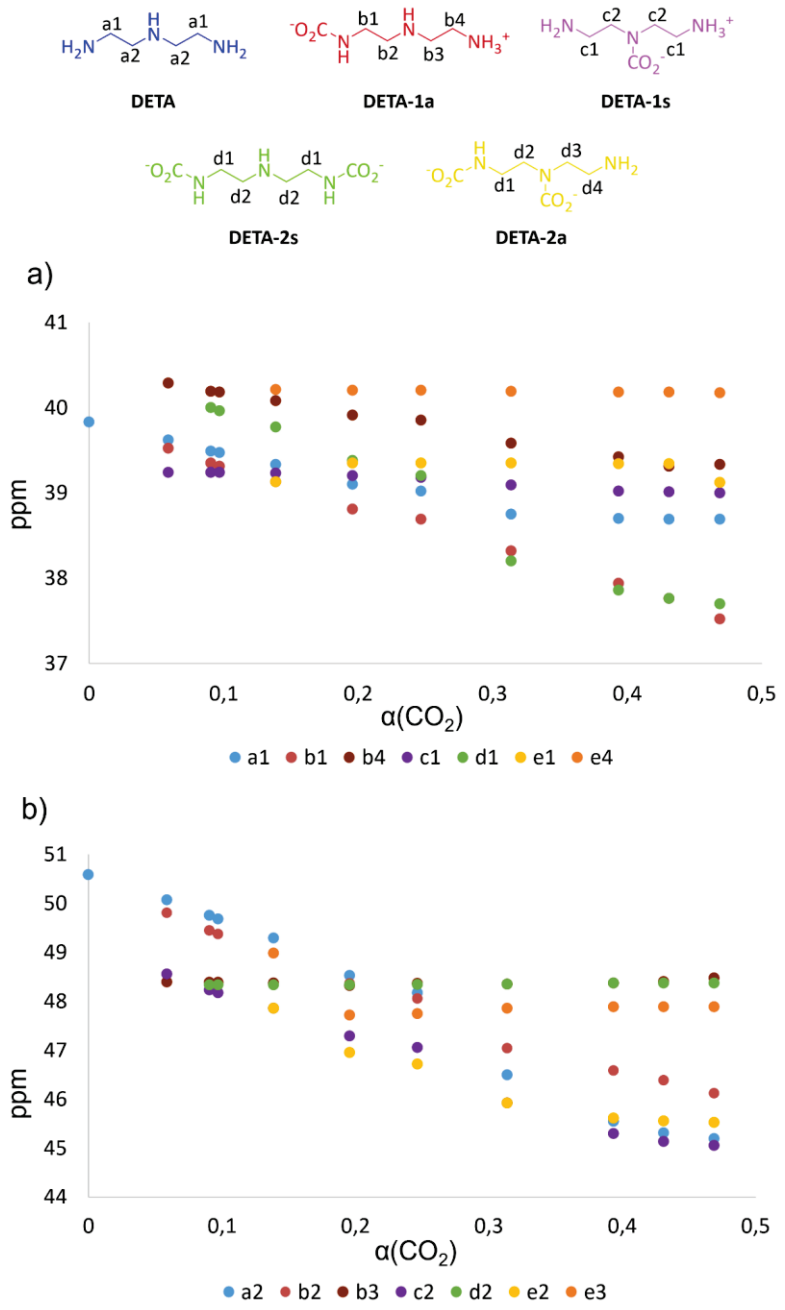

Fig. 138 Evolution of chemical shift for a 0.5M solution of **DETA** in D_2O loaded with CO_2 at 25 °C. a) chemical shift of aliphatic peaks from 37 to 41 ppm; b) chemical shift of aliphatic peaks from 44 to 51 ppm.

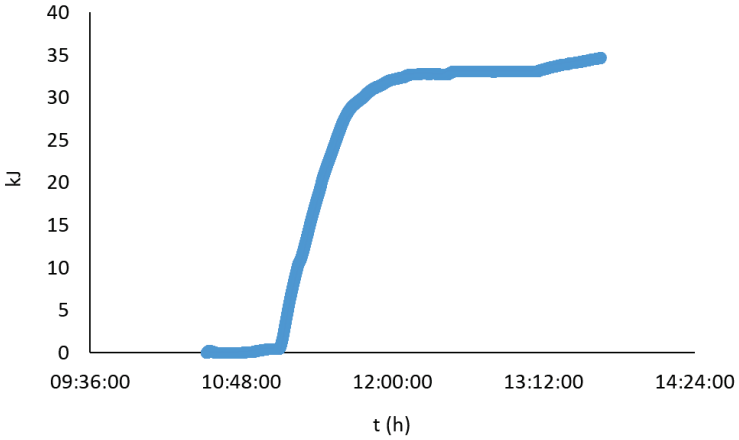

Fig. 139 Reaction enthalpy of a 0.5M aqueous solution of **DETA** upon CO_2 loading. The graph is expressed in $\Delta_r H^\circ$ (kJ) versus reaction time (h).

1.3 Glycine

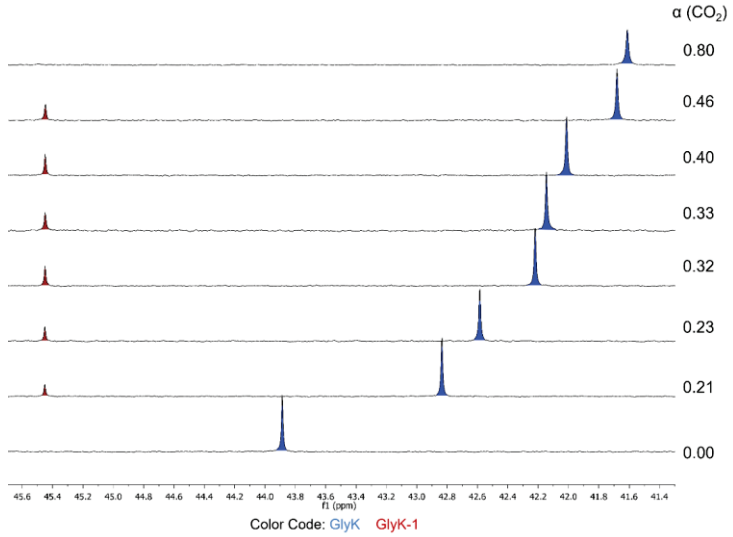

Fig. 140 ^{13}C qNMR spectra evolution for a 0.5M solution of **GlyK** in D_2O at 25 °C. Zoom on sp^3 signals from 41 to 46 ppm.

Annexes

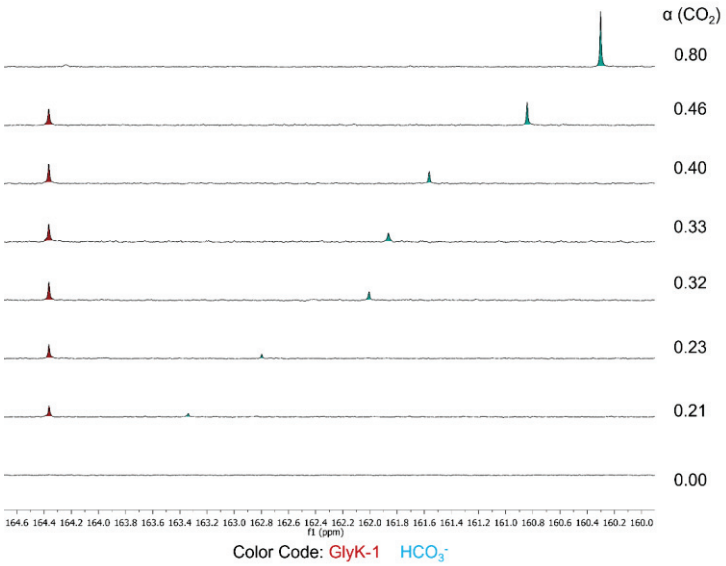

Fig. 141 ^{13}C qNMR spectra evolution for a 0.5M solution of **GlyK** in D_2O at 25 °C. Zoom on sp^2 signals from 160 to 165 ppm.

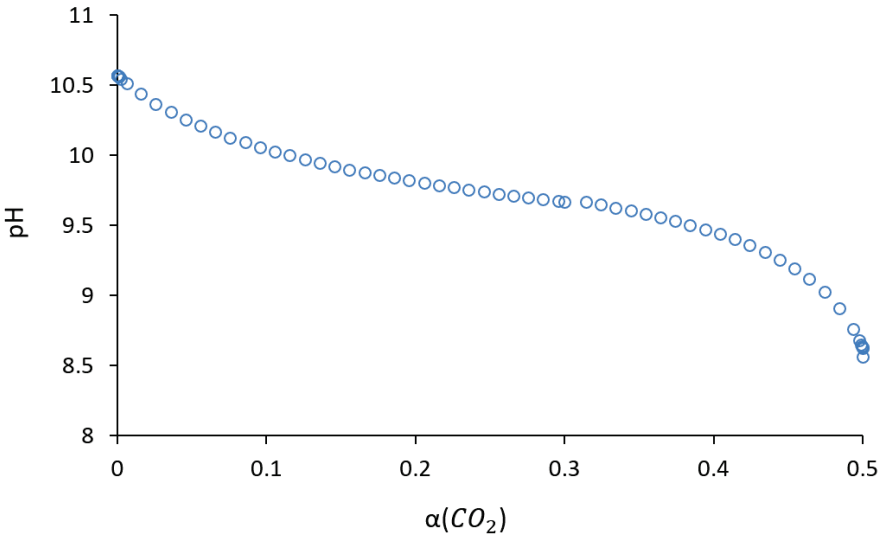

Fig. 142 pH evolution of a 0.5M aqueous solution of **GlyK** upon increasing CO_2 loading at 25 °C.

1.4 *L*-Lysine

The attribution of the ^{13}C NMR signals to the CO_2-loaded species was determined observing the evolution of the stacked spectra and the chemical shift of the species. In Fig.143 are reported the chemical shift of the epsilon -CH_2. In the first spectrum ($\alpha(CO_2) = 0$), the only visible signal is the one of free ***L*-LysK** (blue). Upon increasing CO_2 loading ($\alpha(CO_2) = 0.09$) a second signal appears at $\delta = 41.15$, which was attributed to the ε-CH_2 of the ***L*-LysK-1e** (red). A third signal is visible for $\alpha(CO_2) = 0.21$, which was attributed to the ε-CH_2 of the ***L*-LysK-1a** (purple) ($\delta = 39.5$). At high loading, the monocarbamate ***L*-LysK-1a** (purple) is the most abundant CO_2-loaded species, as confirmed by the pH measure. Furthermore, Fig.145 reports the evolution of the sp^2 signals for the speciation of ***L*-LysK**. The attribution of the carbamate signals was confirmed by the work of Al-Terkawi *et al.*[157]which reported a chemical shift for the epsilon carbamate of δ_{N-CO_2} = 164.8 ppm, while the alpha carbamate was observed at δ_{N-CO_2} = 163.7 ppm.

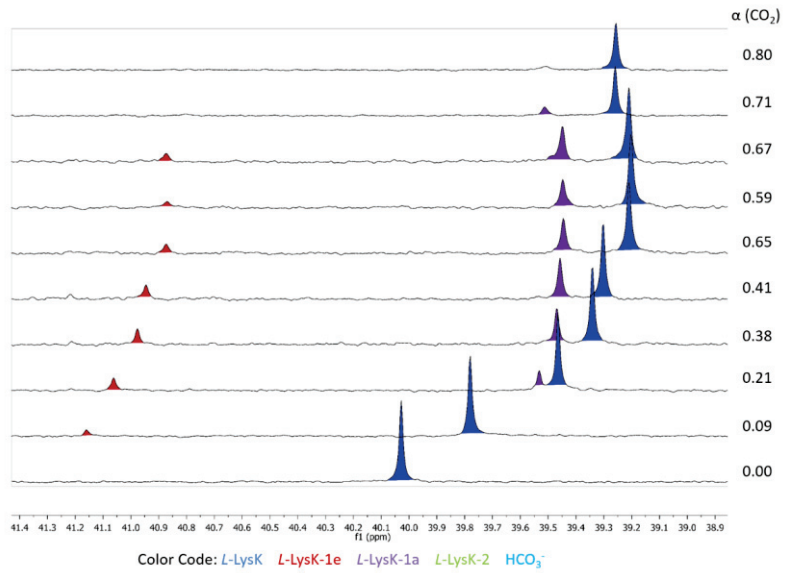

Fig. 143 ^{13}C qNMR spectra evolution for ***L*-LysK** 0.5M in D_2O at 25 °C. Zoom on the epsilon carbon from 38 to 42 ppm.

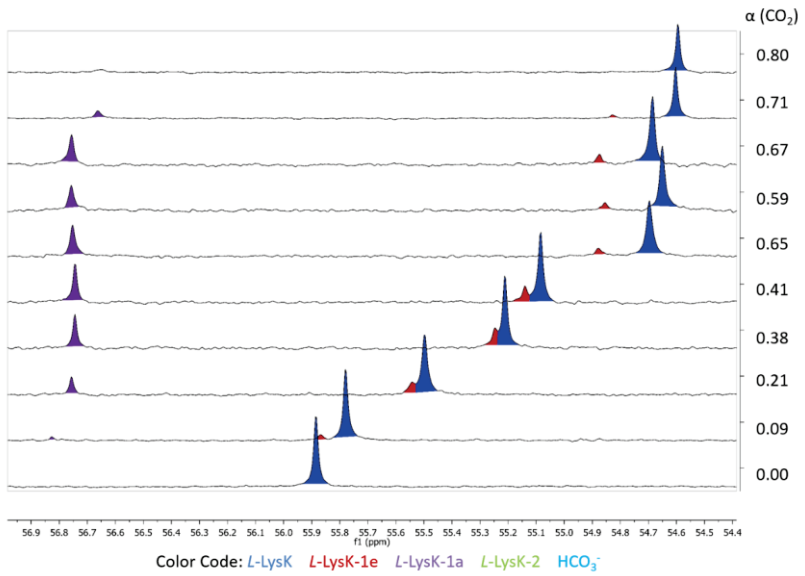

Fig. 144 ^{13}C qNMR spectra evolution for ***L*-LysK** 0.5M in D_2O at 25 °C. Zoom on the alpha carbon from 55 to 57 ppm.

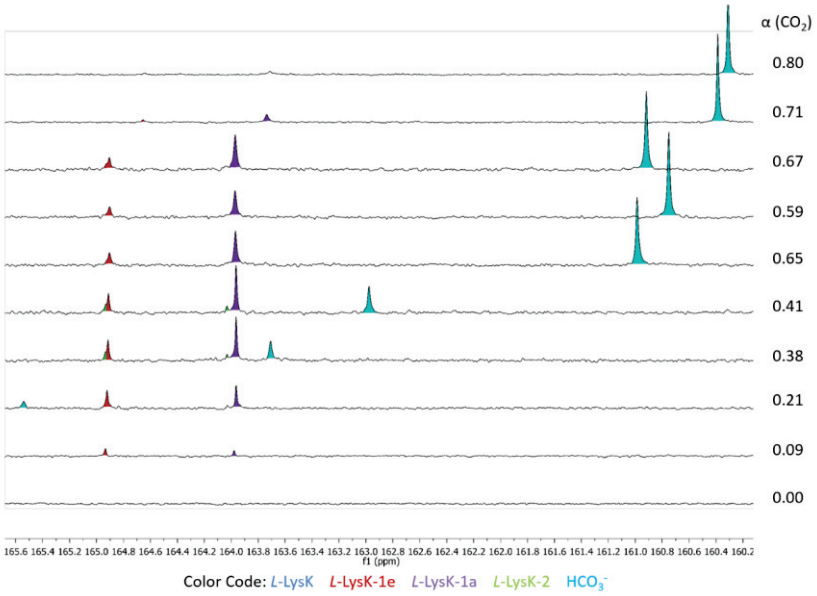

Fig. 145 ^{13}C qNMR spectra evolution for ***L*-LysK** 0.5M in D_2O at 25 °C. Zoom on the sp^2 signals from 160 to 165 ppm.

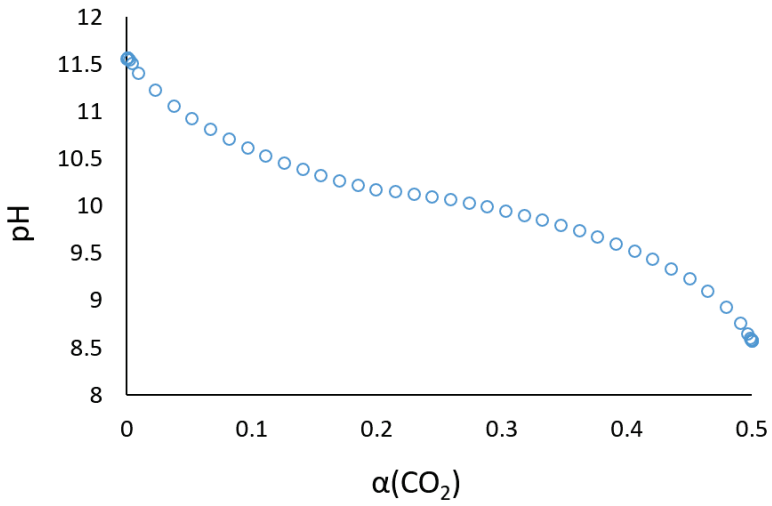

Fig. 146 pH evolution of a 0.5M aqueous solution of ***L*-LysK** upon increasing CO_2 loading at 25 °C.

1.5 *L*-Cysteine

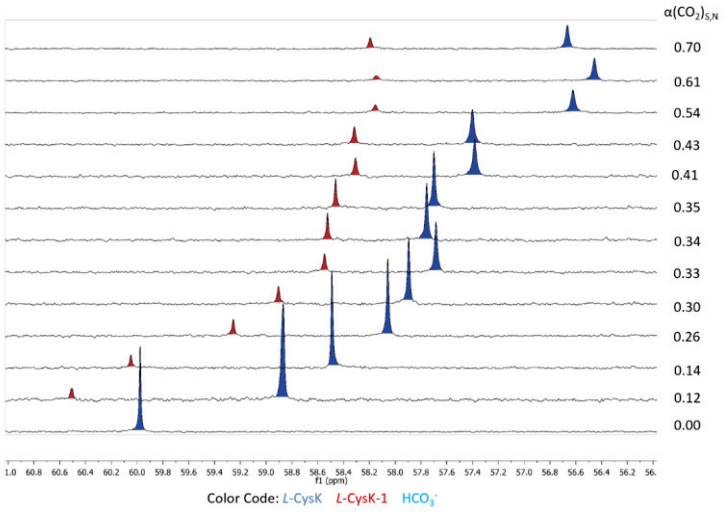

Fig. 147 ^{13}C qNMR spectra evolution for ***L*-CysK** 0.5M in D_2O at 25 °C. Zoom on the sp^3 signals from 56 to 61 ppm.

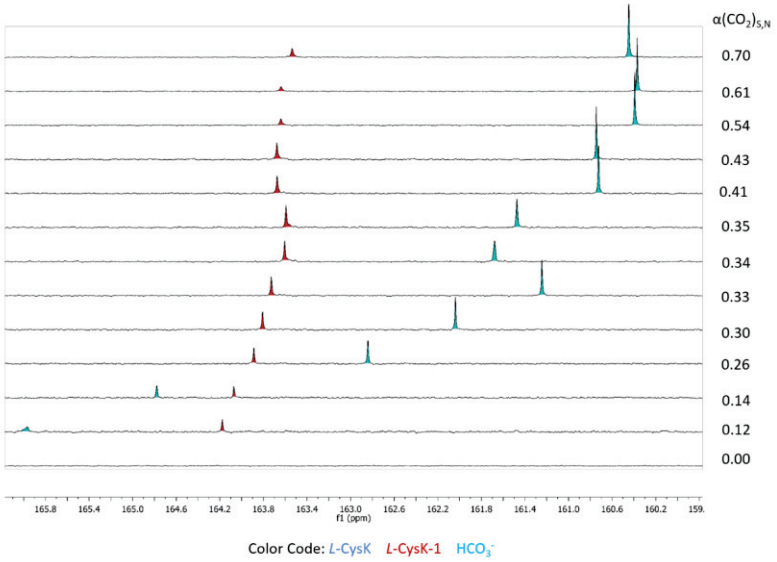

Fig. 148 ^{13}C qNMR spectra evolution for ***L*-CysK** 0.5M in D_2O at 25 °C. Zoom on the sp^2 signals from 160 to 166 ppm.

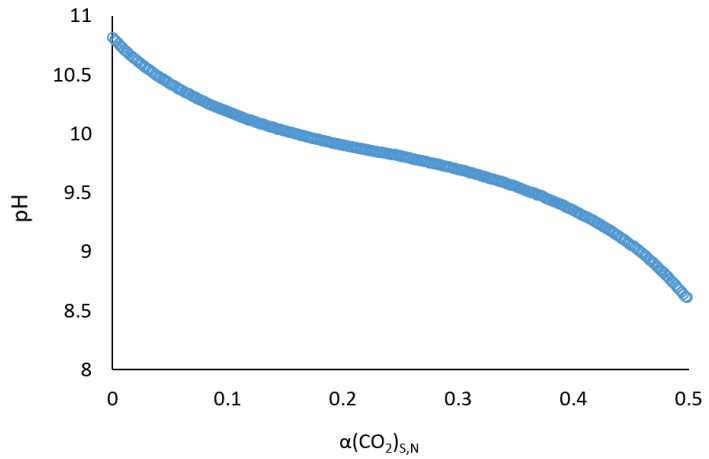

Fig. 149 pH evolution of a 0.5M aqueous solution of ***L*-CysK** upon increasing CO_2 loading at 25 °C.

1.6 *L*-Arginine

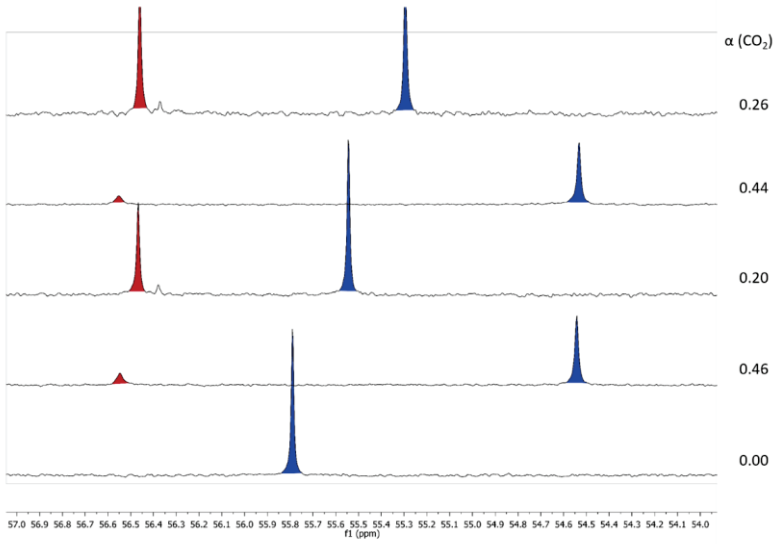

Fig. 150 ^{13}C qNMR spectra for a cyclic capacity experiment performed on a 0.5M solution of ***L*-ArgK** in D_2O at 25 °C. Zoom on sp^3 signals from 53 to 57 ppm.

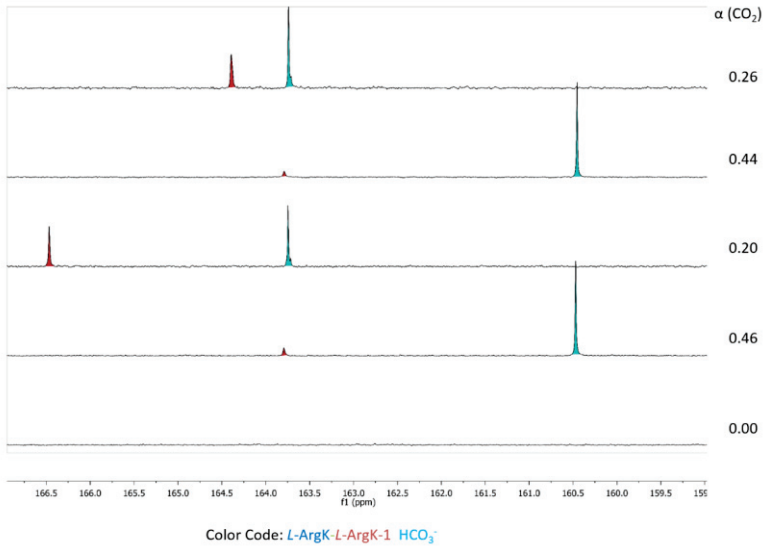

Fig. 151 ^{13}C qNMR spectra for a cyclic capacity experiment performed on a 0.5M solution of ***L*-ArgK** in D_2O at 25 °C. Zoom on sp^2 signals from 159 to 167 ppm.

1.7 *L*-Aspartic Acid

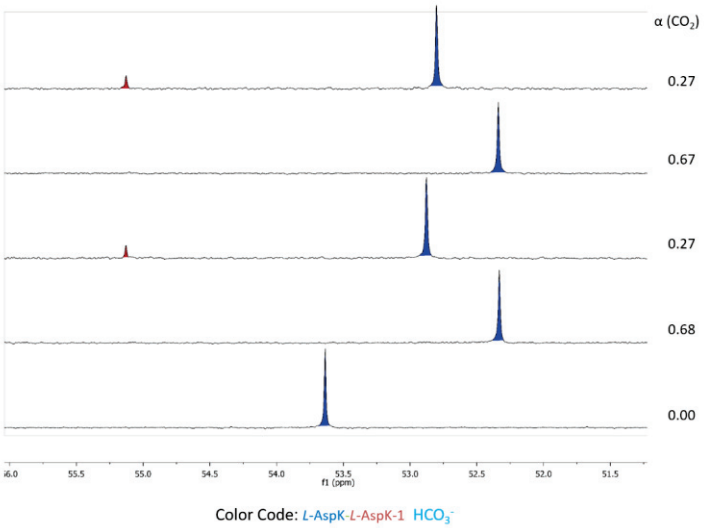

Fig. 152 ^{13}C qNMR spectra for a cyclic capacity experiment performed on a 0.5M solution of ***L*-AspK** in D_2O at 25 °C. Zoom on alpha sp^3 signals from 50 to 56 ppm.

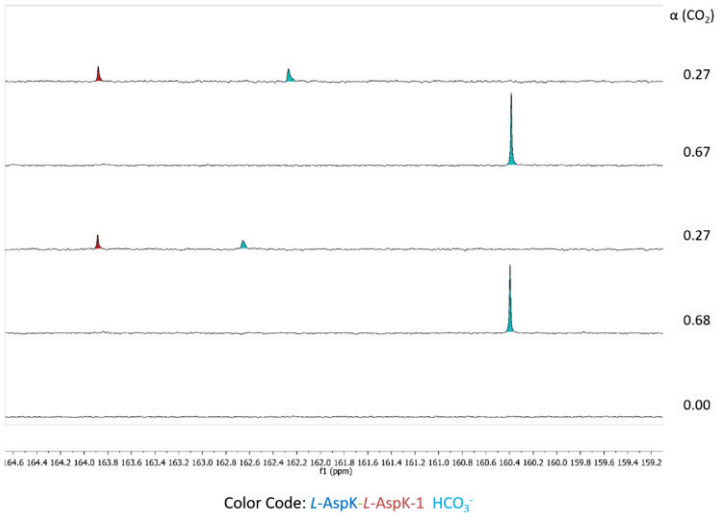

Fig. 153 ^{13}C qNMR spectra for a cyclic capacity experiment performed on a 0.5M solution of ***L*-AspK** in D_2O at 25 °C. Zoom on sp^2 signals from 159 to 165 ppm.

2 Annexes Chapter 3

2.1 EDA and $MgCl_2$

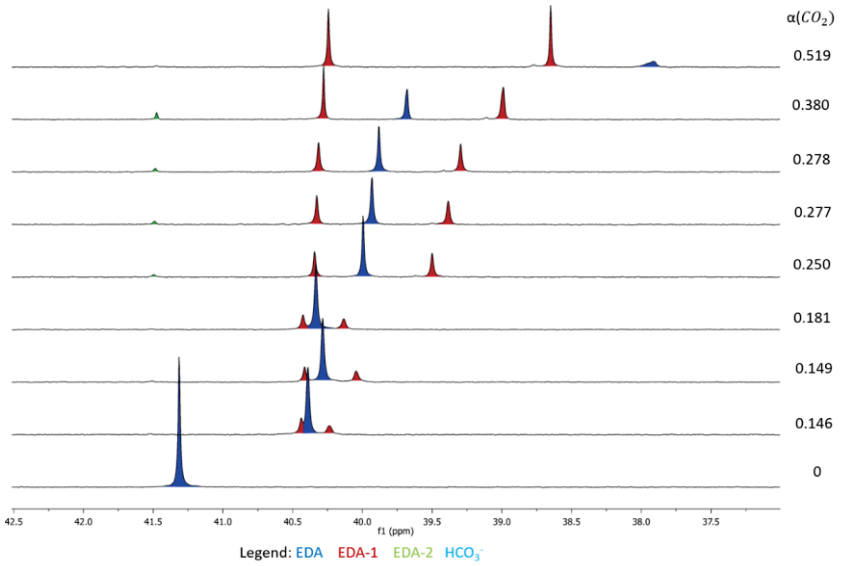

Fig. 154 ^{13}C qNMR spectra evolution for a 0.5M solution of **EDA** with 0.25 equivalents of $MgCl_2$ in D_2O at 25 °C. Zoom on sp^3 signals from 37 to 42.5 ppm.

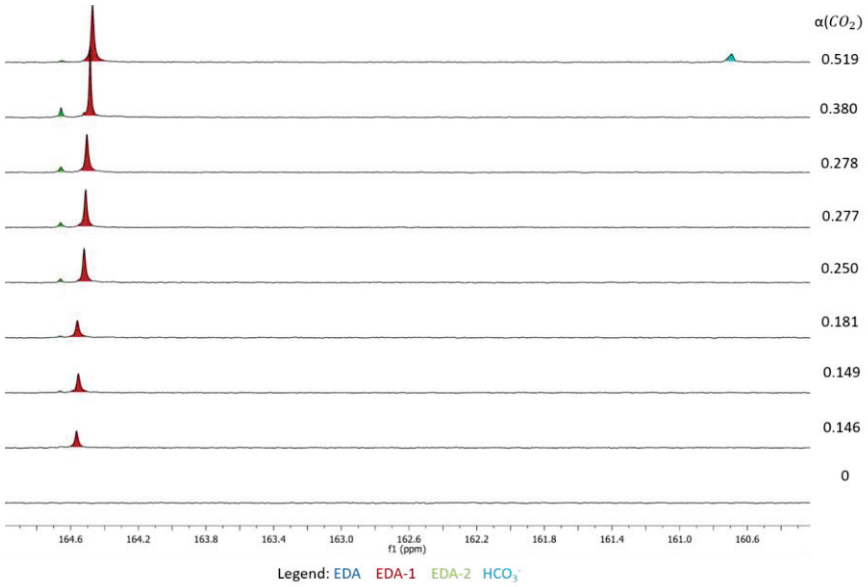

Fig. 155 ^{13}C qNMR spectra evolution for a 0.5M solution of **EDA** with 0.25 equivalents of $MgCl_2$ in D_2O at 25 °C. Zoom on sp^2 signals from 160 to 165 ppm.

2.2 DETA and $MgCl_2$

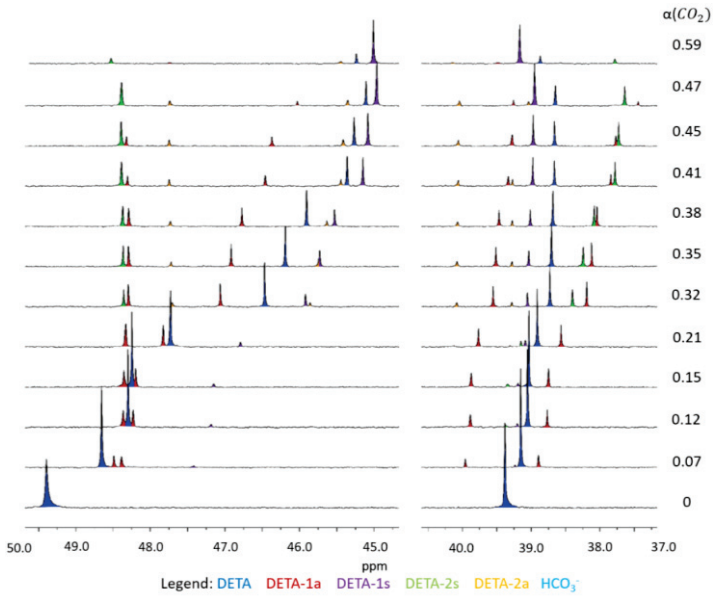

Fig. 156 ^{13}C qNMR spectra evolution for a 0.5M solution of **DETA** with 0.25 equivalents of $MgCl_2$ in D_2O at 25 °C. Zoom on sp^3 signals from 37 to 50 ppm.

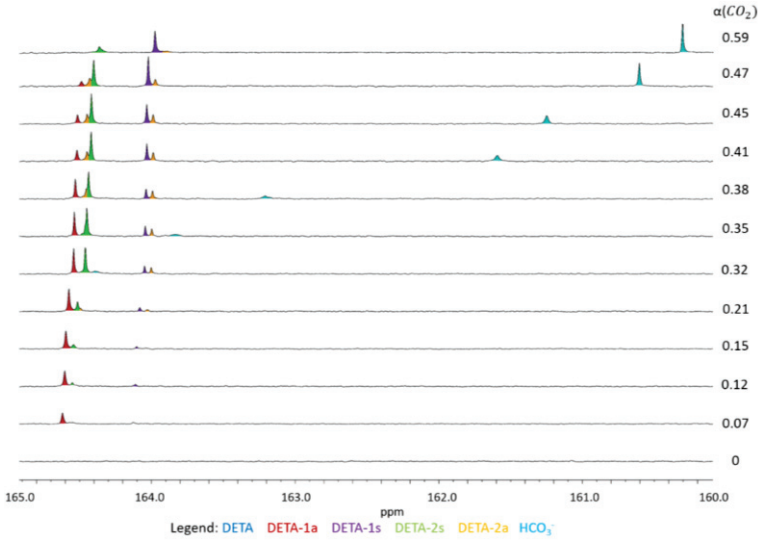

Fig. 157 ^{13}C qNMR spectra evolution for a 0.5M solution of **DETA** with 0.25 equivalents of $MgCl_2$ in D_2O at 25 °C. Zoom on sp^2 signals from 160 to 165 ppm.

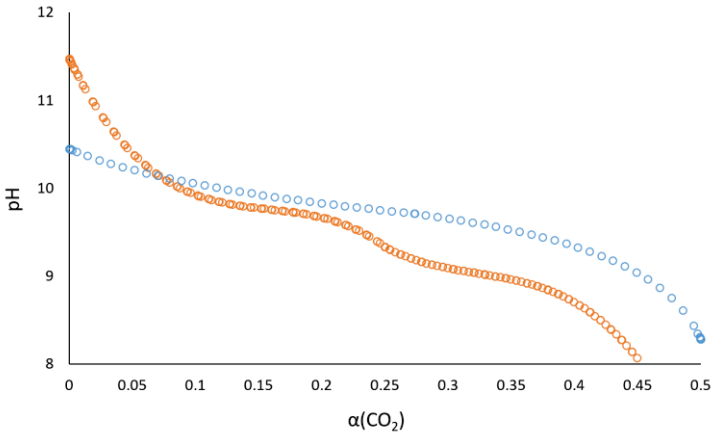

Fig. 158 pH titration at 25 °C of a 0.5M aqueous solution of **DETA** (orange) and a 0.5M aqueous solution of **DETA** with 0.25 equivalents of $MgCl_2$ (blue) upon increasing CO_2 loading.

2.3 Glycine $MgCl_2$

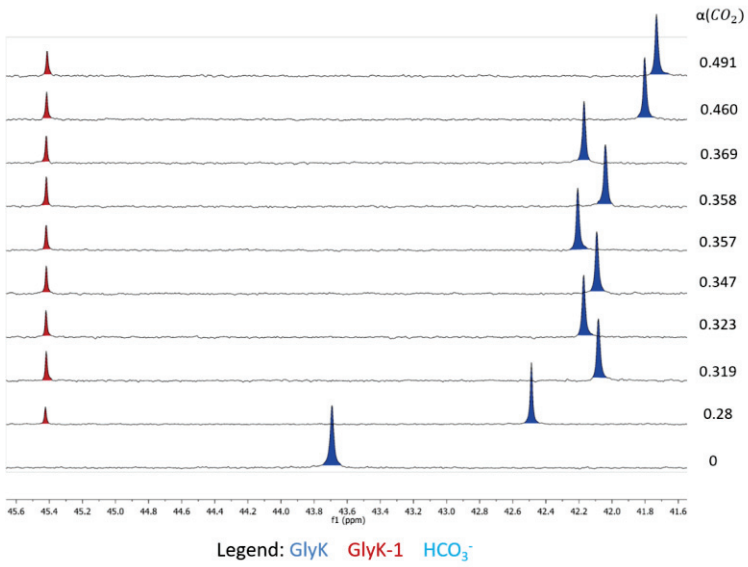

Fig. 159 ^{13}C qNMR spectra evolution for a 0.5M solution of **GlyK** with 0.25 equivalents of MgCl2 in D2O at 25 °C. Zoom on sp3 signals from 41 to 46 ppm.

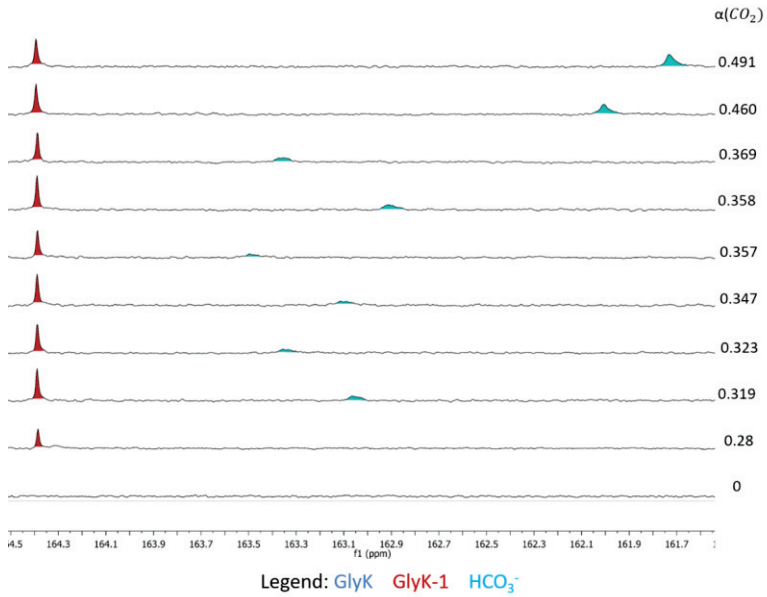

Fig. 160 ^{13}C qNMR spectra evolution for a 0.5M solution of **GlyK** with 0.25 equivalents of MgCl2 in D2O at 25 °C. Zoom on sp2 signals from 161 to 165 ppm.

2.4 *L*-Lysine and $MgCl_2$

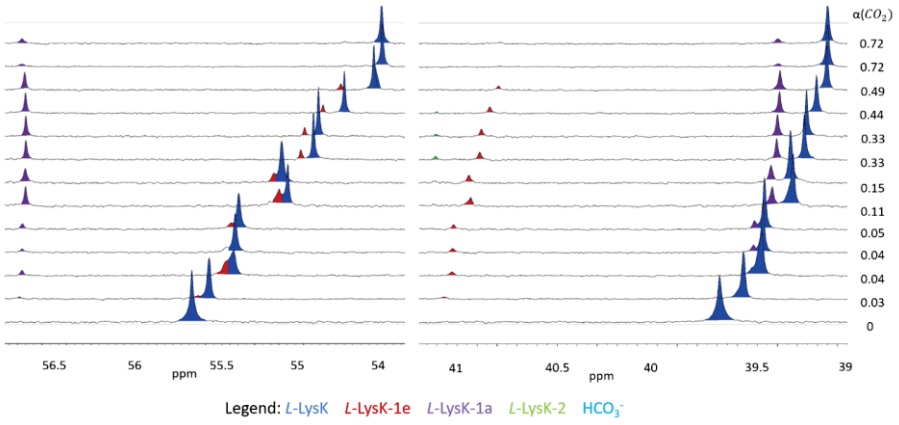

Fig. 161 Evolution of ^{13}C qNMR spectra of a 0.5M solution of ***L*-LysK** in D_2O with 0.25 equivalents of $MgCl_2$. Zoom on the aliphatic signals, 39 to 41 ppm for the epsilon carbon, 54 to 57 ppm for alpha carbon.

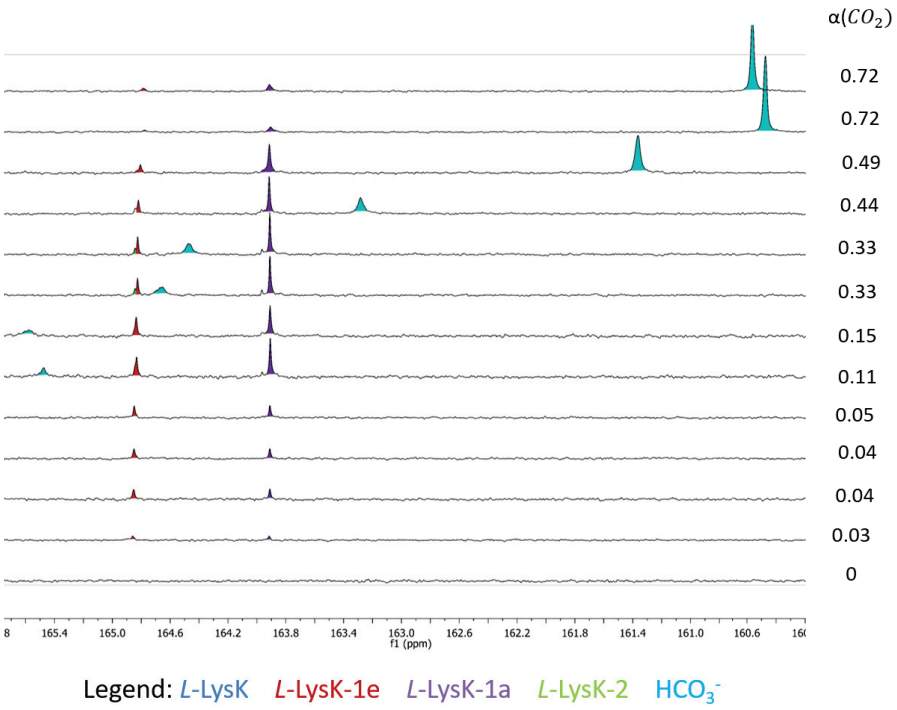

Fig. 162 Evolution of ^{13}C qNMR spectra of a 0.5M solution of ***L*-LysK** in D_2O with 0.25 equivalents of $MgCl_2$. Zoom on the carbonyl signals.

2.5 *L*-Cysteine and $MgCl_2$

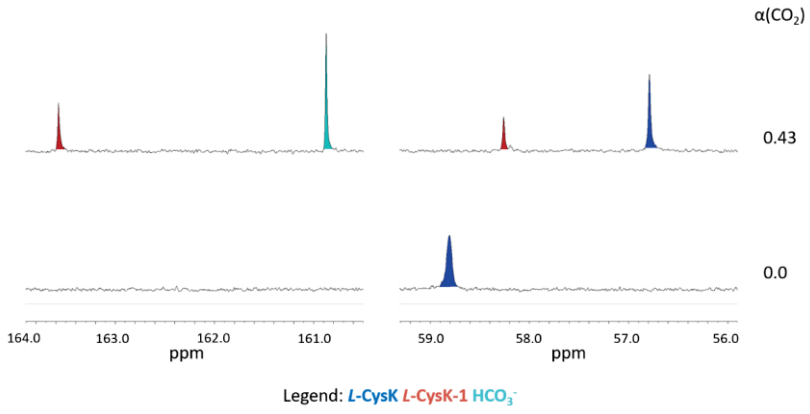

Fig. 163 Stacked ^{13}C spectra of 0.5M ***L*-CysK** in D_2O with 0.125M $MgCl_2$ in absence and in presence of CO_2. Zoom on the aliphatic signal of the alpha carbon (56-59 ppm) and on the carbonyl signal of the CO_2 loaded species (161-164 ppm).

2.6 LAG: DETA and MOx

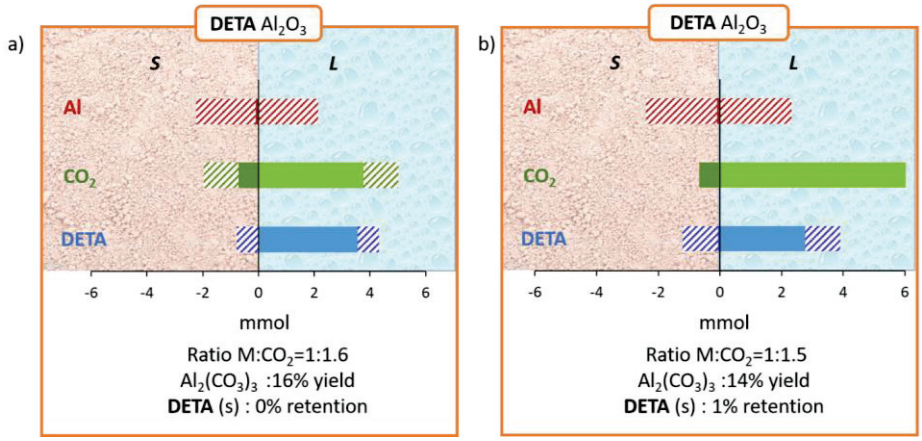

Fig. 164 Results obtained by LAG with a 5M solution of **DETA** in H_2O; grindings performed for 3 cycles of 10 minutes at 500 rpm. a) Al_2O_3, Al:CO_2 = 1:1.6, water washing; b) Al_2O_3, Al:CO_2 = 1:1.5, MeOH washing. Color code: metal (red), CO_2 (green), amine (blue). The graphs are divided into solid fraction (negative values) and liquid fraction (positive values).

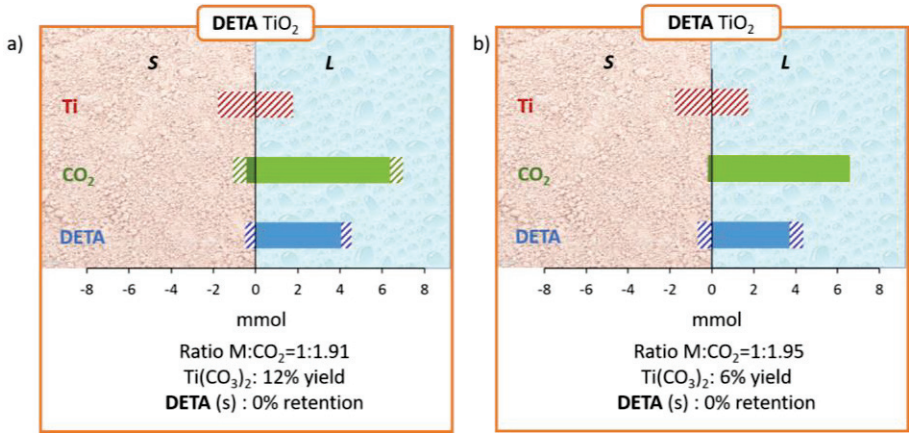

Fig. 165 Results obtained by LAG with a 5M solution of **DETA** in H_2O; grindings performed for 3 cycles of 10 minutes at 500 rpm. a) TiO_2, Ti:CO_2 = 1:1.91, water washing; b) TiO_2, Ti:CO_2 = 1:1.95, MeOH washing. Color code: metal (red), CO_2 (green), amine (blue). The graphs are divided into solid fraction (negative values) and liquid fraction (positive values).

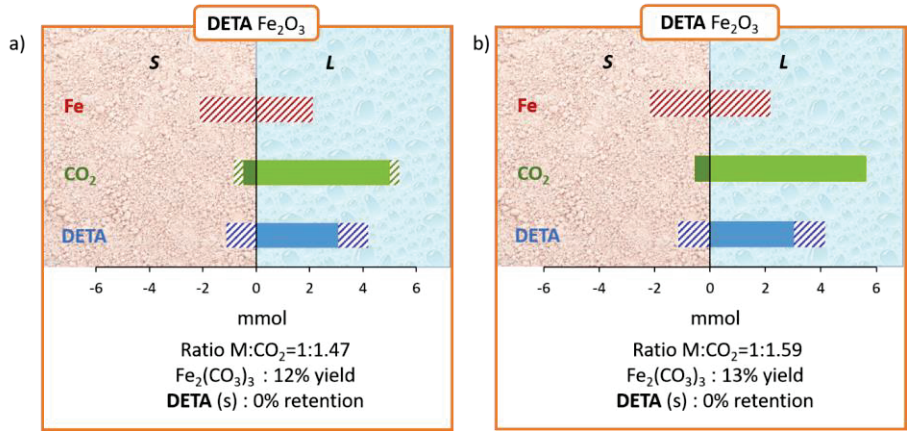

Fig. 166 Results obtained by LAG with a 5M solution of **DETA** in H_2O; grindings performed for 3 cycles of 10 minutes at 500 rpm. a) Fe_2O_3, Fe:CO_2 = 1:1.1.47, water washing; b) Fe_2O_3, Fe:CO_2 = 1:1.59, MeOH washing. Color code: metal (red), CO_2 (green), amine (blue). The graphs are divided into solid fraction (negative values) and liquid fraction (positive values).

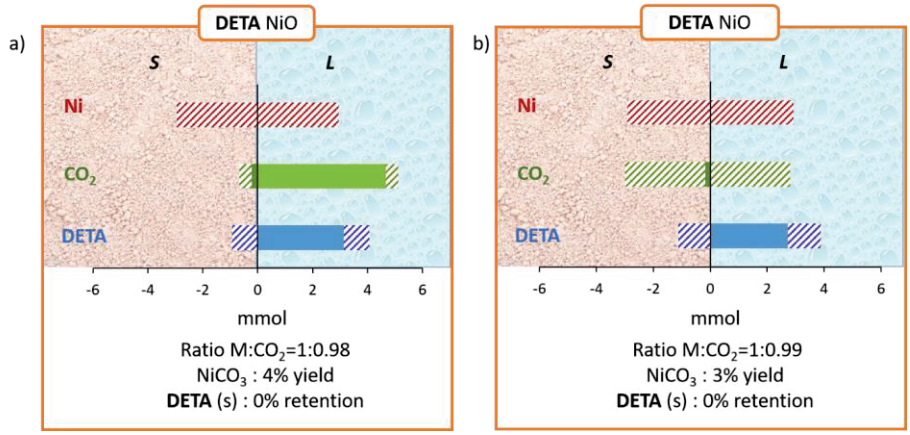

Fig. 167 Results obtained by LAG with a 5M solution of **DETA** in H_2O; grindings performed for 3 cycles of 10 minutes at 500 rpm. a) NiO, Ni:CO_2 = 1:0.98, water washing; b) NiO, Ni:CO_2 = 1:0.99, MeOH washing. Color code: metal (red), CO_2 (green), amine (blue). The graphs are divided into solid fraction (negative values) and liquid fraction (positive values).

2.7 LAG: L-LysK and MgO

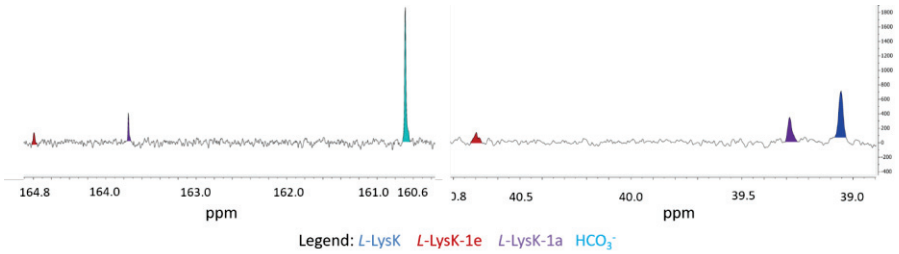

Fig. 168 ^{13}C qNMR spectra of ***L*-LysK**-CO_2(s) loaded at α(CO_2) = 0.79. Zoom on the aliphatic signals of the epsilon carbon (39-41 ppm) and the sp^2 signals (160-164 ppm).

2.8 Neat Grinding, MgO, CaO and GlyK-CO_2(s)

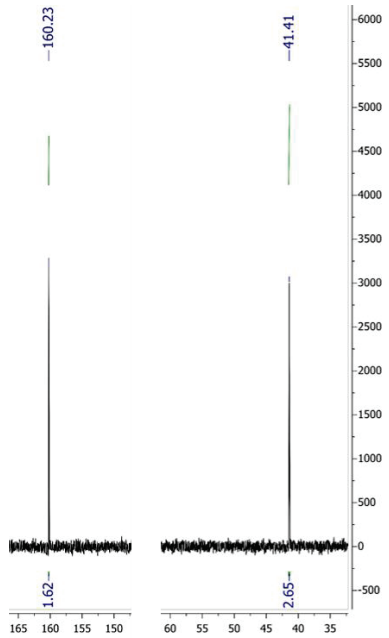

Fig. 169 ^{13}C qNMR spectra of **GlyK**-CO_2(s) loaded at α(CO_2) = 0.61. Zoon on the CH_2 signal (41.41 ppm) and on the bicarbonate peak (160.23 ppm).

2.9 Neat Grinding, MgO and *L*-LysK-CO_2(s)

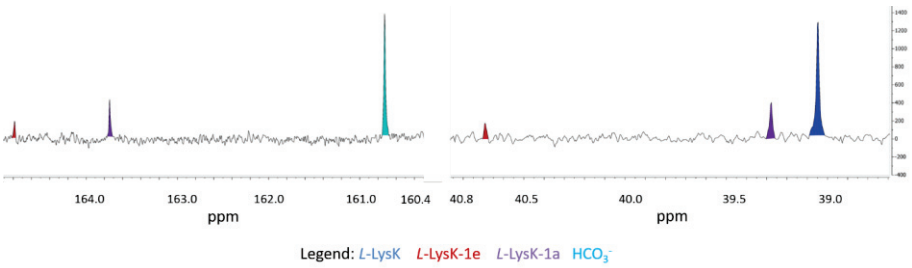

Fig. 170 ^{13}C qNMR spectra of ***L*-LysK**-CO_2(s) loaded at α(CO_2) = 0.57. Zoom on the aliphatic signals of the epsilon carbon (39-41 ppm) and the sp^2 signals (160-164 ppm).

2.10 Neat Grinding, MgO and *L*-CysK -CO_2(s)

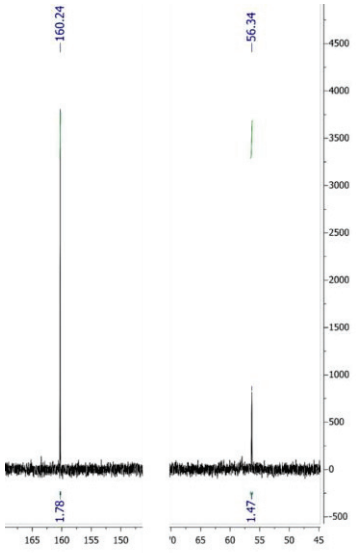

Fig. 171 ^{13}C qNMR spectra of ***L*-CysK**-CO_2(s) loaded at α(CO_2) = 0.61. Zoon on the alpha CH_2 signal (56.34 ppm) and on the bicarbonate peak (160.24 ppm).

2.11 Neat Grinding, CaO and *L*-LysK -CO_2(s)

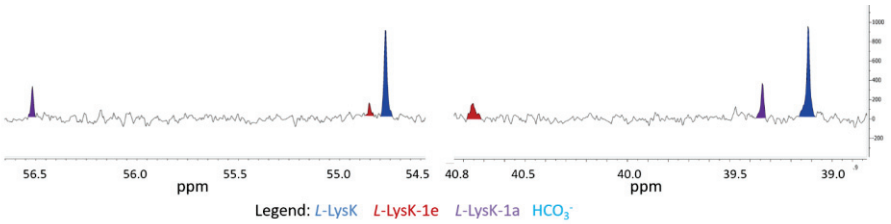

Fig. 172 ^{13}C qNMR spectra of ***L*-LysK**-CO_2(s) loaded at α(CO_2) = 0.77. Zoom on the aliphatic signals of the epsilon carbon (39-41 ppm) and the alpha carbon (54.4-56.5 ppm).

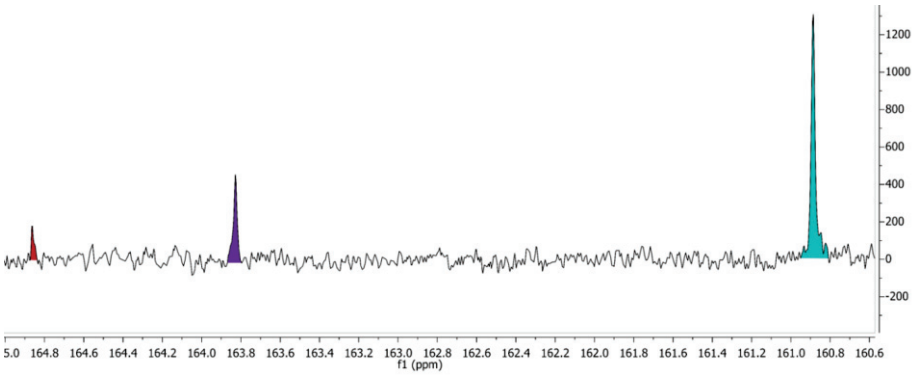

Fig. 173 ^{13}C qNMR spectra of ***L*-LysK**-CO_2(s) loaded at α(CO_2) = 0.77. Zoom on the bicarbonate and carbamate sp^2 signals (160.6-164.8 ppm).

2.12 Neat Grinding, CaO and *L*-CysK -CO_2(s)

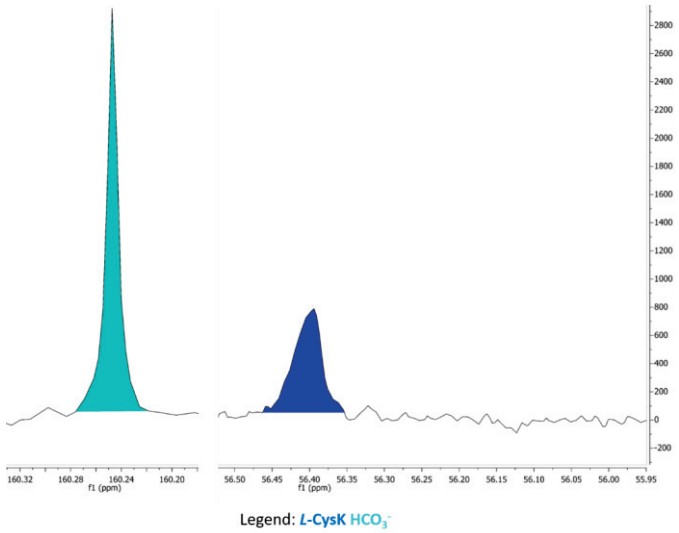

Fig. 174 ^{13}C qNMR spectra of L-CysK-CO_2(s) loaded at α(CO_2) = 0.52. Zoom on the aliphatic signal of the alpha carbon (56.4 ppm) and on the bicarbonate sp^2 signal (160.24 ppm).

3 Annexes Chapter 4

3.1 Description of the soil

Table 50 Initial mmol of metals per gram of soil.

Majors		Minors			
Metal	**mmol/g of soil**	**Metal**	**mmol/g of soil**	**Metal**	**mmol/g of soil**
Mg	0.26	Cr	0.00162	Mn	0.01003
Fe	0.68	Cu	0.00530	As	0.00272
Ca	0.97	Ni	0.00073	Ba	0.00350
Ti	0.07	Co	0.00031	Mo	0.00005
Pb	0.02	Zn	0.00593	Sb	0.00025
Al	2.12	Cd	0.00003	Se	0.00048

Annexes

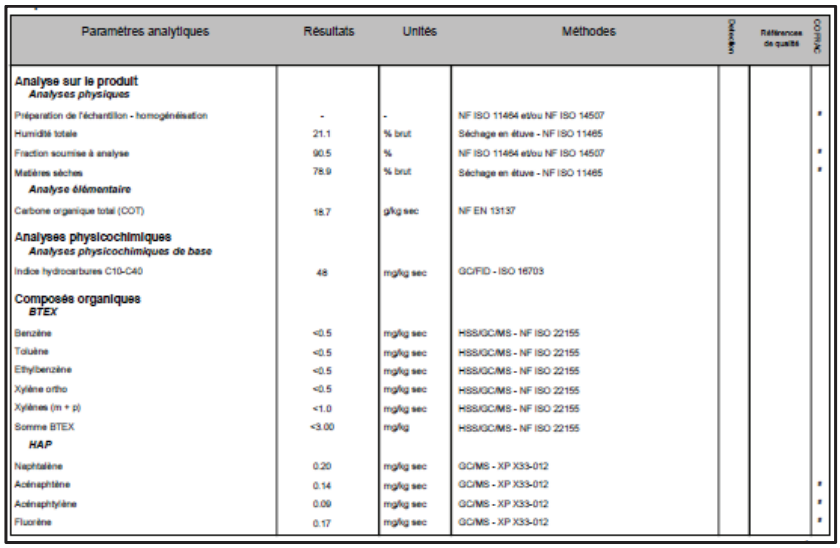

Paramètres analytiques	Résultats	Unités	Méthodes	Qualité	Référence de qualité	COFRAC
Analyse sur le produit						
Analyses physiques						
Préparation de l'échantillon - homogénéisation	-	-	NF ISO 11464 et/ou NF ISO 14507			#
Humidité totale	21.1	% brut	Séchage en étuve - NF ISO 11465			
Fraction soumise à analyse	90.5	%	NF ISO 11464 et/ou NF ISO 14507			#
Matières sèches	78.9	% brut	Séchage en étuve - NF ISO 11465			#
Analyse élémentaire						
Carbone organique total (COT)	18.7	g/kg sec	NF EN 13137			
Analyses physicochimiques						
Analyses physicochimiques de base						
Indice hydrocarbures C10-C40	48	mg/kg sec	GC/FID - ISO 16703			
Composés organiques						
BTEX						
Benzène	<0.5	mg/kg sec	HSS/GC/MS - NF ISO 22155			
Toluène	<0.5	mg/kg sec	HSS/GC/MS - NF ISO 22155			
Ethylbenzène	<0.5	mg/kg sec	HSS/GC/MS - NF ISO 22155			
Xylène ortho	<0.5	mg/kg sec	HSS/GC/MS - NF ISO 22155			
Xylènes (m + p)	<1.0	mg/kg sec	HSS/GC/MS - NF ISO 22155			
Somme BTEX	<3.00	mg/kg	HSS/GC/MS - NF ISO 22155			
HAP						
Naphtalène	0.20	mg/kg sec	GC/MS - XP X33-012			
Acénaphtène	0.14	mg/kg sec	GC/MS - XP X33-012			#
Acénaphtylène	0.09	mg/kg sec	GC/MS - XP X33-012			#
Fluorène	0.17	mg/kg sec	GC/MS - XP X33-012			#

Fig. 175 Nature and abundance of hydrocarbons in the soil.

3.2 Metals omitted

Table 51 Metals omitted in Chapter 4, experiments performed in a stainless-steel reactor.

Reactor	Lixiviant	Metal	Medium ER (%)	SD/2 %
Stainless steel	H_2O	Co	0.7%	0.00144864
		Mo	187.7%	0.20480562
	DETA 0.5 M	Co	13.0%	0.00848042
		Mo	358.5%	0.26720638
	DETA CO2	Co	29.9%	0.04888261
		Mo	252.4%	0.32635365
	LysK 0.5 M	Co	20.6%	0.02456211
		Mo	285.7%	0.60708642
	LysK, CO_2	Co	27.7%	0.02378085
		Mo	256.4%	0.37037994
	GlyK 0.5M	Co	40.7%	0.0325931
		Mo	419.8%	0.49962758
	GlyK, CO_2	Co	32.6%	0.08784817
		Mo	301.2%	0.34311058
	CysK	Co	27.2%	0.03102416
		Mo	636.8%	0.46486255
	CysK, CO2	Co	6.2%	0.01608795
		Mo	354.5%	0.20553629

Annexes

Table 52 Metals omitted in Chapter 4, experiments performed in a tungsten carbide reactor.

Reactor	Lixiviant	Metal	Medium ER (%)	SD/2 %
WC	DETA 0.5M	Ni	210%	2.2636E-06
		Co	36728%	1.0772E-06
		Mo	18%	1.6883E-07
	DETA, CO_2	Ni	164%	2.2636E-06
		Co	27240%	1.0772E-06
		Mo	65%	1.6883E-07
	LysK 0.5M	Co	18453%	1.0772E-06
		Mo	21%	1.6883E-07
	LysK CO_2	Co	11940%	1.0772E-06
		Mo	49%	1.6883E-07
	GlyK 0.5M	Ni	123%	2.2636E-06
		Co	29561%	1.0772E-06
		Mo	37%	1.6883E-07
	GlyK, CO_2	Ni	109%	2.2636E-06
		Co	25627%	1.0772E-06
		Mo	60%	1.6883E-07
	CysK	Co	6805%	1.0772E-06
		Mo	26%	1.6883E-07
	CysK, CO_2	Co	2181%	1.0772E-06
		Mo	51%	1.6883E-07

3.3 Extraction rate vs pH

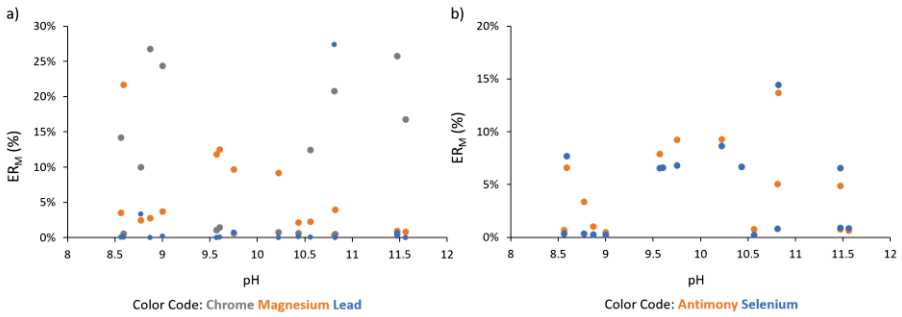

Fig. 176 Metal extraction rate (ER_M (%)) plotted against pH values. The latter refer to the pH values of the leaching solutions discussed in chapter 4. The metals are grouped for their extraction rate interval for clarity; a) chrome (gray), magnesium (orange), lead (blue); b) antimony (orange), selenium (blue).

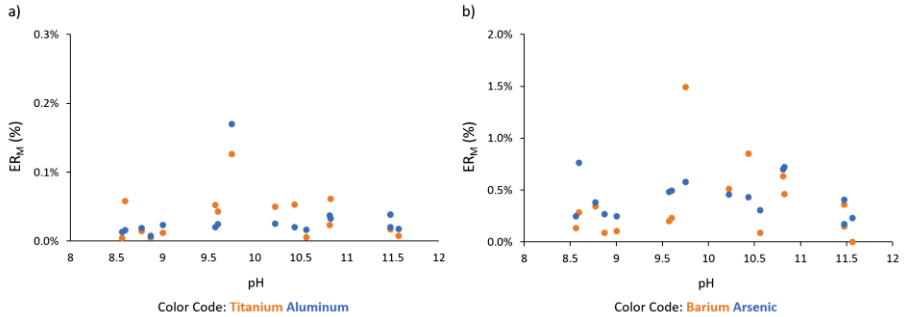

Fig. 177 Metal extraction rate (ER_M (%)) plotted against pH values. The latter refer to the pH values of the leaching solutions discussed in chapter 4. The metals are grouped for their extraction rate interval for clarity; a) titanium (orange), aluminum (blue); b) barium (orange), arsenic (blue).

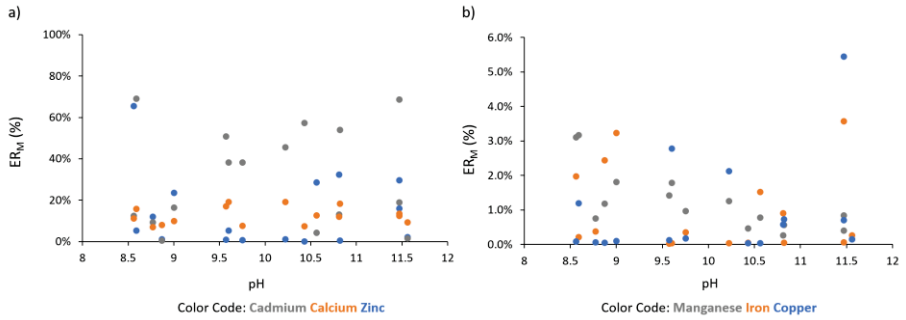

Fig. 178 Metal extraction rate (ER_M (%)) plotted against pH values. The latter refer to the pH values of the leaching solutions discussed in chapter 4. The metals are grouped for their extraction rate interval for clarity; a) cadmium (gray), calcium (orange), zinc (blue); b) manganese (gray), iron (orange), copper (blue).

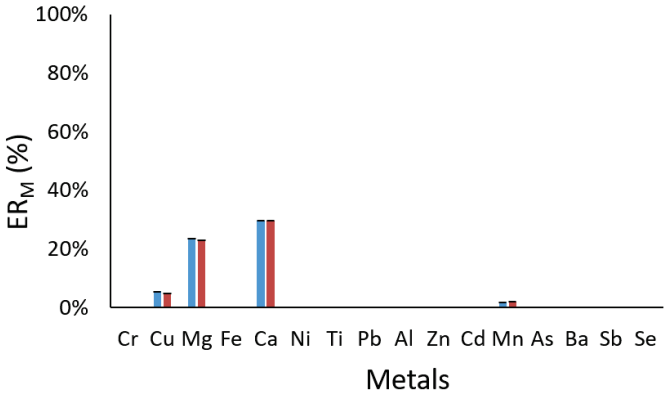

Fig. 179 ICP-OES results for LAG experiments of dried soil treated with 0.1 mL of a 0.5 M aqueous solution of ***L*-CysK** (blue) and ***L*-CysK-CO_2** (red).

Annexes

Bibliography

1. Norahim, N.; Yaisanga, P.; Faungnawakij, K.; Charinpanitkul, T.; Klaysom, C., **2018**, *41*, 211-223.
2. Ahmed, R.; Liu, G.; Yousaf, B.; Abbas, Q.; Ullah, H.; Ali, M. U., *Journal of Cleaner Production* **2020**, *242*, 118409.
3. Bereiter, B.; Eggleston, S.; Schmitt, J.; Nehrbass-Ahles, C.; Stocker, T. F.; Fischer, H.; Kipfstuhl, S.; Chappellaz, J., **2015**, *42*, 542-549.
4. Morice, C. P.; Kennedy, J. J.; Rayner, N. A.; Jones, P. D., **2012**, *117* (D8).
5. A.I.E., *20 Years of Carbon Capture and Storage: Accelerating Future Deployment*. 2016.
6. Friedlingstein, P.; O'Sullivan, M.; Jones, M. W.; Andrew, R. M.; Hauck, J.; Olsen, A.; Peters, G. P.; Peters, W.; Pongratz, J.; Sitch, S.; Le Quéré, C.; Canadell, J. G.; Ciais, P.; Jackson, R. B.; Alin, S.; Aragão, L. E. O. C.; Arneth, A.; Arora, V.; Bates, N. R.; Becker, M.; Benoit-Cattin, A.; Bittig, H. C.; Bopp, L.; Bultan, S.; Chandra, N.; Chevallier, F.; Chini, L. P.; Evans, W.; Florentie, L.; Forster, P. M.; Gasser, T.; Gehlen, M.; Gilfillan, D.; Gkritzalis, T.; Gregor, L.; Gruber, N.; Harris, I.; Hartung, K.; Haverd, V.; Houghton, R. A.; Ilyina, T.; Jain, A. K.; Joetzjer, E.; Kadono, K.; Kato, E.; Kitidis, V.; Korsbakken, J. I.; Landschützer, P.; Lefèvre, N.; Lenton, A.; Lienert, S.; Liu, Z.; Lombardozzi, D.; Marland, G.; Metzl, N.; Munro, D. R.; Nabel, J. E. M. S.; Nakaoka, S. I.; Niwa, Y.; O'Brien, K.; Ono, T.; Palmer, P. I.; Pierrot, D.; Poulter, B.; Resplandy, L.; Robertson, E.; Rödenbeck, C.; Schwinger, J.; Séférian, R.; Skjelvan, I.; Smith, A. J. P.; Sutton, A. J.; Tanhua, T.; Tans, P. P.; Tian, H.; Tilbrook, B.; van der Werf, G.; Vuichard, N.; Walker, A. P.; Wanninkhof, R.; Watson, A. J.; Willis, D.; Wiltshire, A. J.; Yuan, W.; Yue, X.; Zaehle, S., *Earth Syst. Sci. Data* **2020**, *12*, 3269-3340.
7. Rochelle, G. T., *Science* **2009**, *325*.
8. Tapia, J. F. D.; Lee, J.-Y.; Ooi, R. E. H.; Foo, D. C. Y.; Tan, R. R., *Sustainable Production and Consumption* **2018**, *13*, 1-15.
9. Ramezani, R.; Mazinani, S.; Di Felice, R., *Chemical Engineering Science* **2019**, *206*, 187-202.
10. Blamey, J.; Anthony, E. J.; Wang, J.; Fennell, P. S., *Progress in Energy and Combustion Science* **2010**, *36*, 260-279.
11. Erans, M.; Manovic, V.; Anthony, E. J., *Applied Energy* **2016**, *180*, 722-742.
12. Hornberger, M.; Spörl, R.; Scheffknecht, G., *Energy Procedia* **2017**, *114*, 6171-6174.
13. Jansen, D.; Gazzani, M.; Manzolini, G.; Dijk, E. v.; Carbo, M., *International Journal of Greenhouse Gas Control* **2015**, *40*, 167-187.
14. Osman, A. I.; Hefny, M.; Abdel Maksoud, M. I. A.; Elgarahy, A. M.; Rooney, D. W., *Environmental Chemistry Letters* **2021**, *19*, 797-849.
15. Theo, W. L.; Lim, J. S.; Hashim, H.; Mustaffa, A. A.; Ho, W. S., *Applied Energy* **2016**, *183*, 1633-1663.
16. Haszeldine, R. S., *Science* **2009**, *325* (5948), 1647-1652.
17. Holloway, S., *Phil. Trans. R. Soc.* **2007**, *365* (1853), 1095-1107.
18. Dowell, N.; Fennell, P. S.; Shah, N.; Maitland, G. C., *Nat. Clim. Change* **2017**, *7*.

Bibliography

19. Alcalde, J.; Flude, S.; Wilkinson, M.; Johnson, G.; Edlmann, K.; Bond, C. E.; Scott, V.; Gilfillan, S. M. V.; Ogaya, X.; Haszeldine, R. S., *Nature Communications* **2018**, *9*, 2201.

20. Juan Alcaldea, S. F., Mark Wilkinsonb, Gareth Johnsonb*, Katriona Edlmannb, Clare E. Bonda, Vivian Scottb, Stuart M.V. Gilfillanb, Xènia Ogayac and R. Stuart Haszeldineb., Quantifying geological CO2 storage security to deliver on climate mitigation. In *GHGT-14*, Melbourne, Australia, 2018.

21. O'Connor, W. K., Dahlin, David C., Nilsen, David N., Rush, G.E., Walters, Richard P., and Turner, Paul C. , *United States: N. p.* **2001**.

22. Baines, S. J.; Worden, R. H., *Geological Society, London, Special Publications* **2004**, *233*, 1.

23. Hong, S.; Sim, G.; Moon, S.; Park, Y., *Energy & Fuels* **2020**, *34*, 3532-3539.

24. Sanna, A.; Uibu, M.; Caramanna, G.; Kuusik, R.; Maroto-Valer, M. M., *Chemical Society Reviews* **2014**, *43*, 8049-8080.

25. Marocco Stuardi, F.; MacPherson, F.; Leclaire, J., *Current Opinion in Green and Sustainable Chemistry* **2019**, *16*, 71-76.

26. Li, K.; Leigh, W.; Feron, P.; Yu, H.; Tade, M., *Applied Energy* **2016**, *165*, 648-659.

27. Leclaire, J.; Heldebrant, D. J., *Green Chemistry* **2018**, *20*, 5058-5081.

28. Agbonghae, E. O.; Hughes, K. J.; Ingham, D. B.; Ma, L.; Pourkashanian, M., *Industrial & Engineering Chemistry Research* **2014**, *53*, 14815-14829.

29. Cuéllar-Franca, R. M.; Azapagic, A., *Journal of CO_2 Utilization* **2015**, *9*, 82-102.

30. Aladić, K.; Jarni, K.; Barbir, T.; Vidović, S.; Vladić, J.; Bilić, M.; Jokić, S., *Industrial Crops and Products* **2015,** *76*, 472-478.

31. Hughes, A. D.; Black, K. D.; Campbell, I.; Davidson, K.; Kelly, M. S.; Stanley, M. S., *Greenhouse Gases: Science and Technology* **2012**, *2*, 402-407.

32. Brennan, L.; Owende, P., *Renewable and Sustainable Energy Reviews* **2010**, *14*, 557-577.

33. Mikkelsen, M.; Jørgensen, M.; Krebs, F. C., *Energy & Environmental Science* **2010**, *3*, 43-81.

34. Assen, N. v. d.; Sternberg, A.; Kätelhön, A.; Bardow, A., *Faraday Discussions* **2015**, *183*, 291-307.

35. Xiaoding, X.; Moulijn, J. A., *Energy & Fuels* **1996**, *10*, 305-325.

36. Laudenschleger, D.; Ruland, H.; Muhler, M., *Nature Communications* **2020**, *11*, 3898.

37. Meessen, J., *Chemie Ingenieur Technik* **2014**, *86*, 2180-2189.

38. Iijima, T.; Yamaguchi, T., *Applied Catalysis A: General* **2008**, *345*, 12-17.

39. Energy, U. S. D. o., Carbon Dioxide Enhanced Oil Recovery. Energy, Ed. 2010.

40. Oldenburg, C. M.; Pruess, K.; Benson, S. M., *Energy & Fuels* **2001**, *15*, 293-298.

41. Septavaux, J.; Tosi, C.; Jame, P.; Nervi, C.; Gobetto, R.; Leclaire, J., *Nature Chemistry* **2020**.

42. Sanna, A.; Hall, M. R.; Maroto-Valer, M., *Energy & Environmental Science* **2012**, *5*, 7781-7796.

43. Bottoms, R. R. Separating acid gases. US Patent 1783901 2/12/1930, **1930**.

44. Rochelle, G. T., 3 - Conventional amine scrubbing for CO_2 capture. In *Absorption-Based Post-combustion Capture of Carbon Dioxide*, Feron, P. H. M., Ed. Woodhead Publishing: **2016**; pp 35-67.
45. Teir, S., Arasto, A., Sormunen, R., Jussila-suokas, J., Saari, P., **2018**.
46. Kim, S.; Shi, H.; Lee, J. Y., *International Journal of Greenhouse Gas Control* **2016**, *45*, 181-188.
47. Kim, I.; Hoff, K. A.; Mejdell, T., *Energy Procedia* **2014**, *63*, 1446-1455.
48. Kim, I.; Svendsen, H. F., *Industrial & Engineering Chemistry Research* **2007**, *46*, 5803-5809.
49. Kim, Y. E.; Moon, S. J.; Yoon, Y. I.; Jeong, S. K.; Park, K. T.; Bae, S. T.; Nam, S. C., *Separation and Purification Technology* **2014**, *122*, 112-118.
50. McCann, N.; Maeder, M.; Hasse, H., *Energy Procedia* **2011**, *4*, 1542-1549.
51. McCann, N.; Maeder, M.; Hasse, H., *The Journal of Chemical Thermodynamics* **2011**, *43*, 664-669.
52. Septavaux, J.; Germain, G.; Leclaire, J., *Accounts of Chemical Research* **2017**, *50*, 1692-1701.
53. Khanna, R. K.; Moore, M. H., *Spectrochimica Acta Part A: Molecular and Biomolecular Spectroscopy* **1999**, *55*, 961-967.
54. Dijkstra, Z. J.; Doornbos, A. R.; Weyten, H.; Ernsting, J. M.; Elsevier, C. J.; Keurentjes, J. T. F., *The Journal of Supercritical Fluids* **2007**, *41*, 109-114.
55. Versteeg, G. F.; Van Dijck, L. A. J.; Van Swaaij, W. P. M., *Chemical Engineering Communications* **1996**, *144*, 113-158.
56. Crooks, J. E.; Donnellan, J. P., *Journal of the Chemical Society, Perkin Transactions 2* **1989**, 331-333.
57. Caplow, M., *Journal of the American Chemical Society* **1968**, *90*, 6795-6803.
58. Hartono, A.; da Silva, E. F.; Svendsen, H. F., *Chemical Engineering Science* **2009**, *64*, 3205-3213.
59. Bernhardsen, I. M.; Knuutila, H. K., *International Journal of Greenhouse Gas Control* **2017,** *61*, 27-48.
60. Eide-Haugmo, I.; Brakstad, O. G.; Hoff, K. A.; Sørheim, K. R.; da Silva, E. F.; Svendsen, H. F., *Energy Procedia* **2009**, *1*, 1297-1304.
61. Luis, P., *Desalination* **2016**, *380*, 93-99.
62. Rochelle, G.; Chen, E.; Freeman, S.; Van Wagener, D.; Xu, Q.; Voice, A., *Chemical Engineering Journal* **2011**, *171*, 725-733.
63. Hook, R. J., *Industrial & Engineering Chemistry Research* **1997**, *36*, 1779-1790.
64. Davis, J.; Rochelle, G., *Energy Procedia* **2009**, *1*, 327-333.
65. Kim, J.; Lee, J.; Lee, Y.; Kim, H.; Kim, E.; Lee, K. S., *Energy* **2019**, *187*, 115908.
66. Freeman, S. A.; Dugas, R.; Van Wagener, D. H.; Nguyen, T.; Rochelle, G. T., *International Journal of Greenhouse Gas Control* **2010**, *4*, 119-124.
67. Freeman, S. A.; Davis, J.; Rochelle, G. T., *International Journal of Greenhouse Gas Control* **2010**, *4*, 756-761.
68. McCann, N.; Phan, D.; Wang, X.; Conway, W.; Burns, R.; Attalla, M.; Puxty, G.; Maeder, M., *The Journal of Physical Chemistry A* **2009**, *113*, 5022-5029.

69. Cieslarova, Z.; dos Santos, V. B.; do Lago, C. L., *International Journal of Greenhouse Gas Control* **2018**, *76*, 142-149.
70. Nainar, M.; Veawab, A., *Energy Procedia* **2009**, *1*, 231-235.
71. Liu, J.; Li, X.; Zhang, Z.; Li, L.; Bi, Y.; Zhang, L., *Greenhouse Gases: Science and Technology* **2019**, *9*, 349-359.
72. Rochelle, G. T., *Current Opinion in Chemical Engineering* **2012**, *1*, 183-190.
73. Cousins, A.; Huang, S.; Cottrell, A.; Feron, P. H. M.; Chen, E.; Rochelle, G. T., **2015**, *5*, 7-16.
74. Sartori, G.; Ho, W.; Savage, D.; Chludzinski, G.; Wlechert, S. J. S.; methods, p., **1987**, *16*, 171-200.
75. Luo, X.; Liu, S.; Gao, H.; Liao, H.; Tontiwachwuthikul, P.; Liang, Z., *Separation and Purification Technology* **2016**, *169*, 279-288.
76. Brúder, P.; Grimstvedt, A.; Mejdell, T.; Svendsen, H. F., *Chemical Engineering Science* **2011**, *66*, 6193-6198.
77. Rabensteiner, M.; Kinger, G.; Koller, M.; Hochenauer, C., *International Journal of Greenhouse Gas Control* **2016**, *51*, 106-117.
78. Leclaire, J., Guillaume Husson,† Nathalie Devaux,† Vincent Delorme,† Laurence Charles,‡ Fabio Ziarelli,§ Perrine Desbois,⊥ Alexandra Chaumonnot,⊥ Marc Jacquin,⊥ Fre´de´ ric Fotiadu,*,† and Ge´rard Buono†, *J. Am. Chem. Soc.* **2010**, *132*.
79. Muchan, P.; Narku-Tetteh, J.; Saiwan, C.; Idem, R.; Supap, T., *Separation and Purification Technology* **2017**, *184*, 128-134.
80. Singh, P.; Versteeg, G. F., *Process Safety and Environmental Protection* **2008**, *86*, 347-359.
81. Khalili, F.; Rayer, A. V.; Henni, A.; East, A. L. L.; Tontiwachwuthikul, P., Kinetics and Dissociation Constants pKa of Polyamines of Importance in Post-Combustion Carbon Dioxide CO2 Capture Studies. In *Recent Advances in Post-Combustion CO_2 Capture Chemistry*, American Chemical Society: 2012; Vol. 1097, pp 43-70.
82. Ermatchkov, V.; Pérez-Salado Kamps, Á.; Maurer, G., *The Journal of Chemical Thermodynamics* **2003**, *35*, 1277-1289.
83. Zhang, R.; Yang, Q.; Liang, Z.; Puxty, G.; Mulder, R. J.; Cosgriff, J. E.; Yu, H.; Yang, X.; Xue, Y., *Energy & Fuels* **2017**, *31*, 11099-11108.
84. Brown, H. C.; Brewster, J.; Shechter, H. J. J. o. t. A. C. S., **1954**, *76*, 467-474.
85. Pike, S. J.; Hutchinson, J. J.; Hunter, C. A., *Journal of the American Chemical Society* **2017**, *139*, 6700-6706.
86. Zhou, S.; Chen, X.; Nguyen, T.; Voice, A. K.; Rochelle, G. T., **2010**, *3*, 913-918.
87. Hatchell, D.; Namjoshi, O.; Fischer, K.; Rochelle, G. T. J. E. P., **2014**, *63*, 1558-1568.
88. Hirasawa, T.; Shimizu, H., *Current Opinion in Biotechnology* **2016**, *42*, 133-146.
89. Sandeaux, J.; Sandeaux, R.; Gavach, C.; Grib, H.; Sadat, T.; Belhocine, D.; Mameri, N., **1998**, *71*, 267-273.
90. Huang, Q.; Bhatnagar, S.; Remias, J. E.; Selegue, J. P.; Liu, K., *International Journal of Greenhouse Gas Control* **2013**, *19*, 243-250.
91. Zhao, Y.; Shen, S.; Bian, Y.; Yang, Y.-n.; Ghosh, U., *The Journal of Chemical Thermodynamics* **2017**, *111*, 100-105.

92. Aronu, U. E.; Svendsen, H. F.; Hoff, K. A., *International Journal of Greenhouse Gas Control* **2010**, *4*, 771-775.
93. Daubert, T. E. a. D., R.P. , *Physical and Thermodynamic Properties of Pure Chemicals (Data Compilation)*. Hemisphere Publishing Corporation: New York, 1989.
94. EPA Predictive Models and Tools for Assessing Chemicals under the Toxic Substances Control Act (TSCA).
95. Zhang, Z.; Li, Y.; Zhang, W.; Wang, J.; Soltanian, M. R.; Olabi, A. G., *Renewable and Sustainable Energy Reviews* **2018**, *98*, 179-188.
96. Hu, G.; Smith, K. H.; Wu, Y.; Mumford, K. A.; Kentish, S. E.; Stevens, G. W., *Chinese Journal of Chemical Engineering* **2018**, *26*, 2229-2237.
97. Weiss, I. M.; Muth, C.; Drumm, R.; Kirchner, H. O. K., *BMC Biophysics* **2018**, *11*, 2.
98. Lee, S.; Kim, J.-W.; Chae, S.; Bang, J.-H.; Lee, S.-W., *Journal of CO2 Utilization* **2016,** *16*, 336-345.
99. Liu, M.; Gadikota, G., *Energy & Fuels* **2019**, *33*, 1722-1733.
100. Wang, X.; Maroto-Valer, M. M., *Energy* **2013**, *51*, 431-438.
101. Zhao, H.; Park, Y.; Lee, D. H.; Park, A.-H. A., *Physical Chemistry Chemical Physics* **2013**, *15*, 15185-15192.
102. Ji, L.; Yu, H.; Li, K.; Yu, B.; Grigore, M.; Yang, Q.; Wang, X.; Chen, Z.; Zeng, M.; Zhao, S., *Applied Energy* **2018**, *225*, 356-366.
103. Elbaz, A.; Aboulfotoh, A.; Dohdoh, A.; Wahba, A. J. J. M. E. S., **2019**, *10*, 1062-1073.
104. Haug, T. A.; Munz, I. A.; Kleiv, R. A., *Energy Procedia* **2011**, *4*, 5029-5036.
105. Snæbjörnsdóttir, S. Ó.; Sigfússon, B.; Marieni, C.; Goldberg, D.; Gislason, S. R.; Oelkers, E. H., *Nature Reviews Earth & Environment* **2020**, *1*, 90-102.
106. Kim, M.-J.; Jung, S., *Journal of CO2 Utilization* **2020**, *42*, 101306.
107. Udovic, M.; Lestan, D., *Chemosphere* **2012**, *88*, 718-724.
108. Gadikota, G., *Communications Chemistry* **2021**, *4*, 23.
109. Liu, M.; Gadikota, G., *Fuel* **2020**, *275*, 117887.
110. Bonfils, B.; Julcour-Lebigue, C.; Guyot, F.; Bodénan, F.; Chiquet, P.; Bourgeois, F., *International Journal of Greenhouse Gas Control* **2012**, *9*, 334-346.
111. Gadikota, G.; Matter, J.; Kelemen, P.; Park, A.-h. A., *Physical Chemistry Chemical Physics* **2014**, *16*, 4679-4693.
112. Zevenhoven, R.; Slotte, M.; Åbacka, J.; Highfield, J., *Energy* **2016**, *117*, 604-611.
113. Zevenhoven, R.; Fagerlund, J.; Nduagu, E.; Romão, I.; Jie, B.; Highfield, J., *Energy Procedia* **2013**, *37*, 5945-5954.
114. Li, L.; Liu, W.; Qin, Z.; Zhang, G.; Yue, H.; Liang, B.; Tang, S.; Luo, D., *Energy* **2021**, *222*, 120010.
115. Liu, M.; Hohenshil, A.; Gadikota, G., *Energy & Fuels* **2021**, *35*, 8051-8068.
116. Kang, D.; Park, S.; Jo, H.; Park, J., *Chemical Engineering Journal* **2014**, *248*, 200-207.
117. Kim, D.-S.; An, K.-G.; Kim, K.-H., *Journal of Environmental Science and Health, Part A* **2003**, *38*, 839-853.
118. Cioica, N.; Tudora, C.; Iuga, D.; Deak, G.; Matei, M.; Nagy, E. M.; Gyorgy, Z. J. E. S. W. C., **2019,** *112*, 03024.

119. Rulkens, W. H.; Tichy, R.; Grotenhuis, J. T. C., *Water Science and Technology* **1998**, *37*, 27-35.
120. Etim, E. E., *International Journal of Environment and Bioenergy* **2012**, *3*, 120-136.
121. E.O. Dada, K. I. N., A.A. Osuntoki, M.O. Akinola, *Ethiopian Journal of Environmental Studies and Management* **2015**, *8*, 606 – 615.
122. Park, K.; Lee, J.; Sung, J., *Chemosphere* **2013**, *91*, 616-622.
123. Tandy, S.; Bossart, K.; Mueller, R.; Ritschel, J.; Hauser, L.; Schulin, R.; Nowack, B., *Environmental Science & Technology* **2004**, *38*, 937-944.
124. Voice, A. K.; Closmann, F.; Rochelle, G. T., *Energy Procedia* **2013**, *37*, 2118-2132.
125. *The Merck Index - An Encyclopedia of Chemicals, Drugs, and Biologicals.* Royal Society of Chemistry: Cambridge, UK, 2013.
126. Haynes, W. M., *CRC Handbook of chemistry and Physics*. CRC Press Inc.: Boca Raton, FL, 1990-1991.
127. Kirk-Othmer, *Encyclopedia of Chemical Technology*. John Wiley and Sons: New York, NY, 1978; Vol. 1-26.
128. EPA U.S. Environmental Protection Agency. CompTox Chemicals Dashboard. .
129. Sax, N. I. L., R.J., *Hawley's Condensed Chemical Dictionary*. Van Nostrand Rheinhold Co: New York, NY, **1993**.
130. T. Boublík, V. F., E. Hála, *The vapour pressures of pure substances* Elsevier Science Publishers Amsterdam, Oxford, New York, Tokyo: **1984**, *17*.
131. Gaube, J., Boublik, T., Fried, V., & Hala, E. *Berichte der bunsengesellschaft für physikalische chemie*, **1985**, *89*, 352-352.
132. Pfefferle, W.; Möckel, B.; Bathe, B.; Marx, A., Biotechnological Manufacture of Lysine. In *Microbial Production of l-Amino Acids*, Faurie, R.; Thommel, J.; Bathe, B.; Debabov, V. G.; Huebner, S.; Ikeda, M.; Kimura, E.; Marx, A.; Möckel, B.; Mueller, U.; Pfefferle, W., Eds. Springer Berlin Heidelberg: Berlin, Heidelberg, 2003; pp 59-112.
133. Hermann, T., *Journal of Biotechnology* **2003**, *104*, 155-172.
134. Sang Sefidi, V.; Luis, P., *Industrial & Engineering Chemistry Research* **2019**, *58*, 20181-20194.
135. R. Kelle, T. h. a. B. B., L-Lysine Production. In *Handbook of Corynebacterium glutamicum*, Francis, T. a., Ed. 2005; pp 465-482.
136. Mazinani, S.; Ramazani, R.; Samsami, A.; Jahanmiri, A.; Van der Bruggen, B.; Darvishmanesh, S., *Fluid Phase Equilibria* **2015**, *396*, 28-34.
137. Aschenbrenner, O.; Styring, P., *Energy & Environmental Science* **2010**, *3*, 1106-1113.
138. Veawab, A.; Tontiwachwuthikul, P.; Chakma, A., *Industrial & Engineering Chemistry Research* **1999**, *38*, 3917-3924.
139. Davies, D. H.; Burstein, G. T., *Corrosion* **1980**, *36*, 416-422.
140. Chang, Y.-C.; Leron, R. B.; Li, M.-H., *The Journal of Chemical Thermodynamics* **2013**, *64*, 106-113.
141. Hartono, A.; da Silva, E. F.; Grasdalen, H.; Svendsen, H. F., *Industrial & Engineering Chemistry Research* **2007**, *46*, 249-254.

142. Sheng, M.; Xie, C.; Zeng, X.; Sun, B.; Zhang, L.; Chu, G.; Luo, Y.; Chen, J.-F.; Zou, H., *Fuel* **2018**, *234*, 1518-1527.
143. Kim, I.; Svendsen, H. F., *International Journal of Greenhouse Gas Control* **2011**, *5*, 390-395.
144. Mathias, P. M., *Fluid Phase Equilibria* **2014**, *362*, 102-107.
145. Ciftja, A. F.; Hartono, A.; Svendsen, H. F., *Energy Procedia* **2013**, *37*, 1605-1612.
146. Hikita, H.; Asai, S.; Ishikawa, H.; Honda, M., *The Chemical Engineering Journal* **1977**, *14* (1), 27-30.
147. Sada, E.; Kumazawa, H.; Butt, M. A., *The Chemical Engineering Journal* **1977**, *13*, 213-217.
148. Weiland, R. H.; Trass, O., **1971**, *49*, 767-772.
149. Schäffer, A.; Brechtel, K.; Scheffknecht, G., *Fuel* **2012**, *101*, 148-153.
150. Song, H.-J.; Park, S.; Kim, H.; Gaur, A.; Park, J.-W.; Lee, S.-J., *International Journal of Greenhouse Gas Control* **2012**, *11*, 64-72.
151. Kang, D.; Park, S.; Jo, H.; Min, J.; Park, J., *Journal of Chemical & Engineering Data* **2013**, *58*, 1787-1791.
152. Shen, S.; Yang, Y.-n.; Wang, Y.; Ren, S.; Han, J.; Chen, A., *Fluid Phase Equilibria* **2015**, *399*, 40-49.
153. Portugal, A. F.; Sousa, J. M.; Magalhães, F. D.; Mendes, A., *Chemical Engineering Science* **2009**, *64*, 1993-2002.
154. Majchrowicz, M. E.; Brilman, D. W. F.; Groeneveld, M. J., *Energy Procedia* **2009**, *1*, 979-984.
155. Majchrowicz, M. E.; Kersten, S.; Brilman, W., *Industrial & Engineering Chemistry Research* **2014**, *53*, 11460-11467.
156. Aronu, U. E.; Ciftja, A. F.; Kim, I.; Hartono, A., *Energy Procedia* **2013**, *37*, 233-240.
157. Al-Terkawi, A.-A.; Lamaty, F.; Métro, T.-X., *ACS Sustainable Chemistry & Engineering* **2020**, *8*, 13159-13166.
158. Williams, P. A.; Hughes, C. E.; Martin, J.; Courvoisier, E.; Buanz, A. B. M.; Gaisford, S.; Harris, K. D. M., *The Journal of Physical Chemistry C* **2016**, *120*, 9385-9392.
159. Shen, S.; Yang, Y.-n.; Bian, Y.; Zhao, Y., *Environmental Science & Technology* **2016**, *50*, 2054-2063.
160. Shen, S.; Zhao, Y.; Bian, Y.; Wang, Y.; Guo, H.; Li, H., *The Journal of Chemical Thermodynamics* **2017**, *115*, 209-220.
161. Li, C.; Zhao, Y.; Shen, S., *Energy & Fuels* **2019**, *33*, 10090-10098.
162. Epp, B.; Fahlenkamp, H.; Vogt, M., *Energy Procedia* **2011**, *4*, 75-80.
163. Singh, P.; Rheinhardt, J. H.; Olson, J. Z.; Tarakeshwar, P.; Mujica, V.; Buttry, D. A., *Journal of the American Chemical Society* **2017**, *139*, 1033-1036.
164. Harris, D.; Bushnell, E., *The Journal of Physical Chemistry A* **2019**, *123* , 3383-3388.
165. Stueber, D.; Patterson, D.; Mayne, C. L.; Orendt, A. M.; Grant, D. M.; Parry, R. W., *Inorganic Chemistry* **2001**, *40*, 1902-1911.
166. Shen, S.; Yang, Y.-n., *Energy & Fuels* **2016**, *30*, 6585-6596.
167. Bozorgian, A.; Arab Aboosadi, Z.; Mohammadi, A.; Honarvar, B.; Azimi, A., **2020**, *2*, 420-426.

168. Bavoh, C. B.; Lal, B.; Osei, H.; Sabil, K. M.; Mukhtar, H., *Journal of Natural Gas Science and Engineering* **2019**, *64*, 52-71.
169. Sa, J.-H.; Kwak, G.-H.; Lee, B. R.; Ahn, D.; Lee, K.-H., *Physical Chemistry Chemical Physics* **2014**, *16*, 26730-26734.
170. Lehn, J. M., *Chem. Eur. J.* **1999**, *5*.
171. Corbett, P. T.; Leclaire, J.; Vial, L.; West, K. R.; Wietor, J.-L.; Sanders, J. K. M.; Otto, S., *Chem. Rev.* **2006**, *106*.
172. Hu, X. E.; Yu, Q.; Barzagli, F.; Li, C. e.; Fan, M.; Gasem, K. A. M.; Zhang, X.; Shiko, E.; Tian, M.; Luo, X.; Zeng, Z.; Liu, Y.; Zhang, R., *ACS Sustainable Chemistry & Engineering* **2020**, *8*, 6173-6193.
173. Derks, P. W. J.; Huttenhuis, P. J. G.; van Aken, C.; Marsman, J.-H.; Versteeg, G. F., *Energy Procedia* **2011**, *4*, 599-605.
174. Hartono, A.; Aronu, U. E.; Svendsen, H. F., *Energy Procedia* **2011**, *4*, 209-215.
175. Jakobsen, J. P.; Krane, J.; Svendsen, H. F., *Industrial & Engineering Chemistry Research* **2005**, *44*, 9894-9903.
176. Dolomanov, O. V.; Bourhis, L. J.; Gildea, R. J.; Howard, J. A. K.; Puschmann, H., *Journal of Applied Crystallography* **2009**, *42*, 339-341.
177. Böttcher, T.; Kolodkin-Gal, I.; Kolter, R.; Losick, R.; Clardy, J., *Journal of the American Chemical Society* **2013**, *135*, 2927-2930.
178. Guo, D.; Thee, H.; Tan, C. Y.; Chen, J.; Fei, W.; Kentish, S.; Stevens, G. W.; da Silva, G., *Energy & Fuels* **2013**, *27*, 3898-3904.
179. Liu, M.; Asgar, H.; Seifert, S.; Gadikota, G., *Sustainable Energy & Fuels* **2020**, *4*, 1265-1275.
180. Arti, M.; Youn, M. H.; Park, K. T.; Kim, H. J.; Kim, Y. E.; Jeong, S. K., *Energy & Fuels* **2017**, *31*, 763-769.
181. Ji, L.; Zhang, L.; Zheng, X.; Feng, L.; He, Q.; Wei, Y.; Yan, S., *Journal of CO_2 Utilization* **2021**, *51*, 101653.
182. Zhang, W.; Li, J.; Wang, Q.; Qiu, X., *International Journal of Greenhouse Gas Control* **2020**, *97*, 103056.
183. Dubois, L.; Thomas, D., *Energy Procedia* **2013**, *37*, 1648-1657.
184. Zhang, D.; Ghouleh, Z.; Shao, Y., *Journal of CO2 Utilization* **2017**, *21*, 119-131.
185. Chen, J.; Schaef, H. T.; Li, Q.; Vakifahmetoglu, C.; Riman, R. E.; Bowden, M. E.; Rosso, K. M., Carbonation of Wollastonite [$CaSiO_3$] Under Hydrothermal Conditions During Exposure to Gaseous CO_2: Implications for ex situ Mineralization. 2011; Vol. 2011, pp GC51B-0956.
186. A, O., **1976,** *65*, 933-933.
187. Lee, M.-G.; Kang, D.; Yoo, Y.; Jo, H.; Song, H.-J.; Park, J., *Industrial & Engineering Chemistry Research* **2016**, *55*, 11795-11800.
188. Nguyen, T.; Hilliard, M.; Rochelle, G., *Energy Procedia* **2011**, *4*, 1624-1630.
189. Du, Y.; Yuan, Y.; Rochelle, G. T., *International Journal of Greenhouse Gas Control* **2017**, *58*, 1-9.
190. Ardila-Fierro, K. J.; Hernández, J. G., **2021**, *14*, 2145-2162.
191. Tan, D.; García, F., *Chemical Society Reviews* **2019**, *48*, 2274-2292.

192. Heinicke, G.; Hennig, H.-P.; Linke, E.; Steinike, U.; Thiessen, K.-P.; Meyer, K., **1984**, *19*, 1424-1424.
193. Guo, X.; Xiang, D.; Duan, G.; Mou, P., *Waste Management* **2010**, *30*, 4-10.
194. Ou, Z.; Li, J.; Wang, Z., *Environmental Science: Processes & Impacts* **2015**, *17*, 1522-1530.
195. Tan, Q.; Li, J., *Environmental Science & Technology* **2015**, *49*, 5849-5861.
196. Leštan, D.; Luo, C.-l.; Li, X.-d., *Environmental Pollution* **2008**, *153*, 3-13.
197. Peters, R. W.; Shem, L., Use of Chelating Agents for Remediation of Heavy Metal Contaminated Soil. In *Environmental Remediation*, American Chemical Society: 1992; Vol. 509, pp 70-84.
198. Saeki, S., Lee, J., Zhang, Q., Saito, F., *Int. J. Miner. Process* **2004**, *74*, 373–S378.
199. Zhang, Q.; Lu, J.; Saito, F.; Nagata, C.; Ito, Y., *Advanced Powder Technology* **2000**, *11*, 353-359.
200. Zhang, C.; Wang, J.; Bai, J.; Guan, J.; Wu, W.; Guo, C., *Waste Management & Research* **2013**, *31*, 759-763.
201. Zhang, Q.; Wang, J.; Saito, F.; Okura, T.; Nakamura, I., *Chemistry Letters* **2002**, *31*, 1094-1095.
202. Wang, J.; Lu, J.; Zhang, Q.; Saito, F., *Industrial & Engineering Chemistry Research* **2003**, *42*, 5813-5818.
203. Ying, P.; Yu, J.; Su, W., **2021**, *363*, 1246-1271.
204. Friščić, T., *Journal of Materials Chemistry* **2010**, *20*, 7599-7605.
205. T. Friščić, C. M., H. M. Titi, *Angew. Chem.* **2020**, *132*, 1030 – 1041.
206. Friščić, T.; Jones, W., *Crystal Growth & Design* **2009**, *9*, 1621-1637.
207. Blake, I. O.; Leś, A., **1981**, *19*, 463-475.
208. Smith, A. E. M. R. M., *Critical Stability Constants*. Department of Chemistry College of Science Texas A & M University College Station, Texas 1982; Vol. Volume 5 • First Supplement.
209. Clegg, W.; Little, I. R.; Straughan, B. P., *Journal of the Chemical Society, Dalton Transactions* **1986**, 1283-1288.
210. Palacios, E. G.; Juárez-López, G.; Monhemius, A. J., *Hydrometallurgy* **2004**, *72*, 139-148.
211. Zubair, M.; Sirajuddin, M.; Haider, A.; Ullah, K.; Ullah, I.; Munir, A.; Ali, S.; Tahir, M. N., *Inorganica Chimica Acta* **2018**, *482*, 567-578.
212. Notni, J.; Schenk, S.; Görls, H.; Breitzke, H.; Anders, E., *Inorganic Chemistry* **2008**, *47*, 1382-1390.
213. McCowan, C. S.; Groy, T. L.; Caudle, M. T., *Inorganic Chemistry* **2002**, *41*, 1120-1127.
214. Yao, Z.; Li, J.; Xie, H.; Yu, C., *Procedia Environmental Sciences* **2012**, *16*, 722-729.
215. Wasay, S. A.; Barrington, S. F.; Tokunaga, S., *Environmental Technology* **1998**, *19*, 369-379.
216. A. Tessier, P. G. C. C., M. Bisson, *ANALYTICAL CHEMISTRY* **1979**, *51*, 844-851.
217. Qiao, J.; Sun, H.; Luo, X.; Zhang, W.; Mathews, S.; Yin, X., *Chemosphere* **2017**, *167*, 422-428.
218. Mohamed, M., *Journal of Environmental Chemical Engineering* **2013**, *1*, 363-368.

219. Hong, P. K. A.; Jiang, W., Factors in the Selection of Chelating Agents for Extraction of Lead from Contaminated Soil: Effectiveness, Selectivity, and Recoverability. In *Biogeochemistry of Chelating Agents*, American Chemical Society: 2005; Vol. 910, pp 421-432.
220. Martins, J. G.; Neto, I. F. F.; Pinto, I. S. S.; Soares, E. V.; Barros, M. T.; Soares, H. M. V. M., *Journal of Environmental Science and Health, Part A* **2014**, *49*, 344-354.
221. Naghipour, D.; Gharibi, H.; Taghavi, K.; Jaafari, J., *Journal of Environmental Chemical Engineering* **2016**, *4*, 3512-3518.
222. Knepper, T. P., *TrAC Trends in Analytical Chemistry* **2003**, *22*, 708-724.
223. Nörtemann, B., Biodegradation of Chelating Agents: EDTA, DTPA, PDTA, NTA, and EDDS. In *Biogeochemistry of Chelating Agents*, American Chemical Society: 2005; Vol. 910, pp 150-170.
224. Pinto, I. S. S.; Neto, I. F. F.; Soares, H. M. V. M., *Environmental Science and Pollution Research* **2014**, *21*, 11893-11906.
225. Shahid, M.; Austruy, A.; Echevarria, G.; Arshad, M.; Sanaullah, M.; Aslam, M.; Nadeem, M.; Nasim, W.; Dumat, C., *Soil and Sediment Contamination: An International Journal* **2014**, *23*, 389-416.
226. Voglar, D.; Lestan, D., *Chemosphere* **2013**, *91*, 76-82.
227. Jez, E.; Lestan, D., *Chemosphere* **2016**, *151*, 202-209.
228. Jelusic, M.; Lestan, D., *Science of The Total Environment* **2014**, *475*, 132-141.
229. Udovic, M.; Lestan, D., *Chemosphere* **2009**, *74*, 1367-1373.
230. James M. White, R. A. M. a. N. C. L., *[Contribution from the Department of Chemistry, Duquesnb University]* **1956**, 2367-2370.
231. Anderson, M. M. A.-M. D. NOVEL CHROMIUM (III) ALPHA AMINO ACID COMPLEXES. 2007.
232. McAuliffe, C. A.; Murray, S. G., *Inorganica Chimica Acta Reviews* **1972,** *6*, 103-121.
233. Foti, C.; Giuffrè, O.; Lando, G.; Sammartano, S., *Journal of Chemical & Engineering Data* **2009**, *54*, 893-903.
234. Liu, X. Q., Lee, K.S., *Agriculture Science. InTech* **2013**, 119–158.
235. Watson, T. G., **1976**, *96*, 263-268.
236. Dolev, N.; Katz, Z.; Ludmer, Z.; Ullmann, A.; Brauner, N.; Goikhman, R., *Environmental Research* **2020**, *183*, 109140.
237. Brookes, G.; Pettit, L. D., *Journal of the Chemical Society, Dalton Transactions* **1976**, 42-46.
238. Barbara W. Low, F. L. H. a. F. M. R., *Contribution from the Department of Biochemistry, College of Physicians and Surgeons, Columbia University]* **1959**, *81*.
239. Brown2, H. S. a. T. L., *ournal of the American Chemical Society* **1964**, *87*, 1904-1909.
240. BUSCH, G. R. B. a. D. H., *Inorganic Chemistry* **1963**, *5*, 2110-2113.
241. Hoq, M. F.; Shepherd, R. E. J. I. C., **1984**, *23*, 1851-1858.
242. Poisson, G.; Germain, G.; Septavaux, J.; Leclaire, J., *Green Chemistry* **2016**, *18*, 6436-6444.
243. SHUMAN, L. M., **1985**, *140*, 11-22.

244. Förstner, U., Metal Transfer Between Solid and Aqueous Phases. In *Metal Pollution in the Aquatic Environment*, Förstner, U.; Wittmann, G. T. W., Eds. Springer Berlin Heidelberg: Berlin, Heidelberg, 1981; pp 197-270.
245. Clevenger, T. E., *Water, Air, and Soil Pollution* **1990**, *50*, 241-254.
246. Ehsan, S.; Prasher, S. O.; Marshall, W. D., **2006**, *35*, 2084-2091.
247. Martin, B.; Richardson, F. S., *Quarterly Reviews of Biophysics* **1979**, *12*, 181-209.
248. Dressler, L.; Golbik, R.; Ulbrich-Hofmann, R., **2014**, *395*, 791-799.
249. Constable, E. C.; Housecroft, C. E., *Chemical Society Reviews* **2013**, *42*, 1429-1439.
250. George, T. D.; Wendlandt, W. W., *Journal of Inorganic and Nuclear Chemistry* **1963**, *25*, 395-405.
251. Lib, Z.-X. L. a. H.-H., *Acta Cryst.* **2007**, *E63*, 939–941.
252. Casale, A.; De Robertis, A.; De Stefano, C.; Gianguzza, A.; Patanè, G.; Rigano, C.; Sammartano, S., *Thermochimica Acta* **1995**, *255*, 109-141.
253. Gupta, M.; Srivastava, M. N., *Polyhedron* **1985**, *4*, 475-479.
254. Ibrahim, M.; Radadi, R., *International Journal of Electrochemical Science* **2015**, *10*, 4946-4971.
255. Hammes, G. G.; Steinfeld, J. I., *Journal of the American Chemical Society* **1962**, *84*, 4639-4643.
256. Vinokurov, E. G.; Bondar, V. V., *Russian Journal of Coordination Chemistry* **2003**, *29*, 66-72.
257. Farooq, O.; Uddin Malik, A.; Ahmad, N., *Journal of Electroanalytical Chemistry and Interfacial Electrochemistry* **1973**, *46*, 136-140.
258. Jalilehvand, F.; Sisombath, N. S.; Schell, A. C.; Facey, G. A., *Inorganic Chemistry* **2015**, *54*, 2160-2170.
259. Vadas, T. M.; Ahner, B. A., **2009**, *38*, 2245-2252.
260. Dişbudak, A.; Bektaş, S.; Patır, S.; Genç, Ö.; Denizli, A., *Separation and Purification Technology* **2002**, *26*, 273-281.
261. Martin, R.-P.; Mosoni, L.; Sarkar, B. J. J. o. B. C., **1971**, *246* , 5944-5951.
262. Yasui, T.; Shimura, Y., *Bulletin of the Chemical Society of Japan* **1966**, *39*, 604-608.

Resumés

Valorisation of CO_2 capture agents for soil decontamination

The work presented in this thesis focuses on the development of a CCUS technology which integrates carbon capture, mineral carbonation and decontamination of a soil, provided by the cement industry. Natural α amino acids, glycine, *L*-lysine and *L*-cysteine, were investigated via a Dynamic Combinatorial Chemistry approach for their CO_2 capture properties. We herein demonstrated that αAA can reach higher CO_2 loading, higher cyclic capacities and present lower enthalpies of reaction (-68/-72 kJ/mol of CO_2) compared to **MEA**, thus should be considered as potential substitutes to industrial amines in the field of CO_2 capture. The CO_2-loaded amino acids solutions were then investigated for an Integrated Absorption Mineralization process for the mineral carbonation of alkalin^{e-}earth metal oxides, where ***L*-LysK** provided a calcium carbonation yield of 89% with 4% of amine loss. Finally, the amino acids were investigated, both in absence and in presence of CO_2, as washing solutions for the remediation of a polluted soil. **GlyK**, ***L*-LysK** and ***L*-CysK** displayed high extraction efficiency towards nickel, cadmium and lead, while sequestering 57%-70% of CO_2 as mineral carbonate in the soil. The preliminary results reported in this thesis show that amino acids can be considered potential sorbents for CO_2 capture, metal carbonation enhancers as well as efficient chelating agents for metal extraction.

Keywords: CO_2 capture, Dynamic Combinatorial Chemistry, amino acids, mineral carbonation, soil depollution, amine recovery, CCUS

Valorisation des solutions de captage de CO_2 pour la décontamination des sols

Ce travail de thèse s'intéresse au développement d'une technologie CCUS qui intègre le captage du CO_2 ainsi que la carbonatation minérale couplée à la remédiation des sols. Une série d'acides aminés, glycine, *L*-lysine et *L*-cysteine, a été étudiée par une approche de Chimie Combinatoire Dynamique pour leurs propriétés de captage du CO_2. Les résultats observés montrent que les acides aminés peuvent atteindre des taux de charge $\alpha(CO_2)$ et des capacité cycliques élevées, par rapport à la **MEA**, ainsi que des faibles enthalpies de réaction (-68/-72 kJ/mol de CO_2). Nous pouvons en conclure que les acides aminés peuvent être considérés comme substituts de choix aux amines industrielles utilisées pour le captage de CO_2. Les solutions d'acides aminées ont été ensuite étudiés pour un processus de carbonatation minérale d'oxides de métaux alcalino-terreux, intégré au captage du CO_2. En présence de ***L*-LysK**-CO_2 89% de CaO a été carbonaté, avec une perte d'amine limitées à 4%. Le dernier chapitre de ce travail est consacré à l'utilisation des solutions d'acide aminé pour la dépollution de sols. Ce processus de type CCUS inclut le captage de CO_2, sa fixation sous forme de carbonate métallique ainsi que l'extraction de métaux contaminant et la régénération partielle de l'agent aminé. **GlyK**, ***L*-LysK** et ***L*-CysK** ont montré une efficacité d'extraction envers nickel, cadmium et plomb, avec la séquestration de 57%-70% de CO_2 sous forme de carbonate minéral dans le sol. Les résultats préliminaires obtenus dans ce travail de thèse montrent que les acides aminés tels la glycine, la *L*-lysine et la *L*-cysteine peuvent être considéré des potentiels agents d'une stratégie CCUS intégrée et éco-efficiente.

Mots clefs : captage de CO_2, Chimie Combinatoire Dynamique, acides aminés, carbonatation minérale, décontamination des sols, régénération d'amine, CCUS